ISTITUTO SUPERIORE DI SANITÀ

International meeting

Complexity in the living: a problem-oriented approach

Rome, September 28-30, 2004

Proceedings edited by
Romualdo Benigni (a), Alfredo Colosimo (b), Alessandro Giuliani (a),
Paolo Sirabella (b) and Joseph P. Zbilut (c)

(a) Dipartimento di Ambiente e Connessa Prevenzione Primaria, Istituto Superiore di Sanità, Rome, Italy
(b) Dipartimento di Fisiologia Umana e Farmacologia, Università degli Studi di Roma "La Sapienza", Rome, Italy
(c) Department of Molecular Biophysics and Physiology, Rush University Medical Center, Chicago, USA

ISSN 1123-3117
Rapporti ISTISAN 05/20

Istituto Superiore di Sanità
International meeting. Complexity in the living: a problem-oriented approach. Rome, September 28-30, 2004.
Proceedings edited by Romualdo Benigni, Alfredo Colosimo, Alessandro Giuliani, Paolo Sirabella and Joseph P. Zbilut
2005, v, 247 p. Rapporti ISTISAN 05/20

The scientific world has the clear perception that an interdisciplinary approach is urgently needed for attacking the many yet unsolved problems of today science. This attitude has several roots, including the search of biologists for quantitative foundations, and that of physicists for better approaches to the mesoscopic systems. This feeling is highly exacerbated in the field of complexity studies. The Meeting 'Complexity in the Living' attracted scientists from very diverse fields. A most profitable area of interaction resulted to be the description of methods, conceived as "stratagems" used in the different fields to cope with complex and intermingled problems. These good-faith "stratagems" are probably the only strong commonality amongst so diverse scientists, and thus are a basis for an interdisciplinary science. On this ground, the Meeting was characterized by intense discussion and exchange, whose trace is reported in these proceedings.
Key words: Computational biology, Ecology, Systems, Statistics, Interdisciplinary studies.

Istituto Superiore di Sanità
Convegno internazionale. La complessità del vivente: un approccio orientato al problema. Roma, 28-30 settembre 2004.
Atti a cura di Romualdo Benigni, Alfredo Colosimo, Alessandro Giuliani, Paolo Sirabella e Joseph P. Zbilut
2005, v, 247 p. Rapporti ISTISAN 05/20 (in inglese)

Il desiderio di interdisciplinarietà è fortemente sentito nella scienza odierna, soprattutto sull'onda della necessità della biologia di darsi dei fondamenti quantitativi, e della fisica di essere efficace nello studio dei sistemi mesoscopici. Questa sensazione è sentita con ancora maggior forza nell'ambito degli studi sulla complessità. Il convegno 'Complexity in the Living' è stato un'occasione di confronto fra scienziati di diversa estrazione. Un terreno di incontro tra le diverse specializzazioni è stato identificato nei metodi, intesi come 'trucchi del mestiere' utilizzati nei diversi settori per districarsi da situazioni complesse e di difficile interpretazione. Questi trucchi (in senso buono) sono probabilmente uno dei più fertili comun denominatori fra scienziati di differente estrazione e quindi l'ambito in cui una reale interdisciplinarietà può proficuamente fondarsi. Su questo terreno, nei giorni del convegno c'è stato un fitto e accalorato scambio di idee, di cui questi atti riportano la traccia.
Parole chiave: Biologia computazionale, Ecologia, Sistemi, Statistica, Studi interdisciplinari.

Per informazioni su questo documento scrivere a: benigni@iss.it

Il rapporto è accessibile online dal sito di questo Istituto: www.iss.it

Presidente dell'Istituto Superiore di Sanità e Direttore responsabile: *Enrico Garaci*
Registro della Stampa - Tribunale di Roma n. 131/88 del 1° marzo 1988

Redazione*: Paola De Castro, Sara Modigliani* e *Sandra Salinetti*
La responsabilità dei dati scientifici e tecnici è dei singoli autori.

TABLE OF CONTENTS

Foreword v

METHODOLOGICAL BACKGROUND

The inherent complexity of chemistry
Luigi Cerruti 3

Complexity of life via collective mind
Michail Zak 21

Evolutionary neural gas: a scale-free self-organizing neural net without topological constraint
Luigi Lella, Ignazio Licata 43

3D measures of complexity for the assessment of complex trabecular bone structures
Norbert Marwan, Peter Saparin, Wolfgang Gowin, Jürgen Kurths 53

Fine-grained Delaunay triangulation for the solution of diffusion equations in cellular clusters
Roberto Chignola, Edoardo Milotti 59

Reality generation: the fractal temporal perspective
Susie Vrobel 64

ECOLOGICAL AND ENVIRONMENTAL ISSUES

Functional and structural properties of hemoglobins from Atlantic cod (*Gadus morhua l.*) populations from the southern part of the North Sea, the Belt Sea, and the Baltic Sea
Ole Brix, Atle Torbjørnsen Nedenes, Bengt Berdal 71

Evolution, complexity, individual, struggle and co-operation for life
Giovanni Alfredo Zapponi 96

Solar ultraviolet radiation at the earth's surface: factors affecting its impact on human beings
Giuseppe Rocco Casale, Anna Maria Siani, Alfredo Colosimo 106

Decision engineering in complex social-economical systems using self-organized criticality
Roma Siugzdaite, Saulius Norvaisas 111

PHYSIOLOGICAL AND METABOLIC REGULATIONS

Analysis of complex metabolic networks on the basis of optimization principles
Hermann-Georg Holzhütter 121

Aggregation propensity of proteins quantified by hydrophobicity patterns and net charge
Joseph P. Zbilut, Julie C. Mitchell, Alessandro Giuliani, Alfredo Colosimo, Norbert Marwan, Mauro Colafranceschi, Charles L. Webber, Jr. 136

Metabonomic study of transgenic maize
Cesare Manetti, Cristiano Bianchetti, Lorena Casciani, Cecilia Castro, Maurizio Delfini, Maria Enrica Di Cocco, Alfredo Miccheli, Mario Motto, Filippo Conti 152

Prediction of Herg affinity values using independent approaches
Elena Fioravanzo, Nicola Cazzolla, Lucia Durando, Cristina Ferrari, Massimo Mabilia, Rosella Ombrato 158

Inferring the essentiality of different mutations of saccharomyces cerevisiae from the positions of the corresponding enzymes in the metabolic network
Maria Concetta Palombo, Alfredo Colosimo, Alessandro Giuliani, Lorenzo Farina 163

MOLECULAR MODELLING

Changing paradigms in drug discovery
Hugo Kubinyi 171

Computational explorations of the property space of biomolecules
Bernard Testa, Giulio Vistoli, Alessandro Pedretti, Andrzej J. Bojarski, Mateusz Nowak 186

A stochastic and computational method for estimating the folding rates of wild type and mutant proteins
Mario Compiani, Emidio Capriotti, Rita Casadio 200

Adaptive processing of complex data structures in QSPR/QSAR analysis
Alessio Micheli, Antonina Starita 206

Looking for constitutive gene regulation webs by microarray studies: a recursive neural network approach
Monica Francesca Blasi, Ida Casorelli, Alfredo Colosimo, Francesco Simone Blasi, Margherita Bignami, Alessandro Giuliani 209

INTEGRATIVE NEUROSCIENCE

Non invasive brain computer interface for communication and control
Fabio Babiloni, Donatella Mattia, Marco Mattiocco, Alessandro Timperi, Serenella Salinari, Maria G. Marciani, Febo Cincotti 217

Time-dependent measures of dynamical complexity
Paul E. Rapp, Christopher J. Cellucci, Toshio A. A. Watanabe, Richard S. Hernandez 221

Model, dynamical behaviour and synchronization properties in networks of fast-spiking interneurons
Angelo Di Garbo, Alessandro Panarese, Michele Barbi, Santi Chillemi 233

Analyzing spatial distributions of fMRI "bold" signals by RQA variables
Marta Bianciardi, Paolo Sirabella, Gisela E. Hagberg, Alessandro Giuliani, Joseph P. Zbilut, Alfredo Colosimo 238

Otoacoustic emissions at different maturation stages: pre-term and full term subjects comparison
Giovanna Zimatore, Alessandro Giuliani, Stavros Hatzopoulos, Alfredo Colosimo 244

FOREWORD

This report contains a series of contributions originated from the Meeting entitled "Complexity in the living: a modelistic approach", which was held in Rome, September 28-30, 2004. The Meeting has been organised jointly by the Istituto Superiore di Sanità (the Italian National Institute of Health), and the Interdepartmental Research Centre for Models and Information Analysis in Biomedical Systems (CISB) of the University "La Sapienza", Rome. The Meeting was held at CISB. The chapters follow the structure of the sessions of the Meeting, with its division into long lectures and short communications.

In 1997, a previous meeting with the same name was organized by us, and held in the same place with a similar format. At the time, the emphasis was on the methodological and formal issues, more than on the practical applications. In most presentations, specific problems were discussed with the aim of showing how different research fields could take advantage of the use of a few basic, unifying concepts.

In the latter edition of the meeting, the emphasis clearly shifted towards a 'hands-on' perspective. The main question was: once a given data set, in a well defined experimental context, is recognized to be unsuitable for the application of linear and deterministic models, what are the analytical tools available for a satisfactorily descriptive, and possibly predictive approach? This substantial change of perspective derives from the realisation, in recent years, that expectations about the possibility of an all embracing 'complex systems theory' has remained largely unfulfilled; on the contrary, local approaches based on operational measures of complexity have often produced very fruitful results in different fields. This recognition opens the way to new interdisciplinary efforts no longer based on 'shared theories', but on 'shared data analysis approaches'.

The contributions collected in the present volume span many fields, from ecology to neuroscience. In our opinion, this matches perfectly our original intention to present an updated panorama of case-stories-in-complex-systems-analysis. Moreover, the need to be understood by very diverse types of scientists stimulated the lecturers to get rid of excessive details, and to focus instead on the most crucial issues.

The need to approach complex systems with more efficient strategies is not only an internal, academic problem of the scientific community. On the contrary, this need is also linked to a more responsible attitude towards the overwhelming problem of sustainable conditions for the living species on our planet. In fact, the new demands posed by the society to the science have changed in their focus from more specific technological applications (for which the classical reductionist approaches are highly suitable), to wider issues (e.g., global warming, psychiatric disorders epidemics in Western countries, excessive exploitation of natural resources). For these "new problems", new theoretical paradigms are needed: this meeting was designed to go along these lines.

In this light, we believe that this collection of papers demonstrates that consideration of complex phenomena from an interdisciplinary and data-driven perspective is an invaluable source of inspiration for producing smart solutions for otherwise untreatable problems.

Methodological background

Lecture

THE INHERENT COMPLEXITY OF CHEMISTRY

Luigi Cerruti
Dipartimento di Chimica Generale ed Organica Applicata, Università di Torino, Torino, Italy

Introduction

Every scientific discipline has a *peculiar* approach to its specific problems and to more general issues. There are many reasons for a so different disciplinary attitude. The essential *raison d'être* is very deep, because it results from the diverse ontological levels of importance for the different scientific disciplines (1). Other more 'superficial' reasons have their roots in the history and sociology of science (2). We can expect that a theme like complexity may act as a catalyst to amplify the disciplinary differences.

Many of the specific problems of chemistry are inherently complex, and the first part of the present essay deals with the *nature of chemistry* from the point of view of complexity. The second part of the essay considers three crucial topics of the *chemistry of nature*: catalysis, origin of life, Gaia.

What is chemistry?

For a historian the question "What is chemistry?" is not a silly one. The Merriam-Webster Online Dictionary gives a simple definition of chemistry: "science that deals with the composition, structure, and properties of substances and with the transformations that they undergo" (3). This kind of definition is usual and useful in many contexts (e.g. in general chemistry textbooks), however for a chemistry historian it covers only a part of his/her field of research. Of course, it is a fundamental part, and yet only a part. A glimpse to Table 1 is sufficient to question the idealistic simplification of the dictionary definition.

Table 1 lists seven different kinds of components of the 'chemistry system'. Not all the components are pertinent to our discussion, but some will be recalled several times in the following pages. Anyway, it is possible to give an immediate and decisive support to the conception of chemistry as a complex system. Decomposability is an important issue in many scientific fields, from mathematics and computer science to theoretical biology. We can use the concept of decomposability in a soft but significant way referring to a procedure described by John L. Casti. Decomposability it is a property of simple systems. The components of a simple system interact weakly, so we can disconnect one or more of the components and the system will behave more or less as it did before. A suitable example is a ship. She can be a highly complicated system, but from the point of view of decomposability it is not complex; any ship can suffer major damage without dramatically changing her overall seafaring capacity. A complex system with its high degree of interaction is very sensitive to these changes. Disconnecting or damaging any part/component of the system will produce drastic changes in the systems behaviour. It is inconceivable a running chemistry without chemists (component B), or laboratories (component C), and so on until the end of the list.

Table 1. Chemistry as a complex system

System component		Short description and comment
A	*Knowledge*	When chemical knowledge is meant simply as information, it is the most abstract level of the discipline. Because of this abstractness, many times for 'chemistry' it is meant 'chemical information'
B	*Scientists*	Chemists are women and men who produce chemical knowledge. There is no chemical knowledge without chemists; it is necessary to remark this obvious fact because philosophers often describe a science without human actors, something as a disembodied science
C	*Instruments, laboratories, institutions*	These three system components are heterogeneous, but together they let scientists to do their work and to reproduce themselves as scientists.
D	*Documentation and media*	Documentation consists of the material supports which store the texts (books, journal, etc.), as well as the texts themselves
E	*Substances and materials*	See text
F	*Chemical plants and industrial processes*	Chemical plants produce substances/materials for the market, and data for research and control. Industrial chemical processes are extremely different from laboratory processes. See also text
G	*Ethos*	The disciplinary ethos is the set of behaviour rules of the chemical comunity members. This ethos controls also the epistemic behaviour of the chemists. See also text

Chemistry historians and science historians have written many scholarly articles and learned books on any separate item of Table 1, with an empirical demonstration that it is feasible a partial description of a complex system. However, historians are compelled to think in a hermeneutical way, with a recurrent loop between text and context, and they are perfectly aware that they have to cut almost all the ties between the particular research topic and the rest of chemistry (or the rest of science, or the rest of scientific culture, etc.).

Definitions of complexity

John Horgan, a well known freelance journalist and author, published in June 1995 an article entitled "From complexity to perplexity" (4). In this article he mentions the 31 definitions of complexity, collected several years before by Seth Lloyd of the Massachusetts Institute of Technology. Hogan published his scourging essay on *Scientific American*, and in the following years the essay was quoted countless times. It is understandable that a diversified set of definitions might drive to despair mathematicians and logician, but it is not the same case for a chemist (not to mention a historian). Chemists use several definitions of the acid/base couple depending on the context of use of the concept and of the related substances: the 'acidity' of an oxide surface is not the 'acidity' of a sulphuric acid aqueous solution.

In chemistry, complexity is a property of a system and of its behaviour. Two definitions of complexity are useful for our purposes:

Def1*:* a system is complex when it is not possible to describe the system with a unique formal model, and the models in use are not derivable from each other (5).

Def2*:* a system is complex when its behaviour as a whole is not derivable from the properties of its parts.

The first definition was born in the context of theoretical biology, while the second definition is accepted by almost all the non-reductionist researchers. The two definitions have different epistemological traits. Def1 emphasizes the intractability of the complex systems from a unique

point of view; while it recalls itself to reductionist models of analysis, in reality it skilfully challenges them. It does not deny the partial success of this or that formal model, but it asserts that for a complex system there will be always some escaping property or behaviour, and therefore a single formal model will not be never in a position to supplying a total description of the system. Def2 is so widely accepted because it removes the dreary issue of reductionism (6): we notice that a system is complex when in its behaviour comes forth an emergent property, an innovation of different ontological level from that one on which the single parts of the system are set to form the system in examination

Inherent complexity of chemical objects and processes

Any real chemical system presents relevant problems at the microscopic and macroscopic levels, in fact in the system are present *molecules* (micro-level), and *substances* and *materials* (macro-level). The complexity of the 'objects' of chemistry (molecules, substances and materials) is a part of the inherent complexity of chemistry; another part is due to the complexity of the *reactions* running inside the system. At first, these items will be analysed in respect to complexity, and later on some emphasis will be given to the opportunities/difficulties of the quantitative approaches, and to the interplay between the procedures of synthesis and the irreducible individuality of many molecular structures.

For short, the particular problems of materials will not be treated here, but at least a specification is due. The distinction between a substance and a material is not ontological but pragmatic. Iron and propylene are substances with physical and chemical properties, in part referred to substances as such (e.g. melting point), and in part referred to the component particles (e.g. ionisation potential or molecular weight). A substance 'becomes' a material when it is considered its *use* for a purpose, so in the case of iron and propylene we may interested in knowing their modulus of elasticity. A material is not necessarily more 'complex' than a substance; what is of importance is the point of view which is considered.

Molecules and substances

At first sight, it may seem bizarre to think that a *single molecule* could be a *complex system*, but we can dissipate our doubts using the two definitions of complexity given above.

According to Def1: a molecule is complex because even decomposition, its simplest possible reaction, is not describable by a unique model. Thermal decomposition is always possible, and it is described with models different from and not reducible to the models used for the decomposition *via* heterogeneous catalysis.

According to Def2: a molecule is complex because at least one of its inherent properties is not derivable from the properties of its component atoms. Molecular structure does not depend only on the properties of the component atoms but also on their mutual connections. Among the emergent properties two are inherent to any molecule: *organisation* (7) and *stability* (8). A third property emerges when it is formed a molecule, or simply a cluster of atoms: it is the breaking of the spherical symmetry of any isolated atom. When this symmetry breaking becomes stable it is born a completely new microscopic object, a molecule with a *shape*. It is revealing that molecular organisation (structure) and shape are the starting-point of the quantitative determination of the molecular complexity.

On July 18, 1980, the *Journal of the American Chemical Society* received from the Bell Laboratories a short paper with a roaring title: "The First General Index of Molecular

Complexity". Steven Bertz, the author, opened his paper with these words: "Synthetic chemists have been defining a 'complex molecules' in the way that many people define art: they know it when they see it". Bertz' ironic touch was somewhat heavy, but the author's intentions were very ambitious because his "unified index" would take in account "the size, symmetry, branching, rings, multiple bonds, and heteroatoms characteristic of a complex molecule". The use of graph and information theories let Bertz calculate for every molecule a single number C_T, which he presented with a preposterous sentence: "C_T is the first measure of molecular complexity that is completely general" (emphasis added). Thus Bertz put in order all the possible molecules: every molecule corresponded to a number on the real number line, and on this line the word 'measure' acquired a strong sense. According to Bertz, it became "possible to calculate the change in complexity [Δ], upon going from reactant to product in the course of a chemical reaction", and eventually "the process of calculating Δ [could] be repeated for all the steps in a synthetic sequence, thus providing a means to gauge progress toward a complex target molecule" (9).

The history of the last two decades has demonstrated that 'unified indexes' are almost of no use in the laboratory practice. Robert Woodward, perhaps the best organic chemist of the last century, wrote shining pages on his *personal* trains of thought when he was meditating on the best way for climbing from one step to another one in a delicate synthesis. According to Woodward, "there is excitement, adventure, and challenge, and there can be great art, in organic synthesis". From an epistemological point of view the excitement of Woodward and other organic chemists is perfectly understandable because in many times it is the consequence of an unpredictable (hostile) behaviour of certain molecules, also in standard reactions; we may dub as C_{11}-factor this temperamental behaviour of the molecules of interest. In the years following the discovery of the therapeutic use of cortisone, a hard competition started between the major pharmaceutical industries, in order to find a new synthesis, different from the Saret synthesis, controlled by Merck. The crucial step of the Saret synthesis was the introduction of an atom of oxygen in the position C_{11} of the steroid structure of cortisone. The C_{11} position resisted at length, and at last it surrendered to a bacteriological attack by Upjohn. The C_{11}-factor checkmates any C_T number because the C_T numbers and the many similar ones convey the properties of an ideal, isolated molecule, while during a reaction many (really many) molecules interact with other similar and different molecules, with the molecules of solvent, with heat, light, mechanical walls, etc.

Twenty year after the seminal article by Bertz, the mathematical 'measure' of the molecular complexity had no firm base. The judgment of Randić and Plavšić, experts of international fame, was severe: "Complexity, just as many other widely used concepts in chemistry (e.g., aromaticity), has not been rigorously defined, at least for a general case" (10). This sentence should merit some remarks, but I prefer to mention another type of index, related to complexity.

|Descriptor| is a general term, used in several academic fields. Its special meaning in chemistry can be appreciated in the definition (plus *caveat*) given by Todeschini and Consonni: "A molecular descriptor is a number extracted by a well defined algorithm from a molecular representation of a complex system, i.e. the molecule". Todeschini and Consonni are the leaders of the Milano Chemometrics and QSAR Research Group, one of the strongest groups in the field. "There is good reason to believe that often our difficulties in attributing a meaning to this number lie ultimately in the lack of deeper chemical theories and higher level languages and not from esoteric approaches to the descriptor definition" (11). In semantics we speak of 'intensive' meaning (the definition) and of 'extensive' meaning (the set of objects to which the definition can be applied). Also the extensive meaning of |chemical descriptor| can be appreciated from a recent manual published by the Milano QSAR group. Todeschini and Consonni give the definition of about 2,000 different descriptors (12)! This crowd of different descriptions is a

definitive confirm that a molecule is a complex system (see above, Def1), but for an epistemological comment it is better to refer to a smaller, albeit authoritative, set of descriptors.

In 2002 the content of the Chemical Abstract Service (CAS) registry file was enriched with experimental and calculated property data. Here we are not interested in the enormous quantity of substances and properties indexed, but in the ontological qualities of the properties. The five experimental properties are all measured at the macroscopic level. We find a different situation for the calculated properties, where boiling point and flash point are macroscopic properties of substances, while the number of freely rotable bonds and of hydrogen donors/acceptors refer to structural properties of molecules. Among the 14 calculated quantities, there is also the ambitious bioconcentration factor, defined as "the ratio of the concentration of a substance in an aquatic organism to the average concentration of the substance in the surrounding water. Values are calculated at pH 1,4,7,8, and 10 and are derived from the corresponding calculated log D values", where log D is "the logarithm of the partition coefficient between octanol and water at a given pH for the mixture of the neutral and ionic forms of a compound". Log P is "the logarithm of the partition coefficient between octanol and water for the neutral form of a compound" (13). Calculated quantities as the bioconcentration factor, log D and log P are really ambitious because they try to predict the behaviour of complex systems.

The properties with experimental values in the CAS registry are:

- Melting Point
- Boiling Point
- Refractive Index
- Optical Rotatory Power
- Density.

The calculated properties are:

- Bioconcentration Factor
- Boiling Point
- Enthalpy of Vaporization
- Flash Point
- Freely Rotable Bonds
- logD
- logP
- Molecular Weight
- Molar Solubility
- Number of Hydrogen Donors
- Number of Hydrogen Acceptors
- Organic Carbon Adsorption Coefficient (Koc)
- pKa
- Vapor Pressure.

In effect, the above lists collect a mixed bag of properties. Some properties relate to molecules, other ones to substances, and some other ones, as logD and logP, are ambiguous, for reasons which will immediately clear.

Insoluble doubts about solubility

One of the major difficulties of teaching/learning chemistry is that chemists' disciplinary discourse is inherently ambiguous (at least for non-chemists or philosophers) because it refers to two different ontological levels, nearly in any expression. For example, we can consider the following stoichiometric equation:

$$CO + 2H_2 \rightarrow CH_3OH \text{ [1]}$$

This writing refers to the reaction between *three* molecules, one of carbon oxide and two of hydrogen; at the same time it refers to the reaction between two substances, carbon oxide and hydrogen, in the stoichiometric relationship of one mole of carbon oxide and two moles of hydrogen. It is obvious that equation [1] has no meaning for the actual mechanicistic running of the reaction; however the final equilibrium is completely ruled by the stoichiometric quantities. In other words, at the *microscopic level* equation [1] maintains that in certain, *not specified*, way three molecules have to react to give a new single molecule; at the *macroscopic level* equation [1] affirms that the substance carbon oxide reacts with the substance hydrogen in a *precise* stoichiometric relationship.

In the case of equation [1] every first-year chemical student is able to discriminate the two levels of discourse, but in other cases it is not so easy to distinguish the macroscopic level from the microscopic. The investigation of models for solubility is a very active research field both in QSAR (Quantitative Structure-Activity Relationships) and in QSPR (Quantitative Structure-Property Relationships). Solubility is an important property for many substances in several different contexts, from physiological absorption to *in vitro* reactivity for a particular synthesis; unfortunately, solubility is not an easy property to be dealt with. First of all, solubility cannot be an intrinsic property of a substance because it regards the behaviour of the substance under consideration in a particular, specified solvent. So, when we are speaking of solubility, we are always referring (at least) to a couple of substances. The solubility of a substance can be measured with a minimal quantity of the substance, but the quantity is at least of 30 mg, a quantity which is detectable to the naked eye, thus solubility is operationally a macroscopic property. Nevertheless, the solution process takes place for the interactions at the microscopic level between the particles of the solute and the particles of the solvent. This contrast may be well expressed with few classical thermodynamic equations.

For every process at equilibrium and a system at STP conditions it is valid:

$$\Delta G° = \Delta H° - T\Delta S° \text{ [2]}$$

The same $\Delta G°$ value gives us the value of the equilibrium constant of the process:

$$\Delta G° = - RT \ln K \text{ [3]}$$

The equation [2] tells us whether the process is spontaneous ($\Delta G° < 0$), and splits the $\Delta G°$ value in two parts: $\Delta H°$ is the enthalpic part, in our case equivalent to the dissolution heat of the substance; $\Delta S°$ is the entropic part, connected to the variation of the possible states of the system. The equation [3] connects the variation of the free energy with the equilibrium constant, in our case with K_{sp}, the solubility product constant. Equation [3] may be rewritten as:

$$\Delta G° = - RT \ln Ksp \text{ [4]}$$

In regard to the equation [2] an analysis of the relative values of $\Delta G°$, $\Delta H°$, and $T\Delta S°$, demonstrates that also for similar classes of simple compounds (e.g. NaX and AgX, X = a halogen) there are cases in which prevails the enthalpic term, and other cases in which prevails the entropic term. Similar cases "illustrate the difficulties encountered in seeking explanations of solubility in terms of a handful of simple rules; in general each case must be individually subjected to the above sort of analysis before any considerable progress can be made towards understanding the factors which determine solubility" (14). This opinion was expressed many years ago by W.E. Dasent; more recently a IUPAC committee expressed a 'complementary' view: "Thermodynamic analysis of solubility phenomena provides a rational basis for the construction of functions to represent solubility data, and thus aids in evaluation, and sometimes enables thermodynamic quantities to be extracted. Both these aims are often difficult to achieve because of a lack of experimental or theoretical activity coefficients" (15). The reference to the activity coefficients is very important because it points to the thermodynamic origin of our

doubts about the possibility of distinguishing the ontological levels referred to by the word |solubility|.

When we proceed from ideal systems to real ones the equation [4] has no direct and immediate application, because K_{sp} has to be calculated from the activity coefficients and not from the concentrations. Unfortunately we know almost nothing on these notorious coefficients, apart from the fundamental fact that they let us pass from the *measurable* chemical quantities (concentrations) to the *real* quantities of substance which participate to the process. On a general ground we can say that an activity coefficient is an a-dimensional parameter which 'condenses' in its value the whole non-ideality of the system under consideration. Depending on the system under consideration, similar coefficients are not known once and for all, since they feel the effects of the actual situation of the particles (molecules, ions) which compose the substances present in the system. Therefore, a molar quantity as $\Delta G°$, apparently valid for every system, is tracked down to molecular reality of a single, particular system, when it is applied as a function of activities in equations like the equation [4]. Thermodynamics teaches us that the ontological knot which binds the macroscopic substance and the microscopic molecule cannot be completely untied.

Reactions

After the Second World War, in the course of a generation, chemical laboratories thoroughly changed, and chemists of any denomination (including the reluctant organic chemists) changed their attitude toward the physical instrumentation, and learned to use a dozen of different spectroscopies. At the same time, the X-ray structure determination became more and easier with the use of powerful instrumentation, software and computers. Up to then the *interaction among substances* was almost the only source of information about the properties of substances and molecules. After the massive introduction of physical instruments in chemical laboratories, the principal source of information about the microscopic level has become *the interaction between substances and electromagnetic fields* (16).

These impressive changes caused a shift in the disciplinary ethos of organic chemists. Before the introduction of the physical instrumentation the disciplinary prestige had two different and complementary focal points: the determination of difficult structures of natural products and the synthesis of molecules of very complex structure. After the transformation of the chemical laboratory only one disciplinary focus remained: the synthesis of new, extraordinary and/or useful molecules. The synthesis of an organic compound is often similar to the creation of a piece of art for the liberal use of traditional knowledge, plus imagination, ingenuity, and creativity. Ingenuity and creativity are at their best when the chemist is forced to invent a new reaction or to find a better control of a known reaction. In effect, the complexity of a chemical reaction becomes very evident when the chemist, academic as well as industrial, try to control the behaviour of the system in which the reaction runs.

Hints from philosophy of catalysis

Chemists use catalysts to control reactions in laboratories as well as in industrial plants. All living beings (including chemists) live thanks to an enormous number of catalysts, thus catalysis is a field of research in which the intrinsic complexity of the 'disciplinary' chemistry intermingle with the complexity of the 'natural' chemistry. As it will be soon clear, in this context the word |control| is used in a very strong sense, because in the great majority of the

successful cases the catalyst selects a particular reaction pathway from a host of possible pathways (17).

The *virtuality* of most chemical properties is absolutely evident when we describe the *reactivity* of a substance. Here it is appropriate to refer to the detailed protocols, which have to be followed in order to use correctly a substance as a *reagent* (18). In the protocols, we find the instructions for (re)creating the right *context* for the *use* of the reagent. Following this train of thought we see that the property of being a catalyst is exceedingly virtual. Certain cases of catalytic activity seem almost scandalous. I think of the Orito reaction in which platinum, modified by the presence of preadsorbed cinchonidine becomes active for the stereoselective hydrogenation of a α-ketoester. While chemists were able to gain the knowledge necessary to identify new, simpler and more stereoselective (commercial) substances, however, overall, the research left unsolved a crucial aspect of the problem, just the source of the catalytic activity.

We can consider a closed *chemical system*, consisting of a set of chemical substances, each present with certain, and determinate number of moles. At any value of temperature and pressure the evolution of the system *must* obey the laws of thermodynamics. However, in many actual chemical systems the variation of the Gibbs free energy may be negative for a large set of reactions, thus we may describe a *thermodynamic framework* given by all the $\Delta G < 0$, *corresponding to all the possible reactions inside the system*, and in this thermodynamic framework the substances are connected through the usual stoichiometric equations. Nevertheless, as we know, the evolution of the system does not necessarily evolve towards the lowest value of the Gibbs energy, principally because of the kinetic aspect of the permitted reactions. At given temperature and pressure the most evident feature of the thermodynamic framework is built up by the minima corresponding to all the possible mixture of products; these minima are connected by the relative maxima corresponding to the ambiguous substances named 'activated complexes'. On this supporting structure of the classical thermodynamic framework, chemical kinetics introduces/reproduces an essential kinetic feature, the rates of reaction, with their empirically determinate, non-stoichiometric, orders of reaction, and their reference to the macroscopic world of chemical substances. At this point, statistical thermodynamics and quantum chemistry tries to describe, qualitatively and quantitatively, the molecular dynamics, which, at the microscopic level of reality, rules the transformation of molecular systems. We may say that classical and statistical thermodynamics and quantum chemistry give us a vantage-point from which we enjoy a good view on the valleys, cols and saddles of the potential-energy surface. These valleys and passes constitute the 'natural' *kinetic landscape* of any chemical system. The metaphor I am proposing is to consider a catalyst as a contrivance, which modifies the kinetic landscape of a chemical system (19).

To burn butenes

The case of kinetic landscaping which I consider in some formal kinetics details is the selective oxidation of butens. 1-butene, cis- and trans-2-butene and 2-methylpropenes (isobutene) are the four isomers which correspond to the brute formula C_4H_8. In the chemical-industrial jargon, the designation 'n-butenes' refers to mixtures of the first three isomers. The four isomers show differences in their chemical behaviour, and, mostly, their reactivity can be ordered in this way:

isobutene >> 1-butene > 2-butenes

Their main reactions are addition reactions, isomerization and polymerization, but here I am interested in considering the catalytic oxidative dehydrogenation of butenes to maleic anhydride. A simplified reaction scheme may be the following (Figure 1).

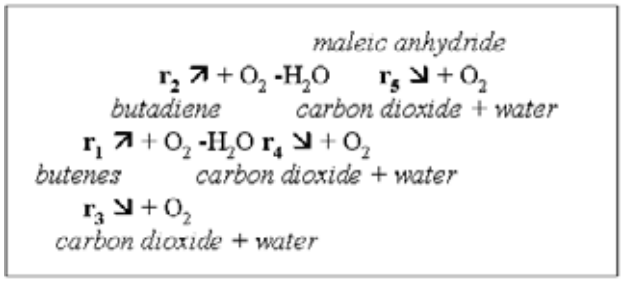

Figure 1. Catalytic oxidative dehydrogenation of butenes to maleic anhydride

Products and reagents are involved in more than one reaction, each occurring with its own rate and stoichiometry; thus, we can describe the rate of any appearing and disappearing substance in this form:

$$r_i = \Sigma_j \alpha_{ij} r_j \quad i = 1,6; j = 1,5$$

where i refers to a substance and j to a reaction rate. α_{ij} is the matrix of the stoichiometric coefficient which permits the description of the evolution of any single species, if the kinetic equations r_1 to r_5 are known. The scheme is *extremely simplified*; for example, any isobutene molecule present in the system is quickly oxidized to carbon oxide, carbon dioxide and water, and any partial, destructive oxidation leads to the presence of carbon oxide. To its turn, with carbon oxide and water it becomes possible the *water gas shift reaction*; with the resulting hydrogen and other carbon oxide it becomes possible the *oxo-process*, or, in a way completely independent from the presence of olefins, it could start a *Fischer-Tropsch reaction*. In a sense, it is difficult to see the borders of the kinetic landscape corresponding to a gaseous mixture of butens and oxygen, at the temperatures between 350 and 450 °C used in industry.

It is to be appreciated that in this vast kinetic landscape the most crowded resorts could be the minima of free energy corresponding to the combustion end products, carbon dioxide and water. As a matter of fact, the ignition temperatures of the four butene isomers (listed at the beginning of this sub-section) are 384, 325, 325 and 465 °C respectively. However, in 1985 were on stream three plants, in Germany and in Japan, in which n-butens and mixed butens were oxidized to maleic anhydride over V_2O_5/P_2O_5 catalyst, with selectivity of about 50-60 mol%.

A similar kinetic landscape (at a lower temperature) may be modified by catalyst containing vanadium pentoxide, along with a variety of other oxides (titanium, zinc, aluminium or antimony oxides). At 200-320 °C it is possible to control the oxidation of n-butens in this way:

$$\begin{matrix} CH_2{=}CH{-}CH_2{-}CH_3 \\ \\ CH_3{-}CH{=}CH{-}CH_3 \end{matrix} \quad \downarrow\uparrow \quad + 2\ O_2 \rightarrow 2\ CH_3COOH$$

If we now write three overall oxidation reactions of butenes in the simplest stoichiometric way, we see at a glance the permanent identity of reagents and the enormous difference of products in the making of maleic anhydride, the production of acetic acid, and the simple combustion:

$$C_4H_8 + 3\ O2 \rightarrow C_4H_2O_3 + 3\ H_2O$$
$$C_4H_8 + 2\ O2 \rightarrow 2\ C_2H_4O_2$$
$$C_4H_8 + 6\ O2 \rightarrow 4\ CO_2 + 4\ H_2O$$

Returning now to the industrial process for obtaining maleic anhydride, the feedstock was the C_4 product from a steam cracker, and it consisted essentially of butenes and butadiene, plus smaller amounts of butanes. Under optimum operating conditions butanes remained unreacted, isobutene burnt to carbon oxides and water, and the n-butenes and butadiene were converted to maleic anhydride. I conclude this point stressing that the C_4 components followed three very different paths: unreacted, completely oxidized, and partially oxidized (in the wanted measure and structural position).

The preceding case demonstrates that chemists are very able to modify the 'natural' kinetic landscapes, and that, as the actual terrestrial landscapes, the kinetic landscapes are very sensitive to change.

Self-catalysis

In 1910 Alfred Lotka sent two very similar articles to the *American Journal of Physical Chemistry* and to the German *Zeitschrift für physikalische Chemie*. The titles of the articles referred to a "theory of periodic reactions", and Lotka demonstrated that oscillating reactions happen when in a set of four reactions one of them produces an intermediate compound which acts self-catalytically on its own formation. Lotka's papers are nearly a century old, and the same time unit can be used for the seminal contribution of Turing, which was published more than half a century ago. It is well known that Alan Turing opened a new research field in 1952, when he published on the *Philosophical Transactions* an essay on "The chemical basis of morphogenesis". Turing was able to predict the spontaneous formation of spatial patterns because in addition to auto-catalytic reactions he considered the diffusion of the reactive species, and in particular different diffusion rates for different species. Turing's essay is very interesting not only for the scientific content, but also for the author's communicative intentions, who tries to explain to the reader the required notions of chemistry and biology. Turing's paper is a very rare and brave example of advanced science blended with popularization; Turing was rightly thinking that the mathematicians who could appreciate the mathematical content were not able to understand the chemical features of the system and its biological consequences.

In spite of Turing's efforts, in the next two decades the study of reaction-diffusion systems was neglected, both at the theoretical level and in laboratory. The most famous case of this delayed interest is that of the reaction discovered by Boris Belousov. Belousov discovered his oscillating reaction before the publication of Turing's paper, but Belusov's attempts of publishing a paper on the reaction were always unsuccessful. The situation of stalemate lasted until Anatol Zhabotinsky, a soviet biophysicist, published his first paper on *Biofizika* in 1964. Eventually a scientific community surfaced at a meeting of the Federation of European Biochemical Societies, held in Prague in 1968 (20). In effect, there was a serious epistemological obstacle to the reception of the same problem of the oscillating reactions. In fact many chemists thought that the spontaneous formation of temporal and space patterns was forbidden by the second law of thermodynamics. This obstacle was dismantled by the work of Ilya Prigogine and his collaborators.

Prigogine's contribution to the understanding of complex chemical system was fundamental for two reasons. The first reason is strictly scientific: a continuous flow of papers and books conveyed the scientific community important, new ideas and proposals (e.g. the dissipative structures). The second reason is more personal, and in a sense sociological. Prigogine's strong personality helped the diffusion of interest in the thermodynamics of irreversible processes not less than the scientific contributions. The enhanced efficacy of the strong couple, science +

personality (21), was demonstrated by the heated debate on the chemical and physical legitimacy of the Brusselator model.

The so-called Brusselator is a model for a reaction-diffusion system which employs the following reactions:

$$A \leftrightarrow X$$
$$B + X \leftrightarrow Y + D$$
$$2X + Y \leftrightarrow 3Y$$
$$X \leftrightarrow E$$

A and B are the reagents, D and E are the end products; X and Y are intermediate compounds. The model was proposed by Prigogine and Lefever in 1968, and it was the first one of this type which was chemically plausible. The model was further elaborated by Prigogine and Glansdorff in 1971 (22), and eventually it was dubbed *Brussellator* by J.J. Tyson in 1973. In the 1980s Prigogine's proposal was attacked by other researchers, especially on an alleged unreality of the termolecular reaction:

$$2X + Y \leftrightarrow 3Y$$

These attacks urged a lively defence, which was published on the *Faraday Transactions* by Prigogine's collaborators. Lefever, Nicolis and Borckmas waved a self-absolving and disengaging banner: "The Brusselator: It does Oscillate all the same". In the paper conclusion (five lines) they wrote: "The doubts and criticisms which have been expressed concerning the physicochemical soundness of the Brusselator model and its use as a prototype for the study of chemical oscillations are completely ill-founded" (23).

Self-chemistries and other self-somethings

In 1990 a group led by Julius Rebek synthesized a molecule called amino adenosine triacid ester (AATE), which itself consists of two components, pentafluorophenyl ester and amino adenosine. When AATE molecules are dissolved in chloroform with the two components, the AATE molecules act as templates for the two components to join up and form new AATE molecules. Thermal motion of the solution then separates the original molecule from the copy. Under ideal conditions, AATE can reproduce itself 1,000,000 times in one second (24). It was the beginning of a promising line of research; an extremely interesting result of this line was published on *Nature* in 2001, under the title "A chiroselective peptide replicator". The researchers led by Reza Ghadiri explains the aim of their investigation: "Given that molecular self-replication and the capacity for selection are necessary conditions for the emergence of life, chiroselective replication of biopolymers seems a particularly attractive process for explaining homochirality in nature". In the paper they report that a 32-residue peptide replicator is capable of efficiently amplifying homochiral products from a racemic mixture of peptide fragments through a chiroselective autocatalytic cycle (25). In a statement released to the NASA Astrobiology Institute Ghadiri affirms that the result is astonishing, "Based on [our] understanding, polypeptides can self-replicate, form complex networks, error correct, form mutual systems, they have all sorts of emergent properties, and they can now do homochiral amplification" (26). It is noteworthy that the *in vitro* research on replicating and evolving molecular systems is flanked by an *in silico* research on artificial chemistries.

Self-reproduction of molecules is a case of the self-organizing phenomena, now under scrutiny in many laboratories. On a more general ground, self-organization refers to spontaneous ordering tendencies observed in certain classes of complex systems, both artificial

and natural. Actual examples in nature and in laboratory range from dust devils and hurricanes to certain sorts of chemical and biological systems, such as Benard cells and chemical oscillators. The topic of self-organization has also been explored also under other rubrics, such as 'emergent structuring', 'self-assembly', 'autocatalysis', and 'autopoiesis'. The scientific discourse on the origin of life is dominated by reflexive prefixes: *auto*- or *self*-catalysis, *self*-assembly, *self*-reproduction, *self*-organisation, and this kind of prefixes are philosophically interesting.

Looking for a self

'Self' is a mysterious philosophical word, but, in our context, the *self*- prefix has essentially a pragmatic meaning. Scientists of many denominations give a 'self' to systems in the form of a well controlled content of information, and in the right conditions these systems exhibit a complex "informed dynamics". Jean-Marie Lehn worked out this concept in many details in the context of suprachemistry. Molecular chemistry has developed a wide range of very powerful procedures for constructing ever more sophisticated molecules from atoms linked by covalent bonds. Beyond molecular chemistry lies supramolecular chemistry, which aims at developing highly complex chemical systems from components interacting via non-covalent intermolecular forces. By the appropriate manipulation of these interactions, supramolecular chemistry became the chemistry of molecular information, involving the storage of information at the molecular level, in the structural features, and its retrieval, transfer, and processing at the supramolecular level, through molecular recognition processes operating via specific interactions. In his words: "Supramolecular chemistry has paved the way toward apprehending chemistry as an information science through the implementation of the concept of molecular information with the aim of gaining progressive control over the spatial (structural) and temporal (dynamic) features of matter and over its complexification through self-organization, the drive to life" (27).

We can now leave this kind of micro-self and go to consider a possible macro-self.

Gaia, at last

James Lovelock, a physical chemist, stated the Gaia hypothesis in 1972, in the journal *Atmospheric Environment*. Shortly after this beginning Lovelock began collaboration with the biologist Lynn Margulis that has continued to this day. The first statement of the hypothesis was: "Life regulates the climate and the chemical composition of the atmosphere at an optimum for itself". After two decades, Lovelock complemented this statement in a very interesting way: In a paper presented in Tokyo in 1992 Lovelock affirms: "The whole system of life and its material environment is self-regulating at a state comfortable for the organisms". In the same paper Lovelock copes with the criticism that he and Margulis had proposed a sentient Gaia, able to control the Earth consciously. Lovelock's answer is adamant: "Nothing was further from our minds. From the start, Gaia has been a top-down systems view of the Earth, the hard science view of a physical chemist with an interest in control theory. This was never some trendy new age pseudo-science" (28).

It is noteworthy that this defence of the scientific nature of Gaia was delivered when the Gaia hypothesis had fully entered in the debates of the scientific community. In 1988 the American Geophysical Union had held its annual Chapman Conference with a clear title: "Scientists on Gaia" (29). Anyway, also now, the scientific discourse on Gaia is very cautious when it faces the question of a definition of Gaia itself. CSA (Cambridge Scientific Abstracts) is

a privately-owned information company located in Bethesda, Maryland. In November 2003 CSA proposed in its "Hot Topics Series" the theme of the dimethylsulphide (DMS) emission, and in the attached glossary the editor gave this definition: "Gaia hypothesis: Earth homeostasis is maintained by active feedback processes operated automatically and unconsciously by the biota" (30). The word |unconsciously| recalls us an old Latin saying which states: *Excusatio non petita accusatio manifesta*.

Also for us the DMS problem is important, but before treating it we can test the epistemological status of Gaia consulting the Google oracle. For the query "Gaia hypothesis" Google signals 18.220 pages, and for the query "Gaia theory" the pages are only 8590. Google's verdict seems clear, but the proportion between hypothesis and theory is reversed if we pass from English to German and Dutch: "Gaia Hypothese" gets 875 pages and "Gaia Theorie" collects 1790 pages. The epistemological status of Gaia remains uncertain.

A tale of seas and clouds

In 1987 Nature published an article whose title contained a really weird adjective: *geophysiological*. The four authors discussed the possible impact of the production of DMS by marine phytoplankton on the global climate. It was known that DMS was an important sulphur-containing atmospheric trace gas of marine biogenic origin, but the authors went far beyond this point. They pointed out that DMS emitted from the oceans might be a precursor of tropospheric aerosols and cloud condensation nuclei, thereby affecting the Earth's radiative balance and possibly constituting a negative feedback to global warming. In this context it was particularly relevant the enhanced albedos of marine stratus and altostratus clouds (31). The names of the authors were Charlson, Lovelock, Andreae, and Warren, and in short time the hypothesis of this kind of geophysiological feedback was dubbed 'the CLAW hypothesis'.

DMS is important *per se* for the global sulphur cycle, because it represents 95% of the natural marine flux of sulphur gases to the atmosphere, and scientists estimate that the flux of marine DMS supplies about 50% of the global biogenic source of sulphur to the atmosphere. This great and various interest in DMS and its fate explains why, in the decade following the initial description, the CLAW hypothesis was the subject of over 700 scientific papers describing the biogeochemistry of DMS, its precursors, and their connection to earth's climate.

The CLAW hypothesis is still somewhat controversial (32), however it is relevant in a research on complexity in chemistry because a multi-step negative feedback phenomenon, such as that envisioned in the CLAW hypothesis, probably cannot be adequately evaluated in the laboratory; it must be done *in situ*. Biochemical researches on the phytoplankton metabolism, and physico-chemical researches on the conversion of DMS to sulphate and methanesulphonic acid, must be complemented by difficult analytical investigation in and on oceans. The whole of chemistry is pertinent to confirm or disprove the CLAW hypothesis.

Crossing the disciplinary borders

The importance of the Gaia theory goes vastly beyond its scientific meaning and not only for the view of Earth as a super-organism (see later discussion) but also for its sociological impact on the organisation of science. The same theory is conceivable only and uniquely in a multidisciplinary context. In this sense, it is exemplary the case of the researches on the dimethylsulphide impact on the global climate. The four authors of the CLAW hypothesis had the following scientific training: Charlson was a chemist, working in the field of atmospheric chemistry; Lovelock was a chemist turned in a physical chemist; Andreae had studied earth

sciences and was an oceanographer; Warren was a meteorologist, specialised in the study of cloud albedo. An interaction scheme emerges from their professional qualification: atmosphere (Charlson), ocean (Andreae) and clouds (Warren) were connected by the syncretistic way of thought of a physical chemist. Also the collaboration between Lovelock and Margulis was so fertile because their scientific background was extremely different: the *trait d'union* was a holistic point of view.

What is life?

In 1944 Erwin Schrödinger published a booklet which in the following decades became one of the most famous works of the last century. The title of the booklet was *What is life?* and since then, despite the gigantic progress of biology, the question mark has not been removed. Half a century after Schrödinger's contribution, for its research in exobiology NASA gave a clean-cut answer to the question and chose the definition proposed by Gerald Joyce. Since 1994 and in several occasions, Joyce, a biochemist, maintained that life is "a self-sustained chemical system capable of undergoing Darwinian evolution". The essential points of the definition are three: life is understood as the activity of a chemical system; the system sustains itself without external intervention, i.e. the process is thermodynamically spontaneous; the system undergoes Darwinian evolution, so it not only self-replicates but reproduces itself with the possibility of errors and competes with other systems.

Given the scientific and technological role of NASA, Joyce's definition has been debated at length. For example it is maintained that NASA's working definition of life is far from ideal, just in the field of exobiology. It risks excluding some novel life forms that could exist, such as ones that replicate so haphazardly that natural selection is not an option. A promising answer to this objection is that evolution without reproduction could be possible.

More legal, ethical and epistemological questions

For me it was a great surprise when I 'discovered' that there was a strong legal basis for the view of our planet as a living being. The Convention on Biological Diversity is a legally binding agreement opened for signature at the Earth Summit in Rio de Janeiro in 1992. By 2002, the Convention had been signed by 175 countries. As such, the Convention has more member countries than the World Trade Organization. The Convention's objectives are: the conservation of biological diversity (for short: biodiversity); the sustainable use of biodiversity's components; and the equitable sharing of benefits derived from genetic resources. (In my opinion the three objectives are in order of increasing difficulty). The Convention defines biodiversity as "the variability among living organisms from all sources, including, *inter alia*, terrestrial, marine and other aquatic ecosystems and the ecological complexes of which they are part: this includes diversity within species, between species and of ecosystems" (33). Before commenting this definition, I quote three other important points. The Convention recognizes "the importance of biological diversity for [...] maintaining life sustaining systems of the biosphere". It acknowledges that "conservation and sustainable use of biological diversity is of critical importance for meeting the food, health and other needs of the growing world population". The Convention affirms that biodiversity has intrinsic value, and that biodiversity and its components have "ecological, genetic, social, economic, scientific, educational, cultural, recreational and aesthetic values". This last point is of an evident ethical import, and it will be recalled later.

I read the text of the Convention for the first time in Italian. As a historian I am very suspicious about the real syntactic and semantic meanings conveyed by a translation, so I looked at the original English text. My question was about the inclusion of the ecosystems among the living organisms, and in a kind of word game I collected the definition of biodiversity also in German, French and Spanish. The German translation was particularly rewarding, because without fear of redundancy it confirms *die Vielfalt der Ökosysteme* (see Table 2).

Table 2. The definition of biological diversity (Convention on Biological Diversity, Rio de Janeiro, 1992)

Language	Texts from "Article 2. Use of Terms"
English	"Biological diversity" means the variability among living organisms from all sources including, inter alia, terrestrial, marine and other aquatic ecosystems and the ecological complexes of which they are part; this includes diversity within species, between species and of ecosystems".
German	"Im Sinne dieses Übereinkommens [...] bedeutet "biologische Vielfalt" die Variabilität unter lebenden Organismen jeglicher Herkunft, darunter unter anderem Land-, Meeres- und sonstige aquatische Ökosysteme und die ökologischen Komplexe, zu denen sie gehören; dies umfaßt die Vielfalt innerhalb der Arten und zwischen den Arten und die Vielfalt der Ökosysteme".
Italian	"Per «diversità biologica» si intende la variabilità tra gli organismi viventi di ogni origine, compresi tra gli altri, gli ecosistemi terrestri, marini e gli altri ecosistemi acquatici, ed i complessi ecologici di cui fanno parte; ciò include la diversità nell'abito di ciascuna specie, e tra le specie degli ecosistemi".
French	"Diversité biologique: Variabilité des organismes vivants de toute origine y compris, entre autres, les écosystèmes terrestres, marins et autres écosystèmes aquatiques et les complexes écologiques dont ils font partie; cela comprend la diversité au sein des espèces et entre espèces ainsi que celle des écosystèmes".
Spanish	"Por diversidad biológica se entiende la variabilidad de organismos vivos de cualquier fuente, incluídos, entre otras cosas, los ecosistemas terrestres y marinos y otros ecosistemas acuáticos y los complejos ecológicos de los que forman parte; comprende la diversidad dentro de cada specie, entre las especies y los ecosistemas".

The specific legal consequences of the definition of an ecosystem as a living organism are not relevant in our discussion, while the ethical and epistemological consequences are really relevant. The Convention affirms that the components of biodiversity have not less than nine different kinds of values: ecological, genetic, social, economic, scientific, educational, cultural, recreational and aesthetic values. If the word |value| has an ethical meaning (and it *has*), biodiversity and its components have a tenth kind of value, that is an ethical value. When we enter in a solitary alpine valley, walking on an old mule track, we feel an intense 'contact with nature': possibly we find ourselves in company with a quiet, great and out of the ordinary being. The 'respect for nature' has its root in the respect for living organisms.

The epistemological consequences of the view of ecosystems as living organisms are challenging. If we drop from Joyce's definition of life the word |Darwinian| we get the simplest description of an ecosystem: "a self-sustained chemical system capable of undergoing evolution". A Darwinian evolution entails selection, and to its turn selection entails many individuals and their participation to the lottery of reproduction. In this biological and usual sense, no single ecosystem may evolve following a Darwinian scheme. However, it is evident that in our world reality ecosystems evolve, reacting to the climate change or to the human intervention. Perhaps, it is possible a non-Darwinian evolution.

A second consequence of the equation ecosystem = living being is that life is no more bound to reproduction. This is an epistemological conclusion of paramount importance. Personally, I think that Gaia is a kind of living super-organism, which was born and will die, but which in the past/present conditions cannot reproduce. Life without reproduction is an interesting scientific and philosophical issue.

Conclusions

The inherent complexity of chemistry is not intractable. In the preceding pages we saw that the use of catalysis is a powerful means for the control of reactions, and auto- or self-catalysis promises to be a powerful means as well. For sake of brevity I did not discuss the new horizon opened by suprachemistry, but this is the moment of mentioning the exiting constructive ability gained in the field of nano-machines. While catalysis controls/selects the reaction pathways, suprachemistry endeavours to control/construct both the pathways and the information content of the synthesised molecules. The molecular information content becomes peculiarly evident just in the nano-machines as those constructed by the research groups of Balzani and Stoddart, because these nano-machines respond with molecular movements and/or light signal to an external stimulation (light signal or chemical signal) (34).

Despite of the immense progress of the last two decades, the inherent complexity is posing new formidable problems to chemists. In fact the most difficult challenges come from fields where chemistry has to work with other disciplines, and not longer side by side on the same problem, but inside the same problem. The superconductive ceramics are a model problem, but chemistry is in the same situation in several other fields of study, from the leading nano-technologies, through the main-stream material science, to more exotic specialities as the Turing patterns. The inherent complexity of chemistry remains inherent, because we cannot change the nature of molecules, substances and reactions. However, chemists are now obliged to become less elusive, and to open their way of thinking to other scientists; put briefly, the inherent complexity of chemistry is no longer a love-affair of lonely chemists.

Notes and references

1. Dupré J. The disorder of things. Metaphysical foundations of the disunity of science. Cambridge: Harvard UP; 1996.
2. Cerruti L. Procedure conoscitive e culture disciplinari. Un'analisi storiografica. Quaderni della Rivista di Storia della Scienza 1992; 2: 83-122.
3. As an Italian (and as a chemist) I was impressed when I 'discovered' that in English the word |chemistry| may be defined as "reaction between two people: the spontaneous reaction of individuals to each other, especially a mutual sense of attraction or understanding"; on line at the URL: http://encarta.msn.com/dictionary_/chemistry.html.
4. Horgan J. From complexity to perplexity. Scientific American 1995;6:74-9.
5. Rosen R. Anticipatory systems. Oxford: Pergamon Press; 1985.
6. Cerruti L. Il riduzionismo. Prospettiva storica e problemi attuali. In: Cerruti L, Mostacci E, Treves S, Turcxo F (Ed.). Atti del XII Congresso della Divisione di Didattica Chimica. Pisa: CNR; 2003. p. 5-30.
7. Del Re G. Ontological status of molecular structure. HYLE - An International Journal for the Philosophy of Chemistry 1998;2(4):81-103.

8. Lewin R. Complexity. Life on the edge of chaos. London: Phoenix; 1997.
9. Bertz SH. The first general index of molecular complexity. J Am Chem Soc 1980;103:3599-601.
10. Randić M, Plavšić D. On the concept of molecular complexity. Croatica Chemica Acta 2002;75:107-16.
11. Milano Chemometrics and QSAR Research Group. Dragon: application for the calculation of molecular descriptors. Milan: University of Milan (updated 20 January 2004, cited 12 September 2004). Available from: http://www.disat.unimib.it/chm/Dragon.htm.
12. Todeschini R, Consonni V, Handbook of Molecular Descriptors. Methods and Principles in Medicinal Chemistry, Weinheim: Wiley-VCH; 2000. The size of the research field is given by the more than 3300 bibliographic references of the handbook.
13. Searching Properties in the CAS Registry File; this page was on line on February 8, 2004, URL: http://www.cas.org/ONLINE/STN/STNOTES/stnote27.html. Also a serious, almost official site changes the page content without changing the address; the sentences I quote in my paper are no more on line.
14. Dasent WE. Inorganic energetic. London: Penguin Books; 1970.
15. IUPAC Subcommittee on Solubility and Equilibrium Data, Introduction to the Solubility Data Series. Solubility of Solids in Liquids, URL: http://www.unileoben.ac.at/~eschedor/sl-intro.html.
16. Cerruti L. Bella e potente. La chimica del Novecento fra scienza e società, Roma: Editori Riuniti; 2003; chapter 12 is on the supersession of classical chemistry.
17. The research field of the philosophy of catalysis was opened many years ago by Alwin Mittasch, a German scientist, technician and philosopher: Mittasch A, Katalyse und Determinismus: ein Beitrag zur Philosophie der Chemie, Berlin: Springer;1937. The field was almost completely neglected until recent years: van Brakel J, On the Neglect of the Philosophy of Chemistry, Foundations of Chemistry, 1999; 1(2):111-174. I gave a contribution to the field in: Cerruti L, Historical and Philosophical Remarks on Ziegler-Natta Catalysts: A Discourse on Industrial Catalysis. HYLE - An International Journal for the Philosophy of Chemistry, 1999;5(1):3-41.
18. Cerruti L. Chemicals as instruments. A language game. HYLE - An International Journal for the Philosophy of Chemistry 1998;4(1):39-61.
19. The phrase 'energy landscape' is widely used in assorted fields as protein folding, the glass transition, and fracture dynamics in solids, where the topography of the multidimensional potential energy landscape is receiving much attention as a useful object of study for understanding complex behaviour in condensed-phase systems.
20. Chance B, Pye EK, Ghosh AK, Hess B (Ed.). Biological and biochemical oscillators. New York: Academic Press; 1973.
21. In his obituary of Prigogine Albert Goldbeter speaks of a "radiating personality"; Goldbeter A, Ilya Prigogine (1917-2003). J Biosci 2003;28(6):657-9.
22. Glansdorff P, Prigogine I. Structure, stabilite et fluctuations. Paris: Masson; 1971.
23. Lefevre R, Nicolis G, Borckmas P. The Brusselator: it does oscillate all the same. J Chem Soc Faraday Trans 1988;84 I (4):1013-23.
24. Tjivikua T, Ballester P, Rebek, J Jr. A self-replicating system. J Am Chem Soc 1990;112:1249-50.
25. Saghatelian A, Yokobayashi Y, Soltani K, Ghadiri MR, A chiroselective peptide replicator. Nature 2001;409:797-801.
26. NASA Astrobiology Institute. Pasadena, CAL, USA; (updated December 26, 2001; cited September 12, 2004). Availble from: http://nai.arc.nasa.gov/news_stories/news_detail.cfm?ID=75.
27. Lehn J-M. Supramolecular chemistry: from molecular information towards self-organization and complex matter. Rep Prog Phys 2004;67:249-65.

28. Lovelock J. The evolving Gaia theory. Tokyo: United Nations University Press; 1992. Last visited: September 12, 2004. Available from: http://www.unu.edu/unupress/lecture1.html.

29. Schneider SH, Boston PJ (Ed.), Scientists on Gaia, Cambridge, MA: MIT Press; 1991.

30. Cambridge Scientific Abstracts. Glossary. Cambridge: Cambridge University Press; 2003. Last visited: September 12, 2004.Available from: http://www.csa.com/hottopics/dimethyl/gloss.html.

31. Charlson RJ, Lovelock JE, Andreae MO, Warren SG, Oceanic phytoplankton, atmospheric sulphur, cloud albedo and climate: a geophysiological feedback, Nature, 1987;326:655-661.

32. Reaser JK, Pomerance R, Thomas PO. Coral bleaching and global climate change: scientific findings and policy recommendations. Conservation biology 2000;14:1500-11.

33. The English text of the Convention and the French translation are on line at the URL: http://www.agora21.org/cdb/index.html. Italian translation in: Postiglione A, Pavan A (Ed.), Etica ambiente sviluppo. La comunità internazionale per una nuova etica dell'ambiente, Napoli: Edizioni Scientifiche Italiane;2001;259-289. Spanish translation on line at the URL: http://www.colciencias.gov.co/simbiosis/pdfs/ley.pdf. German translation on line at the URL: http://www.biosicherheit.de/pdf/aktuell/CBD.pdf.

34. Balzani V, Credi F, Raymo M, Stoddart JF. Artificial molecular machines. Angew Chem Ind Ed 2000;39:3348-91.

Lecture

COMPLEXITY OF LIFE VIA COLLECTIVE MIND

Michail Zak
Jet Propulsion Laboratory, California Institute of Technology,Pasadena, CA, USA

Introduction

The concept of collective mind has appeared recently as a subject of intensive scientific discussions from economical, social, ecological, and computational viewpoints (1). It can be introduced as a set of simple units of intelligence (say, neurons, or interacting agents), which can communicate by exchange of information without an explicit global control. The objectives of the agents may be partly compatible and partly contradictory (i.e., they can cooperate or compete). The exchanging information may be at times inconsistent, often imperfect, non-deterministic and delayed. Nevertheless, observations of working insect colonies, social systems, and scientific communities suggest that such collectives of agents appear to be very successful in achieving global objectives, as well as in learning, memorizing, generalizing and predicting, due to their flexibility, adaptability to environmental changes, and creativity.

The objective of this paper is to introduce a dynamical formalism describing the evolution of the behavior of communicating agents. All the previous attempts to develop models for so called active systems (i.e., systems that possess certain degree of autonomy from the environment that allows them to perform motions that are not directly controlled from outside) have been based upon the principles of Newtonian and statistical mechanics (2). These models appear to be so general that they predict not only physical, but also some biological and economical, as well as social patterns of behavior exploiting such fundamental properties of nonlinear dynamics as attractors. Not withstanding indisputable successes of that approach (neural networks, distributed active systems, etc.) there is still a fundamental limitation that characterizes these models on a dynamical level of description, they propose no difference between a solar system, a swarm of insects, and a stock market. Such a phenomenological reductionism is incompatible with the first principle of progressive biological evolution (3, 4). According to this principle, the evolution of living systems is directed toward the highest levels of complexity if the complexity is measured by an irreducible number of different parts which interact in a well-regulated fashion (although in some particular cases deviations from this general tendency are possible). At the same time, the solutions to the models based upon dissipative Newtonian dynamics eventually approach attractors where the evolution stops (until a "master" reprograms the model). Therefore, such models fail to provide an autonomous progressive evolution of living systems (i.e. evolution leading to increase of complexity).

Let us now extend the dynamical picture to include thermal forces. That will correspond to the stochastic extension of Newtonian models, while the Liouville equation will extend to the so called Fokker-Planck equation that includes thermal force effects through the diffusion term. Actually, it is a well-established fact that evolution of life has a diffusion-based stochastic nature as a result of the multi-choice character of behavior of living systems. Such an extended thermodynamics –based approach is more relevant to model of living systems, and therefore, the simplest living species must obey the second law of thermodynamics as physical particles do. However, then the evolution of living systems (during periods of their isolation) will be

regressive since their entropy will increase (5). As pointed out by R. Gordon (6), a stochastic motion describing physical systems does not have a sense of direction, and therefore, it cannot describe a progressive evolution. As an escape from this paradox, Gordon proposed a concept of differentiating waves (represented by traveling waves of chemical concentration or mechanical deformation) which are asymmetric by their nature, and this asymmetry creates a sense of direction toward progressive evolution. Although the concept of differentiating waves itself seems convincing, it raises several questions to be answered: Who or what arranges the asymmetry of the differentiating waves in the "right" direction? How to incorporate their formalism into statistical mechanics providing progressive evolution without a violation of the second law of thermodynamics? Thus, although the stochastic extension of Newtonian models can be arranged in many different ways (for instance, via relaxation of the Lipcshitz conditions, (7), or by means of opening escape-routes from the attractors), the progressive evolution of living systems cannot be provided.

The limitations discussed above have been addressed in several publications in which the authors were seeking a "border line" between living and non-living systems. It is worth noticing that one of the "most obvious" distinctive properties of the living systems, namely, their intentionality, can be formally disqualified by simple counter-examples; indeed, any mechanical (non-living) system has an "objective" to minimize action (the Hamilton principle) as well as any isolated diffusion-based stochastic (non-living) system has an "objective" to maximize the entropy production ("The Jaynes Principle") (4). The departure from Newtonian models via introduction of dynamics with expectations and feedback from future has been proposed by B. Huberman and his associates; further departure which includes learning nested models of multi-agent systems was introduced by J. Vidal (8). However, despite the fact that the non-Newtonian nature of living systems in these works was captured correctly, there is no global analytical model which would unify the evolution of the agent's state variables and their probabilistic characteristics such as expectations, self-images, etc.

The objective of this paper is to extend the First Principles of classical physics to include phenomenological behavior on living systems, i.e. to develop a new mathematical formalism within the framework of classical dynamics that would allow one to capture the specific properties of natural or artificial living systems such as formation of the collective mind based upon abstract images of the selves and non-selves, exploitation of this collective mind for communications and predictions of future expected characteristics of evolution, as well as for making decisions and implementing the corresponding corrections if the expected scenario is different from the originally planned one. The approach is based upon our previous publications (9-11) which postulate that even a primitive living species possesses additional non-Newtonian properties which are not included in the laws of Newtonian or statistical mechanics. These properties follow from a privileged ability of living systems to possess a self-image (a concept introduced in psychology) and to interact with it. The mathematical formalism is based upon coupling the classical dynamical system (with random components caused by uncertainties in initial conditions as well as by the Langevin forces) representing the motor dynamics with the corresponding Fokker-Planck equation describing the evolution of these uncertainties in terms of the probability density and representing the mental dynamics. The coupling is implemented by the information-based supervising forces that can be associated with the self-awareness. These forces fundamentally change the pattern of the probability evolution, and therefore, leading to a major departure of the behavior of living systems from the patterns of both Newtonian and statistical mechanics. Further extension, analysis, interpretation, and application of this approach to the collective-mind-based communicating agents will be addressed in this paper. It should be stressed that the proposed model is supposed to capture the signature of life on the phenomenological level, i.e., based only upon the observable behavior, and therefore, it

will not include a bio-chemical machinery of metabolism. Such a limitation will not prevent one from using this model for developing artificial living systems as well as for studying some general properties of behavior of natural living systems. Although the proposed model is supposed to be applicable to both open and closed autonomous systems, the attention will be concentrated upon the latter since such properties of living systems as free will, prediction of future, decision making abilities, and especially, the phenomenology of mind, become more transparent there. It should be emphasized that the objective of the proposed approach is NOT to overperform alternative approaches to each PARTICULAR problem (such approaches not only exist, but they may be even more advanced and efficient), but rather to develop a GENERAL strategy (by extending the First Principles of physics) that would be the starting point for ANY particular problem. The impotence of the general strategy can be illustrated by the following example- puzzle: Suppose that a picture is broken into many small pieces that are being mixed up; in order to efficiently reconstruct this picture, one has to know how this picture should look; otherwise the problem becomes combinatorial, and practically, unsolvable. This puzzle is directly related to the Brain research.

Reflective chains: what do you think I think you think…?

We will start with the simplest model of two interacting agents assuming that each agent is represented by an inertionless classical point evolving in physical space. We will also assume that the next future position of each agent depends only upon its own present position and the present position of his opponent. Then their evolutionary model can be represented by the following system of differential equations:

$$\dot{x}_1 = f_1(x_1, x_2) \quad [1]$$

$$\dot{x}_2 = f_2(x_1, x_2) \quad [2]$$

Here $x_1$and x_2 are the state variables for the agent 1 and the agent 2, respectively.

We will start with the assumption that these agents belong to the same class, and therefore, they know the structure of the whole system [1], [2]. However, each of the agents may not know the initial condition of the other one, and therefore, he cannot calculate the current value of his opponent's state variable. As a result of that, the agents try to reconstruct these values using the images of their opponents. This process can be associated with the concept of reflection; in psychology reflection is defined as the ability of a person to create a self-nonself images and interact with them.

Let as turn first to the agent 1. In this view the system [1], [2] looks as following:

$$\dot{x}_{11} = f_1(x_{11}, x_{21}), \quad [3]$$

$$\dot{x}_{21} = f_2(x_{21}, x_{121}) \quad [4]$$

where x_{11} is the self-image of the agent 1, $x_{21}$is the agent's 1 image of the agent 2, and x_{121} is the agent's 1 image of the agent's 2 image of the agent 1.

This system is not closed since it includes an additional 3-index variable x_{121}. In order to find the corresponding equation for this variable, one has to rewrite equations [3], [4] in the 3-index form. But it is easily verifiable that such form will include 4-index variables, etc., i.e., this chain of equations will never be closed. By interchanging the indices 1 and 2 in equations [3] and [4], one arrives at the system describing the view of the agent 2. The situation can be generalized

from two- to n – dimensional systems. It is easy to calculate that the total number of equations for the m-th level of reflection, i.e., for the m-index variables, is

$$N_m = n^m. \quad [5]$$

Thus, the number of equations grows exponentially with the number of the levels of reflections, and it grows linearly with the dimensionality n of the original system. It should be noticed that for each m-th level of reflection, the corresponding system of equations always includes (m+1)-index variables, and therefore, it is always open. Hence, for any quantitative results, this system must be supplemented by a closure, i.e., by additional equations with respect to extra-variables. In order to illustrate how it can be done, let us first reduce equations [1] and [2] to the linear form

$$\dot{x}_1 = a_{11}x_1 + a_{12}x_2, \quad [6]$$

$$\dot{x}_2 = a_{21}x_1 + a_{22}x_2. \quad [7]$$

Taking the position of the agent 1, we can rewrite equation [6] in the form:

$$\dot{x}_1 = a_{11}x_i + a_{12}x_{21}. \quad [8]$$

In which the unknown agent's 2 state variable x_2 is replaced with its value x_{21} to be predicted by the agent 1. Recalling that the agents 1 and 2 belong to the same class, it is reasonable to assume that the agent 1 knows the expected initial value χ_2^0 as well as the initial variance σ_2^0 of the agent's 2 state variable x_2. Based upon that, the agent 1 can predict current values of the agent' 2 state variable as:

$$\begin{aligned} x_{21} &= \chi_2 + \sigma_2 L(t), \\ < L(t) > &= 0, \\ < L(t)L(t') > &= 2\delta(t - t') \end{aligned} \quad [9]$$

where L(t) is a Langevin force represented by a random function with zero mean and a correlation function, i.e. the random force has no bias, and its next values are totally independent upon all the previous values. According to this representation the variable x_{12} has the expected value χ_2 and the variance σ_2. In other words, the prediction consists of random guesses dispersed symmetrically around the expected value while the expected value x_2 as well as the variance σ_2 characterizing this dispersion are to be found. Substituting Equation [9] into Equation [8], one arrives at the following Langevin-type stochastic differential equation, (12)

$$\dot{x}_1 = a_{11}x_1 + a_{12}(\chi_2 + \sigma_2 L) \quad [10]$$

of the agent 1. Similar equation can be written for the agent 2

$$\dot{x}_2 = a_{21}(\chi_1 + \sigma_1 L) + a_{22}x_2. \quad [11]$$

However, from the viewpoint of the agent 1, the last equation may have two different forms

$$\dot{x}_2 = a_{21}x_1 + a_{22}(\chi_2 + \sigma_2 L) \quad [11a]$$

or

$$\dot{x}_2 = a_{21}(\chi_1 + \sigma_1 L) + a_{22}(\chi_2 + \sigma_2 L) \quad [11b]$$

Equation [11a] expresses that the agent 1 assumes that the agent 2 knows the state variable of his opponent (or partner), i.e., x_1. On the contrary, equation [11b] expresses that the agent 1

assumes that the agent 2 does not know the opponent's (or partner) variable and predicts it in the same way in which the agent 1 does. From the viewpoint of the reflection levels, the system [10], [11] is on the first level since each agent uses only the image of his opponent while the systems [10], [11a] and [10], [11b] are on the second level since each agent, in addition, uses the image of the image of the opponent (partner) of itself and his opponent (partner). In order to make our point in the simplest way, we will stay with the first level of reflection, i.e., with the system [10], [11].

Formally these equations are not coupled (unlike their original versions [6], [7]). However, as will be shown below, they are coupled indirectly, via the variables $\chi_1,\chi_2,\sigma_1,\sigma_2$. Indeed, since [6] and [7] can be considered as the Langevin-type stochastic differential equations, the evolution of these variables is governed by the corresponding Fokker-Planck equation (12)

$$\frac{\partial p}{\partial t}+\frac{\partial}{\partial X_1}[(a_{11}X_1+a_{12}\chi_2)p]+\frac{\partial}{\partial X_2}[(a_{21}\chi_1+a_{22}X_2)p]= \\ =(a_{12}^2\sigma_2^2\frac{\partial^2}{\partial X_1^2}+a_{21}^2\sigma_1^2\frac{\partial^2}{\partial X_2^2})p \qquad [12]$$

Here $p(t,X_1,X_2)$ is the joint probability density of distribution of the state variables x_1 and x_2 over the space coordinates X_1 and X_2. Equation [12] describes the evolution of the initial probability density as a result of action of the random forces L(t). This equation must be complemented by the normalization condition

$$\int_{-\infty}^{\infty}\int_{-\infty}^{\infty} pdX_1dX_2=1 \qquad [13]$$

as well as by the definitions of $\chi$and σ

$$\chi_i=\int_{-\infty}^{\infty}\int_{-\infty}^{\infty} X_i\,p\,(t,X_1,X_2)\,dX_1dX_2, \qquad i=1,2. \qquad [14]$$

$$\sigma_i=\int_{-\infty}^{\infty}\int_{-\infty}^{\infty}(X_i-\chi_i)^2\,p\,(t,X_1,X_2)\,dX_1dX_2, \qquad i=1,2. \qquad [15]$$

The system [12]-[15] is closed, and it can be solved subject to the initial and boundary conditions

$$p(0,X_1,X_2,)=p^0(X_1,X_2) \qquad [16]$$

$$p(t,\pm\infty,\pm\infty)=0, \\ \frac{\partial p}{\partial X_i}(t,\pm\infty,\pm\infty)=0, \quad i=1,2 \qquad [17]$$

Substituting [14] and [15] (as the known functions of time found from the solution of this system) into equations [10] and [11], one obtains the solutions for the state variables.

$$x_i=\exp(a_{ii}t)[\int_0^t a_{ij}(\chi_j+\sigma_j L)dt+x_i^0], \\ where\ i,j=1,2;\ i\neq j. \qquad [18]$$

Here x_i^0 is the initial value of the corresponding state variable.

It should be noticed that the solutions [18] are random because of the randomness of the Langevin forces L. That is why for qualitative analysis it is more convenient to stay with the statistical invariants of these solutions i.e., with the means χ_i the variances σ_I expressed by Equations [14] and [15], respectively.

It should be noticed that the same strategy of the solution can be applied to the models describing the second level of reflection, i.e., Equations [10], [11a] or [10][11b] with the only difference that these equations express only the view of the agent 1. After interchanging the indexes 1 and 2 in these equations, one arrives at the similar system expressing the view of the agent 2. Then each agent is supposed to create the image of the model of his opponent (partner), etc.

Dialog as evolutionary game with incomplete information

In this section we will apply the model of two interacting agents presented by equations [10]-[17] to the evolutionary games. The model is intentionally trivialized to make the interaction between the agents easily tractable; at the same time, this model still preserves the distinguished properties of the proposed approach. The general model with many other applications has been discussed in ref. (13). A game here is understood as a special type of an interaction between two agents, which follow certain rules and expecting a certain outcome. A game is evolutionary if the interacting agents change their internal states in order to be successful in the future. Turning to equations [10] and [11], one can see that this model of interacting agents satisfies both of these definitions. Indeed, the state variable x_I can be associated with internal representations of the agents. The right-hand parts of equations [10] and [11] can be considered as the statements made by each of the agent, respectively. Each of those statements depends upon the both state variables as the reactions to the corresponding statements. The left-hand parts of equations [10] and [11] express the changes of the state variables. From these changes the agents calculate the next statements, and that changes the internal states of the agents. It should be noticed that the representations as well as the statements are arbitrary with respect to what one wants to present. In other words, the model captures the grammar without a semantic. It should be recalled that games could be adversary or cooperative. In this section we will deal only with the cooperative games; in particular, the outcome of the game will be to approach the common ground (or mutual belief, or sheared conception) regardless of the initial conditions. Obviously, if the system [10], [11] is stable, i.e., if

$$a_{11} + a_{22} < 0, \qquad a_{11}a_{22} > a_{12}a_{21}, \qquad [19]$$

any initial conditions x_i^0 (i = 1, 2) will lead to the common ground i.e., to the zero solution, under the condition that each agent has a complete information not only about the values of his own state variable, but about the values of the state variable of another agent as well. However, in case of language communications, the information is never complete: it could always be interpreted in many different ways, unless the sender and the receiver have some "expected" mutual belief following from previous knowledge about each other backgrounds, or about the context of the forthcoming dialog. Hence, it would be reasonable to assume that although each agent does not know the values of the state variable of his partner, he, nevertheless, can come up with some random guesses that are characterized by known statistical invariants such as the mean χ and the variance σ. Turning to equation [9], one can recognize that this is exactly the same representation we just mentioned. As shown in the last section, actually it is sufficient for the agent to know only the initial values of these invariants since then their current values are

uniquely determined by the corresponding Fokker-Planck equation [12]. Thus, we have to return to equations [12]-[17] in order to find these invariants. We will demonstrate that for a simple system such as equations [10], [11], one does not need to find the solution to equation [12] subject to the conditions [13]-[17]; instead, the direct equations with respect to the statistical invariants χ and σ can be derived from Equation [12]. Indeed, let us multiply equation [12] by X_i (i = 1, 2) and integrate over the whole space. Then, taking into account the conditions [13] and [17], one obtains the following system of ordinary differential equations with respect to the expected values of the state variables.

$$\dot{\chi}_1 = a_{11}\chi_1 + a_{12}\chi_2, \quad [20]$$

$$\dot{\chi}_2 = a_{21}\chi_1 + a_{22}\chi_2. \quad [21]$$

Obviously the systems [20], [21] and [6], [7] are identical, i.e., the evolution of the state variables (with complete information) and their expectations is described by the same model. (Such a coincidence results from the linearity of the original mode). But it should be noticed that the stability of expectations does not guarantee the stability of the system [10], [11], i.e., the stability of the state variables with incomplete information. Indeed, let us turn to the solution [18] of equations [10] and [11]. Obviously this solution is unstable if $a_{11}>0$ or $a_{22}>0$, regardless of the expectations and variances as functions of time, and even if the first inequality in [19] is satisfied. Therefore, in order to provide the stability of evolution of the state variables with incomplete information, the expectations must be "more stable," i.e., (as it follows from the standard theorems of linear stability theory) the inequalities are to be stronger than [19]

$$a_{11} < 0,\ a_{22} < 0, a_{11}a_{22} > a_{12}a_{21} \quad [22]$$

In our further analysis we will assume that the conditions [22] hold. However, one should notice that these conditions are only necessary, but not yet sufficient for the stability of equations [10] and [11]. In order to derive the sufficient conditions, one has to analyze the evolution of the variances. For that purpose, let us multiply equation [12] by X_i^2 (i =1, 2), and integrate it over the whole space. After transformations similar to those performed above for expectations, one arrives at a system of ODE that is nonlinear with respect to variances and is coupled with equations [20], [21]. For better observability, we will simplify this system by assuming that

$$\chi_1^{\,0} = 0, \chi_2^{\,0} = 0 \quad [23]$$

Then the governing equations for the variances can be written in the following form

$$\dot{\sigma}_1^{\,2} = 2a_{11}\sigma_1^{\,2} + 2a_{12}^{\,2}\sigma_1^{\,2}\sigma_2^{\,2} \quad [24]$$

$$\dot{\sigma}_2^{\,2} = 2a_{22}\sigma_2^{\,2} + 2a_{21}^{\,2}\sigma_2^{\,2}\sigma_1^{\,2} \quad [25]$$

Although this system is still nonlinear, its stability analysis is simple. Indeed, since it has one attractor

$$\sigma_1 = 0, \quad \sigma_2 = 0 \quad [26]$$

and one repeller

$$\sigma_1^{\,2} = -\frac{a_{22}}{a_{21}^{\,2}}, \quad \sigma_1^{\,2} = -\frac{a_{11}}{a_{12}^{\,2}} \quad [27]$$

the stability will be provided if the initial variances are inside the basin of attraction, i.e., if

$$(\sigma_1^{\,0})^2 < -\frac{a_{22}}{a_{21}^{\,2}}, \qquad (\sigma_2^{\,0})^2 < -\frac{a_{11}}{a_{12}^{\,2}} \qquad [28]$$

Thus, the inequalities [22] and [28] are necessary and sufficient for the stability of the system [10], [11] in the simplified case [23]. As follows from [28], the incompleteness of the information measured by the initial variances $\sigma_1^{\,0}$ and $\sigma_2^{\,0}$ is directly responsible for the divergence of the dialog. At the same time, the stability of the original model [6], [7] represented by the conditions [22], increases the allowed degree of the incompleteness that would still preserve the convergence of the dialog.

In conclusion of this section, we will make several remarks. First we will analyze the effect of noise upon the stability of the dialog. For that purpose, we will add additional Langevin forces to equations [6] and [7]:

$$\dot{x}_1 = a_{11}x_1 + a_{12}x_2 + b_1^{\,2}\Gamma_1(t) \qquad [29]$$

$$\dot{x}_2 = a_{21}x_1 + a_{22}x_2 + b_2^{\,2}\Gamma_2(t) \qquad [30]$$

Here $\Gamma_1(t)$ and $\Gamma_2(t)$ are random functions with zero means and with correlation functions equal to a δ-function, and the constants $b_1^{\,2}$, $b_2^{\,2}$ represent the strengths of the noise interference for the agent 1 and 2 respectively. After the transformations similar to those performed above, one arrives at the following stability conditions:

$$(\sigma_1^{\,0})^2 < -\frac{a_{22}}{a_{21}^{\,2}} + \frac{b_1^{\,2}}{a_{21}^{\,2}}, (\sigma_2^{\,0})^2 < -\frac{a_{11}}{a_{12}^{\,2}} + \frac{b_2^{\,0}}{a_{12}^{\,2}} \qquad [31]$$

These conditions demonstrate that the noise interference decreases stability of the dialog by decreasing the upper bound of the initial variances (which are proportional to the degree of incompleteness of information) that are sufficient for the convergence of the dialog to the common ground.

Second, we will assume that each agent is able to stabilize the dialog by applying control (or self-supervising) forces composed of the probability density and its space-derivatives. In order to suppress noise we will choose the following control forces

$$F_1 = -c_1^{\,2}\frac{\partial}{\partial x_1}\ln p, \qquad F_2 = -c_1^{\,2}\frac{\partial}{\partial x_2}\ln p \qquad [32]$$

to be added to the right-hand sides of equations [6] and [7] respectively

$$\dot{x}_1 = a_{11}x_1 + a_{12}x_2 + F_1 \qquad [33]$$

$$\dot{x}_2 = a_{21}x_1 + a_{22}x_2 + F_2 \qquad [34]$$

Here the constants $c_1^{\,2}$ and c represent the strengths of the control forces. Their contribution into the stability conditions is:

$$\begin{aligned}(\sigma_1^{\,0})^2 &< -\frac{a_{22}}{a_{21}^{\,2}} + \frac{b_1^{\,2}}{a_{21}^{\,2}} - \frac{c_1^{\,2}}{a_{21}^{\,2}},\\ (\sigma_2^{\,0}) &< -\frac{a_{11}}{a_{12}^{\,2}} + \frac{b_2^{\,2}}{a_{12}^{\,2}} - \frac{c_2^{\,2}}{a_{12}^{\,2}}.\end{aligned} \qquad [35]$$

As follows from [35], the control forces can completely suppress the effect of noise if

$$c_1 = b_1,\ c_2 = b_2 \qquad [36]$$

Thus, the proposed model consists of three basic components. The first component is the dynamical model of the agents interaction (in the form of a dialog) represented by ODE (see equations [6] and [7]). This model can be associated with the motor dynamics. Since language communications are always incomplete, the motor dynamics has to be complemented by additional information. This information is coming from the collective mind that represents a special knowledge-base (or a context) composed of the abstract images of the agents in terms of their joint probability density; these images capture general characteristics of the agents, their "habits," expected routes of their evolution, possible deviations of the state variables from their expected values, etc., (see equation [12]). From the collective mind [12], each agent can extract the evolution of his own (marginal) probability density p_i.that represents his mental dynamics. In our model, the marginal densities are approximated by the expectations χ_i and the variances σ_i, and therefore, the mental dynamics of the agents is expressed by equations [20], [24], and [21], [25], respectively. The last component of the model is the feedback from the collective mind [12] to the motor dynamics [6], [7] implemented by the control forces [32] (see equations [33] and [34]). These self-supervising forces can be associated with the agent's self-awareness since they are composed only of the internal parameters characterizing the state of the collective mind, while their goal is to effect the motor dynamics in order to achieve a desired out- come of the "game."

The model introduced in this section is, probably, the simplest one that still allows us to present the proof-of-concept using well-observable closed-form analytical solutions. In the next section we will sketch an extension of this model to the general case when only a numerical approach can be applied.

General model

In this section we will generalize the two-dimensional model described by equations [1] and [2] to n-dimension and add the control forces generalizing the forces [32]

$$\dot{x}_{i|i} = f_i(x_{1|i}, x_{2|i}, \ldots x_{n|i}) + \sum_{j=1}^{n} \alpha_{ij} \frac{\partial}{\partial x_{j|i}} \ln\, p(x_{1|i}, \ldots x_{n|i}) \qquad [37]$$

$$\dot{x}_{j|i} = f_j(x_{1|j|i}, \ldots x_{n|j|i}) + \sum_{j=1}^{n} \alpha_{ij} \frac{\partial}{\partial x_{j|i}} \ln\, p(x_{1|j|i}, \ldots x_{n|j|i}), \qquad j \neq i \qquad [38]$$

Here $x_{k|j|i}$ is the state variable of the image of the k-th agent in view of the j-th agent in view of the i-th agent. This two-reflection-system of n^2 equations is still open since additional equations for the three-index-variables are needed. Such equations can be written in the same form as equations [38], however, they will include the four-index-variables, and the total three-reflection-system will still be open. After m reflections one will arrive into n^{m-1} equations with respect to n^m variables. In order to close the system, one has to introduce a mechanism to create the chain of images. For that purpose, let us turn to the Liouville equation [25] that describes the evolution of the joint probability density $p(X_1,\ldots X_n)$. In the same way in which the density $\rho(X)$ in equation [7] describes the self-image of a single agent, equation [25] can be exploited for description of the chain of images in the form of linear regressions

$$x_{j|i} = M(x_j) + \beta_{ji}[x_i - M(x_i)],$$
$$x_{k|j|i} = M(x_{k|j}) + \beta_{kji}[x_i - M(x_i)], etc \quad [39]$$

Here $M(x_j)$ is expected value of x_j, and the regression coefficients β_{ji}, β_{kji}, etc are uniquely defined by the components of the dispersion matrix $[r_{ij}]$ (for instance, $\beta_{i\,j} = r_{ij}^2/r_{ii}$). Thus, all the regressions [39] are determined by the distribution ρ governed by equation [25]. After substitution the regressions [39] into equations [37] and [38], one arrives at a closed system of ODE's and PDE that couples the motor and mental dynamics in view of the i-th agent.

$$\dot{x}_{i|i} = F_i(x_i, Mx_1, ...Mx_n, r_{ks}) +$$
$$+ \frac{\partial}{\partial x_i} \ln \rho_i(x_i, Mx_1, ..Mx_n, r_{ks}) \sum_{j=1}^{n} \alpha_{ij}[1 + \beta_{ij}(r_{ks})], \quad i = 1, ...n \quad [40a]$$

$$\dot{x}_{j|i} = F_j(x_i, Mx_1, ...Mx_n, r_{ks}) +$$
$$+ \frac{\partial}{\partial x_i} \ln \rho_i(x_i, Mx_1, ...Mx_n, r_{ks}, t) \sum_{j=1}^{n} \alpha_{ij}[1 + \beta_{kji}(r_{sq})], \quad i = 1, ...n \quad [40b]$$

$$\frac{\partial \rho_i}{\partial t} = -\frac{\partial}{\partial x_i}\{(\rho_i \sum_{j=1}^{n} F_j) + \frac{\partial}{\partial x_i}[\ln \rho_i] \sum_{i=1}^{n}\sum_{j=1}^{n} \alpha_{ij}(1+\beta)]\}, \; i = 1, ..n \quad [41]$$

Here ρ_i is the joint probability density in view of the i-th agent.

It should be emphasized that equation [41] is characterized not only by nonlinear diffusion, but by a nonlinear drift as well since both of these coefficients depend upon the density moments. Obviously, different agents have different views of the system, and these differences start with different initial conditions and initial densities for different i-ths. Hence, all the systems [40]-[41] evolve independently for different i-ths until an external event couples them.

The structure of the complexity chains, in general, can be different from those described above. Indeed, suppose that all the agents, except the i-th one, shear information about the values of their state variables; therefore, they have to predict only the position of the i-th agent. That can be done via linear regression of x_i onto the rest of the variables

$$x_i = M(x_i) + \sum_{k \neq i} \beta_{ik}[x_k - M(x_k)],$$
$$\beta_{ik} = -\frac{\lambda_{ik}}{\lambda_{ii}}, \qquad [\lambda_{ik}] = [\sigma_{ik}]^{-1} \quad [42]$$

This structure can be generalized to the case when all the agents are divided into several groups such that the agents in the same group shear all the information about their state variables, while the agents from different groups do not. Thus, the proposed model is capable to capture complexity that matches the complexity of life, and that includes behavior of ecological, social as well as economics systems.

Let us discussed in more details the control (or self-supervised) forces F_i. In our previous model, (see Equations [32]), their role was to stabilize the dialog by suppressing noise. In general, their choice depends upon the objective of the cooperating agents. If this objective is formulated in terms of minimization of a functional

$$J = \int \Phi(p, \nabla p, ...) dV \rightarrow \min$$

then, applying the formalism of the control theory, one can find the corresponding control forces. However, one should notice that in the classical control theory, the control forces depend

upon the state variables (14), while here they are composed of the parameters of the collective mind such as expected values and variances of the state variables, and that is why it is better to call them self-supervised forces.

When communicating agents simulate the human society, some emerging objectives can take over and govern the agent's behavior. As an example, consider the principle of reflectivity introduced by V. Lefebvre (15): the subject tends to generate a pattern of behavior such that similarity is established and preserved between the subject and his model of the self "while this principle, is a manifestation of a special cognitive mechanism of self-representation rather than a result of the intellectual efforts of the subject consciously thinking about the self." In terms of our formalism, the following self-supervised forces can implement this principle (see ref. 13)

$$F_i = \gamma_i (\chi_i - x_i)^{\frac{1}{3}}, \qquad \gamma_i = const. \qquad [43]$$

On a large time-scale, one can introduce the principle of maximum complexity stating that a human-like community of agents evolves toward the maximum increase of the complexity of its social structure. In terms of our formalism, such an evolution is achieved by the increase of the number of the levels of reflections, (see Equation [5]). However, a natural constraint for such an increase is the exponential growth of the capacity and resources required.

More practical approach to selection of the self-supervised forces can be adopted from the concept of learning in neural nets. Suppose that these forces are sought in the following parametrised form:

$$F_i = \tanh \sum_{i,j} w_{i,j} p_j, \qquad i.j = 1, 2, ...k$$

in which w_{ij} are constant weights, and p_j is the value of the probability density at a fixed point j of the n-dimensional space $X_1 \ldots X_n$,while k is the number of the points at which the probability density is discretised. Let us assume that our objective is to teach the artificial communicating agents to make correct decisions in response to unexpected changes in external forces or in the objectives. For that purpose, first we have to find an expert whose responses (either rational or intuitive) will be optimal. Then, comparing these responses with the corresponding responses of the model and applying the back-propagation technique, one can find the optimal weights in the self-supervising forces.

Interpretation of the model

In this section we will present and discuss the interpretation of the proposed collective-mind-based model of communicating agents from the viewpoints of mathematics, and physics. We will also propose possible interpretations from viewpoint of biology, psychology, neuro-science, social dynamics and economy, as well as language communications, control theory, and hardware implementation

Mathematical viewpoint

From the mathematical viewpoint the model is represented by the system of the Langevin-type stochastic differential equations (see Equations [10], [11] or Equation [39]) and the corresponding Fokker-Planck equation (see Equation [12] or Equation [40]. The connection between these equations is the following: Equation [39] simulates randomness while Equation [40] manipulates by the values of its probability; therefore, if Equation [39] are run independently many times and statistical analysis of the corresponding solutions is performed, then the calculated probability density will evolve according to Equation [40]. However, the major departure from the classical case here is in the coupling between the Langevin and the Fokker-Planks equations. This coupling is implemented by the self-supervising forces F_i as well

as by the expectations χ_i and the variances σ_i of the state variables (see Equation [39]). As a result of this coupling, the Fokker-Planck equation becomes nonlinear with respect to the probability density, and that, in turn, leads to new fundamental phenomena in the probability space (13). These phenomena include formation of multi-attractor limit sets as well as formation of shock waves, and solitons.

Both phenomena demonstrate a major departure from linear evolution of probability density. The multi-attractor limit sets allow one to introduce an extension of neural nets that can converge to a prescribed type of a stochastic process in the same way in which a regular neural net converges to a prescribed deterministic attractor. An information-based neural net of that type was introduced and analyzed in ref. (13). The shock waves and solitons decrease the rate of disorder by slowing down or even reverse the diffusion. Therefore, these phenomena can play an impotent role in self-organization of active systems. Another new phenomenon representing a special form of entanglement of stochastic processes is illustrated by Equations [10] and [11]. Indeed, formally the stochastic processes described by these equations are independent since Equation [10] does not depend upon x_2 and Equation [11] does not depend upon x_1. However, these processes are coupled via their invariants (see Equations [20] and [21], and that entangles them in a special nonlinear way. It should be noticed that this entanglement implements connection between the agents by mean of the collective mind.

Physical viewpoint

From the physical viewpoint, the model represents a fundamental departure from both Newtonian and statistical mechanics. Indeed, firstly, in Newtonian mechanics the evolution of the probability density (described by the Fokker-Planck equation) is always linear, and it never affects the underlying motion of the corresponding physical system. Secondly, in Newtonian mechanics the Fokker-Planck equation only registers the evolution of the probability density without affecting the corresponding equations of motion, and there are no principles that would determine additional feedback forces. Both of these conditions are violated in the proposed model: due to the self-supervising forces F_i, Equations [39] and [40] are coupled, and that, in turn, makes Equation [40] nonlinear. The same coupling between the evolution of the probability density and the corresponding motion in physical space may cause a decrease of the entropy i.e. a progressive evolution that is strictly forbidden by the statistical mechanics of isolated systems. Thus, the proposed model is non-compatible with both Newtonian and statistical mechanics. At the same time, it is fully consistent with the theory of differential equations and stochastic processes. The only conclusion following from that is that this model can display some "non-Newtonian" features. Formal similarity of the proposed model and quantum mechanics is discussed in refs (11, 13).

Biological viewpoint

From the viewpoint of evolutionary biology, the proposed model illuminates the "border line" between living and non-living systems. The starting point of our biologically inspired interpretation is the second law of thermodynamics that states that the entropy of an isolated system can only increase. This law has a clear probabilistic interpretation: increase of entropy corresponds to the passage of the system from less probable to more probable states, while the highest probability of the most disordered state (which is the state with the highest entropy) follows from a simple combinatorial analysis (3). However, this statement is correct only if there is no Maxwell' sorting demon, i.e., nobody inside the system is rearranging the probability distributions. But this is precisely what the self-supervising feedback is doing: it takes the probability density p from Equation [40], creates functionals or functions of this density, converts them into a force and applies this force to the equation of motion, (see the last three

terms in Equations [39]). As already mentioned above, because of that property of the model, the evolution of the probability density becomes nonlinear, and the entropy may decrease "against the second law of thermodynamics." Obviously the last statement should not be taken literary; indeed, the proposed model captures only those aspects of the living systems that are associated with their behavior, and in particular, with their motor-mental dynamics since they are beyond of the dynamical formalism. Therefore, such physiological processes that are needed for the metabolism are not included into the model. That is why this model is in a formal disagreement with the second law of thermodynamics while the living systems are not. In order to further illustrate the connection between the life-nonlife discrimination and the second law of thermodynamics, consider a small physical particle in a state of random migration due to thermal energy, and compare its diffusion i.e. physical random walk, with a biological random walk performed by a bacterium. The fundamental difference between these two types of motions (that may be indistinguishable in physical space) can be detected in probability space: the probability density evolution of the physical particle is always linear and it has only one attractor: a stationary stochastic process where the motion is trapped. On the contrary, a typical probability density evolution of a biological particle is nonlinear: it can have many different attractors, but eventually each attractor can be departed from without any "help" from outside.

That is how H. Berg (16) describes the random walk of an *E. coli* bacterium: "If a cell can diffuse this well by working at the limit imposed by rotational Brownian movement, why does it bother to tumble? The answer is that the tumble provides the cell with a mechanism for biasing its random walk. When it swims in a spatial gradient of a chemical attractant or repellent and it happens to run in a favorable direction, the probability of tumbling is reduced. As a result, favorable runs are extended, and the cell diffuses with drift". Berg argues that the cell analyzes its sensory cue and generates the bias *internally*, by changing the way in which it rotates its flagella. This description demonstrates that actually a bacterium interacts with the medium, i.e., it is not isolated, and that reconciles its behavior with the second law of thermodynamics. However, since these interactions are beyond the dynamical world, they are incorporated into the proposed model via the self-supervised forces that result from the interactions of a biological particle with "itself," and that formally "violates" the second law of thermodynamics. Thus, the proposed model offers a unified description of the progressive evolution of living systems. Based upon this model, one can formulate and implement (via the reflective chains) the principle of maximum increase of complexity that governs the large-time-scale evolution of living systems. It should be noticed that at this stage, our interpretation is based upon logical extension of the proposed mathematical formalism, and is not yet corroborated by experiments.

Psychological viewpoint

From the viewpoint of psychology the proposed model can be interpreted as representing interactions of the agent with the self-image and the images of other agents via the mechanisms of self-awareness. In order to associate these basic concepts of psychology with our mathematical formalism, we have to recall that living systems can be studied in many different spaces such as physical (or geographical) space as well as abstract (or conceptual) spaces. The latter category includes, for instance, social class space, sociometric space, social distance space, semantic space e.t.c.Turning to our model, one can identify two spaces: the physical space x,t in which the agent state variables $x_i(t)$ evolve,(see Equation [39]), and an abstract space $p(X_1..X_n, t)$ in which the probability density of the agent' state variables evolve (see Equation [40]).The connection with these spaces have been already described earlier: if Equation [39] are run many times starting with randomly chosen initial conditions, as well as with random values of the Langevin forces $L_i(t)$, one will arrive at an ensemble of different random solutions, while Equation [40] will show what is the probability for each of these

solutions to appear. Thus, Equation [40] describes the general picture of evolution of the communicating agents that does not depend upon particular initial conditions. Therefore, the solution to this equation can be interpreted as the evolution of the self- and non-self images of the agents that jointly constitutes the collective mind in the probability space. Based upon that, one can propose the following interpretation of the model of communicating agents: considering the agents as intelligent subjects, one can identify Equation [39] as a model simulating their motor dynamics, i.e. actual motions in physical space, while Equation [40] as the collective mind composed of mental dynamics of the agents. Such an interpretation is evoked by the concept of reflection in psychology (17). Reflection is traditionally understood as the human ability to take the position of an observer in relation to one's own thoughts. In other words, the reflection is the self-awareness via the interaction with the image of the self. Hence, in terms of the phenomenological formalism proposed above, a non-living system may possess the self-image, but it is not equipped with the self-awareness, and therefore, this self-image is not in use. On the contrary, in living systems the self-awareness is represented by the self-supervising forces which send information from the self-image to the motor dynamics. Due to this property that is well-pronounced in the proposed model, an intelligent agent can run its mental dynamics ahead of real time, (since the mental dynamics is fully deterministic, and it does not depend explicitly upon the motor dynamics) and thereby, it can predict future expected values of its state variables; then, by interacting with the self-image via the supervising forces, it can change the expectations if they are not consistent with the objective. Such a self-supervised dynamics provides a major advantage for the corresponding intelligent agents, and especially, for biological species: due to the ability to predict future, they are better equipped for dealing with uncertainties, and that improves their survivability. It should be emphasized that the proposed model, strictly speaking, does not discriminate living systems of different kind in a sense that all of them are characterized by a self-awareness-based feedback from mental to motor dynamics. However, in primitive living systems (such as bacteria or viruses) the self-awareness is reduced to the simplest form that is the self-nonself discrimination; in other words, the difference between the living systems is represented by the level of complexity of that feedback.

Neuro-science viewpoint

From the viewpoint of neuro-science the proposed model represents a special type of neural net. Indeed, reinterpreting an agent's state variable x_i as a neuron's mean soma potential, and assuming that each neuron receives full information from the rest of neurons, one arrives at a conventional neural net [37]. It should be recalled that in this case the self- supervising forces are not needed, and they can be ignored. The departure from the conventional case starts with the incompleteness of information, i.e., when a neuron does not receive the values of the mean soma potentials from the rest of the neurons. This incompleteness is compensated by a "general knowledge" stored in the collective mind [40] and delivered to the neural net via the self-supervising forces F_i. As a result of that, the neural net [39] becomes random, while the evolution of its statistical invariants is described by the collective mind [49]. In order to illuminate the difference between these two cases we will start with a single continuously updated linear neuron with a dissipation feedback

$$\dot{x} = -x \qquad [44]$$

The state variable x eventually approach an attractor x=0 regardless of initial conditions.

$$x = x_0 \exp(-t) \qquad [45]$$

In general case, a multi-dimensional nonlinear neural net may converge to one of the several attractors that can be static, periodic, or chaotic as well. However, one fundamental property remains the same: as soon as these attractors are approached, the evolution stops.

Let us turn now to a stochastic extension of a neuron [44]. This can be done in several ways. One way is to relax the Lipschitz conditions (7). Another way is to introduce a special types of the equilibrium points which are attractors in one direction and repellers in the others. In the both cases the neuron state variable will perform a Brownian motion that can be included in Equation [44] via the Langevin force L(t):

$$\dot{x} = -x + L(t). \qquad [46]$$

Equation [46] has the solution:

$$x = x_0 \exp(-t) + \int_0^t \exp[-(t-t')]L(t')dt' \qquad [47]$$

Equation [47] describes a stochastic process that characterizes the evolution of the neuron state variable. The evolution of the probability density is described by the corresponding Fokker-Planck equation

$$\frac{\partial p}{\partial t} = \frac{\partial}{\partial X}(Xp) + D\frac{\partial^2}{\partial X^2}p\ . \qquad [48]$$

Its solution for the sharp initial value p(x,0)=δ(x→0) is represented by a normal distribution

$$p = \frac{1}{\sqrt{2\pi D'}}\exp[-\frac{X^2}{2D'}], \qquad [49]$$
$$D' = D[1-\exp(-2t)].$$

As t→∞, the distribution tends to the thermodynamical limit with D′→D. Obviously, D>D′, and therefore, the entropy E=LnD√2π approaches its maximum value at t→∞. This result can be extended to the general case of multi-dimentional diffusion-based neural nets. That means that the evolution of such neural nets is always regressive, i.e. their entropy can only increase.

Let us introduce a control force to reverse the increase of the entropy. Within the framework of the Newtonian formalism, the most general control force must depend upon the state variables and time, i.e., F = F(x,t). Substituting this force into Equation [46], and introducing the corresponding changes into Equation [48], in which the drift and the diffusion coefficients are functions of X and t. Then, according to the Boltzman H-theorem (12) the entropy of the system will still monotonously increase regardless of the a particular form of the control force. However, the situation is changed if the control is represented by a self-supervised force composed of the probability density and its derivatives. For the proof of concept, let us choose this force as following

$$F = D\frac{\partial}{\partial x}\ln p \qquad [50]$$

which is applied after t>T. Then Equations [46] and [48] are to be rewritten as

$$\dot{x} = -x + L(t) + D\frac{\partial}{\partial x}\ln p \qquad [51]$$

and

$$\frac{\partial p}{\partial t} = \frac{\partial}{\partial X}[(X - D\frac{\partial}{\partial X}\ln p)p] + D\frac{\partial^2}{\partial X^2}p \qquad [52]$$

respectively. After trivial transformations, Equation [52] is reduced to the form in which the diffusion term is suppressed

$$\frac{\partial p}{\partial t} = \frac{\partial}{\partial X}(Xp). \qquad [53]$$

The solution to this equation that starts from t>T is

$$p = \sqrt{\frac{\beta}{2\pi Y}}\exp[\beta t - \frac{\beta X^2 \exp(2\beta t)}{2DY}, \qquad [55]$$
$$Y = 1 - \exp(-2\beta t).$$

As follows from this solution, the self-supervised force reverses the evolution of the probability density towards the decrease of the entropy, and that makes a self-supervised neuron a "messenger of life."

Thus, the fundamental property of the self-supervised neuron is its ability to create the self-image (Equation [52]) and interact with this image (Equations [53] and [54]). It would be a challenge for a future research to associate the self-supervised neuron with the mirror neuron 9 recently discovered in the monkey) that fires both when performing an action and when the monkey is observing the same action performed by another subject. Indeed, the way in which the self-supervised neuron works is the following. It is assumed that all the communicating agents belong to the same class in a sense that they share the same general properties and habits. It means that although each agent may not know the exact positions of the rest of the agents, he, nevertheless, knows at least such characteristics as their initial positions (to accuracy of initial joint probability density, or, at least, initial expected positions and initial variances). This preliminary experience allows him to reconstruct the evolution of expected positions of the rest of the agents using the collective mind as a knowledge base. *Hence, a self-supervised neuron representing an agent A can be activated by an expected action of an agent B which may not be in a direct contact with the agent A at all, and that can be associated with the mirror properties of the self-supervised neuron.*

The collective properties of self-supervised neurons, i.e., the self-supervised neural nets have a significant advantage over the regular neural nets: they possess a fundamentally new type of attractor – the stochastic attractor that is a very powerful generalization tool. Indeed, it includes a much broader class of motions than static or periodic attractors. In other words, it provides the highest level of abstraction. In addition to that, a stochastic attractor represents the most complex patterns of behavior if the self-supervised net describes a set of interacting agents. Indeed, consider a swarm of insects approaching some attracting pattern. If this pattern is represented by a static or periodic attractor, the motion of the swarm is locked up in a rigid pattern of behavior that may decrease its survivability. On the contrary, if that pattern is represented by a stochastic attractor, the swarm still has a lot of freedom, and only the statistic of the swarm motion is locked up in a certain pattern of behavior. For example, an information-based neural net (13) can approach a stochastic attractor that preserves a prescribed amount of information express via the entropy E.

It should be emphasized that, due to the multi-attractor structure, the proposed model provides the following property: if the system starts from different initial conditions, it may be trapped in a different stochastic pattern. Such a property, in principle, cannot be provided by regular neural nets or cellular automata since they can have only one *stochastic* attractor.

Social and economic viewpoint

One of the basic problem of social theory is to understand "how, with the richness of language and the diversity of artifacts, people can create a dazzlingly rich variety of new yet relatively stable social structures" (18). Within the framework of the dynamical formalism, the proposed model provides some explanations to this puzzle. Indeed, social events are driven by two factors: the individual objectives and social constraints. The first factor is captured by the motor dynamics [39], while the social constraint is created by the collective mind [40]. A balance between these factors (expressed by stochastic attractors) leads to stable social structures, while a misbalance (expressed by stochastic repellers) causes sharp transitions from one social structure to another (revolutions) or to wandering between different repellers (chaos, anarchy). For an artificial "society" of communicating agents, one can assign individual objectives for each agent as well as the collective constrains imposed upon them and study the corresponding social events by analyzing the governing equations [39] and [40]. However, the same strategy is too naïve to be applied to a human society. Indeed, most human as members of a society, do not have rational objectives: they are driven by emotions, inflated ambitions, envy, distorted self- and nonself images, etc. At least some of these concepts can be formalized and incorporated into the model. For instance, one can consider emotions to be proportional to the differences between the state variables and their expectations

$$E_m = c(\chi - x)\,. \qquad [55]$$

Equation [55] easily discriminates positive and negative emotions. Many associated concepts (anger, depression, happiness, indifference, aggressiveness. and ambitions) can be derived from this definition (possibly, in combination with distorted self and non-self images). But the most accurate characteristic of the human nature was captured by cellular automata where each agent copies the behaviors of his closest neighbors (which in turn, copy their neighbors, etc.). As a result, the whole "society" spontaneously moves toward an unknown emerging "objective." Although this global objective is uniquely defined by a local operator that determines how an agent processes the data coming from his neighbors, there is not known any explicit connection between this local operator and the corresponding global objective: only actual numerical runs can detect such a connection. Notwithstanding the ingenuity of his model, one can see its major limitation: the model is not equipped with a collective mind (or by any other type of a knowledge base), and therefore, its usefulness is significantly diminished in case of incompleteness of information. At the same time, our model can be easily transformed into a cellular automata with the collective mind. In order to do that one has to turn to Equation [37], replace the sigmoid function by a local operator, and the time derivative-by the time difference. Then the corresponding Fokker-Planck equation [40] reduces to its discrete version that is Markov chains (10). On the conceptual level, the model remains the same as discussed in the previous sections. This illustrates a possible approach to the social dynamics based upon the proposed model.

From the viewpoint of economics, the proposed model can represent games with incomplete information. Probably, the best illustration of that is the so called minority game which is a simplified model of conflicting situations observed in financial markets (19). It describes a system in which an odd number N of agents is allowed to make two possible choices: 1 or 0, and that divides the agents in two groups while the group with less number of agents wins. Clearly when agents know nothing about the possible strategies of their adversaries, the outcome is totally random. However, if the agents shear some global information about each other (such as the history of the game in the form of the sequence of the last winning choices), the dynamics of the game becomes extremely complex (for instance, it includes such phenomena as the phase transitions). Within the framework of our model, the sheared

information can be stored in the collective mind, and this will provide the agents with the dynamics of interaction between the sheared knowledge and the individual strategies. An exciting challenge for future work is to test the utility of this approach in formalizing shared information as used in section 3.

Language communications viewpoint

Language represents the best example of a communication tool with incomplete information since any message, in general, can be interpreted in many different ways depending upon the context i.e. upon the global information sheared by the sender and the receiver. Therefore, the proposed model is supposed to be relevant for some language-oriented interpretations. Indeed, turning to Equation [39], one can associate the weighted sum of the state variables with the individual interpretations of the collective message made by the agents. The sigmoid functions of these sums form the individual responses of the agents to this message. These responses are completed by the self-supervising forces that compensate the lack of information in the message by exploiting the global sheared information stored in the collective mind, (see Equation [40]). The agent's responses converted into the new values of their state variables are transformed into the next message using the same rules, etc. These rules determined by the structure of Equations [39] and [40] can be associated with the grammar of the underlying language. In particular, they are responsible for the convergence to- or the divergence from the expected objective. It should be noticed that the language structure of the proposed model is invariant with respect to semantics. Hence, in terms of the linguistics terminology that considers three universal structural levels: sound, meaning and grammatical arrangement (20), we are dealing here with the last one. To our opinion, the independence of the proposed model upon the semantics is an advantage rather than a limitation: it allows one to study invariant properties of the language evolution in the same way in which the Shannon information (that represents rather an information capacity) allows one to study the evolution of information regardless of a particular meaning of the transmitted messages.

Let us now try to predict the evolution of language communications based upon the proposed model. As mentioned earlier, the evolution of the living systems is always directed toward the increase of their complexity. In a human society, such a progressive evolution is effectively implemented by increase or the number of reflections in a chain "What do you think I think you think, etc." The society may be stratified into several levels or "clubs" so that inside each club the people will shear more and more global information. This means that the language communications between the members of the same club will be characterized by the increased capacity of the collective mind (see Equation [40]), and decreased information transmitted by the messages (see Equation [39]). In the theoretical limit, these messages will degenerate into a string of symbols, which can be easily decoded by the enormously large collective mind The language communications across the stratified levels will evolve in a different way: as long as the different clubs are drifting apart, the collective mind capacity will be decreasing while the messages will become longer and longer. However, the process of diffusion between these two streams (not included in our model) is very likely.

Control theory viewpoint

The proposed model can be considered as a closed-loop controlled dynamical system known in the engineering control, with the only difference that, unlike the engineering control where the control forces are triggered by the values of the state variables and their time-derivatives, here the control forces are determined by the parameters of the collective mind that implicitly represent the state variables of the underlying system. This type of control can be linked to a so-called reflective control introduced in mathematical psychology by V. Lefebvre (21) since the system is governed by the reflections, i.e., by the parameters characterizing the images rather

than real objects. The mathematical consequences of this property have been discussed in the sub-section A of this section.

Applications and implementations

The proposed model has two types of applications that can be associated with science and technology, respectively. The first type includes theoretical studies of behavior of living systems, and can be performed by direct computer simulations of the system [39], [40]. The second type includes the development of artificial living systems that are supposed to simulate and replace some functions of a human (robots, unmanned spacecrafts, etc.). The most effective way of implementation of these systems is by means of analog devices such as VLSI chips used for neural net's analog simulations. As discussed in the sub-section E of this section, Equation [39] can be treated as regular continuously updated neural nets with additional random forces. Implementation of these forces has been proposed by M. Zak (13) based upon non-Lipschitz dynamics. Equation [40], after approximation of space-derivatives be finite differences, can be easily transformed to a neural-net-like dynamical system that can be implemented by VLSI chips.

Variation formulation

In this section we will propose a variation formulation of the First Principle for Living system phenomenology. First we will generalize the model introduced above using the following neural-net-based vector structure

$$\dot{\bar{x}} = \bar{f} + \alpha \nabla \ln p(x_1, \cdots, x_n, t), \;\; \bar{x} = \{x_1, \cdots, x_n\}, \;\; \bar{f} = \{f_1, \cdots, f_n\} \qquad [56]$$

$$\dot{\rho} = -\nabla \bullet (p\bar{f}) - \alpha \nabla^2 p, \;\; \alpha = const \qquad [57]$$

$$f_i = w_i x_i + w_{ij} \sum \tanh x_j,$$

$$\alpha = W_{ij} r_{ij} + W_{ks} . \sum_{k=1}^{n} \sum_{s=1}^{n} \tanh r_{ks}, \;\; \cdots \qquad [58]$$

$$w_{ij}, W_{ks} \theta = const$$

Eq.[56] and [57] represent the motor and the mental dynamics, respectively. The vector f_i stands for physical forces presented in a parameterized neural-net-based form (see Eq. [58]. The state variables x_i represent velocities rather than positions. The information –based forces are derived from the following scalar

$$\Pi = -\alpha \ln p \qquad [59]$$

This function can be called "the information potential" since its expected value [-M ln p] is equal to the Shannon information capacity H. The gradient of this potential taken with the opposite sign can be identified with the information-based force F = -grad Π. The weight α is expressed by Eq. [58] as parameterized function of the correlation moments r_{ks} that, being a functionals of the joint probability density $p(x_1,...x_n)$, include the reflection paradigm "what do you think I think you think…". It can be demonstrated that the information potential couples the Newtonian dynamics [16] and the corresponding Liouville equation [17] [describing propagation of initial uncertainties) formally in the same way in which the quantum potential couples these equations in quantum mechanics. However, the role of the information potential is different: it can generate a negative diffusion that reverses the evolution toward s decrease of entropy.

Eq. [56] can be reduced to a gradient system if one drops the Newtonian forces f_i and assumes [without a loss of generality) that $\alpha = 1$

$$\dot{\bar{x}} = \nabla \ln p - \nabla \ln \frac{1}{p}$$

Then, the following identity is true along the system's trajectory

$$\frac{d}{dt} \ln \frac{1}{p} = \frac{\partial}{\partial t} \ln \frac{1}{p} + \nabla \ln \frac{1}{p} \bullet \dot{\bar{x}} = \frac{\partial}{\partial t} \ln \frac{1}{p} - |\nabla \ln \frac{1}{p}|^2$$

Let us choose the most probable trajectory recalling that on such a trajectory

$$\nabla p = 0, \quad \nabla^2 p < 0,$$

$$i.e \qquad \frac{\partial}{\partial t} \ln \frac{1}{p} = -\frac{1}{p} \frac{\partial p}{\partial t} = \frac{1}{p} \nabla^2 p < 0$$

Hence

$$\frac{d}{dt} \ln \frac{1}{p} < 0, \qquad i.e \qquad \frac{d}{dt} \ln p > 0, \qquad and \qquad \frac{d}{dt} \Pi < 0$$

Thus, Eq. [56] reduces to the gradient-decent dynamics that *minimizes the information potential Π along the most probable trajectory. This result can be considered as the "objective" of the corresponding living system.*

Data-driven model discovery

In this section the following inverse problem is addressed: given a dynamical system [for instance, brain) as a black box represented by time series of the sensor data (encephalograms); reconstruct the underlying model assuming that it has the form [56],[57], and parameterization [58]. The first step is to extract the stationary components from the time series. This can be done by applying an appropriate set of difference operators (22). Next, based upon the ergodic hypothesis, one can reconstruct the stationary probability density p^0 as a function of the state variables:

$$p^0 = p^0(x_1 ... x_n) \qquad [60]$$

as well as all the moments needed. It is assumed that this function is defined at the points

$$x_i = x_{i1}, x_{i2}, \cdots, x_{iq} \qquad [61]$$

Noticing that p^0 must satisfy the stationary version of Eq.[57]

$$0 = -\nabla \bullet (p\bar{f}) - \alpha \nabla^2 p, \; \alpha = const \qquad [62]$$

and substituting f and α from Eq. [58], one arrives at a linear algebraic equation with respect to the constant parameters w_{ij} and W_{ks} that, for compression, can be denoted and numerated as W_i

$$\sum_{i=1}^{m} A_i W_i = B \qquad i = 1, 2, \cdots, m \qquad [63]$$

where m is the number of the parameters defining the model, and:

$$A_i = A_i(p^0, x_1, ..., x_n), \quad B = B(p^0, x_1, ..., x_n) \qquad [64]$$

are the coefficients at the parameters W_i and the free term, respectively. Introducing values of A_i and B at the points x_{ij} and denoting them as A_{ij}, and B_j, one obtains a linear system of q^n algebraic equations

$$\sum_{i=1}^{m} A_{ij} W_i = B_j, \quad j = 1, 2, ..., q^n \qquad [65]$$

with respect to m unknown parameters. It is reasonable to assume that

$$q^n >> m \qquad [66]$$

so the system becomes overdetermined. The best-fit solution is found via pseudo inverse of the matrix

$$A = \left\{ A_{ij} \right\}, \qquad i.e.\ W = A^* \overline{B} \qquad [67]$$

Here

$$A^* = (A^T A)^{-1} A^T, \ and \ \ \overline{B} = \left\{ B_j \right\} \qquad [68]$$

As soon as the parameters W are found, the model is fully reconstructed, while this model is compatible with the specific properties of living system since it reserves room for progressive evolution, reflection paradigms, etc.

Conclusion

In summary, we have introduced a new mathematical formalism that offers a rich framework for developing models capturing non-Newtonian properties of living systems. The proposed general approach has been focused on the behavior of communicating agents who compensate an incompleteness of exchanged information by means of the collective mind as a context-type of the global sheared knowledge base. Detailed analyses of an example illustrating the proposed formalism as well as discussion of speculations about its scientific and technological applications have been performed.

Acknowledgment

The research described in this paper was performed at Computer Science Department, Neuroscience Program University of Southern California under contract with the National Aeronautic and Space Administration. The effort was sponsored by the Jet Propulsion Laboratory California Institute of Technology.

References

1. Huberman B. The ecology of computation. Amsterdam: North-Holland; 1988.
2. Mikhailov A. Foundations of synergetics. New York: Springer, 1990.
3. Prigogine I. From being to becoming, San Francisco: W.H. Freeman; 1980.

4. Haken H. Information and self-organization. New York: Springer; 1988.
5. Prigogine I. Non-equilibrium statistical mechanics. New York: John Wiley; 1962.
6. Gordon R. The hierarchical genome and differential waves. Singapore: World Scientific; 1999.
7. Zak M. Terminal model of newtonian dynamics. Int J Theor Phys 1992:32:159-90.
8. Vidal J, Durfee E. Learning nested models in an information economy. J Exp Theor Artif Intell 1998;4:12-28.
9. Zak M. Physical invariants of biosignature. Phys Letters A 1999;255:110-8.
10. Zak M. Dynamics of intelligent systems. Int J Theor Phys 2000; 39:2107-40.
11. Zak M. Quantum evolution as a nonlinear markov process. Foundations of Physics L 2002;15:25-37.
12. Risken H. The Fokker-Planck equation. New York: Springer, 1989.
13. Zak M. Self-supervised dynamical systems. Chaos, Solitons & Fractals 2003;19:645-66.
14. Banks SP. Control system engineering. New Jersey: Prentice-Hall; 1986.
15. Lefebvre V. The Law of self-reflextion. Reflexive Processes and Control, 2002.
16. Berg H. Random walks in biology. New Jersey: Princeton University Press; 1983
17. Lefebvre V. The cosmic subject. Moscow: Russian Academy of Science; 1997.
18. Arbib M, Hesse M. The construction of reality. Cambridge: University Press; 1986.
19. Challet D, Zhang YC. On the minority game. Physica A 1998:256;514.
20. Yaguello M. Language through the looking glass. Oxford: Oxford University Press; 1998.
21. Lefebvre V. Algebra of conscience. Kluwer Acad. Publ; 2001.
22. Box GEP. Time Series analysis. New Jersey: Prentice Hall; 1994.

Short communication

EVOLUTIONARY NEURAL GAS: A SCALE-FREE SELF-ORGANIZING NEURAL NET WITHOUT TOPOLOGICAL CONSTRAINT

Luigi Lella (a), Ignazio Licata (b)
(a) Università Politecnica delle Marche, DEIT, Ancona, Italy; E-mail: l.lella@inform.unian.it
(b) Istituto di Cibernetica Non-Lineare per lo Studio dei Sistemi Complessi, Marsala (TP), Italy; E-mail: licata@programmazione.it

Introduction

The self-organizing nets are particularly fit to carry out cluster analysis of non-hierarchic type, by using competitive learning strategies. It makes them the ideal model for the categorizing processes in natural and artificial intelligent systems. The most patent limits of such models lie in making use of deterministic rules and dimensional constraints (1). In observing the evolutive processes, we can see that the system-environment interaction does not let us foresee beforehand what structural organization the net will take, on the contrary it is emerging during the process and often varies along time. These requirements have stimulated some alternative approaches, see the TRN (2) or the GNG (3), but they all are based upon deterministic rules, which thing leads to the coming out of topologies whose final structure is a *Delaunay Triangulation* (4). From a biological viewpoint, this aspect is scarcely plausible because, in some way, it "pilots" the input categorization towards simple schemes whereas the inputs themselves are, in nature, a not well-defined, noise affected and highly aleatory set, so the emerging structures are generally less rigid, endowed with wide local connectivity but quite extended with respect to the clustering nodes.

We delineate here a model without topological constraints led by simple probabilistic rules. The net is considered as a population of nodes where the main events conditioning its evolution, such as the creation or elimination of links and units, depend on the amount of the local and global available resources. In the model defined during the training phase, which is the assimilation of inputs, it has been adopted a *winner takes all* strategy (5). The links of the stronger units are not directly reinforced, when there are low resources the life probability of the weak nodes simply decays. In so doing it comes out a scale-free graph which is a mark, strongly significant from the viewpoint of physics, of self-organizing processes and information amplifying. It is known that this kind of graph can be found in many natural and artificial systems endowed with logical and thermodynamic openness (6, 7). We will see then that the above mentioned structure justifies in accordance with physics the used term of "gas".

Evolutionary algorithm

The net nodes can be considered as individuals of a population living in an ecosystem. The population surviving is granted by two kinds of resources: one is *global*, given by the available space – the net can get M_P units at most –, and the other ones are *local*, given by the distortion

errors D equal to the distances between the input vectors and the vectors (centres or weight vectors) associated to the net units closest to them (the winner units).

The individuals are divided in groups developing around the winners, but they can also establish a link with other groups.

The interaction modalities among individuals depend on the amount of available resources. When there is scarcity of resources the individuals show a tendency to compete each other, when there is abundance of resources the individuals show a tendency to reproduce.

The evolution stops when it is reached the minimization of the expected quantization error D – the average of the distances between the centres of the winners and the corresponding input vectors [1] – which represents an high modelizing level of the inputs and, consequently, a good adaptive outcome.

$$D = 1/K \sum_{i=1}^{K} \left\| x_i - w_j \right\| \qquad [1]$$

Each net training step, corresponding to the introducing of the succession of the input signals (an epoch), can be divided in three phase.

Winner units' selecting (a)

They are selected the units getting the centres closest to the introduced inputs (*WTA strategy*). So the winners are the units closest to the local resources and, consequently, they are the strongest population units showing a tendency to stay in their own zone and no need to establish links with other groups.

Centres updating (b)

During this phase they are updated both the centres of the winners and the ones connected to them. The centres of the winners shift towards the corresponding inputs. The shift is equal to a fraction of the distance (difference vector) separating the centres of the winners from the corresponding inputs. The centres of the units linked to the winners are modified too, but we have now a fraction minor than the distance which separates them from the inputs.

Lets put x the input corresponding to the winner characterized by w centre, and w_{ij} the centres of the units linked to the winners:

$$\begin{aligned} w(t+1) &= w(t) + \alpha(x - w(t)) \\ w_i(t+1) &= w_i(t) + \beta(x - w_i(t)) \end{aligned} \qquad [2]$$

Each unit is characterized not only by a centre, but also by a variable d representing the quadratic distance from the closest local resource. Such variable value mirrors the individual weakness. The smaller the variable value, the greater the individual surviving possibilities.

At each evolutionary step, the value of this variable is set to its maximum. After each updating of the centre w of a unit, which happens when a given input x is introduced, it is calculated the quadratic distance between the two vectors $(||\boldsymbol{x}\text{-}\boldsymbol{w}||^2)$. If the quadratic distance is less than the node weakness, it will become its new value.

Population evolutionary phase (c)

The population of the net nodes evolves by producing new descendants, establishing new connections and eliminating the weaker unities. How it is shown in the Figure 1, all these events are characterized by a probability depending on the availability of the system resources. Each

unit *i, i = [1…N(t)]* where *N(t)* is the actual net dimension (total number of units), can meet the closest winner j with probability P_m.

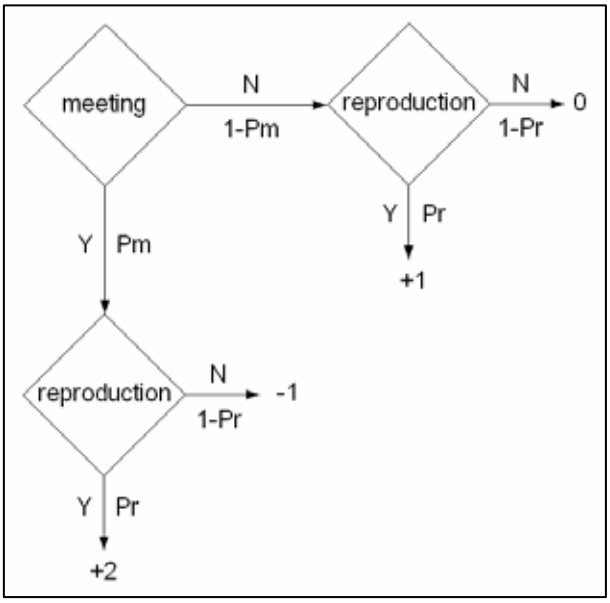

Figure 1. Evolutionary phase of the algorithm

If the meeting takes place the two units establish a link and can interact by reproducing with probability P_r. In this case two new units are created and their centres will be:

$$w_1 = \frac{w_i + \frac{w_i + w_j}{2}}{2}$$
$$w_2 = \frac{w_j + \frac{w_i + w_j}{2}}{2} \qquad [3]$$

If, due to the lack of resources, reproduction does not take place the weakest unit of the population, i.e. the one with the highest debility degree, is removed.

If the *i* unit does not meet any winner, it can interact with its closest unit *k* with probability P_r so producing a new unit whose centre is the following:

$$w = \frac{w_i + w_k}{2} \qquad [4]$$

if we fix a maximum population size, the ratio between $N(t)/N_{max}$ can be seen as a measure of the ecosystem global resources. For example, if the population size is low, the reproduction rate will be high. So we can reasonably put $P_r = 1 - N(t)/N_{max}$. On the contrary, if the population size is high, the higer will be the possibility of connection between two individuals, so we can put $P_m = N(t)/N_{max}$. We can also take into consideration a local resource linked to the expected quantization error: each unit i could meet a winner with a probability given by

$P_m = (N(t)/N_{\max})(1 - D_{\min}/d_i)$, and $P_r = 1 - P_m$, where D_{min} is the average we aim to reach. Obviously, it can happen that the weakness d of the node taken into consideration is inferior than D_{min}, so we have to set: $D_{min}/d < 1$.

The dynamic course of the population size can be studied by two models. The first one takes into consideration only the global resources, the second one takes into account the local resources according to the way they have been defined:

$$\begin{aligned} &N(t+1) = N(t) + 2P_m P_r N(t) - P_m(1-P_r)N(t) + (1-P_m)N(t) - (1-P_m)P_d N(t) = \\ &= 2N_t - 2P_m^2 N(t) = \\ &= 2N(t)\left(1 - \frac{N(t)^2}{M_p^2}\right) \Rightarrow X(t+1) = 2X(t)\left(1 - X(t)^2\right)(first \quad model) \\ &= 2N(t)\left(1 - \frac{N(t)^2}{M_p^2}\left(1 - \frac{D_{\min}}{D}\right)^2\right) \Rightarrow X(t+1) = 2X(t)\left(1 - X(t)^2\left(1 - \frac{D_{\min}}{D}\right)^2\right)(second \quad model) \end{aligned} \qquad [5]$$

where $X(t)$ is the normalized ratio $N(t)/N_{max}$.

Except for the factor $(1 - D_{min}/D)$, the formula reminds the one of the quadratic logistic map by Annunziato and Pizzuti (8) :

$$X(t+1) = aX(t)\left(1 - X(t)^2\right) \qquad [6]$$

The outcome is in concordance with the premises. In fact, the [5] describes an evolutionary history where the self-organization of the initial growing process takes place and it is consequently fallowed saturation, which is linked not only to the global resources but also both to the peculiar distribution within the net of the winners and the configuration of various strength units in the neighbourhood.

Annunziato and Pizzuti proved that at the parameter varying different regimes arise. For $a < 1.7$ there is no chaotic behaviour and we have a simple attractor. For the interval between $1.7 < a < 2.1$ there arise chaotic regimes with a sequence of attractors localized in different zones of the phase space.

Simulations

We have compared the performances of the ENG with the GNG ones in categorizing bidimensional inputs which are uniformly distributed on two different regions. In the former case, the inputs are localized within four square regions; in the latter one, inputs are in a ring region.

As stopping criterion we have chosen the minimization of D (the D_{min} threshold size is equal to $10 - 10^{-1}$). For the GNG the formulae parameters for the updating of the centres are α=0.5, β=0.0005, at each λ=300 steps a new unit is introduced and the maximum age of links is equal to 88. For the two models of ENG the formulae parameters for the centres updating are α=0.05, β=0.0006 and the maximum size has be chosen to be equal to N_{max}=120.

How it is shown in the Figure 2, after the training the GNG vectors are all placed within the input domain, which is to say that the net tends to follow the exact topology of the input signals.

On the contrary, in the ENG some units fall outside the input domain, but the net remains connected by few hubs which give it a scale-free graph structure (Figure 3a and b).

The net structural parameters appear actually to be the typical ones of a scale-free graph. In fact, the low average free path characterizes the net micro-world structure, the high clustering

coefficient shows the presence of considerable aggregations of net units and the distribution of probabilities (links amount) of the nodes' degrees displays a really slow decaying tail, which is to say there exists a restricted amount of nodes establishing much more links than the average.

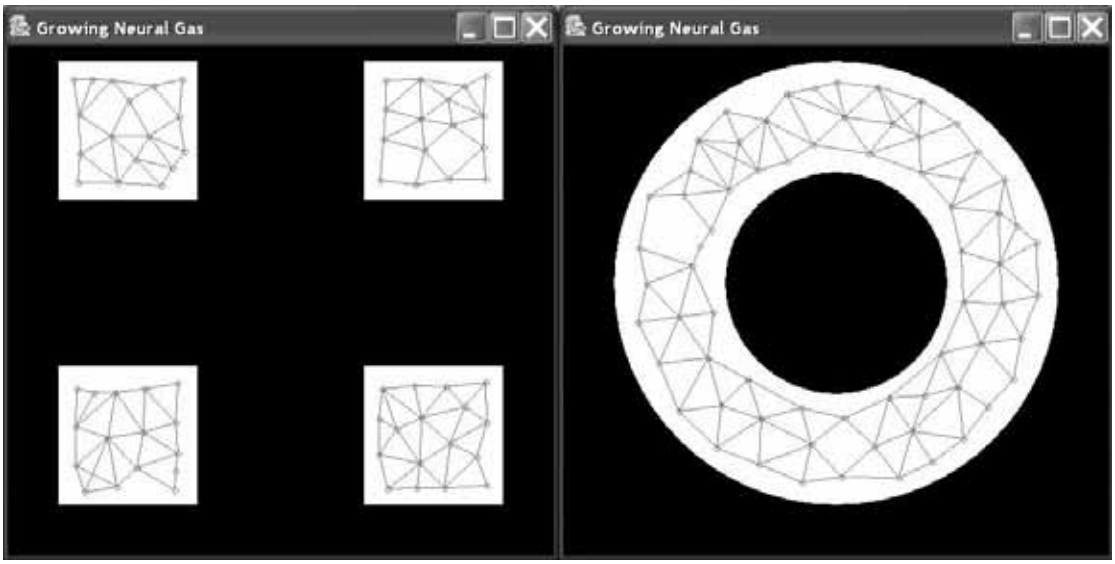

Figure 2. Growing neural gas: simulations

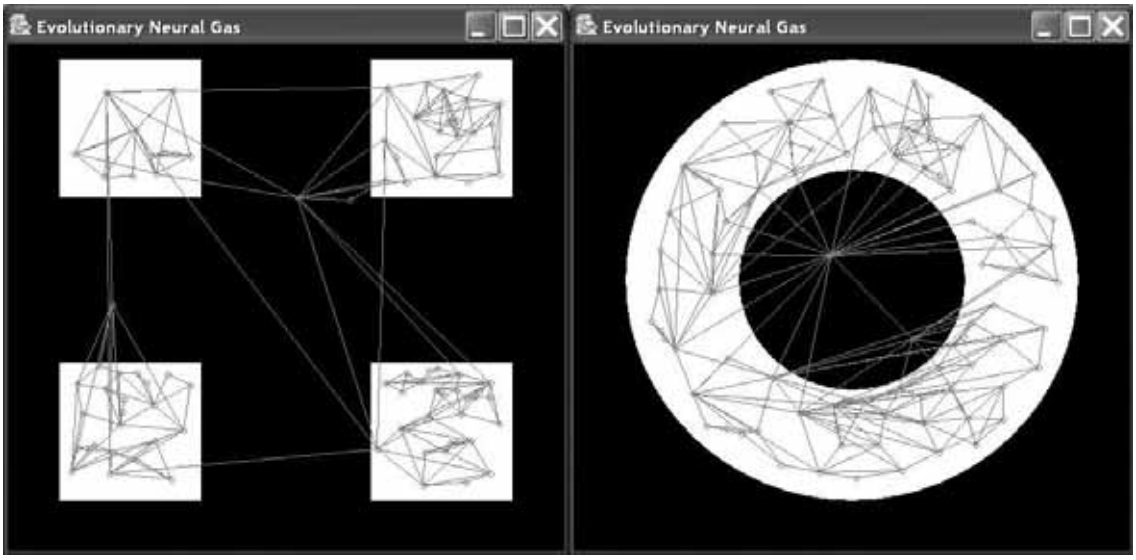

Figure 3a. ENG simulations: first model

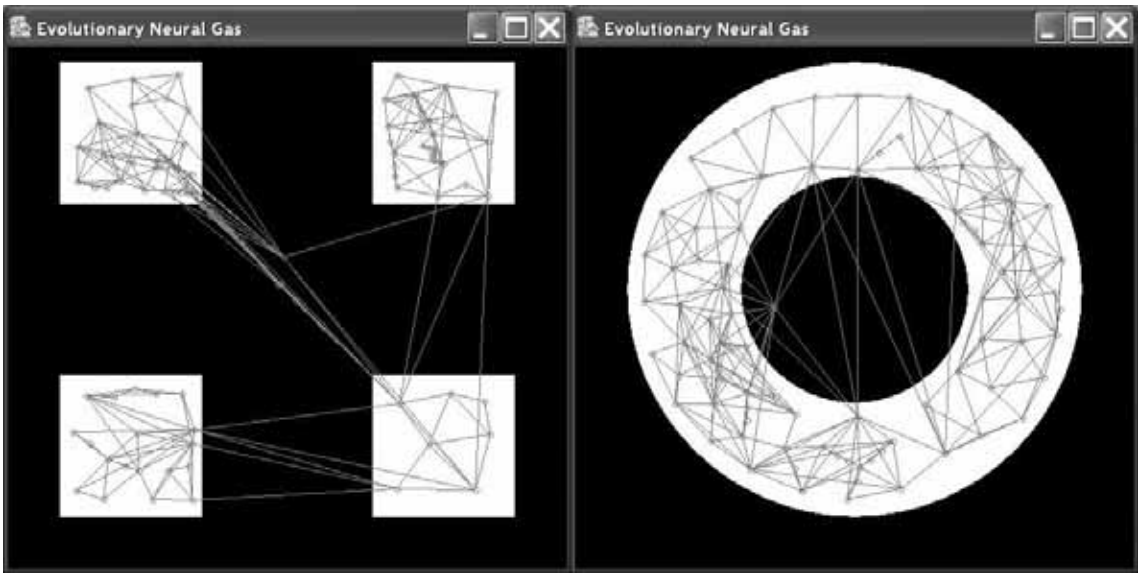

Figure 3b. ENG simulations: second model

How it is shown in Figure 4 (a, b, c), in the GNG the maximum degree that a node can take is about 5, whereas in the ENG we can have nodes establishing more than 8 links.

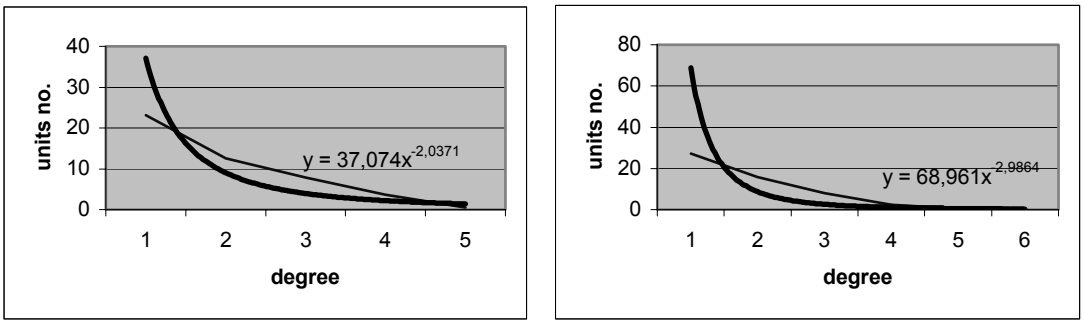

Figure 4a. Average degree distribution in GNG (two different input manifolds)

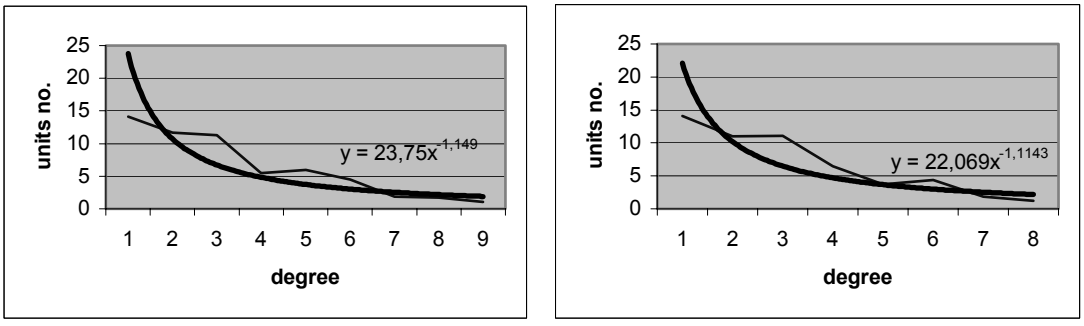

Figure 4b. Average degree distribution in ENG (first model, two different input manifolds)

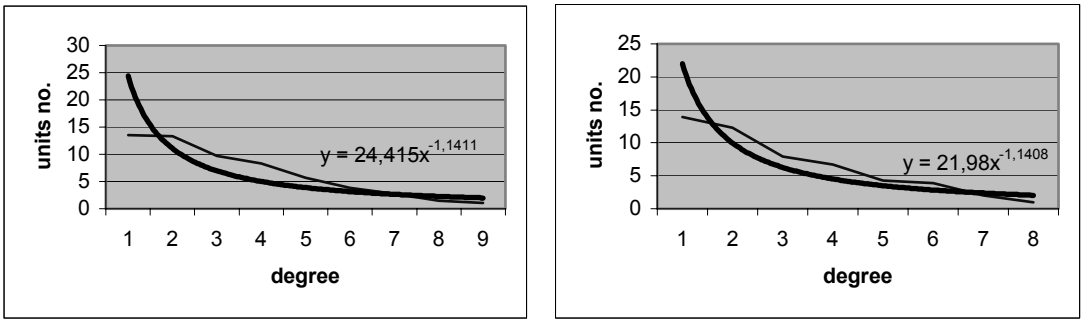

Figure 4c. Average degree distribution in ENG (second model, two different input manifolds)

In Tables 1 and 2 instead we have the average value of the two nets'structural parameters. We got such value by averaging the values of the parameters relative to 30 different nets of the same type and dimension, which has been trained by the same inputs.

The GNG get high average path length and low clustering coefficient, the ENG show short average path length and high clustering coefficient linked to the power law ruling the degree distribution, that's a confirmation of the scale-free features.

Table 1. Comparison of structural parameters (average values, first input manifold)

Parameter	Average path length	Clustering coefficient	Power law exponent
GNG	-	0.49	2.04
ENG (1st)	3.82	0.64	1.15
ENG (2nd)	3.92	0.63	1.14

Table 2. Comparison of structural parameters (average values, second input manifold)

Parameter	Average path length	Clustering coefficient	Power law exponent
GNG	6.4	0.42	2.98
ENG (1st)	3.61	0.58	1.11
ENG (2nd)	3.67	0.59	1.14

The two ENG models share the same structure, in both models they are the winners which create the most of links. They are the privileged units by which each node try to create a link. By making the probabilities also depending on the local D error (Second ENG Model), we obtain a structure more GNG-like, i.e. more gas-like. In fact the conditions to create a new link get much more restrictive, which thing consequently makes the interaction between any of the subset of units and the rest of the net decreasing. So the structure of links seems to extend more uniformly along the region where the inputs are defined, how it is shown in the 2b figure (more patent in the ring distribution of inputs).

In Figure 5 the dynamics of the populations of the two ENG models is represented. In the first model, the population size seems to converge at the final value equal to $0.72N_{max}$, so confirming Annunziato and Pizzuti experimental outcomes.

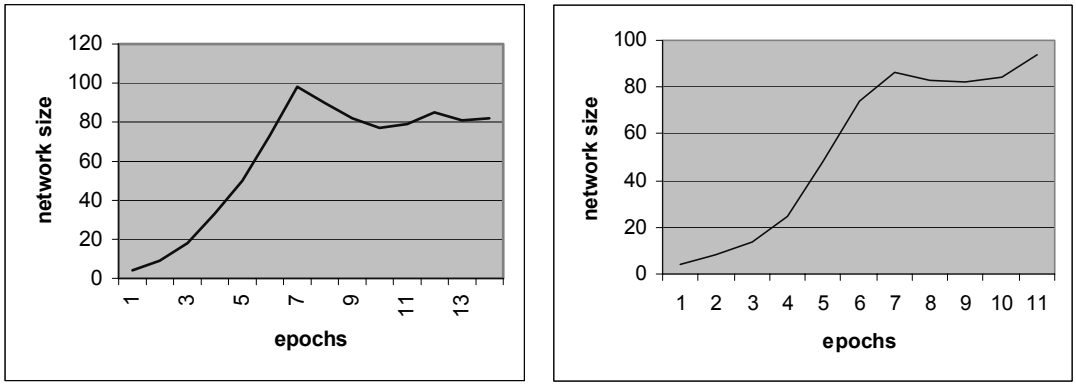

Figure 5. Network size evolution of the two ENG models (first input manifold)

Considering that *d* tends to gradually decrease during the training, how Figure 6 points out, the influence of the ($1-D_{min}/d$) factor tends instead to increase so reducing the effects of the negative effects of the [5] and [6] formulae. It justifies the sudden population increase at the training final steps in the second model.

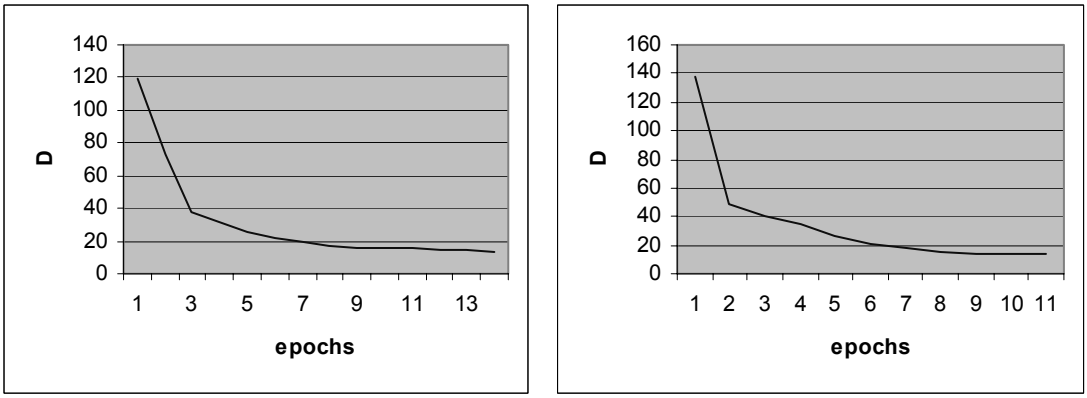

Figure 6. Average D error of the two ENG models (first input manifold)

The sudden increase of units can be mainly recorded around the winners (which get a low *d*). It means that at the final steps of training new units and links keep on growing around the winners, but not among the subgroups of units which became more and more isolated.

If we visualize the phase plane *(X(t),X(t+1))* (Figure 7), we can immediately notice that the punctiform characteristics of the attractor become more marked in the second model. It means that the system tends to mostly converge at a fixed final state. Such behaviour is just due to the scarce interaction among the groups of the net units at the final stages of training.

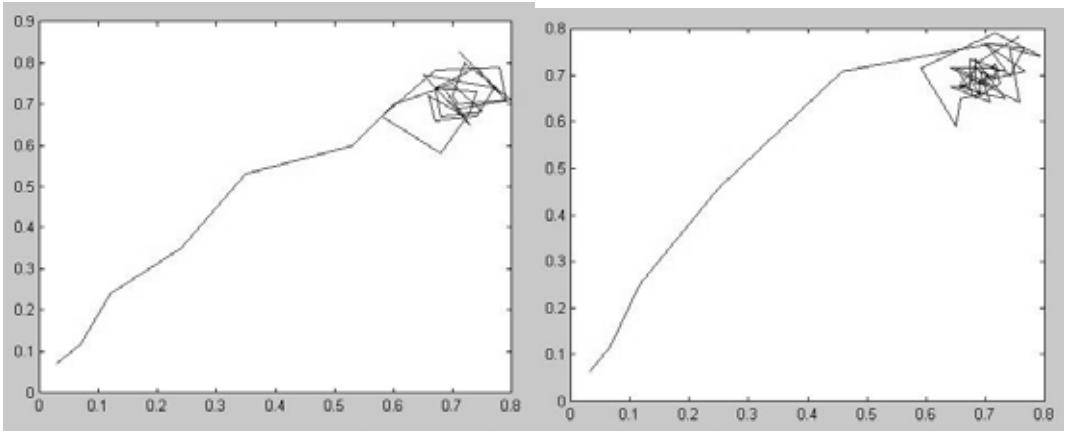

Figure 7. Population dynamics *(X(t),X(t+1))* of the two ENG models (first input manifold)

Conclusions: a physical picture – future developments

The algorithm here developed essentially represents a process of experimental selection analogous with the selection phase in Edelman's model (9, 10). The population evolution of nodes is led by an evolutive strategy which does not use the classical learning rules such as the Hebb law (11). The adopting of a discrete probabilistic model finds its motive in the recent experimental studies showing how groups of neuronal units get wide functional versatility in responding to different stimuli and, vice versa, same stimuli give rise to extremely diversified responses. It points out that a certain "random" component of the cerebral activity is laid on a much more radical level than "noise" and it need a class of models different from the deterministic "traditional"– linear and non – ones (12). The ENG algorithm lets groups of units to form, but does not integrate and synchronize their activity. So the system behaves like a gas made by "neuronal molecules" weakly interacting each others.

The problem of adopting a winner-takes-all strategy is that it is so favoured a process of information localizing, which is totally different from the Edelman dynamic nucleus' hypothesis. A dynamic nucleus is a process, not a specified net element and it is defined by neural interactions rather than by specific localization. In the ENG model is quite easy to get the formation of the dynamic nuclei by connecting selected winners by the diffusion on the activation signal.

Such solution favours the synchronization of the activities of the groups of the net units. In consonance with the "gas" metaphor, we can say that the activation signal "crystallizes" the system around the original scale-free structure, increasing the co-operative integration and the neural complexity essential to the autopoietic large-scale processes of the neural activity.

References

1. Kohonen T. Self-organized formation of topologically correct feature maps. Biol Cybernetics 1982;43:59-69.
2. Martinetz TM, Schultzen KJ. Topology representing networks. Neural Networks 1994:7(3);507-22.

3. Fritzke B. Growing cell structures – A self-organizing network for unsupervised and supervised learning. Neural Networks 1994;7(9):1441-60.
4. Delaunay B. Sur la sphere. Bullettin of the Academy of Sciences USSR 1934;7: 793-800.
5. Chialvo DR, Bak P. Learning from mistakes. Neuroscience 1999;90(4):1137-48.
6. Steyvers M, Tenenbaum J. The large-scale structure of semantic networks. Working draft submitted to Cognitive Science, 2001
7. Albert R, Barabasi A. Topology of evolving networks: local events and universality. Phys Rev Lett 2000;85:5234.
8. Annunziato M, Pizzuti S. Adaptive parametrization of evolutionary algorithms driven by reproduction and competition. In: Axer H, Jantzen J, Berks G (Ed.). Proceedings of ESIT 2000. Aachen, Germany: ESIT; 2000.
9. Edelman GM. Group selection and phasic reentrant signaling: a theory of higher brain function, In: Edelman GM, Mountcastle V (Ed.). The mindful brain. Cambridge: MIT Press; 1978. p. 51-100.
10. Edelman GM. Neural Darwinism: The Theory of Neuronal Group Selection, New York: Basic Books;1987
11. Martinetz TM. Competitive Hebbian learning rule forms perfectly topology preserving maps. In: Geilen P, Kappen C (Ed.). ICANN'93: International Conference on Artificial Neural Networks, Amsterdam: Springer; 1993. p. 427-34.
12. Zbilut JP. Unstable singularities and randomness. Amsterdam: Elsevier; 2004.

Short communication

3D MEASURES OF COMPLEXITY FOR THE ASSESSMENT OF COMPLEX TRABECULAR BONE STRUCTURES

Norbert Marwan (a), Peter Saparin (b), Wolfgang Gowin (b), Jürgen Kurths (a)
(a) Institute of Physics, University of Potsdam, Germany
(b) Charité Campus Benjamin Franklin, University Medicine Berlin, Germany

Introduction

For the assessment of bone stage (e.g. regarding different osteoporotic stages), usually the bone mineral density (BMD) is measured. However, this measurement does not contain any information about the structures inside the bone (Figure 1). Recent work emphasized the importance of analysing the structural changes of trabecular bone (1, 2). Different approaches for the study of trabecular bone were successfully introduced for 2D image analysis, as measures of complexity based on symbolic dynamics. The new available 3D bone images (μCT-data) challenge the development of new 3D measures of complexity, which are able to assess structural changes in trabecular bone. We consider here new developments of 3D measures based on spatial correlation and geometrical properties: Moran's I Index and Shape Index. Histomorphometrical measures are used for comparison with the "golden standard" of investigation of trabecular bone (3).

All of this is work in progress, which means that these measures may not yet be perfect and that the presented results are preliminary.

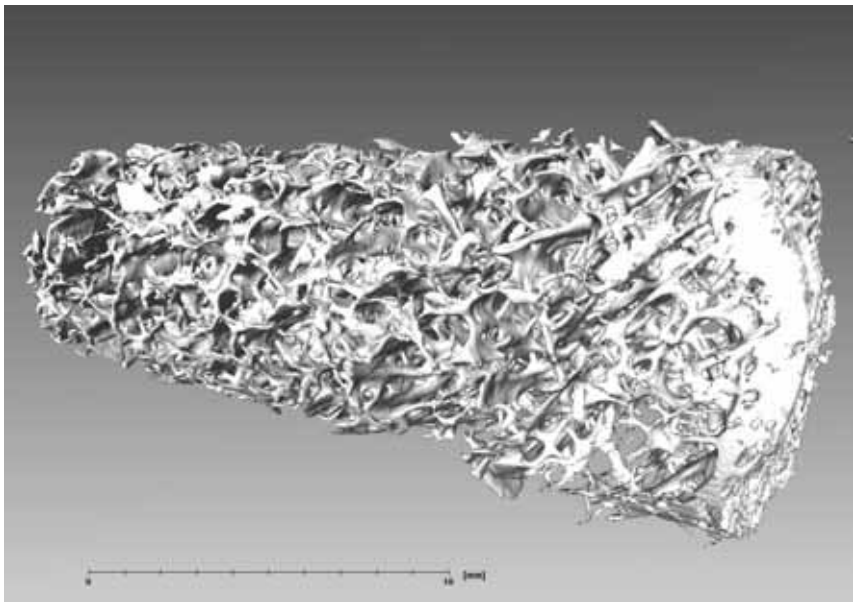

Figure 1. Complex structures in trabecular bone of proximal tibia (3D μCT scan of a biopsy)

Moran's *I* Index

Definition

The Moran test is a kind of a spatial auto-correlation test and was successfully applied in 2D image analysis (4, 5). The Moran's *I* Index for a two-dimensional image is defined by:

$$I = \frac{N}{S_0} \frac{\sum_{j=1}^{d_1 d_2} \sum_{i=1}^{d_1 d_2} \delta_{ij} (x_i - \bar{x})(x_j - \bar{x})}{\sum_{i=1}^{d_1 d_2} (x_i - \bar{x})^2},$$

where $d1$ and $d2$ are the geometric size of the image (columns and rows),
x_i is the value at the specified position,
$\bar{x}$ is the mean of the image,
$\delta_{ij} = 1$ if pixel i and j are adjacent and 0 otherwise,
$N=d_1 d_2$ is the total number of pixels and
$S_0 = \sum\sum \delta_{ij}$ is the number of contiguous pairs ($S_0 = 4d_1 d_2 - 3(d_1 + d_2) + 2$). Its values varies between –1 and +1 (from autocorrelation $I = -1$ to negative autocorrelation $I = +1$; if not correlated, the index will be zero).

For our purpose we have to extend the 2D-definition mentioned above to a 3D-definition:

$$I = \frac{N}{S_0} \frac{\sum_{j=1}^{d_1 d_2 d_3} \sum_{i=1}^{d_1 d_2 d_3} \delta_{ij} (x_i - \bar{x})(x_j - \bar{x})}{\sum_{i=1}^{d_1 d_2 d_3} (x_i - \bar{x})^2},$$

where S_0 is now $S_0 = 13 d_1 d_2 d_3 - 9(d_1 d_2 + d_2 d_3 + d_3 d_1) + 6(d_1 + d_2 + d_3) - 4$.

Pairs of contiguous neighbours must not be counted more than once. Therefore, the considered vicinity of a pixel is not a cube, but a geometric body as shown in Figure 2.

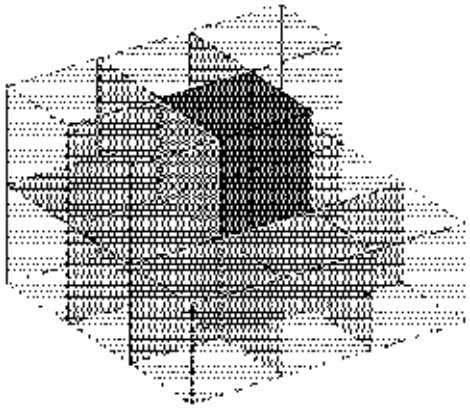

Figure 2. Contiguous neighbours (gray) of a voxel (darkgray) in 3D

A similar measure as the Moran's *I* Index is the Geary's *C* Index, which is an average of the variation $(x_i - x_j)^2$ between adjacent pixels.

This index is inversely related to Moran's *I* Index. However, Moran's *I* Index gives a more global indicator, whereas Geary's *C* coefficient is more sensitive to differences in small neighbourhoods.

In our case of bone and marrow pixels or voxels, these measures are related to an investigation of the interface between bone and marrow.

Moran's *I* Index of proximal tibia

Now we apply the Moran's Index to real μCT bone data gained from proximal tibia biopsies (1cm VOI used). First, we plot the Moran's Index in respect of BV/TV (Figure 3). Next, we plot this index over to the so-called node-terminus ratio, which is a histomorphometrical measure expressing the connectivity of the trabecular network. Whereas both figures reveal a dependence between these measures, the Moran's *I* Index correlates more significantly with the node-terminus ratio (lin.correlation is 0.65; with BV/TV is 0.54). The result of the Geary's *C* Index is similar (here not shown).

From these results we infer, that the measures based on spatial correlations are closely related with the connectivity of the trabecular network.

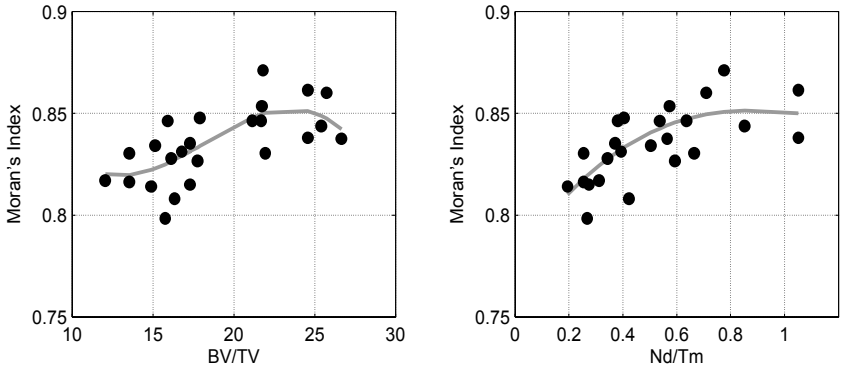

Figure 3. Morans's *I* Index over BV/TV and node-terminus ratio Nd/Tm

Shape Index

Definition

For an object with a given volume, the surface depends on its geometric shape: its surface is minimal for the shape of a sphere:

$$S_{sphere} = \sqrt[3]{36\pi V^2} = \text{minimal.}$$

Therefore, the ratio between the bone surface S_{bone} and the minimal surface S_{sphere}, is introduced:

$$SHI = \frac{S_{bone}}{S_{sphere}}.$$

Such a measure should be able to distinguish between shapes like plates and rods or angular and rounded objects.

This ratio can be computed within gliding boxes in order to get a distribution of this index, which can be further quantified, for instance by using average or entropy.

A brief note about the estimation of the surface and the volume of a discrete three-dimensional object: Our data consist of voxels of zero and one (one means bone and zero means marrow). The simplest approach would be to count the bone voxels for the volume and sum their surfaces. However, these are rather bad estimators for surface and volume – especially when we use an equation in order to compute the minimal surface. Therefore we use an iso-surface algorithm in order to estimate the bone surface and volume. Whereas the code for the iso-surface algorithm for surfaces is widely distributed, for instance for 3D visualization, the code for the volume estimation has not yet been available and was implemented in our group.

Shape Index of proximal tibia

First we are interested in the joint-distributions of the Shape Index and the found volume within small sliding boxes (box size 400µm) regarding different osteoporotic stages (Figure 4).

Due to the bone mass the main point of the distribution slips to higher bone volumes for higher BV/TV. But in the same time this main point moves towards smaller Shape Index values. For higher BV/TV or healthy bone, the distributions are more horizontal, whereas for osteoporotic bone the distributions are more vertical oriented. For the intermediate stage, the distributions seems to be smeared.

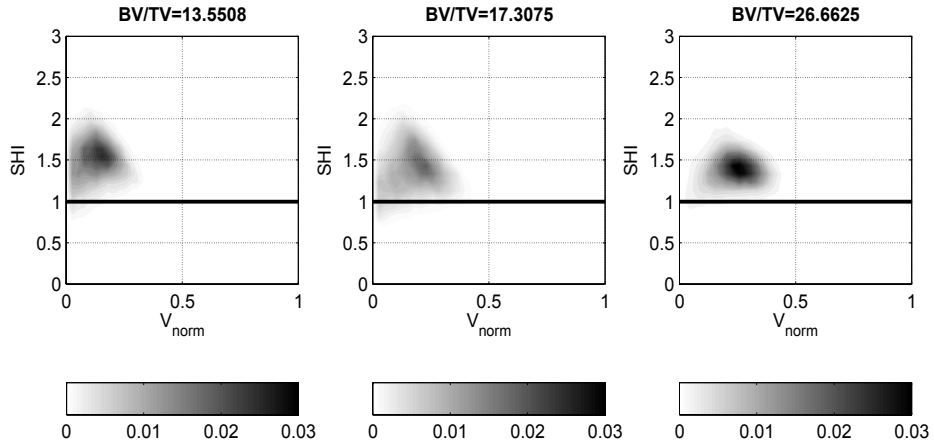

Figure 4. Joint distributions of shape index and bone volume for various osteoporotic stages

Whereas these remarks are only visual inspections of the distributions, these changes can be quantified with statistical measures (Figures 5, 6).

The mean of the shape index and the entropy of its distribution increase for decreasing BV/TV. However, the mean shape index correlates better with a histomorphometrical measure,

the node-terminus ratio, suggesting a correlation between the mean Shape Index and the connectivity. The entropy correlates well with another histomorphometrical measure – the trabecular plate separation. This parameter reveals the relationship between the shape of the distribution and the amount of parallel structures in the trabecular network.

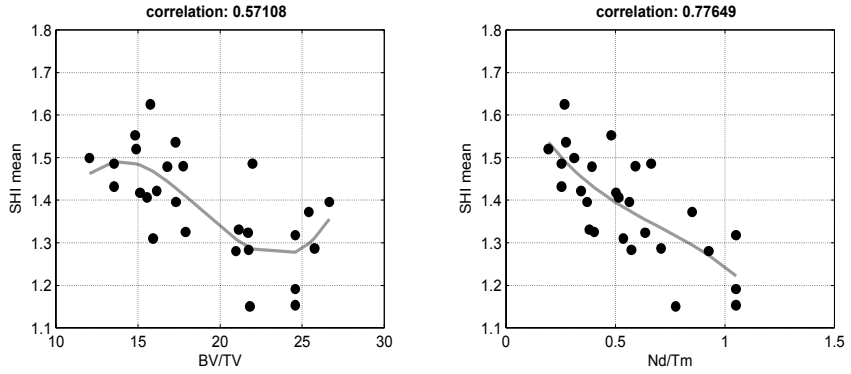

Figure 5. Mean shape as function of BV/TV and node-terminus ratio Nd/Tm

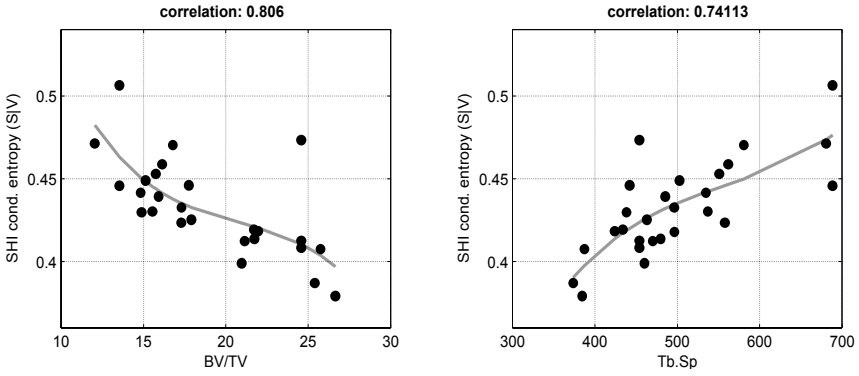

Figure 6. Entropy of Shape Index as function of BV/TV and trabecular plate separation Tb.Sp

Conclusions

In the presented work the well-known 2D measures of complexity Moran's *I* and Geary's *C* Index were successfully adopted to 3D. The Moran's *I* and Geary's *C* Index are related with the network connectivity.

Then a new 3D measure was introduced, which is called Shape Index and which uses simple geometrical features. The Shape Index is related with several histomorphometrical measures (connectivity, parallel plate model, star volume). At the moment this measure is our most promising candidate for the investigation of complex structures in trabecular bone.

Using the proposed measures we found significant changes in 3D bone architecture (connectivity, plate separation) at various stages of osteoporosis.

Acknowledgements

This work is supported by the ESA-Project AO-99-030 Bone 3D (contract #14592).

References

1. Guo XE, Kim CH. Mechanical consequence of trabecular bone loss and its treatment: a three-dimensional model simulation. Bone 2000;30(2):404-11.
2. Silva MJ, Gibson LJ. Modeling the mechanical behavior of vertebral trabecular bone: effects of age-related changes in microstructure. Bone 1997;21(2):191-9.
3. Thomsen JS, Ebbesen EN, Mosekilde Li. A new method of comprehensive static histomorphometry applied on human lumbar vertebral cancellous bone. Bone 2000;27(1):129-38.
4. Chuang K-S, Huang HK. Assessment of noise in a digital image using the joint-count statistic and the Moran test. Physics in Medicine and Biology 1992;37(2):357-69.
5. Chen T-J, Chuang K-S, Wu J, Chen SC, Hwang I-M, Jan M-L. A novel image quality index using Moran I statistics. Journal of Digital Imaging 2003;16(2):210-5.

Short communication

FINE-GRAINED DELAUNAY TRIANGULATION FOR THE SOLUTION OF DIFFUSION EQUATIONS IN CELLULAR CLUSTERS

Roberto Chignola (a), Edoardo Milotti (b)
(a) Dipartimento Scientifico e Tecnologico, Facoltà di Scienze Università di Verona and Istituto Nazionale di Fisica Nucleare, Sezione di Trieste, Verona, Italy
(b)Dipartimento di Fisica, Università di Udine and INFN, Sezione di Trieste, Udine, Italy

Introduction: tumor spheroids

A good understanding of the growth kinetics of tumors is essential to devise better and more effective therapeutic strategies (1). Direct observation *in vivo* of the growth kinetics is not always possible, and a particularly useful *in vitro* technique uses multicell spheroids. Experimental multicell spheroids have volumes that range from about 10-4 mm^3 to about 1 mm^3 and contain as many as 106 cells; they have a complexity which is intermediate between 2D cultures and tumors *in vivo* and display a growth kinetics that is very close to tumors *in vivo* (2, 3).

Since there is no angiogenesis and thus no point transport of nutrients and oxygen, the local environment plays a very important role in the growth of tumor spheroids; experimental observations show that:

- spheroids are layered, and are characterized by an external layer of proliferating cells, by a buried layer of quiescent cells, and by a necrotic core, which is made up of cells either starved or asphyxiated;
- there are strong, measurable oxygen and glucose gradients;
- the structure is not fixed but behaves like a high-viscosity fluid, with a convective transport of cells from the outer layers to the core (4, 5);
- the shape is mostly ball-like, but some spheroids develop fractal-like structures, like dendritic structures on the surface or holes in the bulk.

Multicells tumor spheroids thus act as a clean experimental setup that reproduces many microscopic features of tumors *in vivo*, and captures most of the complex non-linear interactions among cells and with the environment.

Unfortunately, accurate measurements on tumor spheroids need time spans of the order of a couple of months, and environmental conditions are neither very well controllable nor reproducible, and for this reason we are now developing a novel simulator of tumor spheroid growth. Our final aim is a full-fledged in silico simulator of the growth and proliferation of tumor cells, a sort of virtual laboratory where we may experiment at will and have access to all growth variables, and here we describe one important component of this simulator, the diffusion of nutrients, oxygen and other chemicals in the multicell cluster.

Simulator structure and role of diffusion in cell clusters

The simulator structure has already been described in (6) and is shown schematically in Figure 1. The main loop of the simulator includes the following steps:

- *Triangulation*. This step establishes the proximity relations among cells and is essential to reduce the computational complexity to ~ O(N).
- *Diffusion*. The Delaunay triangulation – see for example (7) – performed in the previous step is used as a backbone for diffusion; the dual Voronoi construct is also needed (8). This step is discussed at length in the following sections.
- *Mechanical evolution*. The cell cluster is held together by cellular adhesion forces and is subject to mechanical stress due to volume changes of individual cells as they grow and proliferate, or just shrink and dissolve after necrosis.
- *State evolution*. As they absorb nutrients from the nourishing medium, cells grow and proliferate: this step advances the internal cell clock according to a rather detailed model of cell metabolism (9).
- *Mitosis*. Cells divide and generate new individuals. This step redefines the cluster structure, and together with the mechanical evolution step it sets the need of a new triangulation: the loop starts again until a stop condition is reached.

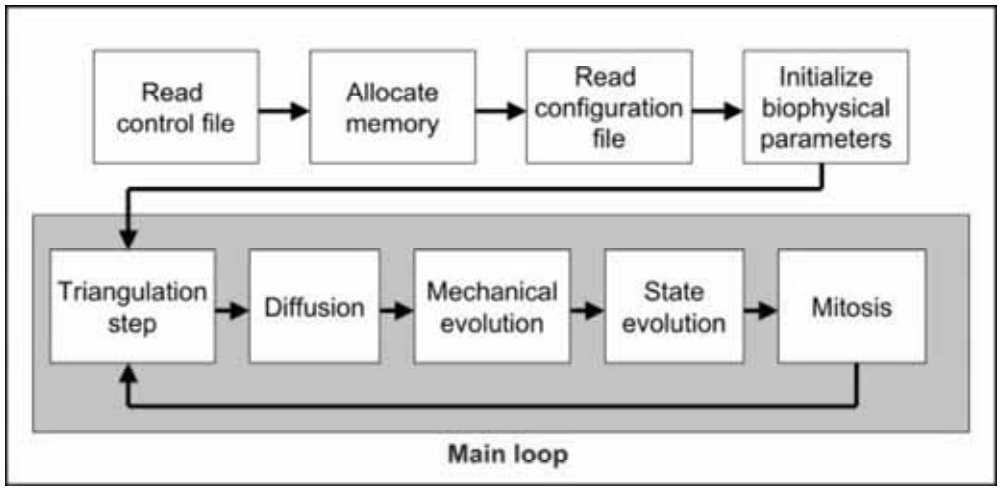

Figure 1. Schematic structure of the simulation program

Here we see that the evolution as a whole is indeed a very complex nonlinear process: growth is influenced by diffusion, growth changes the cluster structure and in turn this changes the way chemicals diffuse in the cluster. The different nutrients interact in the metabolic step and change absorption and consumption and this determines both cell growth and diffusion to neighbouring cells.

One additional detail conjures to make diffusion even more nonlinear than it might appear at first sight; while in most physical contexts one may safely assume the validity of Fick's law:

$$\mathbf{J} = -D\nabla\rho$$

where $\boldsymbol{J}$ is the diffusion current, ρ is the concentration and D is the diffusion coefficient, this is not true for the great majority of molecules in cell biology. Indeed diffusion is in most cases a

complex process, mediated by transporters, specialized proteins that act as carriers across the cell membrane and the diffusion current is described by a Michaelis-Menten equation (10):

$$J = J_{\max} \frac{\Delta\rho}{k_m + \Delta\rho}$$

where J_{max} is the maximum diffusion current, $\Delta\rho$ is the concentration difference on the two sides of the cell membrane, and k_m is a kinetic coefficient which depends on transporter concentration and activity; this means that diffusion can be described correctly only at cell level, and that averaged mathematical descriptions necessarily miss this important point. The Michaelis-Menten diffusion kinetics is equivalent to the standard kinetics at low concentration difference (with $D = J_{\max}\Delta x / k_m$ where Δx is the thickness of the diffusion medium), but it starkly deviates from the linear behaviour as it saturates at large concentration differences.

Complexity estimates

A time-dependent diffusion problem has an associated diffusion equation:

$$\frac{\partial\rho}{\partial t} = -D\nabla^2\rho$$

which in general requires both time and space integration, i.e. an integration over 4 variables. However the diffusion problem can be simplified somewhat if diffusion is so fast that equilibrium is promptly reached and only the space boundary conditions matter: this is indeed the case in small cell clusters.

Take any chemical species that diffuses from the outside to the inside of a cell and assume that its diffusion constant in the membrane is much smaller than the diffusion constant in the cytoplasm, so that its concentration is nearly uniform inside the cell. Now let ρ_{in} and ρ_{out} be the concentrations inside and outside the cell, then if we assume that these concentrations are so low that we can use the standard Fick's law, the diffusion current from the outside to the inside of a membrane is:

$$J = D_m \frac{\rho_{out} - \rho_{in}}{h}$$

where h is the membrane thickness and D_m is the diffusion coefficient in the membrane. If both diffusion and absorption are present, and we let λ be the absorption rate per unit volume, S the cell surface, and V is the cell volume, we obtain the differential formula:

$$\frac{d\rho_{in}}{dt} = D_m \frac{\rho_{out} - \rho_{in}}{h} \frac{S}{V} - \lambda\rho_{in}$$

so that the time constant associated to the exponential transient is $\tau^{-1} = \left(D_m S / hV\right) + \lambda$. For an approximately spherical cell we have $S/V \approx 3/r$, where r is the cell radius, and then $\tau^{-1} \approx \left(3D_m / hr\right) + \lambda$. In the case of oxygen we take the standard values given in (9), and we find that the time constant for simple absorption is $\tau_A \approx 10^7 s$, while when we turn on diffusion this changes to $\tau_{AD} \approx 10^{-2} s$. Since mechanical relaxation of the cell cluster has a time scale of the order of 1-10 s, we see that the diffusion equation for oxygen can safely be solved assuming equilibrium, i.e. $\partial\rho/\partial t \approx 0$; the same considerations hold for other chemicals diffusing in the

cluster. At this point we are left with a Laplace equation which can be solved with a host of different numerical methods (11), and if we take a grid method like that used in the standard relaxation algorithm we can make the following estimate: we need a containment volume which must be larger than a maximum size spheroid, let's say a cube with a 4 mm side, then if we assume a spatial step size of 1μm (approximately one fifth of a cell diameter) there are $6.4 \cdot 10^{10}$ lattice nodes. If we take a 4 byte diffusion variable, this corresponds to a rather large memory of about 256 GB. Moreover if we take a modest 1000 relaxation iterations per lattice node, the algorithm performs about 10^{15} operations and if we run the program on a single 10 GHz processor, the solution of the relaxation algorithm takes (at each time step which is about 1 s of simulated time) about 10^5 s. Even with a smarter, adaptive grid, this cannot be improved by more than about a couple of orders of magnitude. This is a bit too much even if we move the simulation program to a computer cluster, and we need a faster and less memory-consuming algorithm.

Diffusion on the triangulation graphs

The key to a better and faster algorithm is the observation that diffusion for most chemical species is much faster in cytoplasm than in the membrane (about 100 times faster). Therefore we can assume the concentration of any chemical to be approximately uniform inside the cell, and we can consider diffusion over the discrete graph defined by the Delaunay triangulation of the cell cluster.

Solving the diffusion equation on this graph rather than on a lattice approximation of the environment plus cell cluster leads to a dramatic speedup: a 10^6 cell spheroid sorrounded by about 10^7 environmental "pseudocells" (comparatively large regions of the surrounding environment where we assume a uniform concentration), with a total of about 10^7 cells+pseudocells and 1000 relaxation steps per cell (or pseudocell), takes about 10^{10} relaxation steps, which correspond to about 1 s on a 10 GHz processor. The memory space is likewise much smaller, now we need a more modest 40 GB memory. Figure 2 shows a triangulation of a small cluster of cells+pseudocells, and the result of a diffusion calculation.

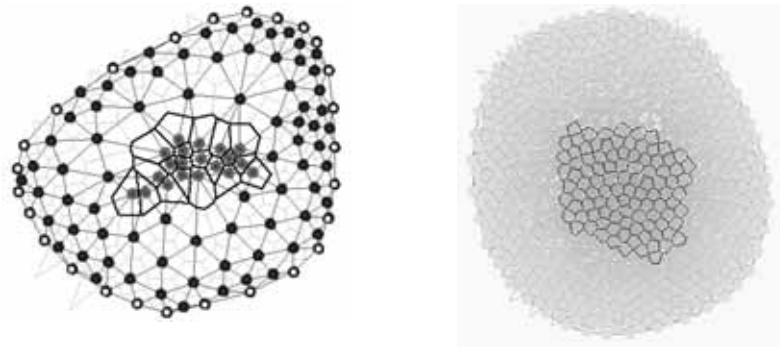

a. **b.**

Figure 2. a) Example of Delaunay triangulation (black segments) of a cell cluster. b) Diffusion calculation

In Panel a) an example of Delaunay triangulation is reported. The boundaries of the interior Voronoy regions are also shown (light gray segments). The black circles are the centers of "pseudocells" that represent the environment. The gray circles are the cell centers. The boundaries of Voronoy regions that contain cells are also shown (thick black segments). In Panel b) are reported the result of diffusion calculation on a small cell cluster plus its environment (gray level corresponds to concentration).

This numerical method is not just faster, it also makes more sense than a lattice approximation: indeed now it is possible to associate to each lattice node the correct Michaelis-Menten kinetics, and it is also possible to introduce complex feedbacks (the concentration of one chemical species influences the diffusion parameters of many other chemicals, and this can be calculate with a straightforward extension of the algorithm). In this way the algorithm captures phenomena associated to cell-sized environmental fluctuations; this would not be important in a linear world, but may greatly change the outcome of the calculations in a system with a well-developed nonlinearity such as a cell cluster. We believe that this may lead ultimately to a better understanding of tumor spheroids and microsized real tumors.

References

1. Norton L. Kinetic concepts in the systemic drug therapy of breast cancer. Semin Oncol 1999;26:11-20.
2. Sutherland RM. Cell and environment interactions in tumor microregions: The multicell spheroid model. Science 1988;240:177-84.
3. Chignola R, et al. Forecasting the growth of multicell tumour spheroids: implications for the dynamic growth of solid tumours. Cell Prolif 2000;33:219-29.
4. McElwain DL and Pettet GJ. Cell migration in multicell spheroids: swimming against the tide. Bull Math Biol 1993;55:655-74.
5. Pettet GJ. The migration of cells in multicell tumor spheroids. Bull Math Bio 2001;63:231-57.
6. Chignola R, Milotti E. Numerical simulation of tumor spheroid dynamics. Physica A 2004;338:261-6.
7. O'Rourke J. Computational geometry in C, New York: Cambridge University Press;1993.
8. Aurenhammer F. Voronoy diagrams – A survey of a fundamental geometric data structure. ACM Comp Surveys 1991;23:345-405.
9. Chignola R, Milotti E. A phenomenological approach to the simulation of metabolism and proliferation stochastic model of metabolism and proliferation dynamics of large tumor cell populations. Phys Biol 2005;2:8-22.
10. Alberts B, Johnson A, Lewis J, Martin R, Roberts K, Walker P. Molecular biology of the cell. 4th ed. New York: Garland Science; 2002.
11. Press WH, Teukolsky SA, Vetterling WT, Flannery BP. C: the art of scientific computing. 2nd ed. New York: Cambridge University Press; 1992.

Short communication

REALITY GENERATION: THE FRACTAL TEMPORAL PERSPECTIVE

Susie Vrobel
The Institute for Fractal Research, Kassel, Germany

Introduction

This paper describes the significance which the structure of the observer's Now can be assigned in time series analysis and ways of modifying the observer's interface.

Time series analysis is usually carried out in retrospect, i.e., we look at a string of data or a plotted graph well after that data was gathered or the event was observed. Direct observation in (almost) real time is usually limited to a succession of temporal events on one Level Of Description (LOD): We cannot detect temporal scaling, e.g., in the self-similar patterns of fore- main- and aftershocks in seismographic data in real time (1). Scaling temporal patterns also occur throughout the living world (2) and are therefore a promising candidate for a differentiated time series analysis which takes account of the interfacial structure of the observer.

Direct, real-time observation takes place in the observer's interface with the world – the Now. This fleeting moment he experiences as a whole, meaningful entity is his only window to the world. So, if an observer wanted to directly observe a temporal scaling pattern in real time – how would this observer's Now need to be structured?

The nested structure of the Now

The German philosopher Edmund Husserl (3) describes the structure of the Now in a phenomenological approach: When we listen to a tune, we hear a succession of musical notes. But we do not perceive simply a succession of unrelated notes – we are able to hear a tune. How come?

We internally connect the note we have just heard with the present one and the tone we anticipate to follow it. Through repeated acts of remembering a tone (retension) and anticipating the next tone (protension) within the memory of the present (Now), we create and are able to perceive a nested temporal pattern within the Now. Thus, the observer creates a simultaneity of retension, the consciousness of the present and protension, all within the Now.

Without memory of the preceding note and no anticipation of the next one, an observer would only perceive a succession of isolated, unrelated notes. But as we are able to perceive a tune and not just a succession of isolated notes, we must assume the Now to provide for both succession and simultaneity.

Succession and simultaneity within the Now generate a nested, fractal structure. It is this extended structure of the Now we have to assume to explain our ability to perceive a tune or any other time series as a meaningful entity.

Let us therefore assume the structure of the Now to be a nested one which contains not only successive events but also temporarily overlapping ones which add the dimension of simultaneity to that of succession. This simultaneity creates a framework time which groups otherwise isolated events into a before and after relation. Without simultaneity, no before and after relations, no related succession, would be possible.

The observer does not generate time, but through his choice of nestings, he generates the structure of the Now.

Fractal time: fractal and non-fractal observers

In my Theory of Fractal Time (4), I have taken account of the observer's nested Now by differentiating between:

- Δt_{length}
  the length of time, which is the number of incompatible temporal extensions in a time series; it describes the succession of events on one LOD.

- Δt_{depth}
  the depth of time, which is the number of compatible temporal extensions in a time series and, therefore, the number of LODs; it reflects simultaneity and provides the framework time which allows us to structure events iṇ Δt_{length}.
  NB: Withouṭ Δt_{depth}, there is no Δt_{length}!

- $\Delta t_{density}$
  the fractal dimension of time, which describes the temporal density of a time series.

A non-fractal observer, who can perceive only isolated notes in a tune or isolated events in a time series, would only be able to observe successive events. Simultaneity and memory formation would be unknown to him, as he would not be able to generate a Temporal Fractal Perspective through continuous nesting. He would live in an eternal succession of unconnected Nows, in which no learning or reflection could take place.

A fractal observer, on the other hand, is able to observe events on a number of LODs. This allows him to generate a Temporal Fractal Perspective, observing succession and simultaneity of events directly, in real time (5).

The Now is an interface between the observer and the world (6). Apart from individuals who are impaired, e.g., by a neurodegenerative disease, we are all fractal observers and see both succession and simultaneity.

Our awareness of this nested perspective, however, appears to be rather limited. It is only when we encounter tangled hierarchies or simply curiosities that the existence of both nested and non-nested perspectives may dawn on us. One such curiosity is the name of the yesterday, today, tomorrow shrub. Its blossoms change within days from deep violet-blue to a light blue and finally to white. As this development is staggered, the shrub always displays blossoms of all three colours. The person who gave the plant its name seems to have looked at it on at least two LODs: on both the plant as a whole, as well as at its individual blossoms, that is, through a fractal interface, a nested Now.

A non-fractal observer who looks at the blossoms of the shrub and their individual development through the successive colours on only one LOD would not come up with a name like yesterday, today, tomorrow. Only a nested interface providing for both simultaneity and succession can generate a Temporal Fractal Perspective, which makes someone refer to the past, the present and the future in the Now.

Temporal natural constraints: the Prime

An observer with a Temporal Fractal Perspective (TFP) may identify scaling structures, i.e., structures which appear on various nested LODs. Scaling is usually a limited property, i.e., there is an "outer" LOD, which hosts the structure covering the largest interval in Δt_{length} and an "inner" LOD with the structure covering the shortest interval in Δt_{length}.

Within such a self-similar domain, we can describe a limitation on the structurability of time by the observer, a Temporal Natural Constraint (TNC): the Prime.

The Prime is the most basic temporal unit within a scaling system - the smallest unit of time which contains the structure recurring on all LODs. It is extended but indivisible in the sense that it cannot contain further nestings.

These smallest, indivisible units of time allow us to relate the nested LODs to each other through their recurring structure. If we set the recurring structure of the Prime as a constant, this Prime Structure Constant provides a translation tool between the LODs of the self-similar domain (7).

Condensation

If the Prime of a temporal structure is set as a constant, the lengths of time Δt_{length}, are condensed on all LODs, to varying degrees. Large intervals of Δt_{length} shrink to a fraction of their original temporal extension. (Imagine superimposing the Prime structures of all LODs – the yardsticks of the various LODs would be condensed.) Condensation occurs for fractal observers only.

For a fractal observer, this condensation generates an extension of the Now, as previously large intervals of Δt_{length} shrink to the extension of the Prime, that smallest, indivisible unit of time.

The Temporal Fractal Perspective is generated by a fractal observer whose Now is differentiated by nested LODs with self-similar structures. As a fractal observer can make out correlations between both successive and simultaneous events in real time, he can, after identifying a Prime, set it as a constant. After the structure of his interface (his Now) has been changed in this way, it now contains the Prime Structure Constant, which enables him to observe a condensed version of originally long intervals in Δt_{length}.

The temporal fractal interface

The Now is our only access to the world. It is the interface between the observer and the system under observation. Non-fractal and fractal observers have generated differently structured Nows, i.e., differently structured interfaces.

As a result, non-fractal and fractal observers obtain different observational results when analyzing a time series. Therefore, we have to take account of the structure of the observer's Now (interface) when we analyse a time series.

"Conventional" retrospect Times Series Analysis can be regarded as a special case of a more general method of Times Series Analysis which differentiates between various structures of the observer's interfacial structures.

In general, we can assume temporal extensions of Δt_{length} of an event to vary, with their individual extensions depending on the observer's Temporal Fractal Perspective.

If two or more observers agreed to modify their interfaces by generating the same number of nested LODs containing the same Prime Structure Constant, the Primes of these interfaces would not only be translation tools between LODs, but also between the interfaces (Nows) of individuals. Shared Primes may also be the result of a selection process. In this case, we should look out for universal Primes.

Universal TNCs

Universal Primes or other TNCs are very probably all around us, rendering possible successful communication as the result of a selection effect. They should be accessible to and shared by a number of fractal observers (if not to all). If this is so, it is likely that we are familiar with them but do not recognize them as Primes.

TNCs need not exhaust themselves in Primes, but could also take the shape of a transition rule (from one LOD to the next). Candidates for such transition rules could be Δtdepth-analogues to known constants which refer to Δt_{length}, e.g., a Δt_{depth}-analogue to Feigenbaum's number (8).

Universal TNCs could reveal "objective" distortions in time (in Δt_{length}), if an experiment showed the existence of a temporal illusion as a result of our Temporal Fractal Perspective. This would require a comparison of observational results of fractal and non-fractal observers.

The observer's role: reality generation

Whether or not there are universal TNCs, individual Temporal Fractal Perspectives can be modified by altering the number of LODs available to the observer (9). This is achieved by means of nesting and de-nesting: Nesting involves the generation of further LODs to increase Δt_{depth}. It further differentiates the observer's Temporal Fractal Perspective. De-nesting takes place when LODs are erased from the observer's Now. An individual left with only one LOD lives in an eternal succession of unconnected, unrelated Nows.

The increasing influence of the observer in the evolving paradigms of time could be shown to start by the replacing of Newtonian absolute time by Einstein's relative concept of time, which allows for observer frames.

Next, quantum mechanics suggests that there is no such thing as an independent observer of reality. The observer or the measuring device participates in the generation of reality.

Rössler's Micro-constructivism (10) introduces an observer-world interface: the Now. As the observer cannot be taken out of the objective structure of the world he wishes to observe, we have to take account of his internal microscopic movements, which alter his interface, his Now. Only a super-observer located outside the system could perceive it without the interfacial distortions people within the system have to put up with. But observers who are part of the system they wish to observe face a Gödel-limit. It is a Strange Loop in Hofstadter's sense (11).

We may, however, modify the structures of our Nows, our interfaces, by nesting or de-nesting, and by extending our Nows by means of condensation.

To conclude, every Time Series Analysis requires a case differentiation in which we state what type of observer is assumed. This is essential, as fractal and non-fractal observers generate very different realities.

References

1. Kagan YY, Knopoff L. Stochastic synthesis of earthquake catalogs. Geophys Res 1981;l 86:B4.
2. Olsen LF, Degn H, Holden AV (Ed.). Chaos in biological systems. London: Plenum Press; 1987. (NATO ASI Series).
3. Husserl E. Vorlesungen zur Phänomenologie des inneren Zeitbewußtseins. (Lectures on the phenomenology of the inner consciousness of time). Tübingen: Niemeyer; 1980 - First published in 1928
4. Vrobel S. Fractal time. Houston: The Institute for Advanced Interdisciplinary Research; 1998.
5. Vrobel S. Fractal time and nested detectors. In: Blackledge JM, Foxon B, Michailkov S (Ed.). Proceedings of the First IMA Conference on Fractal Geometry: Mathematical Techniques, Algorithms and Applications. Leicester, U.K.: DeMontfort University; 2004.
6. Rössler OE. Intra-Observer Chaos: hidden root of quantum mechanics?, In: el Naschie MS, Rössler OE, Prigogine I (Ed.). Quantum Mechanics, Diffusion and Chaotic Fractals, Oxford, England: Pergamon Elsevier Science; 1995.
7. Vrobel S. How to make nature blush: on the construction of a fractal temporal interface. In: Broomhead DS, Luchinskaya EA, McCLintock PVE, Mullin T (Ed.). Stochastics and chaotic dynamics in the lakes. Stochaos, New York: AIP (American Institute of Physics); 2000. p. 557-6.
8. Vrobel S. Fractal time and the gift of natural constraints. Annals of the New York Academy of Sciences 1999;879:172-9.
9. Vrobel S. Ice cubes and hot water bottles, fractals. An interdisciplinary journal on the complex geometry of nature. Singapore: World Scientific; 1997, 5(1):145-51.
10. Rössler OE. Endophysics. Singapore: World Scientific; 1998.
11. Hofstadter DR. Gödel, Escher, Bach - An eternal golden braid. New York: Vintage Books; 1980.

Ecological and environmental issues

Lecture

FUNCTIONAL AND STRUCTURAL PROPERTIES OF HEMOGLOBINS FROM ATLANTIC COD (*GADUS MORHUA L.*) POPULATIONS FROM THE SOUTHERN PART OF THE NORTH SEA, THE BELT SEA, AND THE BALTIC SEA

Ole Brix, Atle Torbjørnsen Nedenes, Bengt Berdal
Department of Biology, University of Bergen, Norway

Introduction

Fish may in their natural environment be exposed to great physical and chemical variations. Fluctuations in ambient hydrographical properties affect not only oxygen availability but also oxygen demand and the oxygen binding properties of the hemoglobins (1). In order to cope with these challenges, fish depend on a flexible and effective gas transporting system based on the principle of ligand-linked conformational changes in tetrameric hemoglobins to ensure an adequate oxygen supply.

In mammalian hemoglobins the tetrameric structure is based on identical and symmetrical $\alpha\beta$ dimers, while in fish tetramers we find unsymmetrical combinations with great variations in α and β monomers (2-4). In contrast to most mammals and birds fish often display hemoglobin multiplicity (iso-hemoglobins) and some fish in the Arctic even lack hemoglobins (5, 4). In addition some species like the Atlantic cod (*Gadus morhua L.*) express polymorph hemoglobins. Atlantic cod is physiologically adapted to the temperate and arctic regions of the North Atlantic, including the North Sea and its adjoining seas (6). The hemoglobin polymorphism of Atlantic cod consist of two main alleles *HbI*1* and *HbI*2*. These can express two homozygote phenotypes labeled *HbI*1/1* and *HbI*2/2*, in addition to a heterozygote *HbI*1/2* (7). Each phenotype consists of 2-5 main iso-hemoglobin components (8). Throughout the geographical range the phenotypes are subject to heterogeneous distribution. The *HbI*1* allele is most common in the southern North Sea, reaching 70% in the British channel. From this centre, the frequency gradually declines to below 10% at the western, northern, and eastern borders of distribution (9). *HbI*2* seem dominant in regions characterized by colder temperatures. It has been suggested that the observed distribution pattern may be governed by the differences in hemoglobin functional properties between phenotypes in relation to the variations in environmental factors, like temperature (10-12). Furthermore, oxygen-binding properties and the iso-hemoglobin ratio are significantly altered in response to long-term temperature acclimation (12). Phenotype *HbI*2/2*, acclimated to cold-water (4 ºC), is characterized by a general increase in oxygen binding performance compared to acclimation at 12 ºC. It appears that phenotype *HbI*1/1* is less affected by acclimation to these two temperatures, retaining a lower overall oxygen affinity (12).

It has previously been shown that cod may regulate their metabolic state by actively seeking colder water layers with more favorable oxygen content and preferred salinity levels (13). Petersen and Steffensen (14) demonstrated that *HbI*2/2* cod preferred lower temperatures

(8.2°C) than *HbI*1/1* cod (15.4 °C) which further underlines the suggestion that the observed distribution pattern may be governed by the differences in hemoglobin functional properties between phenotypes in relation to the variations in environmental factors.

However, optimal hydrographical conditions are rarely available and the fish has to compromise. Ecological parameters, like for instance food access and spawning migrations, may limit the freedom to remain at the most favorable horizontal and vertical position in the water. If exposed to reduced O_2 availability over time, the fish can experience reduction in growth, condition factor, and activity level (15, 16). Under such conditions, the fish may respond by elevating the blood O_2-carrying capacity (i) and by adjusting the hemoglobin-O_2 affinity (ii) (17). The first of these two strategies requires an increase in the number of red blood cells (erythropoesis) and thus increases the metabolic cost in production and circulation of the cells (18). The second possibility involves regulation of ligands that restrain oxygen affinity (19). When oxygen becomes a limiting factor, the fish will produce less ATP, thus causing the hemoglobin-O_2 affinity to increase. This method is observed as a quick response to oxygen demand and hypoxia, but since organic phosphates also work as energy carrying molecules in the body, the lowering of the phosphate pool may imply reduced energy transportation potential within the fish. It is questioned whether this adjustment could be sustainable and productive over longer periods.

Though the southern part of the North Sea, the Belt Sea and the Baltic Sea are located relative close to one another, significantly differences exists both with respect to hydrographical properties and to the distribution of Atlantic cod hemoglobin phenotypes (20, 21).

In the present study, we have investigated the oxygen binding properties of hemoglobin's from wild cod populations as well as ecological and environmental key parameters from these areas in order to understand how environmental factors may influence the distribution pattern of Atlantic cod.

Material and methods

The material used in this study was collected during a two cruises in February (southern North Sea) and April 1999 (Belt Sea and Baltic Sea), onboard the research vessel Heinche (Helgoland). This cruise was a joint project between University of Bergen, Norway and the Alfred Wegener Institute in Bremerhaven, Germany.

Sampling sites

The material for this study was collected within four sampling areas referred to as White Bank, Kiel Bay, Bornholm and Gotland Deep (Figure 1). The Figure shows the locations of the four sampling sites. Spawning areas (shaded) are included to illustrate major distribution areas of cod in the Belt and Baltic region: Baltic cod - East of Bornholm (22) and Belt Sea cod - West of Bornholm (23). Belt and Baltic cod mingle in the transition area marked on the map. These areas were of particular interest because of distinct phenotype frequencies and hydrographical conditions (20). On the White Bank the mean GPS-position was centered at 55°12.05' N and 06°22.42' E based upon 69 stations (STDEV was 04.66' N and 04.46' E, respectively).

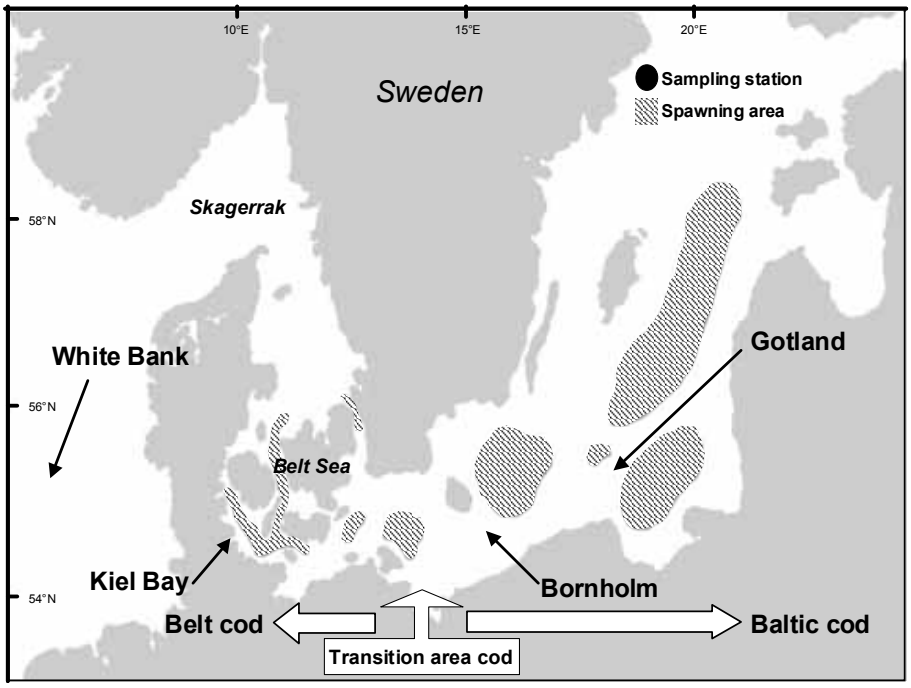

Figure 1. Cod sampling sites

Hydrographical analysis

The following hydrographical data were collected from 30 of the 46 stations trawled in the Belt Sea and the Baltic Sea, and 69 stations on the White Bank (North Sea): Depth, temperature, salinity, and oxygen percentage.

A Current Temperature Depth (CTD) probe (probe ECO056, ME – Meerestechnik – Elektronik) was undertaken, using Multipar 4.4 software, measuring depth in pressure with an accuracy of 0.1 dbar. The probe measured all hydrographical values four times pr. second. Temperature, salinity and oxygen were measured with a resolution of two decimals.

The Multipar software had a depth registration limit of 100 dbar. Depth and surface-temperature was additionally measured with a stationary echo sounder/thermometer. The hydrographical profile for each station was calculated from the total average of all CTD measures (pr. area) rounded down to whole dbar. Average depth was calculated from pooled CTD and echo sounder measures.

Fishing procedure

The cod was collected using a small meshed bottom trawl. The trawl was rigged to collect fish within a vertical range of 5 meters from the sea ground. All trawling sessions lasted 30 minutes, with a speed between 2.5-4.0 knots. Trawling was conducted between 6:00 am and 8:00 pm. For a detailed overview of the material see Table 1.

Table 1. Sampling sites and material collected in February and April 1999

Sampling dates	Area of capture	No. of trawling stations	No. of fish	No. of fish phenotyped	No. of fish O2 analyzed	No. of CTD measurements
9-15.02	White Bank	62	324	279	23	16
12/19/21.04	Kiel Bay	11	381	194	16	9
13-14.04	Bornholm	10	322	149	2	7
15-17.04	Gotland	25	169	152	2	14
Total		**108**	**1196**	**774**	**43**	**46**

Qualitative measures on cod

The following parameters were registered for all fish: total length and weight, sex, weight of gonads, liver, and fullness of gut. The weight of each individual and the abdominal organs were measured to ± 1 gram, while the total length was measured from the snout to the tip of the caudal fork rounded down to the closest cm (24). The condition factor K, was calculated for all phenotyped fish (equation [4]) (25). Stomach contents have been subtracted from the total weight of the fish.

Blood sampling

Cod exceeding 20 cm in length were randomly selected for blood sampling. Specimens below this size were not used due to the small blood volumes. *Aorta ventralis* of each fish was cut and blood was collected from the pericardial chamber with plastic Pasteur pipettes. Approximately 1.5 ml of blood from each fish was carried forward to heparinized 1.8 ml Eppendorf-tubes on ice. Samples were stored in a refrigerator at 4-6 °C, for maximum 24 hours before preparation.

Electrophoresis

A 0.1 ml fraction of each blood sample was isolated in an Eppendorf tube and thereafter centrifuged for 3 minutes at 14000 rpm in a 4 °C cooled centrifuge (Eppendorf 5410). The supernatant was removed and one drop of distilled water was added to lyse the erythrocytes by osmosis. Hemolysat was absorbed into pieces of filter paper before application to agar and polyacrylamid gels for determination of phenotype.

Phenotype analyses were carried out using a flat bed agar gel system described by (7, 26). The isoelectric focusing (IEF) method was prepared according to (27). Both agar and isoelectric focusing gels were stained in Quick stain (Brilliant blue G in perchloric acid) for 0.5 - 2 hours, and de-stained overnight in a solution of 14% acetic acid and 7% methanol (28, 27).

Oxygen binding analysis

Blood samples for oxygen binding analysis were prepared as described by Fyhn (27) and Brix *et al*. (29). Prior to oxygen binding analysis hemolysates were equilibrated using a 100 mM Hepes, 100 mM NaCl buffer (pH ~ 7) in a Sephadex G-25 column. The samples were kept at low temperatures (<4 °C) during preparations. 0.5 ml of each sample was mixed with 100 mM Hepes, 100 mM NaCl buffer, together with 5.5 mM ATP to mimic physiological conditions.

Experimental temperatures of 4 °C and 8 °C were selected based on the approximate upper and lower environmental temperature measured with the CTD device. Each blood sample was divided into two equal volumes, and subsequently buffered to mimic arterial and venous pH (7.5; 8.0) at the two experimental temperatures. The pH electrode was calibrated with a precision buffer (deviation of max ± 0.025 pH units). A 0.5 ml sample of the hemolysat was then transferred to the modified tonometer system for oxygen binding analysis according to the procedure described by Brix *et al*. (29).

Data analysis and statistical methods

The General Linear Model (GLM, SAS Institute Inc.) was used for statistical treatment of length, weight, and condition factor data in combination with Tukey student test (SAS Institute Inc.) for post hoc analysis. Levene's equality test was used to test for variance in the dataset (SAS Institute Inc.)

All structural and most of the functional analyses were made using the software Graphpad Instat, while Statistica version 5.0 or the statistical package in Microsoft Excel 2000 were used for t-tests. Standard deviation (σ) and mean deviation (MD) were both used as a measure of the variation in oxygen affinity (P_{50} values). Significance level was set to $p<0.05$. The term 'near significant' has been used when $0.05<p<0.10$.

The variation in P_{50} values for the phenotypes from the White Bank was analyzed using principal component analysis (PCA; software Sirius 6.6 PRS A/S).

Calculations

Standard deviation (S.D), mean deviation (M.D), and Chi-square (χ^2) values were calculated according to (Zar, 1984).

Owing to dishonest values of oxygen content from the CTD probe, an estimated value of the oxygen partial pressure (P_{O_2}) in the water column was used. A presumed linear decrease in oxygen percent was set to 20% from surface to sea bottom. The partial pressure of oxygen was calculated from:

$$PO_2 = \frac{(BP - VP) \times 20.95 \times O_2}{100} \times mmHg\,, \qquad \text{Equation [1]}$$

where BP is the barometric pressure, VP is the vapor pressure, and 20.95 is the percent O_2 in the equilibrating air, and O_2 is the percent oxygen in the water.

The concentration of oxygen was estimated as:

$$O_2 mg \cdot L^{-1} = \frac{(Table - value^*) \times \%O_2}{100}\,, \qquad \text{Equation [2]}$$

where 'Table-value*' was found in literature (31).

The allele frequency q^{HbI^*} in the cod population was calculated as:

$$q^{HbI^*} = \frac{2 \times H_o + H_e}{2 \times N}\,, \qquad \text{Equation [3]}$$

where H_o=number of homozygotes (*HbI*1/1* or *HbI*2/2*), H_e=number of heterozygotes with relevant allele, N=total number of fish.

The calculation of relative intensity (RI) of the different components was done by the equation:

$$K = \frac{10^5 \times weight}{length^3}, \qquad \text{Equation [4]}$$

where the denominations are in grams and millimeters. Typically the K values vary from 0.8 to 1.6. The lower value is 'an extremely poor fish', while the higher is a fish 'in excellent condition' (32).

The difference in absorption (ΔA) for a given wavelength (i) with respect to the absorption of deoxyhemoglobin is given as:

$$\Delta A_i = A_i - A_{deoxy}. \qquad \text{Equation [5]}$$

The total mean difference from all three nm measured at a given gas mixture was calculated as:

$$\Delta A_x = \frac{\left(\Delta A_{576} + \Delta A_{560} + \Delta A_{541}\right)}{3} \qquad \text{Equation [6]}$$

The total mean difference from each of the four intermediate O_2 saturations was divided by the mean difference of oxy-hemoglobin (100%) to express the percent O_2 saturation:

$$Y = \frac{\Delta A_x}{\Delta A_{oxy}} \qquad \text{Equation [7]}$$

The P_{O_2} of the gas mixture was calculated using equation [1]. The P_{50} value was estimated from Hill Plots by linear regression to quantitatively assess oxygen affinity. The effect of temperature on O_2 binding, expressed as the overall heat of oxygenation (ΔH,.kcal mol^{-1}) was quantified by using a modified van't Hoff equation:

$$\Delta H = -4.574 \times \frac{T_1 \times T_2}{T_2 - T_1} \times \frac{\Delta log P_{50}}{1000}, \qquad \text{Equation [8]}$$

where temperature is in Kelvin (°K). This value includes the heat of O_2 in solution (~ -3 kcal mol^{-1}). The pH sensitivity, expressed by the Bohr factor Φ, was calculated as:

$$\phi = \frac{\Delta \log P_{50}}{\Delta pH} \qquad \text{Equation [9]}$$

The unloading potential ΔP_{O_2} was calculated from the difference in mean P_{50} values for arterial pH (8.0) and venous pH (7.5). Cooperativity of oxygen binding was expressed by the Hill coefficient, n_{50}.

Results

Hydrographic mapping: current, temperature, depth deployments

The purpose of Current, Temperature, Depth (CTD) deployments was to assess the hydrographical situation at the locations. Hydrographical profiles seen in Figure 2 represents the total average of all deployments in each area. Horizontal measures at whole decibars (dbar)

have been pooled, averaged and thereafter plotted for every five meters down to the deepest recorded depth. Profiles are based on nine deployments in Kiel Bay, seven in Bornholm and fourteen in Gotland

Dissolved oxygen (mg/L) and the partial pressure of oxygen (mmHg) in Figure 2 are both calculated based on the percent oxygen measured with CTD.

The current, temperature, and depth (CTD) probe revealed that the White Bank (55°12.05' N, 6°22.42' E) was a stable environment concerning vertical temperature and salinity at the time of measurement (Figure 2). Average depth for the 16 stations was 47.8 meters. Temperature increased from 3.8 in the surface to 5 °C at 10 meters depth. In deeper layers of the water column temperature was stable about 5 °C until 50 meters depth, where the temperature decreased to 4 °C. Thus, no thermo-cline was observed. The salinity ranged between 30 ppt and 34 ppt. Oxygen concentration, based on literature (33), and decreased from 10.7 mg/L at surface to 8.6 mg/L near bottom.

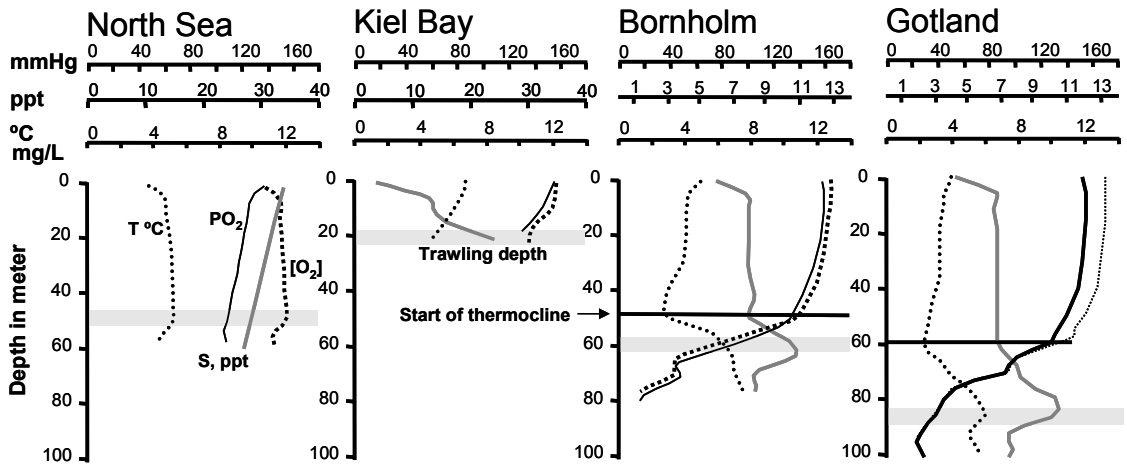

Figure 2. CTD profiles

The current, temperature, and depth (CTD) probe revealed that the White Bank (55°12.05' N, 6°22.42' E) was a stable environment concerning vertical temperature and salinity at the time of measurement (Figure 2.). The Figure reports the CTD profiles featuring the hydrographical conditions with depth from the White Bank in the North Sea, the Belt Sea and the Baltic Sea. Hydrographical values represent the average of pooled CTD measures plotted pr. 5 meters. The average trawling depths are marked to indicate the depth where the majority of fish was collected. Trawling of fish was conducted within five meters above the bottom, in all three stations. Average depth for the 16 stations was 47.8 meters. Temperature increased from 3.8 in the surface to 5 °C at 10 meters depth. In deeper layers of the water column temperature was stable about 5 °C until 50 meters depth, where the temperature decreased to 4 °C. Thus, no thermo-cline was observed. The salinity ranged between 30 ppt and 34 ppt. Oxygen concentration, based on literature (33), and decreased from 10.7 mg/L at surface to 8.6 mg/L near bottom.

Temperatures in the Kiel Bay show a uniform decrease from 6.7 ºC at the surface to 4.7 ºC near the bottom (Figure 2). A sudden change in temperature is located at 48 meters of depth in Bornholm and at 59 meters depth in Gotland. In Bornholm, temperatures in the upper layer

decline from 5 ºC by the surface to 2.9 ºC at the base of the halo-cline. Similarly, the upper layer of Gotland starts at 4 ºC and ends at 2.4 ºC. The temperatures in the lower layers of Bornholm and Gotland increased with depth reaching the highest level in the bottom zone. The total temperature difference within the lower layer is 4.7 ºC in Bornholm, and 3.3 ºC in Gotland. These differences are greater than observed in Kiel Bay (2 ºC).

Salinity increases steeply from the surface towards the bottom in Kiel Bay (4.2 ppt – 24.2 ppt). A halo-cline was observed at 10 meters depth. The upper layer of Bornholm and Gotland is characterized by stable salinities of 8 ppt and 7 ppt, located between ~ 8 meters and the halo-clines. Salinities then continue to increase, reaching their highest concentration (~ 11 ppt) near the bottom.

Oxygen levels in Kiel Bay vary from 12.1 mg/L in the surface water to 9.6 mg/L O2 at 23 meters depth. A similarly high oxygen level was found in the upper layer of the Baltic stations, ranging from 13.3 mg/L to 11 mg/L. Below the halo-cline dissolved oxygen decreases rapidly to a minimum of 1.4 mg/L (12%) in Bornholm and 2 mg/L (17%) in Gotland.

Characterization of hemoglobin phenotypes

Hemoglobin phenotypes were determined by their characteristic patterns and positions on an isoelectric focusing gel (IEF). Agar gel electrophoresis was used supplementary to verify the results from IEF. Of 279 cod phenotyped from the White Bank and 495 cod from the Belt Sea and the Baltic Sea, three different hemoglobin phenotypes were identified. These were the main phenotypes known as *HbI*1/1, HbI*1/2* and *HbI*2/2* (20). From the patterns obtained on an IEF gel we observed that component III was shared by all three phenotypes (Figure 3). The Figure reports an iso-electric focusing gel, illustrating the main phenotypes and approximate iso-electric points (Pi). The band patterns in this figure are the same as observed in our results (8). Phenotype *HbI*2/2b* was not detected among our results, but is inserted to indicate the position of component I. Component I-V are marked with closed dots.

*HbI*1/1* missed component II, while *HbI*2/2* was not in possession of components IV and V. The heterozygote *HbI*1/2* expressed components II-V. Component I was not represented among our samples, but is inserted for illustrational purposes (Figure 3).

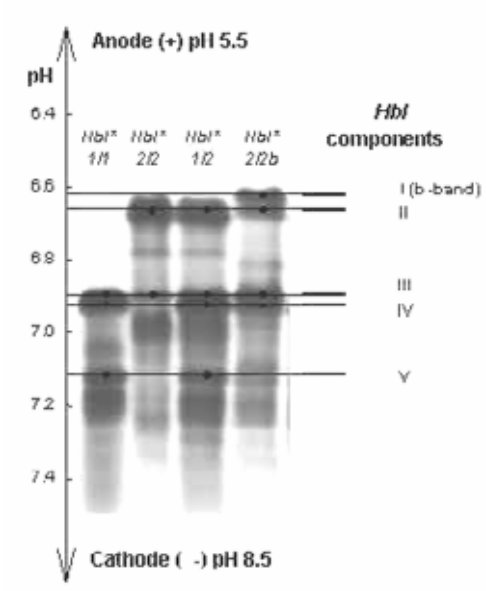

Figure 3. Iso-electric focusing gel of the studied proteins

No observations of band patters deviating from the ones described were found. A general poor quality and resolution of IEF results made further analysis of component intensity impossible.

The distribution of hemoglobin phenotypes

A large difference in the phenotype distribution was observed between the cod from the White Bank, the Belt Sea and Baltic. The *HbI*1* allele is most frequent in the White Bank (q^{HbI*1} = 0.76) followed by Kiel Bay (q^{HbI*1} = 0.61), but rarely encountered in Bornholm (0.10) and Gotland (0.01). In the White Bank *HbI*1/2* is most abundant (0.48), while in Kiel Bay, *HbI*1/1* and *HbI*1/2* are distributed in equal quantities (41%), while *HbI*2/2* is represented in 19% of the fish compared to 10% on the White Bank. Phenotype *HbI*1/1* was not represented in Gotland, but observed in a small amount in Bornholm (4%). The heterozygote HbI*1/2 was more common in Bornholm (13%) and Gotland (3%) compared to *HbI*1/1*. *HbI*2/2* was the dominant phenotype in the Baltic Sea with 83% in Bornholm and 97% in Gotland, respectively.

The Chi-square (χ^2 value (Table 2) gives a measure to the agreement between the observed number of phenotypes and the expected number according to the law of Hardy-Weinberg. In Gotland, we observed a good agreement between results and Hardy-Weinberg distribution, expressed by a low chi-square value (χ^2 = 0.34). The Kiel Bay population experience a slight over-representation of heterozygotes (χ^2= 3.99) while Bornholm (Table 2) has too many *HbI*1/1* homozygotes and few heterozygotes (χ^2= 15.86). The Bornholm station is located close to the transition zone between the Belt and the Baltic Sea (Figure 1). For the White Bank the Chi-constant value (χ^2=0.99) indicated that there were only minor differences between observed and expected values for each phenotype.

Table 2. Relative distribution of phenotypes found at the three locations.

Area of capture	Phenotypes						Nr. offish	q^{HbI*1}	Goodness of fit χ^2
	*HbI*1/1*		*HbI*1/2*		*HbI*2/2*				
	obs.	exp.	obs.	exp.	obs.	exp.			
Kiel Bay	79	72.2	79	92.3	36	29.5	194	0.61	3.99
Bornholm	6	1.5	19	26.8	124	120.7	149	0.10	15.86
Gotland	0	0	4	3	148	149	152	0.01	0.34
White Bank	136	140	154	146	34	38	324	0.66	0.99
Total	221	213.7	256	268.1	342	330.2	819		

Length, weight and condition of cod

In order to look for phenotypic differences in the length, weight and condition of fish, we have employed the General Linear model (GLM; SAS), followed by a Post-Hoc Tukey test. Levene's test for equality was used to test the variance in the dataset. In total 324 cod from the White Bank and 495 cod from the Belt Sea, the Baltic Sea and the Gotland Deep were measured (Table 3). The weight of stomach content was subtracted from the total weight, and the remaining weight was logarithmically transformed. Age data was not available and therefore not included in the statistics.

Table 3. Average length, weight and condition factor for all phenotypes in the White Bank, Kiel Bay, Bornholm and Gotland

Parameter	Hbl Type	White Bank		Kiel Bay		Bornholm		Gotland Deep	
		mean	*SD*	*mean*	*SD*	*mean*	*SD*	*mean*	*SD*
Length *(cm)*	*Hbl*1/1*	59.09	8.95	40.94	11.43	38.67	5.89		
	*Hbl*1/2*	61.96	10.53	40.33	12.03	42.89	6.46	53.50	11.82
	*Hbl*2/2*	57.53	8.73	41.53	14.61	44.32	8.74	45.99	12.10
Weight *(g)*	*Hbl*1/1*	2377.65	1327.41	786.39	697.86	603.18	267.19		
	*Hbl*1/2*	2841.4	2042.161	788.88	783.00	820.95	362.30	1691.60	980.33
	*Hbl*2/2*	2191.84	1246.05	1039.94	1602.20	1006.07	545.64	1188.99	1215.94
Condition	*Hbl*1/1*	1.07	0.16	0.95	0.21	1.00	0.08		
	*Hbl*1/2*	1.07	0.15	0.99	0.43	0.98	0.09	0.99	0.11
	*Hbl*2/2*	1.05	0.16	1.05	0.37	1.03	0.13	1.02	0.20
No of fish	*Hbl*1/1*	136		79		6			
	*Hbl*1/2*	154		79		19		4	
	*Hbl*2/2*	34		36		124		148	

The cod from the White Bank were significantly larger than the cod from the Belt Sea and the Baltic Sea, furthermore *HbI*1/2* cod were significantly longer than both *HbI*1/1* and HbI*2/2 ($p<0.01$ and $p=0.02$), and also heavier ($p=0.025$ and $p=0.076$) when not segregating for sex. There were no differences between the homozygotes, neither in length nor weight. The mean condition factor (K) ranged from 1.05 to 1.075. No significant differences in condition were found between the phenotypes.

The length of cod in Kiel Bay is significantly lower (GLM, $p > 0.05$, $F = 3.01$) than fish from Bornholm. There is no significant difference in length between cod from Bornholm and Gotland. Furthermore the lengths of *HbI*1/2* cod and *HbI*2/2* cod are not significantly different (GLM, $p > 0.11$, $F = 2.14$), however *HbI*1/1* cod are smaller than both *HbI*1/2* cod and *HbI*2/2* cod (Tukey). In all stations, the females were significantly longer than males, and represented by a smaller number (Females n = 183, Males n = 287, the sex could not be determined on all cod). A similar result was obtained for the cod from the North Sea, however, only *HbI*1/2*-females were significantly longer and heavier than the male ($p=0.04$ and $p=0.02$, respectively). The weight of fish followed the same pattern as length for all parameters; location, phenotype and sex.

The condition factor, however, showed that the North Sea cod had a higher condition value than the cod from the Belt Sea and from the Baltic Sea. Furthermore the Baltic cod have a significantly higher condition value compared to Belt cod (GLM, $p > 0.009$, $F = 4.76$). Among the phenotypes *HbI*2/2* shows the highest condition, significantly different from both *HbI*1/1* and *HbI*1/2* in the Belt Sea and the Baltic Sea, while in the North Sea *HbI*1/1* and *HbI*1/2* had the highest condition value. The condition of males was not significantly different from the females.

Oxygen binding studies

Oxygen affinity

The oxygen binding properties are summarized in Table 4. No difference in oxygen binding properties were found between Kiel Bay cod expressing *HbI*1/1* and *HbI*1/2* (t-test $4ºC_{pH\ 7.5}$: $p = 0.50$; $4ºC_{pH\ 8.0}$: $p = 0.83$; $8ºC_{pH\ 7.5}$: $p = 0.86$; $8ºC_{pH\ 8.0}$: $p = 0.60$). The results show a significant

higher oxygen affinity in Baltic cod compared to Belt Sea cod for all temperatures and pH-values tested. Average P_{50} values for the two Baltic *HbI*1/2* specimens ($P_{50;\ pH\ 7.5;\ 4°C}$ = 37.13 mmHg; $P_{50;\ pH\ 7.5;\ 8°C}$ = 30.9 mmHg; $P_{50;\ pH\ 8.0;\ 4°C}$ = 15.18 mmHg; $P_{50;\ pH\ 8.0;\ 8°C}$ = 12.82 mmHg) are lower than values measured for Belt Sea *HbI*1/2* ($P_{50;\ pH\ 7.5;\ 4°C}$ = 45.42 mmHg; $P_{50;\ pH\ 7.5;\ 8°C}$ = 49.25 mmHg; $P_{50;\ pH\ 8.0;\ 4°C}$ = 20.64 mmHg; $P_{50;\ pH\ 8.0;\ 8°C}$ = 17.96 mmHg). *HbI*2/2* from the Baltic Sea were found to bind oxygen at the lowest oxygen tension among samples ($P_{50;\ pH\ 7.5;\ 4°C}$ = missing; $P_{50;\ pH\ 7.5;\ 8°C}$ = 20.77 mmHg; $P_{50;\ pH\ 8.0;\ 4°C}$ = 9.99 mmHg; $P_{50;\ pH\ 8.0;\ 8°C}$ = 9.74 mmHg).

Variability between single samples in each group was measured by calculating the mean deviation (M.D). The mean deviation (Table 3) is generally higher for the Belt Sea samples; (9.48% - 16.82%) compared to the Baltic Sea samples (3.05% – 9.14%).

The results from the White Bank demonstrate great individual differences in half saturation pressures within each phenotype. For the homozygotes, *HbI*1/1* and *HbI*2/2* at pH 7.5, a lower mean deviation (MD) was found at 8 °C than at 4 °C, with 0.10 and 0.16 versus 0.02 and 0.08, respectively. However, this trend was reversed for *HbI*1/2*, which showed a significant higher mean deviation at 8 °C, (0.18) than at 4 °C, (0.07) (p=0.04). At pH 8.0, mean deviation was higher at 8 °C than at 4 °C for all phenotypes, for *HbI*1/1*: 0.28 versus 0.14, *HbI*1/2*: 0.13 versus 0.07 and *HbI*2/2*: 0.12 versus 0.09. In order to analyze the variability in this particular data set we applied a principal component analysis (PCA) (Figure 4a and b). The analysis showed that the linear distance from origo (+) (i.e. all P_{50} values pooled) to the individual P_{50} mean of each phenotype (•) was mostly longer at 8 °C than at 4 °C for both pH values indicating a larger overall variation at 8 °C than at 4 °C. Variation from grand mean is for 8 and 4 °C indicated as broken and solid ellipsis, respectively at pH 7.5 (Figure 4a) and pH 8.0 (Figure 4b).

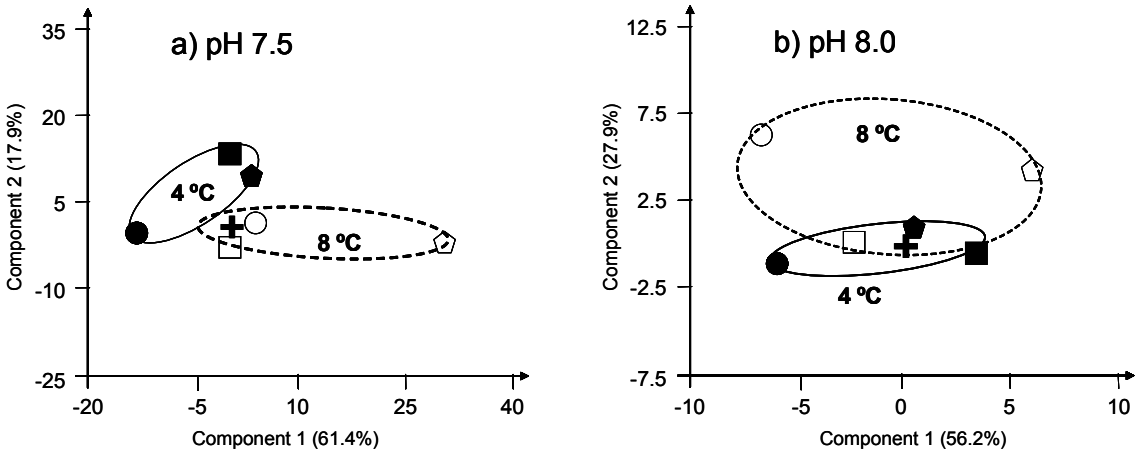

Figure 4. Location of different populations in the component space

At 8 °C the mean of *HbI*1/1* and *HbI*2/2* had a short distance from origo, but the heterozygote had a longer distance along the axis of abscissas describing most of the variation (i.e. 61.4%; Figure 4a). At 4 °C, the distance for *HbI*1/2* and *HbI*2/2* was more along the axis describing only 17.9% of the variation. Figure 4b further show that, except for the close position of *HbI*2/2* at 8 °C to origo, the variation was larger at 8 °C than at 4 °C indicated by a larger broken lined ellipsis.

Belt Sea samples, *HbI*1/1* and *HbI*1/2*, show a relatively lower Bohr factor ϕ at 4 °C and are therefore less pH sensitive at 4 °C (*HbI*1/1*: $\phi_{4°C}$ = -0.76; *HbI*1/2*: $\phi_{4°C}$ = -0.69) than

observed at 8°C (*HbI*1/1*: $\phi_{8°C}$ = -0.82; *HbI*1/2*: $\phi_{8°C}$ = -0.88). The Bohr factor found for Bornholm *HbI*2/2* is the smallest measured ($\phi_{pH\ 8.0}$ = -0.66), indicating low pH sensitivity.

In the White Bank samples *HbI*2/2*, the more anodic phenotype, had the highest average Bohr effect followed by *HbI*1/1* and *HbI*1/2* at both temperatures. Furthermore, at 4 °C, *HbI*2/2* had a significantly higher Bohr factor than *HbI*1/2* ($p<0.001$) and tended towards higher factor than *HbI*1/1* ($p=0.09$). *HbI*1/1* and *HbI*1/2* had similar Bohr effects. The phenotypic differences in pH sensitivity at 8 °C were not so clear.

Table 4. Effect of pH and temperature on P_{50} values for hemoglobin phenotypes from Kiel Bay, Bornholm and Gotland. Number of samples is abbreviated by n.

Area	Hbl Type	n.	Temp. °C	pH	P_{50} mmHg	P_{50} SD	P_{50} MD%	Bohr Factor, ϕ
White Bank	1/1	6	4	7.5	48.47	9.06	16.18	-0.75
		4	4	8.0	20.39	4.12	16.18	
		5	8	7.5	50.97	5.69	8.33	-0.92
		6	8	8.0	18.46	5.79	28.09	
	1/2	8	4	7.5	53.38	4.66	6.98	-0.66
		5	4	8.0	25.02	2.17	6.79	
		9	8	7.5	50.79	10.97	18.04	-0.85
		5	8	8.0	18.86	3.91	13.43	
	2/2	4	4	7.5	56.59	8.80	10.49	-0.99
		4	4	8.0	18.06	2.08	8.98	
		4	8	7.5	47.69	1.27	1.94	-1.04
		3	8	8.0	14.47	2.07	11.58	
Kiel Bay	1/1	7	4	7.5	47.94	7.49	13.64	-0.76
		8	4	8.0	20.33	3.26	12.90	
		8	8	7.5	48.35	11.24	16.82	
		7	8	8.0	18.81	3.19	13.55	-0.82
	1/2	8	4	7.5	45.42	6.71	11.13	-0.69
		8	4	8.0	20.64	2.37	9.48	
		8	8	7.5	49.25	8.78	11.70	
		7	8	8.0	17.96	2.59	9.86	-0.88
Bornholm	2/2	2	4	8.0	9.99		3.05	
		2	8	7.5	20.77		6.00	
		2	8	8.0	9.74		9.14	-0.66
Gotland	1/2	2	4	7.5	37.13		4.23	-0.78
		2	4	8.0	15.18		3.03	
		2	8	7.5	30.9		5.21	
		2	8	8.0	12.82		4.45	-0.76

Discussion

Hydrographical properties

In the North Sea, the sea surface temperature closely follows the air temperature. Also, the seasonal amplitudes are closely similar in shallow water, but the sea surface amplitude is somewhat reduced in deeper water. Any increase in wind speed forces the sea surface temperature to converge even more closely towards the ambient air temperature. Beneath the surface, increasing depths both delay and attenuate surface variability (34).

The salinity, temperature, and depth profile of the White Bank water column (Figure 2) indicated a stable environment both with respect to temperature and salinity. Vertical temperature was roughly the same from surface to bottom with 4 ± 1 °C.

Data from GISST ('Global ice coverage and sea surface temperatures') data-bank show large differences in summer and winter sea surface temperature at 57° N, 7° E (i.e. close to White Bank - 55° N, 6° E). Warmest and coldest mean surface temperatures 1950 – 1969 were in August (17 °C) and March (3 °C), respectively. For comparison the surface temperature outside Lofoten Islands (70° N, 18° E) varied from 11 °C to 4 °C (GISST). Hence, the southern North Sea surface- and sea bed temperatures are among the warmest and most variable temperature regimes experienced by the Atlantic cod within its natural habitat distribution. Furthermore, the shallow regions (depth 25-50 m) and lack of a significant thermo-cline in these areas (Dogger Bank, Southern Bight, German Bight, and White Bank) render the cod impossible to vertically migrate to cooler and deeper water when heat from high surface temperatures is transported vertically.

Temperature recordings along the Torungen-Hirtshals section, however, show a sharp and persistent summer thermo-cline (at 30 to 50 m) in Skagerrak (35). This section across the Skagerrak reaches depths of about 700 m. Below 200 m the seasonal temperature cycle is considerably attenuated, being slightly lower during summer (5-6 °C) than winter (~ 7 °C) (35). Such depths may act as a cooling niche for cod avoiding hot summer temperatures. Atlantic cod are known to have thermoregulatory behavior when confronted with changes in temperature. Though an acute increase in temperature of only 2.5 °C increased oxygen consumption of cod significantly (36), it appears that the cod by this behavior seek to avoid the more energetically costly acclimation processes.

Juvenile cod has been shown to prefer temperatures that correlate closely with seasonal changes in the temperature of the inshore waters they inhabited (37). This preference pattern carried on even if the cod was held at constant temperature over winter, indicating that some internal cycle operating independently of environmental temperature cause temperature preference to change seasonally (37). It has furthermore been demonstrated that cod actively seek water with high oxygen content and low temperatures (38). It should be noted that the so-called optimal combination of temperature and oxygen levels obtained in these studies do not take food availability and predation into account, which may explain that the cod is distributed more northerly that our studies would indicate.

With an annual surface temperature fluctuation from 3 °C to 17 °C and a near constant salinity of 30-34 ppt in the White Bank area (39, 40) the oxygen content is estimated to vary between 10.6 to 7.8 mg O_2 L^{-1} (31). The shallow southern North Sea is assumed to be well-oxygenated from surface to bottom, due to the dynamics of the Atlantic Gulf. A monitoring cruise reported a minimum oxygen concentration of 73 –75% of the Danish west coast, regardless of depth (39). Therefore low levels of oxygen are not experienced by Atlantic cod living in the White Bank area in contrast to the Belt Sea and the Baltic Sea cod (41).

In contrast the brackish-water of the Baltic Sea influences the diversity, composition and distribution of the Baltic fish. Hydrographical conditions in the Belt Sea and the Baltic Sea are well understood from the nature of the contributing environmental factors. The Kattegat and Belt Sea constitute the transition area between the Baltic proper and the North Sea. This relatively shallow water acts as a sill, restricting the water exchange. Furthermore, large volumes of fresh water runoff into the Baltic Sea create an upper layer of low salinity water. Subsequently, water with higher salinity is gathered in a deeper layer below the halo-cline. The annual discharge from rivers, precipitation, and evaporation causes the mean sea level in the southern Baltic proper to be a few centimeters higher than the level in Kattegat, thereby forcing the low salinity surface level through the Belt Sea. Strong westerly winds must shove the lower

water layer past the transition area in order to transport saline and oxygenated water from the North Sea into the Baltic proper. This phenomenon is infrequent, thus leading to water stagnation and reduced oxygen concentration in the bottom layer of the Baltic Sea, over time. Low oxygen and salinity levels in the Baltic Sea can prevail for years (42).

The hydrographic profile obtained for Kiel Bay displays well-oxygenated water (~ 80% saturated), with relatively homogenous cold temperatures in the whole water column, and a rapidly increasing salinity gradient towards the bottom. According to (43), oxygen concentration of bottom water in the Belt Sea and Kattegat is high during the winter, with over 80% saturation, but starts to decrease after spring bloom in March. Water exchange may temporarily stop the decrease during spring and summer, but a lower mean saturation of 40% is reached within the period July to October. Incidents of oxygen depletion in bottom water are observed nearly each summer in the Southern Kattegat, in the Sound and in the Belt Sea.

Profiles from Bornholm and Gotland, both show similar trends in hydrographical properties. Annual temperatures in the Baltic Sea vary from 0 – 18 ºC in the surface layer, and 3 – 6 ºC below the halo-cline (44). Salinity levels vary between 0 – 16 ppt in the upper layer and 9 – 18 ppt in the lower layer. The oxygen content in the bottom region of the Bornholm and Gotland regions is normally in the range 0-2.9 mg/L, resulting in a weak positive redox potential. In some cases, this level may become negative because of the additional oxygen needed to oxidize the sulphur content in the water (42). The present study share the same overall hydrographical features as found by (22), except for minor deviations in salinity. This difference can be explained by the gradual decrease in saline water due to lack of inflowing water from the North Sea (44). The annual hydrographical conditions in the lower layer may change with inflows. Normally, these fluctuations are infrequent and small, thus providing a stable environment throughout the year.

HbI phenotypes

The cod phenotyped in the present study expressed component patterns belonging to the three main phenotypes (7, 8). Husebø (45) observed a low number of cod expressing rare band patterns (IEF) in the Lillebelt and Øresund area. These patterns were absent in the present material probably due to the fact that these sub-phenotypes generally account only a small percentage (1-2%) of individuals in a population (46).

The heterogeneous geographic distribution of hemoglobin phenotypes in cod has been subject for many studies since the early 1960's. Natural selection has been used to explain differences in phenotype clines. After the discovery of a functional correlation between oxygen binding properties and temperature, several rapports have documented correlations between phenotypes and depth, and local season variations (20, 48, 10, 47, 11, 45).

*HbI*1/1* and *HbI*1/2* dominate in the White Bank (89.5% of all phenotyped cod) suggesting that these blood types may be energetically more advantageous than the less frequent *HbI*2/2*. *HbI*1* allele frequency of 0.66 (Table 2) corresponds with previous frequencies found in southern North Sea: 0.6 – 0.7 (46), 0.55 – 0.72 (20), 0.58 (49), and 0.65 (11). Seasonal variations in southern, central, and northern North Sea allele frequency have been reported (20, 10, 11, 45).

The hemoglobin phenotypes in the White Bank were not in complete Hardy Weinberg equilibrium at the time of capture (Table 2; χ^2=0.99). This suggests some migration, selection, mutation or inconsistency in casual crossing among the individuals in the population, the latter two factors presumably being less important. In the North Sea, surface currents transport fertilized cod eggs and larvae. Therefore, it is difficult to trace the origins of eggs and the fates of the larvae after their pelagic phase since those early stages can be neither tagged nor

phenotyped. It cannot be ruled out that larvae from different spawning grounds are mixed together in a common gene pool from which the regional stocks recruit fry either at random or selectively. Phenotypes from the North Sea, sampled from different seasons and places over the past ten years, offer little support to the view that cod spawning ground populations are genotypically distinct (49).

We found that cod expressing the *HbI*1* allele also was widely distributed in the Belt Sea (61%), but scarce in the Baltic Sea (1 - 10%). These results are in good agreement with the phenotype frequencies previously found by (20). Similarly, eelpout (*Zoarces viviparous*) from Kattegat populations are almost exclusively represented by *HbI*1*, while only 10% is present in the Baltic (50, 51). A survey conducted in 1967 – 68, in the north, south and central Baltic, recorded an average frequency of ~ 35% *HbI*1* from 1305 cod (52, 11). With a $\chi^2 = 74$, the Hardy-Weinberg distribution shows greater genetic imbalance than observed among our samples (Table 2). This disparity in phenotype frequency ratio may be related to the mixing of Belt and Baltic stocks (53). From an environmental point of view, these discrepancies between our results may be related to local or seasonal differences in hydrographical conditions at the time and place of sampling. However, we have not been able to obtain literature to support this explanation. On the background of differentiated vertical positioning of hemoglobins, as described by Karpov *et al.* (47), we cannot rule out the possibility that fishing depth and fishing equipment may have some bearing on the phenotype frequency in the catch. Our cod was collected using a bottom trawl, in the layer with warmest water and lowest oxygen level.

Generally, phenotype distribution can be influenced by factors like selection, mutation, migration or genetic drift. In the absence of critical observations, and experimental data, it is not possible to decide the degree of influence from these factors. To obtain an overview of the *in vivo* genetic process, phenotype data must be used in combination with other information, such as tag-recapture data and hydrographical data, measured throughout different life stages. Selection based on differential mortality among phenotypes is likely to be most significant in the vulnerable larval and juvenile stages.

The Baltic and Belt Sea cod populations live in different ecological habitats with separate spawning grounds. The cod stocks in the Baltic Sea are treated by ICES as two separate stocks. One stock occurs to the east of 15 ºE and forms spawning aggregations here. The second stock occurs to the west of 15 ºE. It is also well established that genetic exchange between cod populations is limited (54). However, the two stocks mixes to some extent, especially during the juvenile stage and outside the spawning season. The difference in hydrographical properties and the geographical distance between the Belt Sea and the Baltic Sea partially restrict cod populations from intermingling (55). The poor fit of the chi square test for Bornholm is most likely due to this area being a transition zone with some degree of overlap between the two different phenotype ratios (53). As for the over-representation of heterozygotes observed in Kiel Bay, this may relate to the uneven ratio of males to females described in our samples (56).

A correlation between hydrographical conditions and phenotype distribution is evident in the Baltic Sea and the Gulf of St. Lawrence along the Canadian east coast. Despite of the great genetic divergence found throughout the geographic distance across the Atlantic Ocean, cod populations in both these regions show almost identical phenotype frequencies (98% *HbI*2*) (9, 57). Water properties in the Baltic Sea and the Gulf of St. Lawrence are both characterized by annual low temperatures (4-6 °C), hypoxic bottom conditions, and some degree of halo-cline formation. On the other hand, the salinity level in the Baltic Sea is considerable lower (7-18 ppt) than found in the Gulf of St. Lawrence (33 ppt) (44). From the similar properties observed in these two regions, it seems plausible that temperature may constitute a significant factor concerning the distribution of phenotypes. However, low environmental oxygen levels are also a common denominator, and may act as a supplementary factor in the distribution of

phenotypes. Salinity, on the other hand, does not appear to be decisive for this distribution, due to of the distinct difference in salinity found in these two regions.

Phenotype and size correlations

The trends observed in size and condition data showed that Baltic populations (sex pooled) had greater average size and better condition compared to the Belt Sea population. There was no significant difference between the two Baltic populations. Phenotypic differences in size and condition was observed between *HbI*1/1* and *HbI*2/2*, *HbI*1/2* and *HbI*2/2*, but not between *HbI*1/1* and *HbI*1/2*. Overall, cod with *HbI*2/2* had the greatest average size and condition among the phenotypes. Females were generally larger than males, but showed no difference in condition factor. The number of females was significantly lower than the share of males.

Previous studies show higher growth rates among wild cod with phenotype *HbI*2/2* (58). This correlation has also been described for juvenile wild cod, in which average lengths were greatest for *HbI*2/2*, intermediate for *HbI*1/2* and smallest for *HbI*1/1* (59). Salvanes and Hart (60) observed a higher capture success and more active foraging in young cod with phenotype *HbI*2/2*. On the contrary, other authors have not been able to detect differences between phenotype and growth in natural and semi-natural environments (61, 62). In the controlled tank experiment of Nævdal *et al.* (63), cod with *HbI*2/2* had the highest growth rate at 6, 10 and 14°C. Turbot, having a similar hemoglobin polymorph system to cod, also show higher growth rates for *HbI*2/2* at low (10 °C) and optimal temperatures (16 °C) (64). Phenotypic differences have also been reported in relation to the sex ratio of cod in Danish waters, and in the Trondheim fjord (65, 66).

It appears that phenotype dependent growth rates can be more difficult to interpret in wild environments than under controlled experimental conditions. Growth patterns are often subject to complex patterns of population dynamics and variations in ecological conditions. Our data may indicate a correlation between phenotype and size. Thus, the material at hand imparts several uncertain and unaccountable factors, demanding a cautionary interpretation of the data. Among others, we lack knowledge of the fish's age, year-class and food availability, which is important for direct comparison of size between fish. Our sample size is relatively small and presents a great spread in the phenotype ratio at the respective sampling locations. In addition, we should expect population specific bias. Furthermore, the localities sampled were native spawning sites. This may partly describe the differences in size and number observed between males and females.

As mention previously, we may experience an inhomogeneous distribution of phenotypes and year classes at different hydrographical conditions. If segregation of phenotypes were to be present within a region, this could be manifested as genetic heterogeneity in samples and in turn affect growth rates, catch rates, mortality rates as well as spatial and temporal distribution of the phenotypes.

Based on our present size data, it seems difficult to determine whether *HbI*2/2* individuals have an adaptive significance and thus represent a selection potential at the locations examined.

Oxygen binding properties of hemoglobins

Results from tonometric studies show that Baltic hemoglobins bind oxygen at lower O_2 tensions compared to Belt Sea hemoglobins. Dissimilar oxygen affinities were observed between Belt Sea *HbI*1/2*, and Baltic *HbI*1/2*, while little difference is found when comparing average affinities in Belt Sea *HbI*1/1* and *HbI*1/2*. In Belt Sea hemoglobins, individual P_{50}

variation was remarkably high (M.D = 9.48 – 16.82%), thus representing a spectra of oxygen binding properties rather than unidirectional trends. For Baltic hemoglobins, variation seemed lower (M.D = 3.03 – 9.14%), tending toward high oxygen affinity combined with low sensitivity to pH.

Our results indicate some disagreements with results from previous laboratory experiments. Firstly, according to the results of Karpov and Novikov (10) we would expect to find a strong effect of temperature on oxygen affinity in *HbI*2/2*, and low temperature effect in *HbI*1/1*. Secondly, the oxygen affinity in the range 4 – 8 ºC should be highest for *HbI*2/2*, lowest for *HbI*1/1* and medium for *HbI*1/2*. In our results we found that *HbI*2/2* had the highest affinity, combined with a small temperature effect (ΔH = 0.94 kcal*mol^{-1}). However, the data from the North Sea cod indicates that *HbI*2/2* may also include a low O_2 affinity level similar to that obtained in our Belt Sea *HbI*1/1*, and *HbI*1/2* hemoglobins. These discrepancies can be ascribed to differences in acclimation background. The experiment of (10) measured the oxygen binding properties of whole blood (pH 7.5) from three White Sea cod, all with unknown acclimation backgrounds. Their measuring technique was different from ours, and their use of buffer components is not described. With this background, the results in these two experiments are not directly comparable. Later acclimation experiments demonstrated clearly that oxygen affinity of hemoglobins change significantly in cod acclimated to 4 ºC compared to cod acclimated to 12 ºC over a period of 12 months (12). With a strong influence of temperature acclimation on hemoglobins, we expect a higher variability in wild cod populations due to exposure to different environmental habitats and individual acclimation backgrounds. The variability in P_{50} values observed in our experiment is high (M.D = 3.05-16.82%) compared to measurements (M.D < 3%) gathered from pre-acclimated (7-10 ºC) cod stripped of organic phosphates (29).

Some of the variation in P_{50} values observed may be attributed to unequal effects of ATP on different types of components, and furthermore the miscellaneous configurations of these components. Preliminary experiments have revealed that 3 mM of ATP is sufficient for full saturation of cod hemoglobins. So far, no work has been done to investigate the individual properties of hemoglobin components in cod and their isolated response to ATP. We expect to find a larger impact of ATP on the most anodic components because of their higher affinities for organic phosphates. Some of the difference in functional properties between the phenotypes can be related to the presence of an extra group of the amino acid Histidin in *HbI*1* components (67). Histidin groups play a major role in buffering blood at physiological pH-values (68).

The apparent strategy employed by active species, such as rainbow trout, is to utilize low-affinity hemoglobins (high P_{50}) in conjunction with high arterial P_{O2} values. Oxygen binding properties of this category were recognized in the Kiel Bay hemoglobins, and similarly in wild North Sea cod populations. Sluggish species, such as carp (*Cyprinius carpio*), flounder (*Platichthys stellatus*), and eel (*Anguilla sp.*) typically utilize relatively high-affinity hemoglobins (low P_{50}) in conjunction with low arterial P_{O2} values. These characteristics fit the observations from Baltic *HbI*1/2,* and particularly *HbI*2/2*. Both these groups displayed high O_2 affinity, combined with relatively small Bohr effects, and increased cooperativity. Within the framework of the MWC model, an accurate calculation of cooperativity should not be based on less than fifteen different saturation values for a single oxygen-binding curve (69). Since our calculations were based on the regression from only four measures, the validity of these must be interpreted with caution.

Adjustments to either of these strategies provide a trade-off situation for the fish (70). High-affinity hemoglobin in combination with low arterial P_{O2} is advantageous for optimizing oxygen extraction efficiency from the water, because it assures a large water-to-blood oxygen partial pressure gradient. The fish thereby reduces its ventilatory requirement and thus the

energetic costs. A disadvantage of low P_{O2} in the water is the associated reduction in the O_2 diffusion gradient between blood and tissues. This strategy is therefore appropriate for fish that are not very active, or fish living in hypoxic environments. In active species with high metabolic demands, high arterial P_{O2} values in concert with low-affinity hemoglobin permits a large O_2 diffusion gradient between blood and tissues, thus increasing the O_2 unloading potential. The disadvantage of such a strategy is the resultant low efficiency of O_2 extraction from the water and the accompanying high cost of ventilation. This may be compensated for by a higher cooperativity (n_{50}) of O_2 binding, normally associated with low affinity hemoglobins (70). It appears that Belt Sea cod hemoglobins, present in well-aerated water, are configured to enhance the water-to-blood O_2 diffusion gradient.

Correlations between oxygen binding abilities and environmental conditions

Cod subjected to hypoxic water within the critical oxygen tension limit (P_c) will counteract this state by increasing the rate of ventilation. Different fish species show dissimilar tolerance toward hypoxic thresholds (71). Such differences are also present within species, and may result from disparities in the *in novo* physiological state. Claireaux *et al.* (36) observed that cod subjected to an oxygen gradient avoid oxygen tensions below ~ 67 mmHg, but make short voluntary excursions down to ~25 mmHg if food is offered. According to Plante *et al.* (72), the mortality rate for cod at 15 mmHg was 100% after 96 hours exposure (2 and 6 ºC), although all the fish survived short-term exposure to 15 mmHg. Fifty percent of the cod survived 96 hours at 32 mmHg (LC^{96h}_{50}), while 5% died subjected to 43 mmHg. No casualties were reported at oxygen tension above 52 mmHg. The experiment of Scholz and Waller (73) describes a lower tolerance to hypoxia presented by an LC^{24h}_{50} value of 59 mmHg O_2 (35 ppt at 8 ºC). These results may be explained by the choice of fish selected for the experiment. Scholz and Waller used cod from the North Sea, which we predict consisted of about 60% of the *HbI*1* allele, with an acclimation background from well oxygenated water. Contrary, the experiments of Plante *et al.* (72) have employed fish from the Canadian coast with a predicted frequency of approximately 90% *HbI*2*.

Figure 5 displays the hydrographical profiles from White Bank, Kiel Bay, Bornholm and Gotland Deep. The profile is combined with the P_{50} values found for haemoglobins at the respective stations. The scaling of oxygen tensions derived from hydrographical data is synchronised with experimental pO_2. Dotted lines in the lower graphs marks the mortality percentage of Canadian cod (LC) at 96 hours exposure to hypoxic levels (pO_2) of 15 and 52 (P_c) mmHg (the levels for 32 and 43 mmHg are not shown), measured at 28 ppt salinity, at 2 and 6 ºC (72). The critical O_2 tension, P_c, is equal to LC_0 (96h). For Bornholm and Gotland, shaded boxes to the right constitute the oxygen interval inhabited by 90% of cod (pO_2 range = 75 – 131 mmHg) (22). The shaded triangles in the lower graphs represent the oxygen tension available with corresponding temperature. Habitat temperature range and experimental temperatures (4 and 8 ºC) are marked on the lower temperature axis. The symbols for different phenotypes are: *HbI*1/1* white pie and circle symbol; *HbI*1/2* grey pie and five angled symbol in grey; *HbI*2/2* black pie and square symbol. Closed symbols are venous condition (pH=7.5), while open symbols correspond to the arterial condition (pH=8.0).

Using 52 mmHg as a lower critical oxygen pressure we observe from Figure 5 that this value is reached at ~ 65 meters depth in Bornholm and ~ 80 meters depth in Gotland, respectively. The oxygen tension is lowest near the bottom and slightly lower in the Bornholm waters (17 mmHg, 11%) compared to Gotland (25 mmHg, 16%). In Kiel Bay, we found general high oxygen content near the bottom ~ 136 mmHg, thus not limiting for oxygen uptake.

We expect that most of the cod collected was intercepted at the bottom. However, some of the fish may have been caught at shallower depths in the period when the trawl was submerged or hauled. Considering the low level of oxygen near the bottom, we find it most likely that the cod found at this level were temporary visitors, not permanently inhabiting this region.

According to a hydro acoustic study from Bornholm by Tomkiewicz *et al.* (22) 90% of the cod was distributed at oxygen levels between 75 – 131 mmHg. Of the remaining 10%, less than 5% of the fish were observed at oxygen levels below 3.6 mg/L while close to 5% was found above 131 mmHg. Within a salinity range of 7 – 15.5 ppt, 90% of cod were found between 11.2 and 15 ppt. Ninety percent of the fish were distributed between 4.6 °C and 6.1 °C. The highest abundance of fish was located between 40 – 60 meters of depth, with no fish found shallower than the halo-cline at 40 meters. Generally, the highest distribution of cod was found at the highest oxygen levels and the highest salinity levels. There was no correlation between fish distribution and water temperature, indicating that cod had no specific temperature preference at these conditions.

Behavioral studies conducted under controlled temperature conditions confirm that cod actively seek water properties with the highest oxygen content combined with the lowest temperatures (13, 74). Cod are also observed to avoid new temperature conditions, thus showing thermoregulatory behavior (36). According to Schurmann and Steffensen (38), a reduction of oxygen saturation to 45 mmHg has no effect on the preferred temperature of cod. A further reduction to below 30 mmHg lead to an immediate decrease in selected temperature.

However, other studies found no evidence of lowered tolerance to hypoxia at temperatures ranging from 2 ºC to 6 ºC, and at salinities between 7-28 ppt (75, 72). It appears that the relatively small temperature range (3-6 ºC) observed in the Baltic habitat may be a less significant factor affecting the respiration capacity. This observation corresponds with the low temperature sensitivity observed in the Baltic *HbI*2/2* cod, which is most common in this region. Moreover, the low oxygen tension present in the Baltic will affect the fish relative to the degree of hypoxia.

By combining the hydrographical oxygen tensions in the water at each capture site with the respective P_{50} -values of phenotypes, we obtain a picture of the O_2 availability to the hemoglobin O_2 binding features (Figure 5). This model can only give an idea of the O_2 binding threshold, because the P_{50} values represent single arterial and venous values, and not a complete oxygen-binding curve. Under *in vivo* conditions, the hemoglobins would operate in the upper part of the oxygen-binding curve, normally circulating between 90% of the total capacity at venous and 100% at arterial saturation (76). From Figure 5 we see that venous P_{50} values from Kiel Bay are close to the critical oxygen tension (P_c = 52 mmHg). At this level hemoglobins are barely able to reach their half saturation points. Evaluating the oxygen affinity of Kiel Bay hemoglobins at the lowest oxygen tension found in Bornholm, we see that arterial half saturation is not achieved at 15 mmHg. In Bornholm, native *HbI*2/2* have a high affinity, and are fully able to reach half saturation at both arterial and venous values (Figure 5). However, at the lowest bottom levels < 20 mmHg the O_2 partial pressure is insufficient for half saturation of the hemoglobins. Nevertheless, a full saturation at the lower bottom O_2 levels for both stations would probably not be possible, unless ATP concentrations are lowered. *HbI*1/2* fish are able to half saturate their blood at 52 mmHg, but they are not able to fully saturate it at this level. Their flexibility in the lower bottom zone may be less than for *HbI*2/2* fish. This may mean that a lower bottom niche concerning food, etc. may be open for the *HbI*2/2* fish, and limited for the other phenotypes. Theoretically, Kiel Bay cod of all phenotypes can tolerate the O_2 tensions found at the highest distribution of cod in Bornholm, but these would most likely experience respiratory problems slightly below this level.

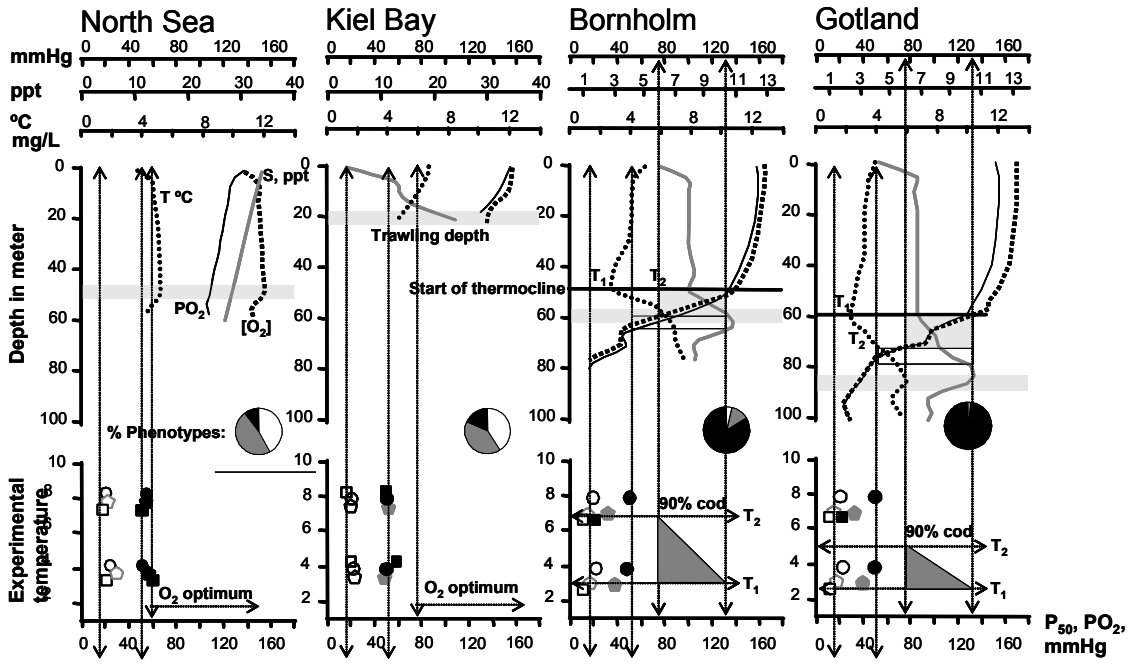

Figure 5. Hydrographical profiles and P_{50} values from White Bank, Kiel Bay, Bornholm and Gotland Deep

It appears that Baltic cod are restricted to the hydrographical properties within narrow zones established by low salinity levels above the halo-cline, and low oxygen levels in the bottom region. This leaves the fish with a sustainable habitat measuring ~10 meters vertically in Bornholm, and ~15 meters in Gotland. Higher and more preferable salinities can be found near the bottom, but are compromised by the parallel drop in oxygen tension. The cod in this region may descend to layers with less oxygen in order to find food, but must return to shallower depths with higher P_{O2} in order to regain an effective respiration, which may also increase the total metabolic support. Chabot and Dutil (77) documented that low oxygen levels made cod throw up the food they had eaten. As soon as the metabolic scope was restored (more than 45% O_2) digestion was resumed and food re-swallowed. They also found that growth rate was directly related to oxygen availability, and that 97% of the reduction in growth was explained by reduced food consumption.

Water temperature is a powerful factor influencing both the fish distribution and behavior (13, 36). For cod, the thermal preferendum range is reported to be 11-14 ºC (37). However, two major factors might keep the cod from this optimum; (1) the niche is not available in the ecosystem it inhabits, (2) there are interactions between temperatures and other abiotic and biotic niches (78). In the range where metabolism demands high respiratory efficiency, such as under hypoxia or high temperatures, acclimation of hemoglobin types to achieve higher oxygen affinity may play an important role (12). Energetic economy is crucial for cod living in marginal habitats. However, if oxygen remains a non-limiting factor and poses no extra energetic cost, the need for hemoglobin acclimation may become less important in maintaining the physiological state. Our results from Kiel Bay cod hemoglobins demonstrate low oxygen affinity combined with a generally high variance in oxygen binding properties.

Conclusion

Wild Baltic cod acclimated to low temperatures and low oxygen levels have higher oxygen-binding affinities compared to wild Belt Sea and North Sea cod. *HbI*2/2* cod, acclimated to the Baltic Sea environment, shows an increased potential in binding O_2 at low oxygen levels. This adaptation may be highly relevant for Baltic cod because their habitat is restricted by an upper vertical limit created by water of low salinity and a lower vertical limit due to lethally low oxygen levels. Being able to cope with lower O_2 partial pressures the *HbI*2/2* cod extend its ecological niche, and could explain its great success in the Baltic Sea.

Based on the results we conclude that climate changes may influence the general distribution of Atlantic cod phenotypes, causing a northward migration of *HbI*1/1* if water temperature increases. Further we will expect the conditions in the Baltic Sea to become worse with a larger reduction in the oxygen levels, which means that even *HbI*2/2* will disappear from the area. This would restrict the distribution area of *HbI*2/2* to marginal regions in the north except from fiords with shelves along the cost line of Norway were we may find reduction in water oxygen tensions combined with colder water.

Acknowledgement

The study was supported by EU CONTRACT N° ENV4 CT97-0596.
We would like to thank Alfred Wegener Institute (AWI) in Bremerhaven, Germany, and in particular all onboard the research vessel Heinche (Helgoland) for the possibility to participate on the cruise and for their helpfulness collecting the material. We further appreciate the superb technical assistance of Solveig Thorkildsen, Dept. of Biology University of Bergen.

References

1. Wood SC, Lenfant C. Evolution of respiratory processes. New York: Marcel Dekker; 1979
2. Wilkins NP. Hemoglobin polymorphism in cod, whiting and pollack in Scottish waters. Conceil International pour l'Exploration de la Mer 1971;161:60-3.
3. Gillen RG, Riggs A. The hemoglobins of a fresh-water teleost, Cichlasoma cyanoguttatum (Biard and Girard). II. Subunit structure and oxygen equlibria of the isolated components. Arch Biochem Biophys 1973;154:348-59.
4. Powers DA. Molecular ecology of teleost fish hemoglobins: Strategies for adapting to changing environments. Am Zool 1980; 20:139-62.
5. Ruud JT. Vertebrates without erythrocytes and blood pigment. Nature 1954;173:848-50.
6. Jamieson A, Thomson D. Blood proteins in North Sea cod (Gadus morua L.) In: Hansen B, Jones BW (Ed.). Proceedings from XIIth Europ. Conf. Anim. Blood Groups Biochem. Polymorph. Bp. 1972. Copenhagen, Denmark. 1972. p. 585-591.
7. Sick K. Hemoglobin polymorphism in fishes. Nature 1961;192:894-6.
8. Fyhn UEH, Brix O, Nævdal G, Johansen T. New variants of the hemoglobins of Atlantic cod: a tool for discriminating between coastal and Arctic cod populations. ICES Mar Sci Symp 1994;198:666-70.
9. Smith PJ, Jamieson A, Birley AJ. Electrophoretic studies and the stock concept in marine teleosts. J Conseil 1990;47:231-45.

10. Karpov AK, Novikov GG. Hemoglobin alloforms in cod, Gadus morhua (Gadiformes, Gadidae), their functional characteristics and occurrence in populations. J Ichthyol 1980;6:45-9.
11. Jamieson A, Birley AJ. The demography of a hemoglobin polymorphism in the Atlantic cod, Gadus morhua L. J Fish Biol 1989;35:193-204.
12. Brix O, Thorkildsen S, Colosimo A. Temperature acclimation modulates the oxygen binding properties of the Atlantic cod (Gadus morhua L.) genotypes—HbI*1/1, HbI*1/2, and HbI*2/2—by changing the concentrations of their major hemoglobin components (results from growth studies at different temperatures). Comp Biochem Physiol A 2004;138:241-51.
13. D'amours D. The distribution of cod (Gadus morhua) in relation to temperature and oxygen level in the Gulf of St. Lawrence. Fish Oceanogr 1993;2:24-9.
14. Petersen MF, Steffensen JF. Preferred temperature of juvenile Atlantic cod Gadus morhua with different hemoglobin genotypes at normoxia and moderate hypoxia. J Exp Biol 2003;206:359-64.
15. Fry FEJ. The effect of environmental factors on the physiology of fish. In: Hoar WS, Randall DJ (Ed.). Environmental relations and behaviour. New York: Academic Press; 1971. p. 1-98.
16. Brett JR, Groves TDD. Physiological energetics. In: Hoar WS, Randall DJ, Brett JR (Ed.). Fish physiology, New York: Academic Press; 1979. p. 279-352.
17. Ali MA. Environmental Biology of fishes. In: Houston AH, editor. Components of the hematological response of fishes to environmental temperature change. New York: Plenum Press; 1980. p. 241-98.
18. Milnor WR. Cardiovascular physiology. New York: Oxford University Press; 1990.
19. Weber RE, Jensen FB. Functional adaptations in hemoglobins from ectothermic vertebrates. Ann. Rev Physiol 1988;50:161-79.
20. Sick K. Hemoglobin polymorphism of cod in the Baltic and the Danish Belt Sea. Hereditas 1965;54:19-48.
21. Pocklington R. The Gulf of St. Lawrence and the Baltic Sea: Two different Organic Systems. Deutsche Hydrogr Zeitschr 1986;39:41-90.
22. Tomkiewicz J, Lehmann K, St. John M. Oceanographic influences on the distribution of Baltic cod, Gadus morhua, during spawning in the Bornholm Basin of the Baltic Sea. Fish Oceanogr 1998;7:48-62.
23. MacKenzie BR, St. John MA, Wieland K. Eastern Baltic cod: perspectives from existing data on processes affecting growth and survival of eggs and larvae. Mar Ecol Progr Ser 1996;134:265-81.
24. Fotland Å, Borge A, Gjøsæter H, Mjanger H. Håndbok for prøvetaking av fisk og krepsdyr. Bergen: Havforskningsinstituttet. 1997.
25. Fulton T. Rate of growth of seas fishes. Sci Invest Fish Div Scot Rept 1902:20:12-24.
26. Jørstad KE. Genetic analyses of cod in northern Norway. In: Dahl E, Danielsen DS, Moksness E, Solemdal P (Ed.). The propagation of cod, Gadus morhua L. Flødevigen rapportserie 1. 1984:745-60.
27. Fyhn UEH. Heterogeneity of fish hemoglobins. Bergen: Department of Fisheries and Marine Biology, University of Bergen; 1991.
28. McFarland G. The staining of starch gels with Coomassie Brilliant Blue G 250 acid solution. Experentia 1977;33:16-68.
29. Brix O, Forås E, Strand I. Genetic variation and functional properties of Atlantic cod hemoglobins: Introducing a modified tonometric method for studying fragile hemoglobins. Comp Biochem Physiol A. 1998;119: 575-83.
30. Zar JH. Biostatistical analysis. London: Prentice-Hall; 1984.
31. Colt J. Computation of dissolved gas concentrations in water as functions of temperature, salinity and pressure. Bethesda, MD: American Fisheries Society; 1984. (Special Publication, 14).

32. Barnham C, Baxter A. Condition factor, K, for salmonid fish. Natural Resources and Environment. Fisheries Notes, 1998; 5.

33. Colt J. Computation of dissolved gas concentrations in water as functions of temperature, salinity and pressure. Bethesda, MD: American Fisheries Society; 1984. (Special Publication, 14).

34. Lane A, Prandle D. Inter-annual variability in the temperature of the North Sea. Continental Shelf Research 1996;16(11):1489-1507.

35. Danielssen DS, Svendsen E, Ostrowski M. Long-term hydrographic variation in the Skagerrak based on the section Torungen – Hirtshals. ICES Journal of Marine Science 1996;53:917-25.

36. Claireaux G, Webber DM, Kerr SR, Boutilier RG. Physiology and behavior of free-swimming Atlantic Cod (Gadus morhua) facing fluctuating temperature conditions. J Exp Biol 1995;198:49-60.

37. Clark DS, Green JM. Seasonal variation in temperature preference of juvenile Atlantic cod (Gadus morhua) with evidence supporting an energetic basis for their diel vertical migration. Can J Zool 1991;69:1302-7.

38. Schurmann H, Steffensen JF. Lethal oxygen levels at different temperatures and the preffered temperature during hypoxia of the Atlantic cod, (Gadus morhua L.). J Fish Biol 1992;41:927-34.

39. Aertebjerg G. Monitoring Cruise r/v Gunnar Thorson in the Sound, Kattegat, Skagerrak, North Sea, Belt Sea and Arkona Sea. Cruise no.203, 6-17 August 2001. Roskilde, Denmark: National Environmental Research Institute; 2001. (Monitoring Cruise Report).

40. Jones JE, Howarth MJ. Salinity models of the southern North Sea. Continental Shelf Research 1995;15(6):705-27.

41. Nehring D, Matthaus W. Current trends in hydrographic and chemical-parameters and eutrophication in the Baltic Sea. Internationale Revue der Gesamten Hydrobiologie 1991;76(3):297-316.

42. Swedish Environmental Protection Agency. Environmental quality in Swedish coast and sea. Final report. Stockholm, Sweden; Official Statistics of Sweden; 2001.

43. Aertebjerg G. State of the marine environment of the Baltic Sea regions. Kattegat and Belt Sea: Third periodic assessment of the state of the marine environment of the Baltic Sea. Balt Sea Environ Proc 1996;1:107-28.

44. Pocklington R. The Gulf of St. Lawrence and the Baltic Sea: Two different Organic Systems. Deutsche Hydrogr Zeitschr 1986;39:41-90.

45. Husebø Å. Geografisk fordeling av hemoglobintyper hos torsk, Gadus morhua L. Bergen: Cand. scient. thesis: Institute of fisheries and Marine biology, University of Bergen; 1995.

46. Frydenberg O, Moller D, Naevdal G, Sick K. Hemoglobin polymorphism in Norwegian cod populations. Hereditas 1965;53:257-71.

47. Karpov AK, Osinov AG, Novikov GG. Protein polymorphism in Atlantic cod, Gadus morhua (Gadidae), of the White Sea. J Ichthyol 1984;24:71-9.

48. Møller D. The relationship between arctic and coastal cod in their immature stages illustrated by frequencies of genetic characters. Fiskeridir Skr Ser Havunders 1969;15:220-33.

49. Jamieson A, Thomson D. Butyric esterase differences in Atlantic cod, Gadus morua L. J Fish Biol 1972;35:193-204.

50. Christiansen FB, Frydenberg O. Geographical patterns of four polymorphisms in Zoarces viviparus as evidence of selection. Genetics 1974;77:765-70.

51. Hjorth JP, Simonsen V. Genetics of Zoarces populations. VIII Geographic variation common to the polymorphic loci Hb-I and Est-111. Hereditas 1975;81:173-84.

52. Jamieson A, Otterlind G. The use of cod blood protein polymorphisms in the Belt Sea, the Sound and the Baltic Sea. Cons Int Explor Mer 1971;161:55-9.

53. Otterlind G. Cod migration and transplantation experiments in the Baltic. Sonerdruck Zeitschr angewandte Ichtyol 1985;1:3-16.

54. Boutilier RG. Physiological ecology in cold ocean fisheries: a case study in Atlantic cod. In: Pörtner HO, Playle R (Ed.). Cold ocean physiology. Cambridge: University Press;1998. p. 463-89.

55. Mork J, Ryman N, Ståhl G, Utter F, Sundnes G. Genetic variation in Atlantic cod (Gadus morhua L.) throughout its range. Can J Fish Aquat Sci 1985;42:1580-7.

56. Hedrick PW. Population biology, the evolution and ecology of populations. Boston: Jones and Barlett Publishers; 1984.

57. Arnason E, Petersen PH, Palsson S. Mitochondrial cytochrome b DNA sequence variation of Atlantic cod, Gadus morhua, from the Baltic and the White Seas. Hereditas 1998;129:37-43.

58. Mork J, Giskeødegård R, Sundnes G. Population genetic studies in cod (Gadus morhua L.) by means of the hemoglobin polymorphism; observations in a Norwegian coastal population. Fiskeridir Skri Serie Havunder 1984;17: 449-71.

59. Mork J, Giskeødegård R, Sundnes G. Hemoglobin polymorphism in Gadus morhua: Genotypic difference in maturing age and within season gonad maturation. Helgoländer Meeresunters 1983;36:313-22.

60. Salvanes AGV, Hart PJB. Is individual variation in competitive performance of reared juvenile cod influenced by hemoglobin genotype? Sarsia 2000;85:265-74.

61. Gjøsæter J, Jørstad K, Nævdal G, Thorkildsen S. Genotype distributions of cod from the Norwegian Skagerrak coast. Sarsia 1992;76:255-9.

62. Jørstad KE, Nævdal G. Studies on associations between genotypes and growth rate in juvenile cod. ICES Ma. Sci Symp., 1994;198:671-5.

63. Nævdal G, Folkvord A, Otterlei E, Thorkildsen S. Growth-rate related to genotype of 0-group cod at 3 environmental temperatures. Sarsia 1992;77:71-3.

64. Imsland AK, Folkvord A, Jonsdottir ODB, Stefansson SO. Effects of exposure to extended photoperiods during the first winter on long-term growth and age at first maturity in turbot (Scophthalmus maximus). Aquaculture 1997;159:125-41.

65. Frydenberg O, Tönnes Nielsen J, Simonsen V. The maintenance of the hemoglobin polymorphism of the cod. Jap J Genet 1969;44:160-5.

66. Mork J, Giskeødegård R, Sundnes G. The hemoglobin polymorphism in Atlantic cod (Gadus morhua L.); genotype differences in somatic growth and in maturing age in natural populations. In: Dahl E, Danielsen DS, Moksness E, Solemdal P (Ed.). The propagation of cod, Gadus morhua L. Flødevigen rapportserie 1 1984:721-32.

67. Rattazzi MC, Pik C. Hemoglobin polymorphism in the cod (Gadus morhua): a single peptide difference. Nature 1965;206:489-91.

68. Perry SF, Tufts B. Fish respiration. San Diego: Academic Press; 1998

69. Monod J, Wyman J, Changeaux JP. On the nature of allosteric transitions: a plausible model. J Mol Biol 1956;12:88-118.

70. Malte H, Weber RE. The effect of shape and position of the oxygen equilibrium curve on extraction and ventilation requirement in fishes. Resp Physiol 1987;70: 221-8.

71. Davis JC. Minimal dissolved oxygen requirements of aquatic life with emphasis on Canadian species. J Fish Res Board Can 1975;32:2295-332.

72. Plante S, Chabot D, Dutil J. Hypoxia tolerance in Atlantic cod. J Fish Biol 1998;53:1342-56.

73. Scholz U, Waller U. The oxygen requirements of 3 fish species from the German Bight - cod Gadus morhua, plaice Pleuronectes platessa, and dab Limanda limanda. J Appl Ichthyol 1992;8:72-6.

74. Schurmann H, Steffensen JF. Spontaneous swimming activity of Atlantic cod Gadus morhua exposed to graded hypoxia at 3 temperatures. J Exp Biol 1994;197:129-42.

75. Claireaux G, Dutil JD. Physiological response of the Atlantic cod (Gadus morhua) to hypoxia at various environmental salinities. J Exp Biol 1992;163:97-118.

76. Houston AH, Murad A. Erythrodynamics in fish: recovery of the goldfish, Carassius auratus from acute anemia. Can J Zool 1995;73:411-8.

77. Chabot D, Dutil JD. Reduced growth of Atlantic cod in non-lethal hypoxic conditions. J Fish Biol 1999;55:472-91.

78. Magnuson JJ, Destasio BT. Global warming: implications for freshwater and marine fish. SEB seminar series. In: Wood CM, McDonald DG (Ed.). Thermal niche of fishes and global warming Cambridge: Cambridge University Press; 1996. p. 377-408.

Lecture

EVOLUTION, COMPLEXITY, INDIVIDUAL, STRUGGLE AND CO-OPERATION FOR LIFE

Giovanni Alfredo Zapponi
Dipartimento di Tecnologie e Salute, Istituto Superiore di Sanità, Rome

"To ask for a definition of life is to ask a something on which proverbially no satisfactory agreement obtains"
(C.H. Waddington, 1968)

This paper is aimed at remembering the important pioneer studies and theories by A.J. Lotka, I. Prigogine, J. Maynard Smith, M. Eigen, C.H. Waddington, D. Levins, R.C Lewontin and M. Ageno (limiting the list to a few names), that still represent a fundamental reference for what was defined as theoretical biology. Most of their ideas and principles still represent the basis of the theoretical approaches, and, in particular, for the system theory, application to biology.

An attempt of deriving some ideas on the evolution process is here presented, that are based on a 'complexity' point of view.

Darwin principle: a too simplified formulation

"A process which led from amoeba to man appeared to philosophers to be obviously a progress - though whether the amoeba would agree with this opinion is not known"
(B. Russell, 1914, cited by A.J. Lotka, in Ref.6).

It is today largely accepted that the concepts and tools of system theory and a 'complexity' point of view may provide a suitable approach for the examination of the Charles Darwin principles of random variation, environmental selection, struggle for life leading to the survival of the fittest. As mentioned by Darwin himself, the principle of struggle for survival was suggested by the T. R. Malthus theory, while an attentive consideration the centuries-old experience and practical criteria of horse and dog breeders (who, following a substantially non - Lamarkian criterion, select and mate the individuals most suitable for their purposes, progressively improving the offspring characters) was an important element for the definition of the principle of character hereditary transmission. The thoroughly closely investigation of spatial distribution, differences and analogies of biological species (in particular during the Beagle ship voyage) provided objective data further stimulating the theory development. This fundamental Darwin work succeeded in putting together many categories of data, experiences, attentive observations and theoretical evaluations into a coherent, rational and revolutionary theory, constituting an important step in the direction of a theoretical biology and of a 'complexity' approach for investigating biological systems.

The simplest and common formulation of the Darwin principle – random variation and environmental selection – certainly does not exhaust all his thought. It is however the mostly discussed and known. Whenever regarded through the criteria of system theory approach, it might be considered as the 'local' point of view of an observer whose attention is 'locally' focused on the particular species and on the stimuli that it receives. In other words, the relationship between the species and the environment is generally assumed to be unidirectional, as the one of a "selector" subject with a "selected" object, in which only the first has the capability of conditioning the latter. This subject-object opposition, basic in the language and human thinking structure, may be thought to also include the one between a creator subject and a created object.

There is no doubt that the Darwin principles, also in their simplest formulation, maintains its validity (as for instance shown by the continuous increase of antibiotic-resistant pathogens that had been and are selected after the extended use of antibiotics); their consideration within a "complexity" point of view is however certainly useful.

Increasing complexity of interactions: time scales

"The 'discovery' of the geological time has been the necessary condition for the first, global interpretation of the evolution process, proposed by Charles Darwin more than 130 years ago" (4)

As underlined by Ageno (1), living organisms are not necessarily 'tending' towards higher organisation levels. The evolution process from simpler to more complex organisms cannot be considered as characterised by a directional and oriented pattern, but rather by something as a complicated landscape. Moreover, available data and estimates provide the indication of the extinction of 99% or more of the species appeared in the world (2), and, from the other hand, the clear evidence of a very large amount (in terms of number and mass) of very simple organisms presently coexisting together with much more complex ones, clearly testifies that evolution towards higher organisation levels is not a general trend (based on this, it has been argued that bacteria could be "the fittest") (3). It is worthwhile noticing that observations in some way similar were also presented by C. Darwin.

As is known, the first simplest forms of life (primordial prokariotes) are estimated to have appeared earlier than 3.5 billions years ago and, presumably, 3.8-4.0 billions years ago, while the first eukaryote cells presumably appeared around 1.0-1.2 billions years ago, followed, around 600 millions years ago, by the first multicellular organisms with shell or skeleton. The life moved from the water to the terrestrial environment about 430 millions years ago, the first mammals appeared around 240 millions years ago, and the genus homo about 2 millions years ago (1, 8).

A first possible observation is that the initial phase of evolution, leading to the appearance of the first prokaryotic cells, may be considered to have required a relatively short time period (at least in "geological time units"). In fact, radioactive dating indicates that the earth's crust solidified about 4.6 billions of years ago; afterwards, further time was necessary for a suitable reduction of earth surface temperature and for the formation of the first atmosphere, through degassing (5). This means that the first prokaryotes appeared presumably less than 1 billion years after the establishment of earth suitable conditions. It is worthwhile noticing that the time period between the appearance of the first prokaryotes and the appearance of the first eukaryotes

was much longer (in the order of 3 billion years). As already said, the following steps were, in geological time, relatively rapid. Lastly, the first *homo* is assumed to have appeared something less than 1 billion of years after the first eukaryotes. This means, in some way paradoxically, that the transition from eukaryotes to *homo* required much less time than the one from prokaryotes to eukaryotes (so that, if time is assumed as the only criterion, the evolution from the first eukaryotes to man could be considered to have been less "problematic" than the one from prokaryotes to eukaryotes).

This is an interesting point, suggesting that the "eukaryote revolution" has created the conditions essential for an "easy" transition towards more complex structures.

This time scale is of major interest. The time series and time trend analysis commonly used in physical and biological studies (generally with much shorter time units) may be of help in the analysis of these processes. The "stasis and punctuate change" theory (3), hereafter briefly discussed, has been largely founded on time scale-related considerations on biological evolution, pointing out its discontinuities and sudden changes.

Increasing complexity of interactions: struggle for life, cooperation, stability and instability

"The organisms do not experiment environments: create them" (2)

"Symbiosis: Progress through co-operation" (4)

"The instances cited should be sufficient to demonstrate how effectively resourceful nature makes use, in her economy, of instability, with its cumulative potency, as a progressive force; as well as of stability, the essentially conservative element in evolution" (6)

"Biological systems are individualised, not repetitive as the physical systems" (1).

As discussed by Lewontin (2), the biological organisms cannot be simply considered the passive consequence of external actions and stimuli. Rather, the whole interactions among the organisms and within organisms constitute something much more complex, and the organisms actively contributed to the creation of the environment, so that their changes are selected by an environment that they have contributed to create. This is true also at a "global" level.

As widely recognised, an oxidising atmosphere is considered as non appropriate for the development of the first forms of life. According to the original Haldane (19) theory, that has found large support by successive studies (e.g., see *ref.* 1), the original atmosphere of our planet, suitable to consent the easy formation of the principal amino-acids in the presence of solar UV radiation, was constituted by a gas mixture including the four elements essential for life, H, O, N and C, but with the absence of free oxygen. Available evidences indicate a transition, about two billions years ago, towards an oxidising, free oxygen rich atmosphere. This change has been attributed to the action of photosynthetic organisms (e.g., cyanobacteria) biochemically transforming carbon dioxide and water into carbohydrates and progressively releasing large quantities of molecular oxygen into the environment and starting the oxidation process (5). The oxygen diffusion in the atmosphere also led to the ozone layer formation, and, consequently, to a significant reduction of ultra violet radiation intensity at the soil level, therefore consenting the existence of the present life forms. A new equilibrium was reached, with the oxygen use in metabolic processes (oxidising metabolism), and the appearance of respiration processes. Life

spread out of water and vegetation invaded the earth (7) (5). It could be observed that in this transition also some positive feed-back chain could have arisen, speeding up the process (e.g., the consequences of vegetation diffusion). In conclusion, a certainly "global" transformation of the environment has been caused, or, in some way, has been "selected", by biological organisms.

The important theory formulated by Eigen (5) has provided a fundamental model, based on the auto-catalysis principle (i.e., on a process characterised by a positive feed-back), of the pre-biotic processes suitable to lead to the formation of the first living organisms. The simplest form of the model entails the interaction of two sets of molecules, the first of them constituted by "nucleic acid-like" molecules, able to self-reproduce and to catalyse the synthesis of a second type of molecules, that, in turn, catalyse the reproduction of the first ones (this latter molecule category might be constituted by "protein-like" molecules or by RNA molecules capable of catalysing the replication). The more general hypercycle model is an extension of the simplest form, constituted by a cyclic connection of single reproduction cycles, with an integration of more "genes" and more catalytic processes. This kind of association, whenever emerging by chance in a biochemical system, may survive and diffuse in it, starting a further evolution process towards a more complex DNA genome-protein based system. The "RNA-catalysed RNA replication" model (5) (8) (9), assumes a condition ("RNA World") in which the genetic information is residing in a RNA molecule sequence and another RNA catalyses the replication properties, while the "Protein World" hypothesis gives the same role to proteins (e.g., *ref.* 10).

It is worthwhile noticing that, as specified by Eigen (5), the hypercycle model has remarkable analogies with the RNA virus structure and biological action, so that it cannot be considered only a theoretical hypothesis, but rather its principles finds support by observable biological processes (the 'auto-catalytic properties' of viruses are so efficient to allow them a very rapid auto-replication within the infected cells and their invasion: "RNA-viruses are natural hypercycles", *ref.* 5) (It is however important to specify that Eigen does not consider RNA or other viruses as possible candidates for a first from of life, because they cannot develop in the absence of a host cell and, rather, may be assumed to be the product of a pre-existing form of life).

Moreover, in a system like the hypercycle, the "internal" selection has a major role: the meaning of mutations of the hypercycle nucleic acids will be mostly determined by their capability of improving or reducing the efficiency of the whole cycle, in terms of replication potential (5).

The universality of the code (even if some minor differences have been identified in some cases) appears as an exceptional feature within the context of the extremely high variability of the life forms, and may represent a major topic in the "complexity" research. Eigen hypothesises that the universal character of the cellular genetic code and of the bio-synthesis mechanism might be attributed to a "once for ever" decision: the properties of the hypercycle, endowed with an extremely high selective potential within a pre-biotic environment and, consequently with the capability of predominate in it, as well as with the capability of reaching a high stability level, may make it a candidate for this event (5).

The development of eukaryotes, probably "the most important and deep discontinuity in evolution" (1), was a fundamental step toward a complexity level that opened the way to a further extremely wide and rapid evolution, and, according to J.R. Reichholf (4),it may be considered a "progress trough co-operation" based on symbiosis. There is today a large agreement on the hypothesis, developed in detail by L. Margulis (11, 12), of the origin of eukaryotes as the result of the incorporation (presumably within a predator-prey relationship), by a prokaryote cell (possibly a primitive mycoplasma), of other specific co-existing prokaryotes. As is known, eukaryote cell organs, as mitochondria (producing energy rich

phosphoric compounds – ATP through an oxidising metabolism) and chloroplasts (effecting the photo-synthesis) have their own independent DNA, their own membrane and may reproduce themselves autonomously within the host cell. Moreover, they have structures and properties largely analogous to the ones of prokaryotic organisms capable of effecting oxidising metabolism or photosynthesis. Similar considerations hold for other structures of eukaryotic cells, that are composed by tubulins (centrioles, kinetosomas, eukaryotic cilia and flagella, mitotic apparatus), that are hypothesised to have derived from incorporated prokaryotic spirochete-like organisms. According to this theory, the formation of animal and vegetal eukaryotes cells respectively implied the incorporation of three and four different types of prokaryotes in the 'hosting cell' internal environment (in the case of vegetal eukaryote cells also the photo-synthesiser prokaryotes) (1).

Necessary conditions for this result obviously were the survival and the achievement of an equilibrium of the 'guest' organisms within the 'host cell' internal environment, the establishment of suitable symbiotic interactions (which implies specific characteristics of the 'ingested' and the 'ingesting' organisms), as well as a process suitable to replicate this more "complex" new cell without the loss of its new acquired characteristics (that means the co-ordinated reproduction of the organisms associated in this new form). A condition possibly facilitating the survival of the 'guest' organisms within the 'host' organisms could have been some similarity of the internal cell environment to the 'primordial broth'.

Some conditions may have facilitated this process; for instance, a possible process leading to the incorporation of a mitochondrion-like prokaryote by an other prokaryote (presumably a proto-mycoplasma) could have included several steps: loss and diffusion of some amount of energy reach molecules in the area close to their producer (the mitochondrion-like prokaryote); an approaching of the second prokaryote (proto-mycoplasma-like), stimulated by the presence of these molecules; then, the phagocytosis of the first by the latter organism (1).

It is worthwhile underlining that the "bricks" with which the eukaryote cell was constructed were complex and significantly evolved organisms, provided with remarkable capabilities (e.g., photosynthesis, or oxidising metabolism, or mobility in the environment through flagella or other means, or using matter and energy produced by other organisms, or predation). Moreover, the establishment of an effective symbiosis (or in common words, a 'co-operation') cannot be thought to have been immediate and easy (e.g., this implied the presence of the suitable organisms in specific areas and specific time periods and the emergence of new, suitable and non-competitive interactions among them). Moreover, the transformation of an 'ingestion' process into a stable symbiosis condition certainly may be not considered a simple and obvious event. This could, at least in part, explain the long time passed between the appearance of prokaryotes and the appearance of eukaryotes.

Such symbiotic association provided the eukaryote cells with enormous advantages for further evolution, as their high energy availability, the redundancy of their bio-synthetic structures and apparatuses, their availability of complex and efficient internal regulation system, their high flexibility and adaptation capability, their possibility of reaching a larger volume in comparison with the one possible for prokaryotes, their capability of establishing together an effective association and, consequently, of producing multi-cellular entities (not possible for prokaryotes). However, it is useful to remind here an important observation by S.J. Gould (3): prokaryotes continue to be perfectly and efficiently adapted to the environment, where today they exist in extremely high quantities; their "limits" did not pose many problems for their survival capability.

This clearly means that survival capacity does not necessarily imply a higher evolution and higher complexity level.

According to the available data and evaluations, the formation of multi-cellular organisms, through the aggregation (or the association) of eukaryotes, appears to have taken place after a time period much shorter than the one elapsed for the preceding step. As is known, the actual possibility of production of a multi-cellular organism from a set of eukaryotic cells is demonstrated by the observable reproductive cycle of a relatively common amoeba (*dictyostelium discoideum*). These amoebas, which normally assume the form of common unicellular eukaryotic organisms able to move in the environment, in scarce or no nourishment conditions may converge together guided by chemical signals and form a pseudo-plasmodium. This process is reversible: when the environmental conditions improve, spores are emitted by the mature new formed organism, so that, finally, individual amoebas diffuse again into the environment (1).

It is worthwhile underlining that in all the above discussed processes (at biochemical and biological levels) a main role is constantly assumed by the association and symbiosis of proper components. In this whole context, the principle of a "co-operation for life" (suggested as a keyword by J.H. Reichholf, *ref.* 4) appears to have a role at least as important as the one of the principle "struggle" or "competition for life".

The principle that stability of biological systems is a necessary condition for their survival, as well as the principle that an absolute and eternal stability prevents any change and therefore any evolution, at a first glance may both appear to have a tautological character. However, this tautological character disappears whenever the dialectics of stability/instability is examined in the light of objective observations and of a theoretical approach including a 'complexity' point of view.

The recent theory of macro-evolution, based on the principle of stasis and equilibrium periods followed by a very rapid shift into new developmental paths (termed as "stasis punctuated by change"), recently investigated thoroughly by Gould (3), is of main interest in this discussion. As is known, this theory is based on many evidences, deriving from studies and dating of fossils, that suggest limited or no changes for very long time periods, preceded or followed by great changes (e.g., appearance or disappearance of one or more species or of some ecosystems) taking place in relatively short periods. From the point of view here adopted, this could be regarded as a sequence of stability and instability states. The above cited sentence by A.J. Lotka (6): "an effectively resourceful nature makes use, in her economy, of instability with its cumulative potency, as a progressive force: as well a of stability, the essentially conservative in evolution", even if presented about eighty years ago, is today still fully valuable.

The positive and negative feed-back processes, and, in a broader sense, the instability or stability conditions, largely studied in system theory and objectively observed in biological and biochemical systems, may provide an important tool to investigate and describe the evolution processes. It is worthwhile underlining that within this paradigm the single individual may acquire an important meaning and significance, not emerging in most of other theoretical approaches. The above mentioned M. Eigen autocatalytic models (the various forms of hypercycle theory) imply that even one single molecule emerging by chance within a biochemical system, capable of establishing catalytic interaction(s) with other present molecules, may in principle start an association capable to survive and diffuse into such system, possibly invading it. In broader terms, according to I. Prigogine (13), the new component(s) with auto-catalysing or mutual-catalysing properties, even if arising in the system at infinitesimal level (the adjective 'infinitesimal', used by Prigogine, is important), may introduce new interactions competing with the pre-existing ones: the structural stability or instability of the system with respect to this perturbation will determine the evolution of the new component(s) and of the whole system (in the first case – i.e., stability – the new component will not survive, while in the second case, – i.e., instability – the whole system will change its

structure, including new components and interactions, or, at worst, could also undergo to disruption). This possibility of infinitesimal components (single molecules, single cells) to acquire significance under specific condition may be thought to be a specific property of biological and biochemical systems. Early works by I. Prigogine have formally shown the possibility of these processes. The "hopeful monster" theory, originally proposed by Goldschmidt and more recently re-examined by Gould (3), may be in some way included in the same paradigm (the hopeful monster has been defined as a mutant organism, endowed with new and suitable adaptation features, not available to the other organisms present in a specific niche – therefore, comparatively, "monster" –, providing it with a high competition level – therefore, "hopeful" –).

On the other hand, as already discussed, it is obvious that only biological systems with an appropriate level of stability may survive, resisting to the large majority of perturbations of external or internal origin. This stability, preserving system existence and making them available to further evolution, is not absolute, so that specific and sporadic events may cause changes increasing the complexity and fitness levels.

The "homeostasis" principle of living beings (the holding constant of some essential parameters of biological systems) makes part of this paradigm. As discussed by Maynard Smith (14), the persistence of ecosystems (and, in general, of biological systems) presumably implies that the interactions within them and of them with the external reality have a highly non casual character, but, rather, are the consequence of some form of selection (this assumption widens the objects of selection with the inclusion of the interactions).

Moreover, the extension of the homeostasis principle into the homeorhesis principle (the holding constant of a time extended course of change, i.e., a "trajectory" in the phase space), and the related theory of "chreods" (canalised trajectories behaving as "attractors of nearby trajectories") by C.H. Waddington (15) have provided an essential framework for theoretically studying the morphogenetic and developmental biological processes.

As far as competition in ecology is concerned, some considerations by J. Maynard Smith (14) (based on A. Lotka and V. Volterra studies) are particularly interesting: an equilibrium may arise between or among in the competing species only if the intra-specific regulation (auto-inhibition, auto-regulation of the population growth) prevails on the inter-specific one (reciprocal inhibition, reciprocal regulation of growth); otherwise, the two (or more) species will not coexist (one or more of them will disappear). This means that a competition excess may be destructive.

Levins (16) presented important considerations about the analysis of system structure and of some system relevant component properties. For instance, he underlines that system components (or subsystems that are component of a higher level system), which are characterised by a rate of change much slower than the one of the other ones, may in practice act as process constants, at least during a specific and limited time period (the simplest example is the driving action of rocks on the water flowing over them; the erosion interaction of water on rocks may be obviously neglected in the short term analysis of water flow processes for which the rock structure is a determinant; however, this is not true in a much longer time period). This methodological approach (the example mentioned is only a small part of it), based on the principle of considering the different time rates of changes ("inertia") of the different system components is certainly useful for simplifying the system analysis.

A detailed discussion of methodological tools for system analysis is out of the scopes of this paper. It may be however useful to mention that, as is known, the whole or a selected part of the interactions taking place in the analysed process may be formally described through appropriate mathematical models, and/or systems of differential equations (or of finite difference equations), and/or computer simulation procedures. These tools allow to test and/or suggest

theoretical hypotheses, to simulate evolution patterns, to carry out predictions, to verify the stability of the examined or hypothesised systems in relation to specific perturbations, to analyse the possible consequences deriving by the introduction of one or more new variables (e.g., new individuals or species or new environmental factors) as well as the possible consequences of changes of some interaction pattern. A long tradition exists in this field, starting with the very important pioneer work by A.J. Lotka (6) and V. Volterra (17) and uninterruptedly continuing up to day. The 'complexity-oriented' approach based on these methods has been fruitful and has widened the scientific research on biological evolution, allowing to insert available data into a logical scheme (e.g., as discussed by Maynand Smith and Szathmary, *ref.* 8). There is much work to do in this field.

Lastly, Lewontin (2), criticising the common simplified statement that genes make the proteins and are self replicating, underlines that genes, by alone, are not in condition of doing anything. Rather, a protein is produced by a complex chemical system, involving many other proteins and using the specific nucleotide sequence of the involved gene as scheme.

These observations appropriately introduce a largely discussed old problem: the properties of a complex system are simply the consequence of the ones of the components or, rather, new properties emerge from complexity? (i.e., in simpler words, the whole is more than the sum of components?). There is a Zen philosophy koan (i.e. a question that stimulates the awakening of one's true/deep/pure meditation) in some way relevant: "every one knows what is the sound caused by clapping two hands: what the sound caused by clapping only one hand is ?" - according to Lewontin, what is the meaning of a DNA molecule without a biochemical system capable to make a correct use of it?).

The above mentioned point of view by Lewontin reminds, in some way, the obvious observation that a word does not mean anything without a language and a culture, and it is useless without writers and/or speakers and readers and/or listeners. It is perfectly clear that a DNA molecule acquires its effective biological meaning whenever it is adequately inserted in a cellular system, capable (when it is appropriate) of reading, decoding, translating and then using its message. Moreover, the cellular system has to protect and preserve this information source. Lastly, in order to make evolution possible, this cellular system also needs to be able to interpret and use the new message possibly arising by chance as consequence of a mutation (something like the extension of a language to include and use new words). Eigen observes that the transition from non-living to living structures has taken place as consequence of the increasing capability of treating information in a "nearly intelligent way", and that the information and its use by biological entities is a property far beyond of chemistry as we know it (even if biochemistry provides its tools) Finally, the biological evolution may be assumed to be not *a priori* predictable by the presence and characteristics of the original chemical and physical environment.

An appropriate level of complexity is necessary for life, leading to the existence of structures capable of preserving the information necessary for their existence, of replicating themselves and of undergoing to changes, within a dialectics of stability-instability.

It is worthwhile noticing that the human culture (that is 'information') was and is preserved and stored (in human minds, on stones, on papyrus, in books, images, musical notes, museums, CDs, etc.), is communicated, and, therefore, 'replicated' (orally, through writing, education and training, arts, customs, mass media, imitation, person-to-person communication, familial communication, etc.), and undergoes to changes (due to new ideas and theories, practical experience, suffering and joy, exchanges among different human groups, the capability - sometimes - to learn from history, disruptive events - including war -, assimilation, protest, discussion, economical bounds, hopeful thinking, ethics, sympathy and solidarity, etc.). In some way, the evolution of culture has some structural analogies with biological evolution, of which represents, in some way, a continuation.

Tentative conclusions

"Nature must be considered as a whole if she is to be understood in detail"
(Bunge, cited by A.J. Lotka, in Ref. 6)

As a possible conclusion, some point might be underlined:
- in a complex biological system the single individual may be important;
- there are good reasons for assuming that, in biological evolution, also a principle of *co-operation for life* has a fundamental role, together with the principle of *struggle for life*;
- the selection is not only unidirectional;
- living organisms have contributed to create ('to select') the environment (in a broad sense);
- the development of *homo* from eukaryote cell appears to have required a time period much shorter than the one for the development of eukaryote from prokaryote cell;
- survival capability does not necessarily require evolution towards a more complex structure (the case of bacteria);
- the fittest is not necessarily the best (in the usual meaning of this word);
- also interactions among components biological systems and ecosystems may undergo to selection;
- negative and positive feed-back interactions, and stability and instability conditions, are all important in evolution processes;
- evolution is not only a slow gradual process;
- the succession of stable states, separated by instability conditions and relatively rapid changes, may constitute another basic evolution process (macro-evolution theories);
- coexistence of different populations is allowed by self-regulation and is disrupted by crude competition;
- during limited time periods, slowly changing components of a biological system, because of their inertia, are scarcely influenced by the other ones and exert on them nearly constant unidirectional interactions;
- the significance, in a broad sense, of biological units, depends on the 'complexity' of which they make part;
- the evolution of human culture has some structural analogies with biological evolution;
- between a strong crude armed individual and a gentle mother with her children, who is the fittest ? The last one, in the long term (hopefully).

Acknowledgements

Gratitude is here expressed to Dr. R. Benigni, for stimulating me to re-thinking the topics of this paper, to Dr. P. Del Giudice, for his useful comments and to Prof. Somenzi of Philosophy of Science, who has introduced me to these arguments – decades ago –.

References

1. Ageno M. Le radici della biologia. Milano: Feltrinelli, 1986.
2. Lewontin RC. Biology as ideology. The doctrine of DNA. Concord, Ontario, Canada: Anansi Press Limited, 1991.
3. Gould SJ. The structure of evolutionary theory, Cambridge: Harvard University Press, 2002 (Italian version: La struttura della teoria dell'evoluzione". Torino: Codice Edizioni, 2003.

4. Reichholf JH. Der Shopferische Impuls. Eine neue Sicht der Evolution. Munchen: Deutsher Taschenbuch Verlag GmbH and Co., K.G, 1992 (Italian version: L'impulso creativo. Milano: Garzanti, 1995)
5. Eigen M. Stufen zum Leben. München: R. Piper GMBH & Co; 1987. (Italian version: Gradini verso la vita. Milano: Adelphi Ed.; 1992).
6. Lotka AJ. Elements of mathematical biology. New York: Dover Publications; 1924 (revised version, 1956).
7. Levine JS. The early atmosphere: a new picture. Sci Act 1986;23(1):6-16.
8. Maynard Smith J, Szathmary E. The origins of life. Oxford: Oxford University Press; 1999 (Italian version: Le origini della vita. Torino: G. Einaudi; 2001).
9. Joyce GF. The antiquity of RNA-based evolution. Nature 2002; 418, 214-20.
10. Ikehara K. Origins of gene, genetic code, protein and life: Comprehensive view of life system from GNC-SNS primitive genetic code hypothesis. J Biosci 2002;27(2):165-186.
11. Margulis L. Origin of eukaryotic cell. New Haven and London: Yale University Press; 1970.
12. Margulis L. Symbiosis in evolution: life and its environment on the early earth. S. Francisco: Freeman; 1981.
13. Prigogine I, Stengers I. La Nouvelle Alliance. Paris: Gallimard; 1981.
14. Maynard Smith J. Models in ecology. London: Cambridge University Press; 1970.
15. Waddington CH. The basic ideas of biology. In: Waddington CH (Ed.). Towards a theoretical biology – Prolegomena. Edinburg, UK: Edinburgh University Press; 1968.
16. Levins R. Complex systems. In: Waddington CH (Ed.). Towards a Theoretical biology – Drafts. Edinburg, UK: Edinburgh University Press; 1970.
17. Volterra V. Variazione e fluttuazioni del numero di individui in specie di animali conviventi. Memorie dell'Accademia Nazionale dei Lincei, 1926, 6,(2): 31-7.

Short communication

SOLAR ULTRAVIOLET RADIATION AT THE EARTH'S SURFACE: FACTORS AFFECTING ITS IMPACT ON HUMAN BEINGS

Giuseppe Rocco Casale (a), Anna Maria Siani (a), Alfredo Colosimo (b)
(a) Department of Physics, University of Rome "La Sapienza", Rome, Italy
(b) Department of Human Physiology and Pharmacology, University of Rome "La Sapienza", Rome, Italy

Introduction

The ultraviolet (UV) region spans the wavelength range from 200 to 400 nm and accounts for less than 9% of the solar output (around 120 Wm^{-2}). UV radiation reaching the earth's surface is controlled by many factors such as astrophysical (sun's activity), astronomical (earth-sun distance, solar elevation), atmospheric (absorption and scattering due to gases, such as ozone, aerosols and clouds) and geographical (altitude, albedo, surface orientation) (1).

Solar ultraviolet radiation is usually classified as UV-A (315-400 nm), as UV-B (280-315 nm) and as UV-C (200-280 nm) (2). The UV portion of spectrum relevant to environmental biology is restricted to the UV-B and UV-A ranges. Wavelengths shorter than 280 nm are completely absorbed before reaching the biosphere, UV-B radiation is efficiently but not completely blocked by atmospheric ozone while atmospheric constituents affect UV-A radiation less. The established effect of stratospheric ozone depletion has given rise to concern about its effect on the ecosystems and on human health (3).

The need to identify possible threats to the biosphere requires proper sensors capable to directly detect biological effects caused by ambient UV radiation and possess high sensitivity to small changes of UV-B (4). Polysulphone dosimeters are reliable, portable, and cost-effective, which makes them a suitable choice.

The study of the factors affecting UV impact on people is characterized by an inner complexity due to the need of combining the accurate determination of the ambient UV radiation with the analysis of its biological effects.

Environmental UV radiation

The evolution and growth of most aquatic and terrestrial life forms is influenced by several environmental variables including the intensity of UV radiation at the earth's surface or under water. The negative correlation between spectral UV-B radiation and total ozone has been properly documented (3). If all other variables (astrophysical, astronomical, atmospheric and geographical) were constant, the degree of UV attenuation would depend only on ozone variability. However, the understanding of all processes affecting surface UV radiation is rather more complicated. Therefore, to quantify the effect of all parameters at different times and space scales is a cumbersome procedure.

The local noon erythemal UV irradiance as measured by TOMS onboard Earth Probe satellite on June 21st 2003, in which regional scale variability is superimposed on the latitudinal

gradient determined by the differential sun illumination, shows that at the global scale, the main factor driving the UV irradiation is the latitude. On the contrary, the UV daily dose in Italy is mainly determined by the altitude of the sites and by climatological atmospheric patterns.

Measuring UV radiation

UV measurements are carried out via different independent instruments with various output formats and without standard calibration procedures (6). The classification of UV sensors is based on their spectral resolution: spectroradiometers (that measure the intensity of radiation every 1 nm or less), moderate and narrow-band radiometers (that measure in bands of ~10 nm) and broad-band radiometers (measuring in a specific range, usually UV-B, UV-A or a combination of both).

The accuracy of instruments, currently estimated at 5% for the best maintained spectroradiometers, is vital for the credibility of UV data. In spectral measurements the uncertainty increases at wavelengths below 300 nm, where the solar signal is weak and masked by instrumental noise (7). Broad-band instruments have higher uncertainty than spectroradiometers.

The impact of environmental UV radiation requires knowledge of action spectra of biological systems, namely of functions expressing the effectiveness of the electromagnetic radiation in causing a specific response of the biological system.

Action spectra have been used for several critical biological responses: DNA damage, inactivation of human fibroblast, keratinocytes and melanocytes, minimal erythema, squamous cell carcinoma in mice, malignant melanoma in fish and plant damage. In Figure 1 the action spectra for some selected UV-related effects (eryhtema, carcinogenesis in mice, photosynthesis inhibition and DNA damage) are shown. The relative response among different spectra is normalised to unity at 300 nm to allow an intercomparison. However, even when measurements of UV radiation are highly accurate, the biologically effective irradiance can vary substantially as a result of experimental errors in the action spectra (such as a too narrow waveband) and the underlying hypothesis of additive spectral effects, which is not always satisfied in nature (8).

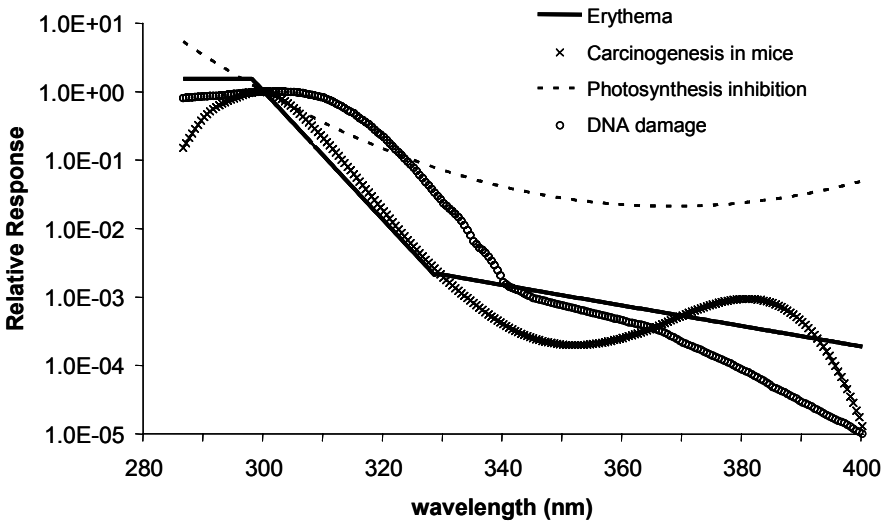

Figure 1. Action spectra for selected UV effects

In addition to the UV measurements, radiative transfer models are available to determine UV irradiances on the ground. Some of them are sophisticated multiple scattering codes based on a neural network approach and contribute to improve the understanding of complicated scattering and absorption processes in the atmosphere.

Human UV exposure

The relationship between UV radiation and its biological consequences has been studied already for several years (9). Interest in this subject increased as a result of recent findings on stratospheric ozone decrease and the consequential increase of solar UV at ground. When UV photons impinge on people, the difficulty of the problem further increases, because solar exposures vary according to the length of time spent outdoors, the time of day and the period of the year, type of activity undertaken, body posture, and the UV protective used [10]. Depending on the amount of available ambient UV radiation, the individual response is determined by: (a) the amount of absorbed UV dose (hourly, daily, monthly, etc.); (b) the characteristics of the interface radiation-matter (epidermis); (c) the photoreactions occurring in the inner layers.

Polysulphone personal dosimetry

The documented worldwide increase in skin cancer cases in recent years has stimulated research on the acute and chronic effects of UV radiation on protected/unprotected skin and eyes.

Polysulphone (PS) dosimetry (11) is oriented towards the understanding of the role of (a), (b) and (c) on target groups. They have been widely used to quantify personal UV exposure of humans in different settings during ordinary daily activities (12).

PS dosimeters, small devices requiring no external power input, are made up of a thin film (usually 40 μm) with spectral sensitivity similar to the erythemal response. In Figure 2 the polysulphone dosimetry device for the study of the distribution of UV radiation on the human body is shown. A dosimeter (left) is made by attaching a PS film on a PVC holder (size 3 cm x 3 cm with a 1.6 cm x 1.2 cm aperture). It can be used on manikins too (right).

Figure 2. Polysulphone dosimetry device for the study of the distribution of UV radiation on the human body

When the dosimeter is exposed to solar UV, the diphenyl sulphone group in polysulphone absorbs UV at wavelengths shorter than 330 nm and an increase of optical absorbancy occurs. Since the largest change in the optical absorbancy, before and after the UV exposure, is at 330 nm, measurements of optical absorbancy change at this wavelength can be related to the ambient UV dose through a calibration curve. By using measured ambient UV irradiances in combination with an understanding of the distribution of solar UV in the human body, estimates of long term exposures can be determined. PS dosimeters cannot be reused after exposure to the sun.

Results and conclusions

Experiments carried out in Rome and vicinity during the summer of 2004, both with manikins and volunteer bathers, show that PS dosimeters targeting specific population groups, allow for quantitative measurements of personal UV exposures. The measured doses on different sites of the human body can be determined by a calibration curve (Figure 3). Each point refers to the change in absorbancy (vertical axis) recorded by a single dosimeter after a fixed exposure time. On the horizontal axis, the corresponding ambient dose as measured by a reference instrument is reported

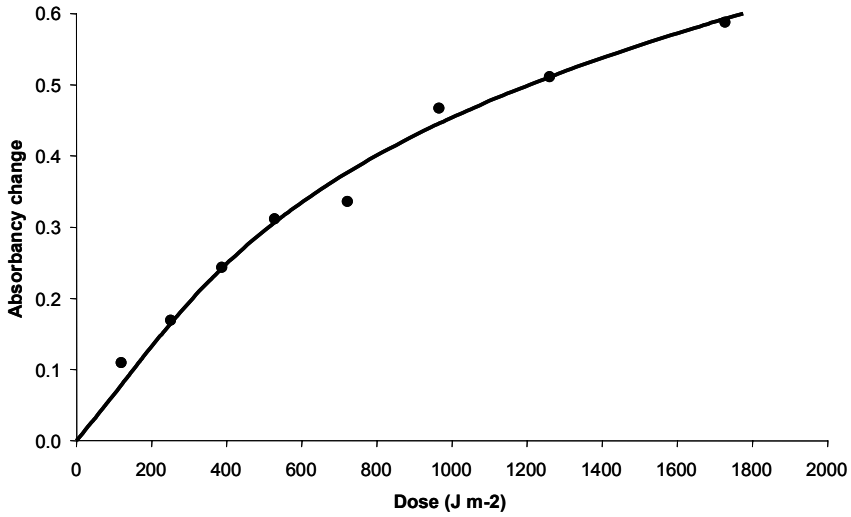

Figure 3. Calibration curve for evaluating personal exposures from changes of dosimeter absorbancy (Rome, July 2nd 2004)

Preliminary results obtained with manikins are presented in Table 1 for supine and sitting postures.

Table 1. Percentage of personal dose with respect to ambient dose for two different postures

Posture	Shoulder	Breast	Cheek
Supine	21%	59%	63%
Sitting	83%	93%	102%

Doses affecting human beings are influenced mainly by the orientation of the body surface respect to the sun. UV dose tends to increase when the portion of body is exposed towards the incoming direct radiation. The albedo effect of the ground increases the percentage of personal dose more in the sitting than in the supine posture. In the sitting posture the dose is 1.6 (breast and cheeks) and 4 (shoulders) greater than the supine. Note also that the albedo effect, in combination with local atmospheric parameters, can enhance personal exposure beyond ambient level (102% for cheeks). Results are congruent with those obtained on volunteer bathers with a single dosimeter on the breast. Doses on individuals are modulated not only by the orientation of the body respect to the sun but also by the length of time spent in the shade. The values of volunteers exposure doses are up to 60% of ambient dose.

A proper methodology for measuring the level of UV radiation on different parts of the body, based on polysulphone dosimetry, has been discussed and tested. Results can be interpreted only if the local characterization of ambient UV radiation is taken into account. Future efforts will be addressed at the search for biological markers whose modification is a direct or indirect effect of UV radiation. Moreover, possible correlations between markers and personal absorbed doses will be studied.

References

1. Kerr JB. Understanding the factors that affect surface UV radiation. In: Demaret R, Edwards O, Ferguson W (Ed.). Proceedings of the 48th SPIE's Meeting, International Symposium on Optical Science and Technology; 2003 Aug 3-8; S.Diego (CA). 2003. p. 686-98.
2. Diffey BL. What is light? Photodermatol Photoimmunol Photomed 2002;18:68-74.
3. World Meteorological Organization. Scientific assessment of ozone depletion. Geneva (Switzerland): WMO; 2003. (Report No. 47. 2002 Global Ozone Research and Monitoring Project).
4. Webb A. Measuring UV radiation: a discussion of dosimeter properties, uses and limitations. J Photochem Photobiol B 1995;31:9-13.
5. Meloni D, Casale GR, Siani AM, Calmieri S, Cappellani F. Solar UV dose patterns in Italy. Photochem Photobiol 2000;71:681-90.
6. World Meteorological Organization. Guidelines for Site Quality Control of UV Monitoring . Geneva (Switzerland): WMO; 1998. (Report No. 126. Global Atmosphere Watch).
7. World Meteorological Organization. Instruments to measure solar ultraviolet radiation, part 1: spectral instrument. Geneva (Switzerland): WMO; 2001. (Report No. 125. Global Atmosphere Watch).
8. Horneck G. Quantification of the biological effectiveness of environmental UV radiation. J Photochem Photobiol B 1995;31:43-9.
9. Diffey BL. Solar ultraviolet radiation effects on biological systems. Phys Med Biol 1991;36:299-328.
10. Diffey BL. Ultraviolet radiation and human health. Clinics in Dermatology 1998;16:83-9.
11. Davis A, Deane GHW, Diffey BL. Possible dosimeter for ultraviolet radiation. Nature 1976;261:169-70.
12. Kimlin MG. Techniques for assessing human UV exposures. In: Demaret R, Edwards O, Ferguson W (Ed.). Proceedings of the 48th SPIE's Meeting, International Symposium on Optical Science and Technology; 2003 Aug 3-8; S.Diego (CA). 2003. p. 197-206.

Short communication

DECISION ENGINEERING IN COMPLEX SOCIAL-ECONOMICAL SYSTEMS USING SELF-ORGANIZED CRITICALITY

Roma Siugzdaite, Saulius Norvaisas
Institute of Mathematics and Informatics, Vilnius, Lithuania
E-mail: roma.siugzdaite@rst.lt*;* saunor@ktl.mii.lt

Introduction

Complexity is one of the most important features when we talk about natural, social or even artificial systems. Complex systems exhibit behavior that differs from the sum of the individual component behaviors. P.Bak defines systems with large variability as complex (1). Systems or projects at any scale do not function as isolated projects or segments, but rather as a network that serves to move people, material, energy and information from one place to another. Complex systems theory can help us to explain this variability and the sometimes-unpredictable behavior of pavement networks.

In this paper we involve Self-Organized Criticality (SOC) theory to analyze urban as well as electricity production data. SOC is the name for the tendency in many large interactive systems to evolve toward a critical state in which events in the system follow a simple power law. Self-organized criticality is the only model or mathematical description that has led to a holistic theory of dynamical systems.

In theory of *adaptive* decision-making the main task is to find values of dynamical parameters to satisfy local optimum criterion. In contrary, for the long-term strategies there is important to search for the systems global optimal solution. In this case we have to take into consideration the main features of SOC systems such as resistance not only to inner non-linear interactions but also to outer influences, positive innovations and destructive perturbations. We assume that the systems criticality simplifies the long-term optimal solutions finding. We will show that complex systems in SOC state are maximally adaptive. Meanwhile external changes of the system, which is taken out or didn't reach SOC state, can determine system loss or total collapse.

Study of a urban system

In our analysis, because we are interested only in global characteristic of the system, a urban system is a physical concentration of people and buildings. We assume that number of people in every city is proportional to the number of buildings; therefore we can model growing of cities only by modeling the houses system dynamics. With reference to statistical sources we can gain comprehensive "rank-size" plots from different countries, compare them and colligate results. Big countries such as USA during recent decade have almost perfect "rank-size" distribution with a 45^{o} slope and with small fluctuations every year. However it is also common to smaller countries as Lithuania, Sweden, Estonia and Norway (Figure 1). From these graphs we suppose

that urban systems from analyzed countries are settled and have above-mentioned global property – SOC – placed as a line in logarithmic rank-size plot.

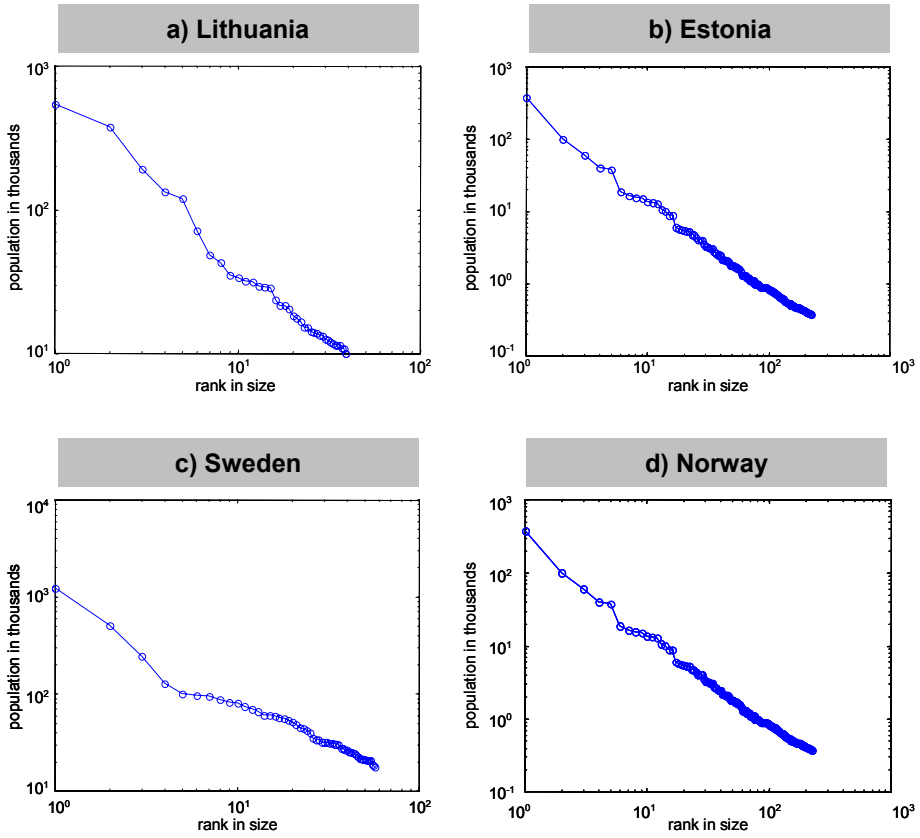

Figure 1. Distribution of population to city rank

The morphology of system of cities may be regarded as a balance between ordered and chaotic structuring elements, a phenomenon, which has already been identified for some cellular automata by Stephen Wolfram (1984) and Chris Langton (1990).

Let's look into medium level – cities in a country. As cities are physical agglomerations of population and housing, it is thought that there exists a threshold along the population-size continuum of settlements at which a village becomes a town, although this threshold varies significantly in space and over time. How to find the threshold? The earliest formal proposal was Zipf's law: the rule can be written as:

$$P_r = \frac{P_1}{r^{\alpha}}$$

where α is a scaling constant. Urbanization is a self-organizing system without any influence from outside, where any bigger fluctuation about the threshold causes system's dynamical changes in space. According to the theory in reality we should obtain the slope of 'rank-size' curve close to –1. But an urban system is dynamic, so one-year measurement is a static value in time, thereby we can see on of the small deviations from SOC state. Fluctuations in time are

available from the data of several years. Then it's a question of population census frequency and data retrieval though. Small variations fulfill conditions practically.

We show these graphs of populations from Lithuania, Estonia, Sweden and Norway in 2003 where the link to 'rank-size' is implied graphically (Figure 1).

Results of the real data statistical analysis (Table 1) show that the slope of these curves is close to expected with small permissible variations. Positive or negative variations conclude the lack or surplus of big or small cities.

Table 1. Scaling constant of Zipf's law

Country	Slope constant
Lithuania	-0.89
Estonia	-1.11
Sweden	-0.89
Norway	-0.76

CA model URBACAM

A cellular automaton is chosen as a modelling tool, because ODE or PDE are not able to describe global behaviour of the system and also they can't show spatial system dynamics in time. CA are discrete in time and space, meanwhile differential equations are discrete only in time.

According to the theory of cellular automaton, the global behaviour of a self-organizing system is governed by locally defined transmission rules. For an urban system, a fundamental question is to what extend urban development is locally specified process.

The model URBACAM (URBAnistic Cellular Automata Model) (7) is the same as done in my PhD thesis. What model parameters will cause an emergence? How sensitive they are to small changes?

However, most applications of cellular automaton models in urban research apply to a larger neighbourhood size than applications in natural sciences. This is probably of difficulties in justifying transition rules in behavioural terms. In our case transition rules are free from number of neighbours, so we can analyse situations with number of neighbours from 8 to 80. Some examples with different neighbourhoods: Moore neighbourhood {8}, extended Moore Neighbourhood {24}, {48} and {80}.

Mathematical model description

The simulated cities grow on a regular quadratic (n x n)-grid with identical cell automata located at each grid position (i,j). In our case, a grid dimension of $n=100$ is chosen to optimise computational costs that scale with n x n.

Let $S^t_{x_{ij}}$ be the state of a cell x_{ij} at the location i,j at time t. $S^t_{x_{ij}}$ belongs to a finite number of states of cells in the cellular space.

Each cell automata can take one of the certain state from a set $S=S_{empty} \cup S_{active} \cup S_{fixed}$, where $S_{active}=\{houses\}$, $S_{fixed}=\{forest, rivers, roads\}$. State transitions are possible from an empty into an active state (growing) and backspace (decaying).

Let $W^t_{x_{ij}}$ be the weight of the cell at time *t.* Then the weight of the cell's neighbourhood at time *t* will be $\widetilde{W}^t_{x_{ij}}$. So, if the cell $x_{ij} \in S_{active} \cup S_{fixed}$, then its neighbourhood weight is:

$$\widetilde{W}^{t+1}_{x_{ij}} = 0; \qquad [1]$$

if the cell $x_{ij} \in S_{empty}$,

$$\widetilde{W}^{t+1}_{x_{ij}} = f(W^t_{x_{ij}}, W^t_{\Omega_{x_{ij}}}) = \sum_{k=i-1}^{i+1} \sum_{l=j-1}^{j+1} W^t_{x_{kl}}; \qquad [2]$$

where $\Omega_{x_{ij}}$ represents a set of cells at the neighbourhood of cell x_{ij} ,

$W^t_{\Omega_{x_{ij}}}$ is a set of weights of cells $\Omega_{x_{ij}}$ at time t, and *f* is a function. In a growing process active cells neighbourhood doesn't weight anything.

If consider the cell itself as a member of its neighbourhood, then

$$W^{t+1}_{x_{ij}} = f(W^t_{\Omega_{x_{ij}}}) \qquad [3]$$

In our case transition function is random and depends on the total weight of cells distribution.

$$random\left\{\frac{\widetilde{W}^t_{x_{ij}}}{\widetilde{W}^t_{S_{empty}}}\right\} \in [0..1]; \Rightarrow x^{t+1}_{gq} \qquad [4]$$

x^{t+1}_{gq} - the element that will become active in *(t+1)* step.

Chaotic nature of urban development is modelled with probabilistic component of simulation model. Consequently, we never might expect two simulations to be identically and simulation runs will differ from the observed situation at least quantitatively, but not necessary qualitatively. So, we have to find parameters and their confidence intervals for a country that settled in self-organized critical state.

Calculations

Which values of parameters describe an emergent of global phenomenon – SOC – in our model? To find these values the grid of [*100 x 100*] elements is not sufficient, because most of all we can get only 3 ranks of clusters (agglomerates). For experimentation this grid is very good, but for better quality of results we need 200x200, 300x300 or even bigger grid. But then we face problems because of computer capacity and need to use more powerful ones.

Calculations in order to find parameters' were done on [100 x 100] grid. So, it wasn't found an optimal size of lattice in this paper.

After analysing calculation data we found graphs on how spatial distribution depends on number of neighbours and parameter values, that show SOC.

Here is some examples how looks like spatial distribution according to number of neighbours (Figure 2).

Figure 2. Simulation results with different number of neighbours

Moore neighbourhood is used the most often, because of its simplicity and small expenditure of calculation time and computer memory. The more neighbours we have the more widely houses are spread spatially, so it's only one-way to get more small clusters. Another way is to increase the weight of "empty" cell. Hence changing one parameter value influences changes of other two, as evidenced in Figure 3.

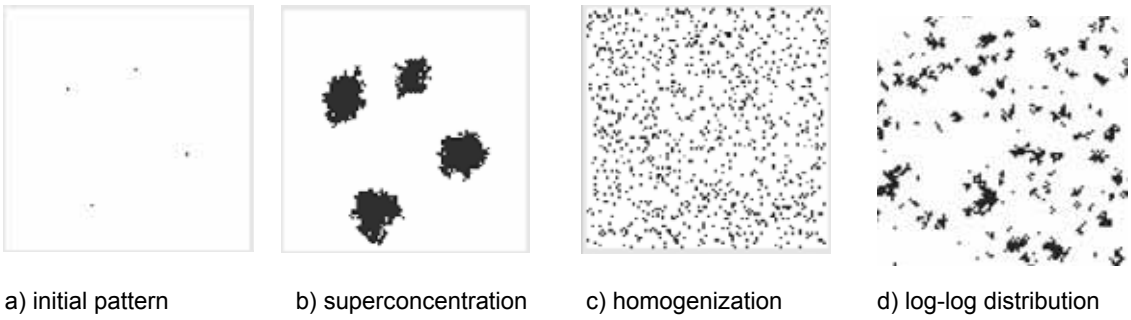

Figure 3. Spatial distribution according to weights of cells

There are two ways to find parameters for SOC: theoretical and practical way. Theoretically it is necessary to find ruling parameter or a set of parameters. Empirically it is possible with a lot of calculations and applying statistical methods.

Doing calculations with program URBACAM we can observe all evolutionary process from the beginning, we can stop it and change parameters: we can control it, because we see how it reshapes in time. Geometrical distribution should show dynamical balance between homogeneity (with even distribution of S_{empty} and S_{active}) and centralization (with S_{active} increasing dominance). After a lot of calculations we supposed that initial parameter for S_{empty} should be 3, and for S_{active} – 800. S_{fixed} cells don't play an important role in this case. With these initial values good result was reached in most cases comparing with other values. And again, we never might expect two simulations to be identically because of probabilistic component in our model (Figure 4).

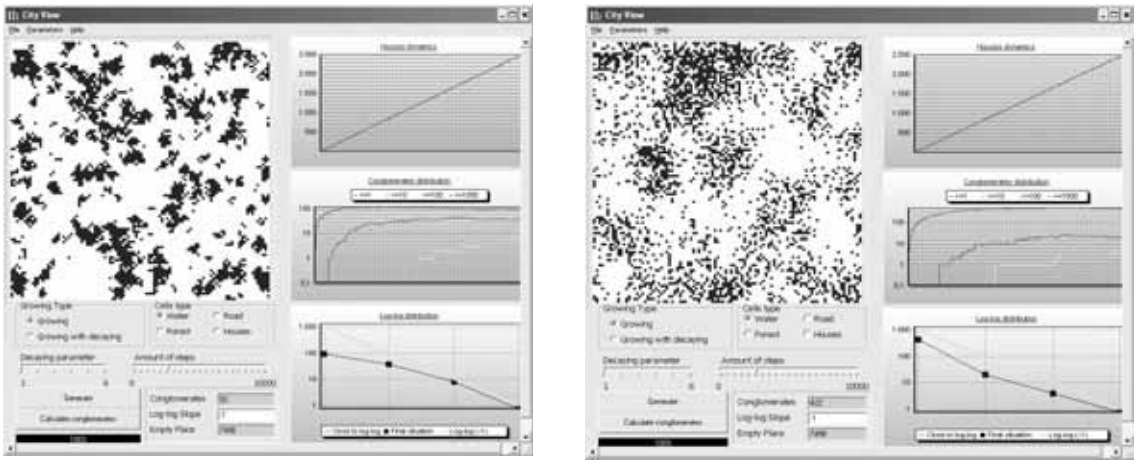

a) S_{active} =800, S_{empty} =3, Moore neighbourhood b) S_{active} =800, S_{empty} =3, 80 neighbours

Figures 4. SOC with different neighbours

Results and conclusions

Proposed model offers not only geographical urban and energetics system characteristics (distribution structure) and dynamics, but also integral characteristics that selfsame important in decision-making. When we have real system deviance from SOC state, taken decision must re-establish this state. That allows us to answer both questions 'what capacity and how many generators' and 'where to build them'. The same rule is valid for urban development. Hence SOC method is combined method that enable identify both parameters of system geometry and system dynamical characteristics.

Cellular automata constitute a powerful tool for understanding cities at more than one level. Micro level: local interactions have simple rules; macro level: global spatial behaviour is able to reflect any geographical situation. Generally many countries are close to SOC in main aspects and they are going to reach this state without any influence from outside, so finding certain parameters for that case allows us to make decisions about further urban development. As self-organizing structure, cities system is inherently complex object. So, to find ruling parameters empirically needs a lot of calculations and time. Certain parameters for SOC state such as neighbourhood and S_{empty}, S_{active} were found in computer experiments.

Decision making in energetics we perceive as a policy of investment in long term development of energetics economy, considering the structure of generators instead of total dynamic characteristics of energy capacity. Generators rank distribution law unambiguously identifies the energetic systems structure. Ideally the system of generators should be in self-organized critical state that reflects naturally formed urban system state. Because of lack of data accessibility we couldn't verify presence of this consistent pattern in various countries except in Lithuania. Accordingly we consider it as operating *ad hoc* hypothesis.

References

1. Bak P. How Nature Works. 1st ed. Berlin: Springer-Verlag; 1996.

2. Batty M, Desillas J, Duxbury E. The discrete dynamics of small-scale spatial events: agent-based models of mobility in carnivals and street parades. Int J Geo Inf Scie 2003;17:673-97.
3. Siugzdaite R, Norvaisas S. Energetics as self-organized system: methodological aspects. Nonlinear Analysis: Modelling and Control 2002; 7:123-37.
4. White R. Cities and cellular automata. Discrete dynamics in nature and society 1998:2:111-25.
5. Batty M, Longley P. Fractal cities: a geometry of form and function. London: Academic Press; 1994.
6. Batty M, Xie Y. From cells to cities. Environment and Planning B 1994;21:31-48.
7. Siugzdaite R, Norvaisas S. Country's urban process modelling with cellular automata. Town planning and architecture 2003;4:31-42.

Physiological and metabolic regulations

Lecture

ANALYSIS OF COMPLEX METABOLIC NETWORKS ON THE BASIS OF OPTIMIZATION PRINCIPLES

Hermann-Georg Holzhütter
Institute of Biochemistry, Humboldt-University Berlin, Berlin, Germany (hergo@charite.de)

Introduction

Complex cellular functions such as motility, growth, replication, defence against toxic compounds and repair of molecular damages are ultimately linked to metabolic processes. Metabolic processes can be grossly subdivided into chemical reactions and membrane transport processes, most of them being catalysed by enzymes and facilitated by specific membrane transporters. The activity of these proteins can be modulated by varies modes of regulation such as allosteric effectors, reversible phosphorylation and temporal gene expression. These regulatory mechanisms operative on the molecular level have been evolved during natural evolution and enable the cell to adapt its metabolic activities to specific functional requirements.

Mathematical modelling of metabolic networks has a long tradition in computational biochemistry (for a historical overview see (1)). Mathematical models of metabolic systems allow to study the systems behaviour by means of computer-based 'in silico' simulations. This type of mathematical analysis may provide deeper insights into the regulation and control of the metabolic system studied (2). Moreover, kinetic simulations of metabolic networks may partially replace time-consuming and expensive experiments to explore possible metabolic alterations of the cell induced by varying external conditions (e.g. pH-value, concentration of substrates, concentration of toxic compounds, concentration of signalling molecules) and thus may provide a valuable heuristics for future experimental work.

Mechanistic kinetic modelling of metabolic networks needs detailed rate equations for each of the participating metabolic processes. Derivation of a reliable rate equation requires knowledge of all physiological effectors influencing the activity of the catalyzing enzyme and the determination of rate-versus-concentration relationships for all these effectors. Thus, realistic mathematical modelling of a metabolic pathway turns out to be a tedious, time-consuming enterprise which up to now has been successfully undertaken only for very few pathways as, for example, the main metabolic pathways of erythrocytes (3-9) or glycolysis in yeast cells (10). For most metabolic pathways and most cell types the available enzyme-kinetic knowledge is currently still insufficient to allow for a realistic mathematical modelling.

To obtain at least a qualitative estimate of stationary metabolic flux rates without knowing the detailed kinetics of individual processes the so-called flux-balance analysis (FBA) has been proposed (11). FBA makes use of the fact that under steady-state conditions the sum of fluxes producing or degrading any 'internal' metabolite has to be zero. Application of this method is based on only two prerequisites: (a) the stoichiometry of the metabolic network under consideration has to be known and (b) an evaluation criterion is needed to pick out the most likely flux distribution among all those flux distributions that are compatible with the steady-state conditions. The topology of the metabolic network is given in terms of the so-called stoichiometric matrix relating the time-dependent variation of the metabolite concentrations to the fluxes through all metabolic processes for which an enzyme or transport protein is available

in a given cell type. The topology of central metabolic pathways is meanwhile available for numerous cell types (see e.g. http://www.genome.ad.jp/kegg). In the first place, this is the result of intensive enzymological work carried out during the last four decades. More recently, the sequencing of complete genomes and the development of bio-statistical techniques to map genes onto proteins enable the prediction of metabolic pathways even if the biochemical identification and characterization of the underlying enzymes is not available yet.

The Darwinian interpretation of natural evolution considers existing biological systems as outcome of an optimization process in that the permanent change of phenotype properties due to mutation and selection leads to an optimal adaptation of an organism to given environmental conditions. Based on this hypothesis, several optimization studies have been performed in the field of metabolic regulation aimed at the prediction of enzyme-kinetic properties and enzyme concentration profiles ensuring optimal performance of metabolic pathways (12-20). In previous applications of FBA the optimal production of biomass has been used as optimality criterion (20). Whereas the maximization of biomass production as the primary objective of the cellular metabolism makes sense for primitive cells such as bacteria that are born to duplicate, application of FBA to cells with more sophisticated ambitions needs a more general criterion. Here it is proposed to settle this criterion on the principle of flux minimization: Given the value of functionally relevant 'target' fluxes, i.e. those fluxes that are directly coupled with cellular functions, the most likely distribution of stationary fluxes within the metabolic network will be such that the weighted sum of all fluxes becomes a minimum. This principle is backed up by the fact that increasing the flux through any reaction of a metabolic network requires some 'effort'. This effort can be split into two different categories. First, some *metabolic effort* in terms of energy and other valuable resources (e.g. essential amino acids) is required to synthesize a sufficiently high amount of enzymes and transport proteins. Second, some *evolutionary effort* has been required to improve the specificity, catalytic efficiency and regulatory control of an enzyme during the long-term process of natural evolution. Whereas the metabolic effort can be measured in units of energy or mass flow, the evolutionary effort is a measure for the likelihood of favourable mutational events to occur that increase the fidelity of an enzyme in the context of the metabolic network. The principle of flux minimization is based on the plausible assumption that during the early phase of natural evolution the competition for limited external resources represented a permanent pressure on living cells to fulfil their functions with minimal effort.

Employing the principle of flux minimization for the calculation of stationary metabolic fluxes results in the solution of a constrained linear optimization problem: Consider the set of all flux distributions meeting the flux-balance-relations dictated by the stoichiometry of the system and pick out the distribution for which the total flux becomes a minimum. The first part of the presentation briefly outlines the mathematical basis of the method. The second part presents an application of the method to the metabolism of erythrocytes.

Method

Basic definitions

We define the metabolic network of a specific cell by the fluxes v_j ($j=1,2,\ldots,n_r$) through all reactions for which at least one enzyme (or transport protein) can be expressed and by the metabolites S_i ($i=1,2,\ldots,n_m$) involved in these reactions. The stoichiometric matrix indicates how flux v_j affects the concentration of metabolite S_i: (i): $N_{i,j} > 0$ – $N_{i,j}$ molecules of metabolite (i) are formed during a single reaction (j), $N_{ij} < 0$ – $N_{i,j}$ molecules of metabolite (i) are consumed during a single reaction (j), $N_{ij} = 0$ – metabolite (i) is not involved in reaction (j). For example,

for the flux v_8 through the chemical reaction $2S_1 + S_2 \xrightarrow{v_8} S_3 + 3S_4$, the elements of the stoichiometric matrix read N_{18}=-2, N_{28}=-1, N_{38}=1, N_{48}=3.

In general, the fluxes v_j may be positive or negative, i.e. the net reaction may proceed either into forward or backward direction. To deal with non-negative variables, the flux v_j is decomposed into an irreversible forward flux $v_j^{(+)}$ (net reaction proceeds from left to right) and an irreversible backward flux $v_j^{(-)}$, (net reaction proceeds from right to left):

$$\begin{aligned} v_j &= v_j^{(+)} - v_j^{(-)} \\ v_j^{(+)} &= v_j\ \Theta(v_j),\ v_j^{(-)} = v_j\left[\Theta(v_j) - 1\right] \end{aligned} \qquad [1]$$

$\Theta(x)$ denotes the unit-step function, i.e. by definition only one of the two components $v_j^{(+)}$ and $v_j^{(-)}$ can be different from zero. The forward direction is defined as that which would ensure a positive Gibbs free energy change under standard conditions (where all reagents are present at unit concentrations); at these standard conditions the backward flux is defined to be zero. The steady-state fluxes have to obey the flux-balance conditions

$$\sum_{j=1}^{n_r} N_{ij}\ v_j = \sum_{j=1}^{n_r} N_{ij}\left(v_j^{(+)} - v_j^{(-)}\right) = 0 \qquad (i=1,\ldots,n_m) \qquad [2]$$

representing the principle of conservation of mass for a homogeneous reaction system. The flux balance conditions [2] constitute a homogeneous system of linear equations with respect to the unknown fluxes. For realistic metabolic systems the number of fluxes is larger than the number of metabolites, i.e. $n_r > n_m$. Thus equation system [2] is underdetermined. i.e. it possesses an infinite number of solutions.

Setting target fluxes through functionally essential reactions: the load function

To accomplish a particular functional state of the cell, the fluxes through a certain number (n_t) of 'target' reactions have to be maintained at non-zero values. Some of the target reactions as, for example, the production of energy (ATP) or the synthesis of membrane phospholipids, are permanently required to ensure cell integrity. Other target reactions as, for example, the synthesis of a hormone or the detoxification of a pharmaceutical may be only temporarily required. The selection of target fluxes is somewhat arbitrary. For example, the demand for a continuous synthesis of phospholipids can be instantiated by introducing the total amount of phospholipids as a model variable and putting either the flux of phospholipids degradation or the flux of phospholipids synthesis to a non-vanishing value

(Relative) deviations of the target fluxes v_j ($j = j_1, j_2, \ldots, j_{nt}$) from given fixed load values l_i are measured by the *load function*

$$L = \frac{1}{n_t} \sum_{i=1}^{n_t} \frac{v_{j_i}}{l_i} \qquad [3]$$

We demand

$$v_{j_i} \le l_i \qquad (i=1,2,\ldots,n_t) \qquad [4]$$

so that the load function is restricted to the range $[0 \le L \le 1]$. L = 1 means that all target flux exactly meet the demanded load values.

Flux constraints arising from the availability of external metabolites

The non-equilibrium state of biochemical reaction systems is maintained by a steady uptake of energy-rich, low-entropy substrates and release of low-energy, high-entropy products. The absence of a certain substrate associated with the exchange flux v_i can be expressed by forcing the uptake component of the flux to zero

$$v_i^{(uptake)} = 0 \qquad [5]$$

Upper boundary for fluxes

Due to physical laws governing the maximal number of collisions between an enzyme and its substrates per time unit, the flux capacity of any enzyme-catalyzed reaction must have an upper boundary,

$$v_j < v_{max} \qquad [6]$$

The turnover rate of a catalytically perfect enzyme is determined by the on-rate constant for the formation of the enzyme-substrate complex which is of the order $\approx 10^8$ M^{-1} s^{-1}. The concentration of substrates and enzymes is typically below 10^{-3} M and 10^{-9} M, respectively. Thus, an ample estimate of the value of v_{max} should be 3.6 x 10^2 mM / h. This value was used in the following calculations.

Thermodynamic evaluation of fluxes: Irreversibility of reactions

The direction of any flux v_j is dictated by the change of Gibbs free energy,

$$\Delta G_j = \Delta G_j^{(0)} + RT \ln\left(\frac{\prod_{i=1}^{n}[S_i]^{N_{ij}^{(+)}}}{\prod_{i=1}^{n}[S_i]^{N_{ij}^{(-)}}}\right) \quad \text{with } N_{ij}^{(+)} = N_{ij} \text{ if } N_{ij} \geq 0,\ N_{ij}^{(-)} = -N_{ij} \text{ if } N_{ij} \leq 0 \qquad [7]$$

$\Delta G_j^{(0)}$ denotes the change of Gibbs free energy under the condition that all reactants are present at unit concentrations (= 1 mol/l). $\Delta G_j^{(0)}$ can be expressed through the thermo dynamical equilibrium constant K_j^{equ},

$$\Delta G_j^{(0)} = -RT \ln\left(K_j^{equ}\right) \qquad [8]$$

where RT = 2.48 kJ/mol at room temperature (T=25^{0}C). As stated above, all reactions of the network will be notated such that under standard conditions $\Delta G_j^{(0)} \leq 0$ $(K_j^{equ} \geq 1)$ and thus $v_j > 0$ $(v_j^{(-)} = 0)$. The second term in the right-hand side of equation [7] depends upon the actual concentrations of the reactants which under cellular conditions may strongly deviate from unit concentrations. With accumulating concentrations of the reaction products (appearing in the nominator) and/or vanishing concentrations of the reaction substrates (appearing in the denominator) the concentration-dependent term in [7] may assume arbitrarily large negative values, i.e. in principle the direction of a chemical reaction can always be reversed provided that other reactions in the system are capable of accomplishing the required change in the concentration of the reactants. For example, the standard free energy change of the glycolytic reaction (*glycerol aldehyde phosphate → dihydroxy acetone phosphate*) catalyzed by the

enzyme triose phosphate isomerase amounts to $\Delta G^{(0)} = -7.94$ kJ/mol ($K_{TIM}^{equ} = 24.6$). Nevertheless, under cellular conditions the net reaction proceeds into backward direction (dihydroxy acetone phosphate → glyceraldehyde phosphate) as the reaction substrate glycerol aldehyde phosphate is rapidly converted into 1,3-bisphosphoglycerate along the glycolytic pathway. This example shows that a sharp classification into reversible and irreversible reactions on the sole basis of $\Delta G^{(0)}$ can be problematic. Instead, we will use the value of the equilibrium constant as weighting factor in the definition of the objective function evaluating the fluxes (see below).

Flux evaluation function

In order to measure the total flux in the network we introduce the flux evaluation function

$$\Phi_v = \frac{1}{n_r} \sum_{j=1, j\neq \text{target fluxes}}^{n_r} \left(\frac{1}{\sqrt{1 + (K_j^{equ})^2}} v_j^{(+)} + \frac{K_j^{equ}}{\sqrt{1 + (K_j^{equ})^2}} v_j^{(-)} \right) \quad [9]$$

defined as the weighted sum over all internal fluxes except the target fluxes. Weighting of the backward flux with the thermodynamic equilibrium constant takes into account the thermodynamic effort connected with reversing the 'natural' direction of the flux (see above). Reciprocal weighting of the forward and backward fluxes is necessary because the value of the flux evaluation function should not depend on the way how we define the forward direction (changing this definition, i.e. exchanging substrates and products, means to inverse the equilibrium constant).

Setting the flux-minimization problem

As outlined above, the optimization strategy followed in this work consists in the accomplishment of the given target fluxes at a minimum of the internal fluxes. To this end, we solve the minimization problem

$$F = \Phi_v + \lambda (1 - L) \rightarrow \text{MINIMUM!} \quad [10]$$

The first term of the objective function F evaluates the internal fluxes The second term of F measures the deviation of the load function defined in equation [3] from the ideal value L = 1. Solution of the minimization problem [10] means to find the best possible compromise between reducing on one hand the internal fluxes (i.e. in the ideal case to make $\Phi_v \rightarrow 0$) and on the other hand preventing larger deviations of the target fluxes from the demanded load values (in the worst case $L \rightarrow 0$). In order to give priority to the fulfilment of the load conditions we choose a sufficiently high value for the parameter λ, i.e.

$$\lambda > \text{MAX}\left\{ \frac{1}{n_r} \sum_{j=1, j\neq \text{target fluxes}}^{n_r} \left(\frac{1}{\sqrt{1 + (K_j^{equ})^2}} v_j^{(+)} + \frac{K_j^{equ}}{\sqrt{1 + (K_j^{equ})^2}} v_j^{(-)} \right) \right\} \quad [11]$$

Because the highest physically feasible value of all fluxes is constraint by v_{max} (see [6]) condition [11] with choosing $\lambda = v_{max}$.

In the following we will speak of the *flux-minimized steady-state* of the metabolic network if the flux distribution satisfies the side constraints [2], [4], [5] and [6] and solves the minimization problem [10].

Results

Flux-minimized steady-states of the erythrocyte metabolism at unconstraint internal fluxes

The above outlined method was applied to the metabolic scheme for erythrocytes depicted in Figure 1. Note that the reaction arrows point into the direction of the net reaction under standard conditions which for the reactions R_3, R_5, R_6, R_7, R_{11} and R_{29} differs from the direction under *in vivo* conditions. The scheme takes into account two cardinal metabolic pathways of this cell: glycolysis including the so-called 2,3-bisphosphoglycerate shunt, and the pentose phosphate cycle constituted of an oxidative and a non-oxidative part. The model comprises 30 reactions and 29 metabolites, whereby only 25 metabolites are independent because there are 4 conservation conditions: AMP + ADP + ATP = const. = A, NAD + NADH = const. = ND, NADP + NADPH = const. = NDP, GSH + $\frac{1}{2}$GSSG = const. = G. Note that in the shown reaction scheme the orientation of the arrows corresponds to the 'natural' direction of the reactions which, as declared above, is defined as that direction which would ensure a positive Gibbs free energy change under standard conditions

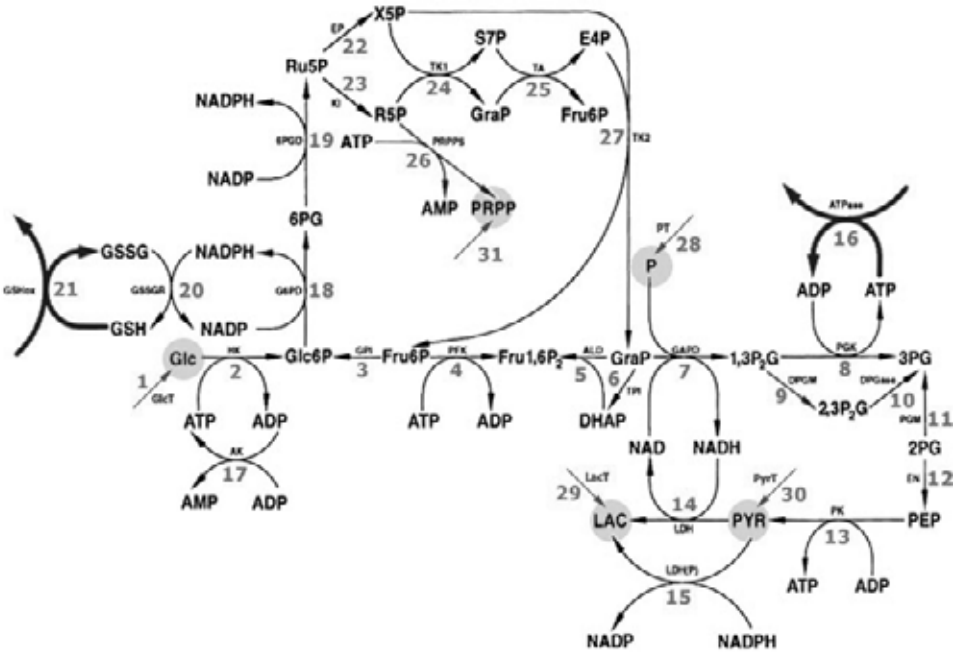

Figure 1. Metabolic network in erythrocytes

For the calculation of stationary and time-dependent states of the reaction scheme in Figure 1 a comprehensive mathematical model was used that takes into account the detailed kinetics of the participating enzymes (8). The mathematical model has been shown to provide reliable simulations of time-dependent and stationary metabolic states of the erythrocyte under a variety of external conditions. Thus, metabolic steady states computed by means of the kinetic model can be used to assess the reliability of flux rates computed by means of the flux minimization

method. The target reactions considered in this example are: (i) ATP-utilization (v_{16}) which is mostly spent on the Na/K-ATPase to maintain Na/K-gradients across the plasma membrane, (ii) GSH-oxidation (v_{21}) to prevent oxidative damage of cellular proteins and lipids, (iii) formation of 2,3-BPG (v_9) required to modulate oxygen affinity of haemoglobin and (iv) synthesis of PRPP (v_{26}) required for the salvage of adenine nucleotides. The magnitude of these 4 target reactions depends on the specific 'external' conditions of the cell as, for example, osmolarity of the blood (or preservation medium), oxidative stress caused by reactive oxygen species or lowering of the oxygen tension during hypoxia.

Owing to the linear flux dependencies imposed by the 25 flux-balance conditions there exist only 5 independent fluxes through which the remaining 25 fluxes can be expressed as linear combinations. Four of these five independent fluxes are the target fluxes; the fifth independent (non-target) flux is chosen to be v_1, the rate of glucose uptake into the cell. Thus, given the values of the 4 target fluxes v_9, v_{16}, v_{21} and v_{26}, the values of all other stationary fluxes are fully determined by the value of the glucose uptake flux. Calculation of the stationary state by means of the flux-minimization method can thus be easily accomplished by expressing all fluxes through linear combinations of the target fluxes and the glucose uptake flux and determining the minimum of the objective function [10] with respect to the flux v_1 of glucose uptake. This yields the value $v_1 = 1.51$ mM/h. Figure 2 compares the flux values obtained by the flux-minimization methods and by kinetic modelling *in vivo* values of the target fluxes: $v_9 = 0.49$ mM/h, $v_{16} = 2.38$ mM/h, $v_{21} = 0.093$ mM/h, $v_{26} = 0.026$ mM/h. For a better visualization, fluxes possessing low and high values are shown in two different panels.

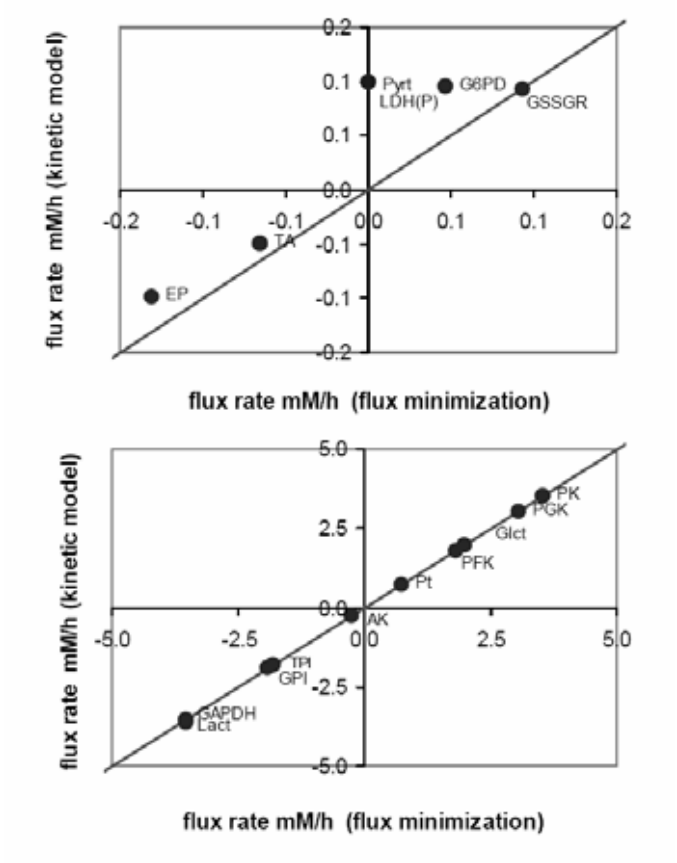

Figure 2 Comparison of fluxes obtained by the flux minimization method and by kinetic modelling

The excellent overall correlation (r^2=0.9997) cannot hide that larger relative differences remain for the minor fluxes mostly pertaining to the hexose monophosphate shunt. This is plausible considering that under normal *in vivo* conditions the glycolytic flux is well determined by the demand of ATP utilization being by far the largest target flux of the system.

The fluxes through the oxidative and non-oxidative pentose phosphate pathway are less strictly determined by the target fluxes: Synthesis of PRPP can be brought about along either branches and the flux through the oxidative pentose phosphate pathway is not only determined by the NADPH consumption of the glutathione reductase but also by the flux through the NADP-dependent lactate dehydrogenase. This accounts for the weaker performance of the flux-minimization method with respect to the minor fluxes through the hexose monophosphate shunt. Nevertheless, the absolute differences are still acceptable considering that the experimental uncertainty of flux measurements (e.g. by tracer methods) is at least of the same order of magnitude. The most striking discrepancies occur with respect to the flux rate through the NADP-dependent lactate dehydrogenase reaction and, as a consequence of that, the pyruvate uptake. The flux-minimization method predicts a vanishing flux through the LDH(P) reaction so that the release of lactate equals exactly the glycolytic flux. In contrast, the kinetic model yields a non-vanishing flux through the LDH(P) reaction having approximately the same magnitude as the fluxes in the oxidative pentose phosphate pathway. The additional consumption of pyruvate by the LDH(P) has to be compensated by a non-vanishing pyruvate uptake. Moreover, the flux through the oxidative pentose phosphate pathway is also higher than predicted by the flux-minimization method because a non-zero flux through the LDH(P) reaction is associated with an additional consumption of NADPH required for the reduction of GSSG. This discrepancy results from the fact that the flux-minimization method will force some of the fluxes to zero if alternative reactions or pathways exist in the network that are 'cheaper' according to the flux evaluation criterion [9]. However, strictly vanishing zero-fluxes can never be expected in any branch of the network if the substrates of the reaction are present in finite concentrations because enzyme activities cannot be completely switched-off by any regulatory mechanism. Therefore, zero-fluxes predicted by the flux-minimization method have to be interpreted as 'small' fluxes compared with other fluxes in the network. As the fluxes through the NADP-dependent lactate dehydrogenase reaction and the pyruvate exchange calculated by means of the kinetic model belong to the group of small fluxes the prediction of a zero-flux (= 'small' flux) is in qualitative agreement with predictions of the kinetic model.

In order to check whether the flux minimization method is capable of providing reasonable estimates of stationary fluxes within a physiologically reliable range of the target fluxes steady state flux distributions of the system were calculated at different combinations of target fluxes where the values of each of the target fluxes was either normal, increased by a factor of 2 or decreased by a factor of ½. For these 81 different combinations of target fluxes the values of 3 representative flux rates obtained by flux minimization and by kinetic modelling are plotted against each other in Figure 3. The correlation between these values is very high. Both methods provide almost identical flux rates of glucose uptake. However, the flux rates through the two branches of the hexose monophosphate shunt exhibit a constant shift against each other which is mostly due to the fact that the flux-minimization method puts the flux through the NADP-dependent lactate dehydrogenase to zero whereas the value calculated by means of the kinetic model is about 0.1 mM/h for all 81 cases. To balance the NADPH utilized by the LDH(P) reaction the flux through the oxidative pentose phosphate pathway is actually higher then the flux through the NADPH consuming of glutathione reductase reaction. This causes an extra supply of ribose phosphates for the PRPP synthesis. Thus, the flux through the oxidative pentose phosphate pathway is still high enough to satisfy the supply of the PRPP synthetase with ribose phosphates where the flux minimization method already predicts negative fluxes

through the non-oxidative pentose phosphate pathway. Increasing the flux through the PRPP synthetase more than twofold, negative flux rates through the non-oxidative pentose phosphate pathway will also be predicted by the kinetic model (data not shown).

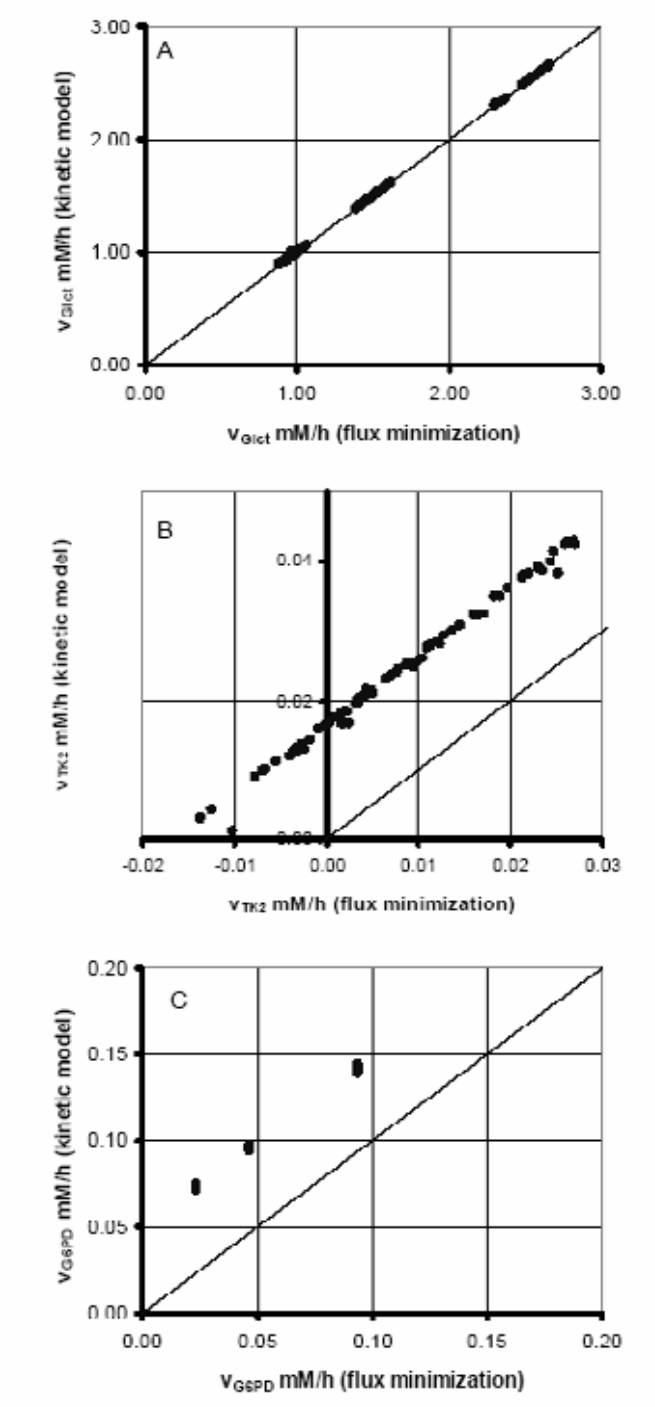

Figure 3. Comparison of fluxes obtained by the flux minimization method and by kinetic modelling at various combinations of target fluxes

Flux-minimized steady-states of the erythrocyte metabolism at constraint fluxes

The above calculations have been performed under the assumption that – except the existence of an upper (very high) boundary for fluxes imposed by physical constraints (see [6]) – there are no limitations of the internal fluxes. This assumption ignores the existence of maximal capacities of the underlying enzymes. Moreover, fluxes may be seriously restricted if the supply of fuel substrates is limited by depletion of external resources or if the maximal activity of enzymes becomes restricted either due to an enzyme defect or to the presence of an enzyme inhibitor. Enzymopathies, i.e. inborn enzyme defects causing a metabolic disorder, have been reported for many enzymes of the erythrocyte. The most prominent enzyme defect with about 400.000.000 cases worldwide is the defect of the glucose-6-phosphate dehydrogenase (G6PD). A diminished activity of the G6PD (or of any other enzyme) usually gives rise to a decrease of the target fluxes thus affecting the viability of the cell.

To study the possible impact of reduced enzyme activities on the flux distribution we solved the minimization problem [10] by systematically restraining the flux through any of the 30 reactions between 0% and 100% of the normal value obtained as solution of the unconstrained problem. According to the behaviour of the load function one may distinguish two types of reactions: (i) the network is capable of compensating the restrained flux by increasing the fluxes in other parts of the network, i.e. the value of the load function can be kept at unity but this has to be paid with progressively increasing flux evaluation values, (ii) the network is not capable of compensating the flux constraint by increasing the flux through alternative branches of the network, i.e. the load function decreases with decreasing values of the upper bound that is put to the flux under consideration and at least one of the target fluxes tends towards zero. In the latter case (ii) the catalyzing enzyme is termed essential as its removal is connected with the disabling of at least one target reaction.

Intriguingly, constraining the flux through a non-essential reaction (case i) implies zero-fluxes through other reactions which can be also switched of without lowering the value of the load function. In other words, the non-essential reactions can be arranged in certain clusters of simultaneously dispensable reactions. This leads to eight different variants of reduced erythrocyte networks depicted in Table 1.

The question arises, however, whether these reduced metabolic networks that still fulfil all constraints of the above outlined minimization approach are indeed feasible from the kinetic view point. This was tested with the aid of a comprehensive mathematical model [8] describing the kinetics of the erythrocyte network shown in Figure 1. Kinetic feasibility of a proposed sub-network was assessed by putting in the model equations the v_{max} -values of the omitted enzymes to zero, constraining the fluxes through the four target reactions to the values given above and trying to determine a stationary solution of this system by means of a global non-linear regression method (Large-scale solver, http://www.frontsys.com/]. If a locally stable stationary solution was found the sub-network was classified as kinetically feasible. This regression calculation was performed by step-wise decreasing the maximal activities of the disabled enzymes in order to avoid the numerical procedure to start too far from the attractor of a stable steady-state. Although it cannot be guarantied that stable stationary solutions can always be found by this strategy the inability to reach a stable kinetic steady-state for five sub-networks can be made plausible by kinetic arguments (see below). The calculations have shown that stable stationary solutions of the kinetic model exist for only three out of the eight sub-networks predicted by the flux-minimization procedure (variants A, B and C in Table 1). Intriguingly, these three kinetically feasible sub-networks exhibit the lowest values of the flux evaluation

function. Note that the kinetically feasible network variant B represents the smallest network lacking four reactions.

Table 1. Erythrocyte sub-networks generated by constraining the flux through an individual reaction to zero

Disabled reaction	Variants of reduced network	Cluster of simultaneously dispensable enzymes	Cluster of simultaneously dispensable reactions	Φ
Glct	H	Glct, HK	v1, v2	3.215
HK	H	Glct, HK	v1, v2	3.215
GPI	E	GPI	v3	0.667
PFK	G	PFK, ALD, TPI	v4, v5, v6	1.597
ALD	G	PFK, ALD, TPI	v4, v5, v6	1.597
TPI	G	PFK, ALD, TPI	v4, v5, v6	1.597
GAPDH	*			
PGK	*			
DPGM				
DPGase	*			
PGM	*			
EN	*			
PK	*			
LDH	*			
ATPase				
AK	*			
G6PD	C	G6PD, 6PGD	v18, v19	0.505
6PGD	C	G6PD, 6PGD	v18, v19	0.505
GSSGR	*			
GSHox				
EP	B	KI, TK, TA	v22, v24, v25, v27	0.501
KI	D	KI	v23	0.516
TK	B	KI, TK, TA	v22, v24, v25, v27	0.501
TA	B	KI, TK, TA	v22, v24, v25, v27	0.501
PRPPS				
Pt				
Lact	F	Lact	v29	0.822
Pyrt	A	Pyrt	v15, v30	0.499

* = essential enzyme

Based on the finding that kinetically feasible sub-networks are characterized by a very small increase of the flux evaluation function compared with the value of the full network we have repeated the calculation of flux distribution at restrained fluxes, but now additionally constraining the value of the flux evaluation function Φ_v to the value obtained for the unconstrained minimization problem. With this additional constraint the value of the load function always decreases irrespective of the constrained flux (see Figure 4). The curves were produced by solving the minimization problem (10) by constraining the flux through the indicated reaction between 0% and 100% of the normal value and constraining the upper bound for the flux evaluation function to the value obtained for the unconstrained problem. The dotted line indicates the threshold value for the load function below which metabolic disorder is expected. Measuring the impact of the individual fluxes on the metabolic fitness of the cell by the % flux reduction at which the load function has dropped by 10% (from 1 to 0.9) one arrives at a ranking of the fluxes (enzymes) that is in close concordance with that obtained on the basis of flux control coefficients using the comprehensive kinetic model.

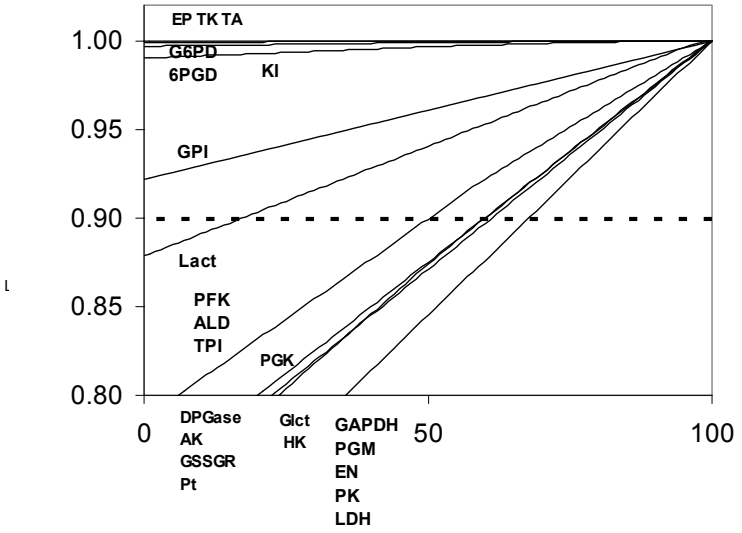

Figure 4. Load function versus % normal flux (i.e., flux obtained for the unconstrained problem) for the various reactions of the erythrocyte network

Discussion

Biology is now facing the era of systems biology. Different types of biological information (DNA, RNA, protein, protein interactions, enzymes, metabolites) can be used to build up mathematical models of the gene-regulatory, signal transducing and metabolic networks of a cell and to integrate them into whole-cell 'in silico' models. The predictive capacity of such models will increase the more details of the underlying elementary processes can be incorporated. With respect to metabolic networks the current situation is such that only for a few pathways and a few cell types sufficient enzyme-kinetic knowledge is available to build up realistic kinetic models. As the number of enzymological studies is dramatically decreasing since 1998 (according to a statistics based on entries of enzymological papers into the data base http://www.brenda.uni-koeln.de) there is little hope that this situation will improve in the near future.

Structural modelling approaches have been proposed as alternatives to mechanism-based kinetic modelling to better understand the architecture and regulation of metabolic networks. These approaches have in common that they work without enzyme-kinetic information. Only the stoichiometry of the system and, if available, some plausible side conditions constraining the external fluxes are used as input. Schuster and co-workers (21) have developed a theoretical method to decompose the stationary fluxes in a metabolic network into elementary flux modes defined as smallest sets of enzymes that can operate at steady state, with all enzymes weighted by the relative flux they need to carry out for the mode to function. These elementary flux modes have strong similarities with the so called extreme pathways forming a basis in the space of flux distributions restrained by inequality relations (22, 24). Both types of decomposition allow the definition of metabolic pathways in a rigorous quantitative and systemic way (22, 23). Moreover, they have been successfully applied to assess the robustness of metabolic networks

against insertions or deletion of certain enzymes. However, these decomposition methods are not suited to calculate the flux rates in metabolic systems. For this purpose, Palsson and co-workers have developed a theoretical approach commonly referred to as flux balance analysis (FBA) (26). This method postulates that the most likely distribution of stationary fluxes in the metabolic network has to be optimal with respect to a feasible optimization criterion. The definition of the optimization criterion is the key point of the whole approach. It is the common view that principles governing the design of cells, tissues and organisms can only be grasped in the context of natural evolution. In Darwinian sense, natural evolution is a permanent optimization process leading to the survival of phenotypes that are best adapted to their natural environment. With respect to metabolism, best adaptation to environmental conditions may involves multiple properties like robustness against fluctuations in the supply with external substrates or relative insensitivity to alterations in the structure and function of the underlying proteins (enzymes, transporters). It thus has to be doubted that a single evolutionary principle alone may account for the sophisticated regulation of metabolic systems of currently existing cells. Resting the computational prediction of system properties on a single optimization criterion a priori holds a considerable degree of arbitrariness. This principal objection holds of course also true for the approach proposed in this paper.

In previous applications of FBA the maximization of biomass production was used as such an optimization criterion. However, studying the metabolism of multifunctional vertebrate cells as, for example, hepatocytes or nerve cells, the maximal production of biomass can hardly be taken as an appropriate optimization criterion. Therefore, this paper proposes a new variant of flux-balance analysis that relies on the principle of flux minimization. This principle captures the obvious fact that gaining functional fitness with minimal expense of external resources and along the shortest route in the evolutionary landscape must have been a decisive selection factor during natural evolution of cellular systems. For the special case that the functionality of a cell is reducible to rapid self-reproduction, gaining a maximal biomass production at given total flux is obviously equivalent with maintaining a given rate of biomass production at a minimum of the total flux. Insofar the principle of maximal biomass production is a special case of the more general principle of flux minimization. It has to be noted furthermore, that minimization of fluxes in a metabolic system is closely linked to minimization of enzyme levels because both properties are directly related to each other. It is a well-known feature of gene regulation to switch off enzymes that belong to temporarily "jobless" metabolic pathways.

The mathematical formulation of the proposed optimization principle consists in the definition of an objective function which is to be minimized under the side constraints that the steady-state conditions (flux balances) are met with respect to all internal metabolites. In the definition of the flux evaluation function [9] the backward direction of fluxes (with respect to the 'natural' direction of the reaction under standard conditions) is weighted by the thermodynamic equilibrium constant of the reaction to take into account that reversing the direction of fluxes becomes more and more unfavourable from the thermodynamic view point the larger the thermodynamic equilibrium constant of the reaction. Although this way of weighting the backward fluxes is purely empirical and lacks straightforward physical or chemical reasoning it has the advantage of avoiding any a priori assumptions on the irreversibility of reactions.

Applying the flux minimization method to cellular metabolic networks one has to identify the so called target fluxes, i.e. those fluxes that are directly linked to the physiological functions of the cell. Target fluxes can be subdivided into 'basic' fluxes that are permanently required at almost constant level to ensure stability and integrity of the cell and 'variable' target fluxes that may vary according to the external conditions of the cell or its current functions in the context of the hosting organism. For the metabolic network of the erythrocyte discussed in this paper,

the production of ATP can be considered a basic target flux amounting to 1-2 mM/h irrespective of the specific external conditions of the cell (27). In contrast, the other 3 target fluxes can be termed as variable ones because they may significantly change under conditions of cellular stress, as for example, oxidative damages caused by certain pharmaceuticals or lowered oxygen saturation of haemoglobin in various forms of hypoxia. In general, the target fluxes of a metabolic network can be found within the set of fluxes connecting the network with neighbouring networks or with the environment (excretion of compounds). However, some basic knowledge about the functions of a given cell type and the metabolic prerequisites to enable these functions will be necessary to arrive at a reasonable selection of target fluxes.

The reliability of stationary fluxes predicted by the flux minimization method was assessed for a metabolic scheme of the energy- and redox metabolism of erythrocytes for which a comprehensive and validated kinetic model was available. Varying the values of the target fluxes between 50% and 200% of their normal values, the numerical values predicted by the flux minimization method are in good agreement with those calculated on the basis of the kinetic model. The remaining systematic discrepancies are due to a wrong prediction of the flux through the NADP-dependent lactate dehydrogenase reaction. This fact brings up a weak but inevitable point of the theoretical concept in that it allows to put the flux through a reaction exactly to zero even if the enzyme catalyzing this reaction (which cannot be down-regulated in the anucleated erythrocyte) and the substrates fuelling the reaction are both present. On the other hand, despite some systematic differences to the results of kinetic modelling, the flux minimization method correctly describes the flux changes induced by changes of the target fluxes. This property could render the flux-minimization method a valuable tool for predicting metabolic changes to external perturbations.

Putting all results together the flux-minimization method should be considered as a serious alternative to currently existing structure-based concepts to assess stationary flux distributions in metabolic networks if detailed kinetic information is lacking.

References

1. Heinrich R, Schuster St. The Regulation of cellular systems. New York: Chapman and Hall; 1996.
2. Fell D. Understanding the control of metabolism. London: Portland Press; 1997.
3. Rapoport TA, Heinrich R. Mathematical analysis of multienzyme systems. I. Modelling of the glycolysis of human erythrocytes. Biosystems 1975:7;120-9.
4. Schauer M, Heinrich R, Rapoport SM. Mathematical modelling of glycolysis and adenine nucleotide metabolism of human erythrocytes. I. Reaction-kinetic statements, analysis of *in vivo* state and determination of starting conditions for *in vitro* experiments. Acta Biol Med Ger 1981;40:1659-82.
5. Schauer M, Heinrich R, Rapoport SM. Mathematical modelling of glycolysis and of adenine nucleotide metabolism of human erythrocytes. II. Simulation of adenine nucleotide breakdown following glucose depletion. Acta Biol Med Ger 1981;40:1683-97.
6. Heinrich R. Mathematical models of metabolic systems: general principles and control of glycolysis and membrane transport in erythrocytes. Biomed Biochim Acta 1985;44:913-27.
7. Schuster R, Holzhütter HG, Jacobasch G. Interrelations between glycolysis and the hexose monophosphate shunt in erythrocytes as studied on the basis of a mathematical model. Biosystems 1988;22:19-36.
8. Schuster R, Holzhütter HG. Use of mathematical models for predicting the metabolic effect of large-scale enzyme activity alterations. Application to enzyme deficiencies of red blood cells. Eur J Biochem 1995;229:403-18.

9. Jamshidi N, Edwards JS, Fahland T, Church GM, Palsson BO. Dynamic simulation of the human red blood cell metabolic network. Bioinformatics 2001;17:286-7.
10. Teusink B, Passarge J, Reijenga CA, Esgalhado E, van der Weijden CC, Schepper M, Walsh MC, Bakker BM, van Dam K, Westerhoff HV, Snoep JL. Can yeast glycolysis be understood in terms of *in vitro* kinetics of the constituent enzymes? Testing biochemistry. Eur J Biochem 2000;267:5313-29.
11. Cornish-Bowden A, Cardenas ML. Metabolic balance sheets. Nature 2002;420:129-30.
12. Heinrich R, Holzhütter HG, Schuster S. A theoretical approach to the evolution and structural design of enzymatic networks: linear enzymatic chains, branched pathways and glycolysis of erythrocytes. Bull Math Biol 1987;49:539-95.
13. Heinrich R, Schuster S, Holzhütter HG. Mathematical analysis of enzymic reaction systems using optimization principles. Eur J Biochem 1991;201:1-21.
14. Pettersson G. Optimal kinetic design of enzymes in a linear metabolic pathway. Biochim Biophys Acta 1993;1164:1-7.
15. Melendez-Hevia E, Waddell TG, Heinrich R, Montero F. Theoretical approaches to the evolutionary optimization of glycolysis – a chemical analysis. Eur J Biochem 1997;244:527-43.
16. Klipp E, Heinrich R. Competition for enzymes in metabolic pathways: implications for optimal distributions of enzyme concentrations and for the distribution of flux control. Biosystems 1999;54:1-14.
17. Varner J, Ramkrishna D. Application of cybernetic models to metabolic engineering: investigation of storage pathways. Biotechnol Bioeng 1998;58:282-91.
18. Varner J, Ramkrishna D. Metabolic engineering from a cybernetic perspective. 1. Theoretical preliminaries. Biotechnol Prog 1999;15:407-25.
19. Klipp E, Heinrich R, Hermann-Georg Holzhütter HG. Prediction of Temporal Gene Expression: Metabolic Optimisation by Re-Distribution of Enzyme Activities. Eur J Biochem 2002;269:5406–13.
20. Edwards JS, Ibarra RU, Palsson BO. In silico predictions of Escherichia coli metabolic capabilities are consistent with experimental data. Nat Biotechnol 2001;19:125-30.
21. Schuster S, Dandekar T, Fell DA. Detection of elementary flux modes in biochemical networks: a promising tool for pathway analysis and metabolic engineering. Trends Biotechnol 1999;17:53-60.
22. Schilling CH, Letscher D, Palsson BO. Theory for the systemic definition of metabolic pathways and their use in interpreting metabolic function from a pathway-oriented perspective. J Theor Biol. 2000; 203: 229-48.
23. Dandekar T, Moldenhauer F, Bulik S, Bertram H, Schuster S. A method for classifying metabolites in topological pathway analyses based on minimization of pathway number. Biosystems 2003;70:255-70.
24. Wiback SJ, Palsson BO. Extreme pathway analysis of human red blood cell metabolism. Biophys J 2002;83:808-18.
25. Stelling J, Klamt S, Bettenbrock K, Schuster S, Gilles ED. Metabolic network structure determines key aspects of functionality and regulation. Nature 2002;420:190-3.
26. Varma A, Palsson BO. Metabolic flux balancing- basic concepts, scientific and practical use. Bio-Technol 1994;12:994-8.
27. Schobersberger W, Tschann M, Hasibeder W, Steidl M, Herold M, Nachbauer W, Koller A. Consequences of 6 weeks of strength training on red cell O_2 transport and iron status. Eur J Appl Physiol Occup Physiol 1990;60:163-8.

Lecture

AGGREGATION PROPENSITY OF PROTEINS QUANTIFIED BY HYDROPHOBICITY PATTERNS AND NET CHARGE

Joseph P. Zbilut (a), Julie C. Mitchell (b), Alessandro Giuliani (c), Alfredo Colosimo (d), Norbert Marwan (e), Mauro Colafranceschi (c, d), Charles L. Webber, Jr. (f)
(a) Department of Molecular Biophysics and Physiology, Rush University Medical Center, Chicago, IL USA
(b) Departments of Mathematics and Biochemistry, University of Wisconsin-Madison, Madison, USA
(c) Dipartimento di Ambiente e Connessa Prevenzione Primaria, Istituto Superiore di Sanitá, Rome, Italy
(d) Department of Human Physiology and Pharmacology, University of Rome "La Sapienza", Rome, Italy
(e) Nonlinear Dynamics Group, Institute of Physics, University of Potsdam, Potsdam, Germany
(f) Department of Physiology, Loyola University Medical Center, Maywood, IL USA

Introduction

It has been well appreciated that the native state fold of proteins is in some way dependent upon the physico-chemical properties of their amino acid sequence, most notably, hydrophobicity (1-3). More recently it has been recognized that the actual folding process is of a stochastic nature, and also includes the possibility of forming aggregates that ultimately can be physiologically harmful. A growing body of evidence suggests that this involves partially or completely unfolded proteins (4). Yet, what factors specifically promote the formation of aggregates as opposed to native folds under relatively normal conditions remain undecided.

Recently, we have proposed that some key features of protein hydrophobicity patterns analyzed by a nonlinear signal processing technique, recurrence quantification analysis (RQA), provide some necessary conditions for aggregation. A significant finding included a correspondence between short deterministic patches of hydrophobicity distribution along the sequence, what we term *laminarity,* [LAM, (*L*)], with 3-D "unstructured" portions of acylphosphatase (AcP). It was shown that the "ruggedness" of the hydrophobicity as measured by the derivative of hydrophobic change [what we term TREND, (*T*)], coincided with Dunker's "disorder" index of proteins (5). Beyond this, a counterpoint was defined as the degree of laminarity. Specifically, in an analysis of the protein engineering experiments of Chiti *et al*. (6) it was shown that aggregation sensitive zones vs. folding sensitive zones were distinguished by the two complementary concepts of trend/laminarity (7). The implication is that these areas may be inherently unstable, and somehow involved in the promotion of (at least) partial unfolding and aggregation. Indeed, it has been shown that regions tend to be involved in binding/folding events (8). The degree at which these conditions exist probabilistically determines the propensity for aggregation. What was not determined is the effect of total charge on the probabilities. Additionally, we suggested that these features may be related mathematically to provide some correlation with aggregation behavior.

In a follow-up study, Chiti, *et al*. (9) addressed the question of charge *a propos* of aggregation again using AcP mutants which minimally affected hydrophobicity, α-helical and β-sheet propensities. Thus, using selected mutations and the results of their previous work, these authors came to the conclusions that increase of net charge (not solely local) aids in avoiding aggregation. In our analysis, we confirm, in part, their observations and make further distinctions on the basis

of: 1) RQA variables and 2) a quantitative model of aggregation propensity, taking into account hydrophobicity patterns and charge. Surprisingly, the model, even if inspired by a specific problem (effects of mutations on aggregation propensity of AcP) is correlated significantly with aggregation propensities in a diverse set of proteins, suggesting a phenomenological index. Moreover, the formula predicting the effect of mutations on aggregation propensity, is also able to locate, at the extreme of a statistical distribution, all the proteins giving rise to highly structured DNA-protein assemblies (histones) and RNA binding proteins present in a large set of 1141 proteins randomly selected from the SWISS-PROT data base.

Materials and methods

Data sets

The data which inspired our model are in a seminal paper by Chiti *et al*. (6) (hereafter referred to as C1), and concern the effect of different mutations on acylphosphatase (AcP) aggregation propensity. A second Chiti *et al.* (9) data set (C2) dealt with the effects of charge. The model was also applied to a set of diverse peptides and proteins whose aggregation propensity was known by Chiti *et al*. (10) (C3). This set was composed of data from the literature specifying aggregation rates by different techniques, and were normalized by wild type aggregation values to allow for comparative analyses.

The protein population used as a test for the aggregation formula included 1141 proteins randomly chosen from the SWISS-PROT repository in order to avoid any selection bias (11) and constituting a representative sample of all known eukaryotic sequences. These proteins are available at ftp://ftp.ebi.ac.uk/pub/contrib/swissprot/testsets/signal. We utilized a subset made of eukaryotic proteins that are not secreted and thus do not have the bias of an N-terminal signal peptide, potentially imposing an externally driven correlation of protein sequences.

Recurrence plots

Eckmann *et al*. (12) introduced a tool which can visualize the recurrence of states $\mathbf{x}_i$ in a phase space. Usually, a phase space has a higher dimension than can be readily visualized. Higher dimensional phase spaces can only be visualized by projection into the two or three dimensional sub-spaces. However, Eckmann's tool enables one to investigate the *m*-dimensional phase space sequence through a two-dimensional representation of its recurrences. Such a recurrence of a state at time *i* at a different time *j* is pictured within a squared matrix with black and white dots, where black dots mark a recurrence, and both axes are the ordered sequences. This representation is called recurrence plot (RP). Such an RP can be mathematically expressed as:

$$\mathbf{R}_{i,j} = \Theta\,(\varepsilon - \|\,\mathbf{x}_i - \mathbf{x}_j\|),\ \mathbf{x}_i \in \Re^m,\ i,j=1,\ldots,N \qquad [1]$$

where $\mathbf{R}_{i,j}$ is the recurrence, N is the number of considered states $\mathbf{x}_i$, ε is a threshold distance, m the embedding dimension, $\|\cdot\|$ a norm and $\Theta(\cdot)$ the Heaviside function. (The threshold distance, ε, determines if a given point is considered recurrent).

The initial purpose of RPs was the visual inspection of higher dimensional correlations. The advantage of RPs is that they can also be applied to rather short, nonlinear, and even nonstationary data. The RPs exhibit characteristic large scale and small scale patterns. The former patterns were denoted by Eckmann *et al*. (12) as *typology* and the latter as *texture*. The typology offers a global impression which can be characterized as *homogeneous*, *periodic*, *drift* and *disrupted*.

Recurrence quantifiers in recurrence plots

Closer inspection of the RPs reveals small scale structures (the texture) which are *single dots*, *diagonal lines* as well as *vertical* and *horizontal lines* (the combinations of vertical and horizontal lines form rectangular clusters of recurrence points). In particular:

- *Single, isolated recurrence points* can occur if states are rare, if they do not persist or fluctuate heavily. However, they are not a unique sign of chance or noise.
- A *diagonal line* $\mathbf{R}_{i+k,j+k} = 1$ (for k=1,…, l, where l is the length of the diagonal line) occurs when a segment of the numerical series runs parallel to another segment, i.e., the sequence visits the same region of the phase space at different intervals. The length of this diagonal line is determined by the duration of such similar local evolution of the segments. The direction of these diagonal structures is parallel to the Line Of Identity (LOI), represented by the main diagonal in RPs, indicating the parallel running of sequences for the same evolution.
- A *vertical (horizontal) line* $\mathbf{R}_{i,j+k} = 1$ (for $k = 1, \ldots, v$, where v is the length of the vertical line) marks a length in which a state does not change or changes very slowly. It seems that the state is trapped.

Because visual inspection is difficult, and dependent upon the resolution of the output device (monitor/printer), a quantification of recurrence plots was developed by Zbilut and Webber (13, 14) and extended with new measures of complexity by Marwan *et al*. (15). In the original definition of the RPs, the neighborhood is a ball (i.e. L_2-norm is used) and its radius is chosen in such a way that it contains a fixed amount of states $\mathbf{x}_j$ (12). (The original Eckmann *et al*. algorithm used a nearest neighbor method to choose the recurrences and the resultant RP was not symmetrical.) The most commonly used neighborhood is that with a fixed radius ε. For RPs this neighborhood was first used by Zbilut and Webber (14). A fixed radius means that $\mathbf{R}_{i,j} = \mathbf{R}_{j,i}$, resulting in a symmetric RP (see Table 1 for a formulation of the variables).

These measures can be computed in windows along the main diagonal, which allows for a study of their spatial dependence, and can be used to detect state transitions. Another possibility is to define these measures for each diagonal parallel to the main diagonal separately (16). Windowed versions are also available.

Recurrence in protein sequences

The numerical series studied in this work are protein sequences coded by the hydrophobicity of the constituent residues. Discrete time and spatial series (like non branching polymers) are completely congruent mathematical objects, given they are both linear arrangements of discrete subsequent elements with a fixed and well defined ordering. Switching from time series to protein primary structures, the dynamical concept of "state" corresponds to a patch of consecutive monomeric units of length equal to the embedding dimension.

Each protein sequence was coded by means of the Miyazawa-Jernigan hydrophobicity scale (MJ) of aminoacid residues (17). This scale corresponds to the first eigenvalue of the contact energy matrix as reported at: http://us.expasy.org/tools/pscale/Hphob.Miyazawa.html, a choice dictated by our previous analysis of a 1141 random sample of protein sequences from the SWISS-PROT Database (see above). In that case, we demonstrated that the MJ was the code producing the largest separation in distance space for obtained patterns, as compared to a random assortment of amino acids.

Table 1. RQA Measures

Measure	Definition
Recurrence, *REC*	Percentage of recurrence points in an RP: $REC = \frac{1}{N^2} \sum_{i,j=1}^{N} R_{i,j}$
Determinism, *DET*	Percentage of recurrence points which form diagonal lines: $DET = \frac{\sum_{l=l_{\min}}^{N} lP(l)}{\sum_{i,j}^{N} R_{i,j}}$ P(l) is the histogram of the lengths l of the diagonal lines.
Laminarity, *LAM*	Percentage of recurrence points which form vertical lines: $LAM = \frac{\sum_{\upsilon=\upsilon_{\min}}^{N} \upsilon P(\upsilon)}{\sum_{\upsilon=1}^{N} \upsilon P(\upsilon)}$ P(v) is the histogram of the lengths v of the vertical lines.
Trapping time, *TT*	Average length of vertical lines: $TT = \frac{\sum_{\upsilon=\upsilon_{\min}}^{N} \upsilon P(\upsilon)}{\sum_{\upsilon=\upsilon_{\min}}^{N} P(\upsilon)}$
Longest diagonal line, L_{max}	Length of the longest diagonal line: $L_{\max} = \max\left(\{l_i; i = 1,\ldots,N_l\}\right)$
Longest vertical line, V_{max}	Length of longest vertical line: $V_{\max} = \max\left(\{\upsilon_l; l = 1,\ldots,L\}\right)$
Divergence, *DIV*	Inverse of L_{max} : $DIV = \frac{1}{L_{\max}}$ Related to the largest positive Lyapunov exponent, but does not correspond to it.
Entropy, *ENT*	Shannon entropy of the distribution of the diagonal line lengths p(l): $ENT = -\sum_{l=l_{\min}}^{N} p(l) \ln p(l)$
Trend, *TREND*	Paling of the RP towards its edges: $TREND = \frac{\sum_{i=1}^{N-2} [i - (N-2)](REC_i - \langle REC_i \rangle)}{\sum_{i=1}^{N-2} [i = (N-2)/2]^2}$

The application of RQA implies an *a priori* setting of the working parameters embedding dimension, radius, and line (the minimum number of adjacent recurrent points to be considered as deterministic). On the basis of studies of the maximal information content of protein sequences (at embedding 3) as well as our previous analyses, the above parameters were set to: embedding dimension = 3; radius = 6**,** and line = 2. The radius was determined by finding the shelf singularity of hydrophobicity as defined by the RQA variable DET (17-21). Because of the size of the SWISS-PROT Database, the radius was set to obtain approximately 1% REC values, which, in practice, ensures achievement of the singularity.

Results

Empirical refinements and model validation

In order to develop a general empirical model of aggregation we first focused attention on the data of C2 which was used to evaluate the effect of net charge on AcP folding. Our aim was to determine a simple functional relationship between RQA variables, charge (*Q*), and aggregation indexes.

As indicated by Chiti *et al*. (9), an inverse relationship emerged between aggregation rate and net charge. To determine whether such a relationship was also exhibited by any recurrence variable, six RQA variables (REC, DET, ENT, MAXL, TREND and LAM) were entered into a stepwise regression analysis for aggregation rate (*Agg*) changes between mutants (mut) and wild type (wt) AcP, expressed as $\ln(\nu_{mut} / \nu_{wt})$. TREND was shown to be the most significant and, moreover, TREND explained the majority of variance ($p = 0.000001$). As a result, TREND was chosen to explore the charge/aggregation dependency.

When a general linear model, based only upon charge and TREND, was applied to aggregation data, a statistically significant interaction term between TREND and *Q* was found ($r = 0.802$, $p = 0.0002$) suggesting that a straightforward linear model was inappropriate (16). Careful consideration of the relationship between TREND and LAM point to the fact that LAM is a modifier of TREND, namely that repetitive deterministic patches affect the overall TREND calculation. This view is also supported by the finding that short deterministic patches, termed "singular," are an important factor in protein folding. Thus, one possible formulation of these considerations could be:

$$Agg = Const + a(|T|^{L} * |Q|). \quad [2]$$

LAM, in turn, can be further specified by the Trapping Time (TT), i.e. the average length of the laminar segments as a "weighting" term. Thus, the relationship among RQA variables was formulated as a tower function, *|T|^(L^TT)*, with LAM being expressed as decimal fraction. This function, which conveys the idea of statistical "singularity" and is also mathematically singular, insofar as it does not admit continuous derivatives near T = 0, was included in the following empirical formula:

$$Agg = Const + a(|T|^{(L^{TT})} * |Q|). \quad [3]$$

The singularity near $T = 0$ is particularly bad, as $0 < L^{TT} < 1$ implies that the derivative blows up near this point, rather than simply being undefined. Notice that in expressions [2] and [3] *a* is an adjustable parameter and *T* the absolute value is taken, without loss of generality. *Q* is the value of the net charge associated with the protein sequence and was calculated from the total number of positively and negatively charged residues at neutral pH. This was done in order to avoid presumptions of e.g., lower pH as might be obtained in specific experimental conditions, and to standardize the calculation. In this respect, it should be noted that the data sets of C1 and C2 were obtained with a pH of 5.5 involving primarily a single positive change relative to the histidine residue.

Again, *Q* was found to be significantly related to the *|T|^(L^TT)* function via significant interaction ($r = 0.79$; $p = .0002$; Figure 1). Note that the calculated function is nonlinear, and is plotted as a linear graph for convenience. To further validate this function, the original AcP data set (C1) was added to the regression evaluation for the entire set of tested mutations in addition to mutations known to be significant for aggregation. With this addendum, the results were an *r* of 0.798, and $p = 0.001$ (Figure 2).

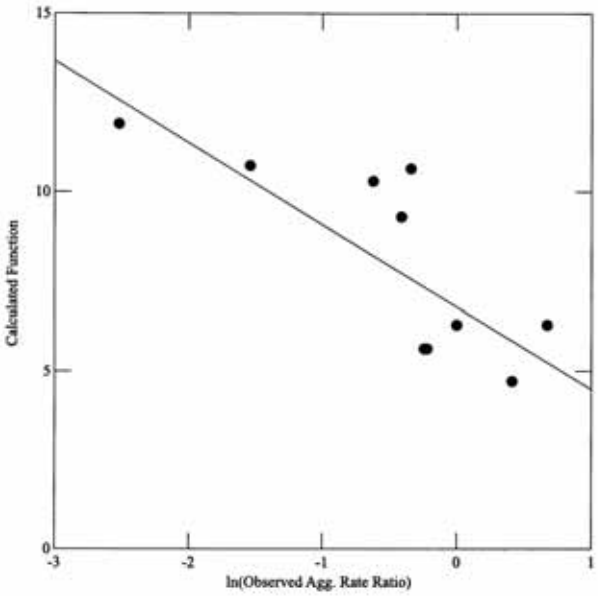

Figure 1. Calculated *vs* observed aggregation rates of AcP variants (data set C2)

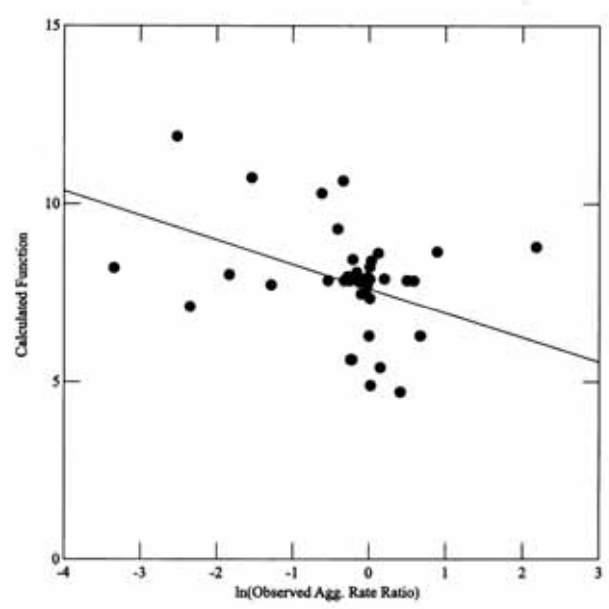

Figure 2. Calculated *vs* observed aggregation rates of AcP variants (data set C2) and mutants (data set C1) combined

Subsequently, the findings were extended to a new set of peptides whose aggregation rates are available from the literature (C3). By fitting a model using change scores of hydrophobicity, α coil and β sheet free energy, as well as charge to the prediction of aggregation rate they obtained an $r = 0.860$, $p < 0.0001$. Using Eq. 3, we obtained $r = 0.642$, $p = 0.0003$ (Figure 3).

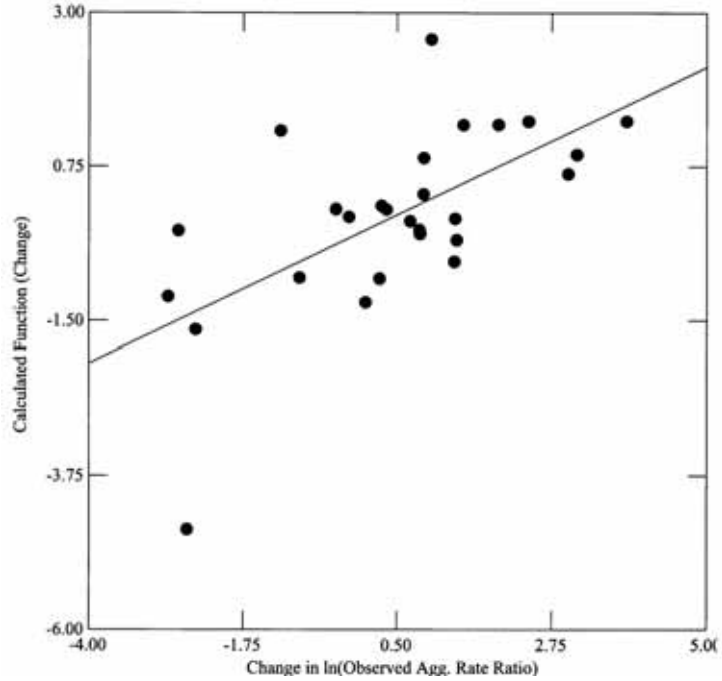

Figure 3. Data from C3 data set (see details in the text)

It is important to note that although our model the *r* value is less than that obtained by the authors for C3; it is calculated solely on the basis of hydrophobicty patterns and calculated net charge at neutral pH and, perhaps more importantly, is an *ab initio* model. This is to emphasize that the C3 data used three factors, whereas our model is based on two. In fact it was based on an independent data set (the AcP system) totally unrelated to C3 data set made of a diverse set of peptides from the literature.

Mathematical considerations

The following section outlines mathematical details of the aggregation model. Although not essential to understanding the remainder of the paper, these details will be of interest to many readers. The crucial point to be made in analyzing the partial derivatives of the recurrence model is that the aggregation propensity, *F*, is non-Lipschitz as a function of the TREND variable, *T*. The significance of this is that the rate of change in aggregation is unbounded as a function of *T* near *T = 0*. Thus, a small perturbation of *T* can result in radically different aggregation behavior, and inherent randomness in the biological system can cause instability and unpredictability. This supports the essential stochastic nature of the process by the inherent instability of TREND as suggested by our previous paper.

The simple function (ignoring the weighting factor), $F(Q,T) = |T|^L \cdot |Q|$ illustrates the differentiability of the aggregation model. First, consider the derivative of $A(Q) = |Q|$. The function $|Q|/Q$ is a good way to represent $A(Q)$, because $A'(Q) = 1$ for $Q > 0$, and $A'(Q) = -1$ for $Q < 0$, and the value is undefined at $Q = 0$.

The function $sign(A)$ is identical to *A'*, *on the domain of A'*, however $sign(A)$ is defined and equal to zero at $Q = 0$. This is not true of the derivative of *A'*. The domain of definition is relevant near the axes $Q = 0$ and $T = 0$, and we will see it is a somewhat subtle issue.

Looking at the symbolic derivatives, we have

$$\begin{aligned}\frac{dF}{dQ} &= |T|^L \cdot A'(Q) \\ &= |T|^L \cdot \frac{|Q|}{Q} \\ &= \left(\frac{1}{Q}\right)\left(|T|^L \cdot |Q|\right)\end{aligned} \quad [4]$$

Then $\frac{dF}{dQ}$ is non Lipschitz (no continuous derivatives) as a function of *T*, and it is discontinuous as a function of *Q*. Because $|Q|/Q$ remains bounded near $Q = 0$, the formula extends continuously at (0,0), but it is undefined for $Q = 0$, $T \neq 0$. Looking at the partial derivative with respect to *T*, we see that $\frac{dF}{dT}$ is continuous as a function of *Q* but unbounded as a function of *T* near $T = 0$ (for $0<L<1$):

$$\begin{aligned}\frac{dF}{dT} &= (L \cdot |T|^{L-1} \cdot A'(T)) \cdot |Q| \\ &= (L \cdot |T|^{L-1} \cdot \frac{|T|}{T}) \cdot |Q| \\ &= \left(\frac{L}{T}\right)\left(|T|^L \cdot |Q|\right)\end{aligned} \quad [5]$$

Near $T = 0$, $\frac{dF}{dT}$ is non Lipschitz (for any value of *Q*), and initial value problems for the equation:

$$\nabla F = \left(\frac{dF}{dQ}, \frac{dF}{dT}\right) = \left(\frac{1}{Q}, \frac{L}{T}\right) \cdot F \quad [6]$$

no longer have unique solutions. This is specifically the case for any trajectory emanating from $T = 0$ (Figure 4). The practical implication is that $F = 0$ is an improbable state for globular proteins.

General applications of the model

Although these calculations may be significant, actual understanding of the involved mechanisms may be deceiving since they reflect "change scores" (22). This is to say that certain putatively important contextual variables are ignored in favor of examining the variables of interest. In other words, only the change of the mutant amino acid relatively to the wild type as characterized by the formula elements is considered. Thus, while the variables of interest may

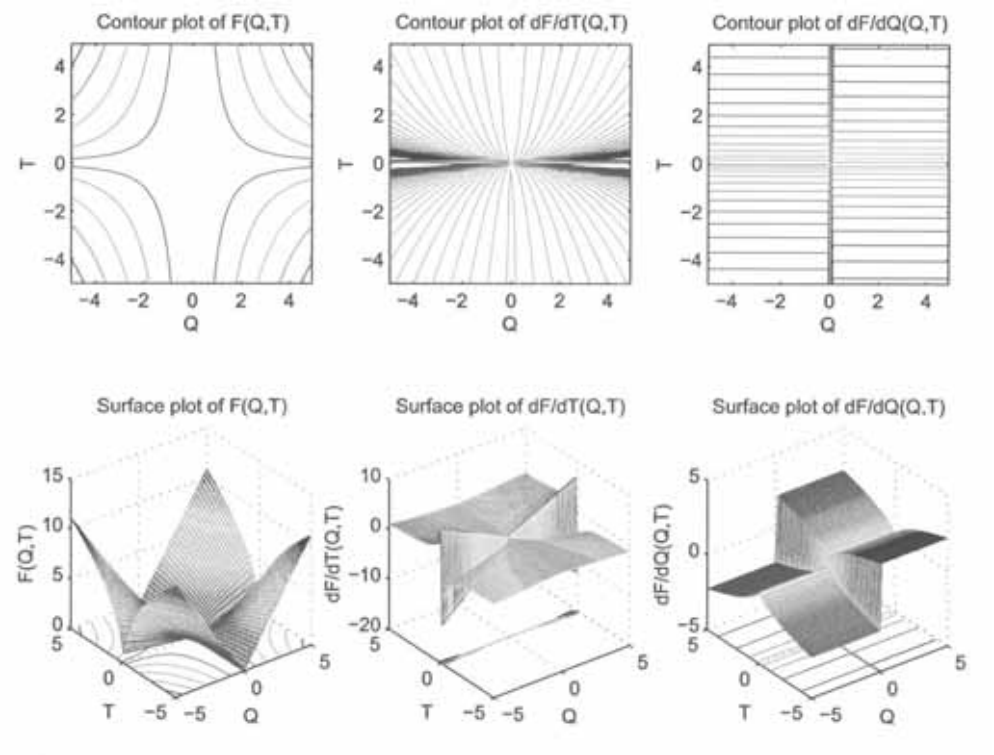

Figure 4. Graphs of the nonlinear function describing the singularities at (0,0), and related derivatives, for *L* = 0.5

be found to have noteworthy effects, ignored variables are not examined, although "controlled," given the fact that they have not changed. Another common application of change scores is the basis for "repeated measures" analysis of variance. Clearly, the most obvious ignored variable in the present case is peptide length. Consequently, a canonical analysis for the observed fluorescence by length and charge, partialing out the effects of Eq. 2 was performed and demonstrated a significant effect for peptide length ($p = 0.04$). These results, however, should be taken with caution since there is a restriction in range with 16 of the 27 mutations being equal to or less than 42 amino acids in length.

Thus a naive inclusion of protein length in a function may be premature. However, based on strictly formal arguments, one would assume that any net charge effects would be affected by Coulomb's inverse square law; i.e., the "net" electrostatic effects would not be linear, and are proportional to $1/Length^2$. This is not to suggest that this relation is definitive since, as is well known, molecular electrostatic forces are confounded by other factors, such as, e.g., van der Waals forces; or that there are specific point charge effects. However, in this respect, we were guided by the experience of Plaxco *et al*. (23) and Ivankov *et al*. (24) who revised their observation of contact order being important in protein folding to include protein size/length. This is to say that the "net" effects are screened by distance along the chain. Nonetheless, this may serve as a first approximation of length effect. To this end, Eq. 3 was normalized for length and recurrences by the relation:

$$Agg = \frac{|T|^{(L^{TT})}}{REC} * \frac{|Q|}{Length^2} \qquad [7]$$

As a first test of this normalization procedure, the C3 data were recalculated according to Eq. 7. Interestingly, the *r* dropped to 0.136 (p = NS). As was previously noted, however, 16 of the 27 mutants are equal to or less than 42 residues in length (n = 16, mean = 34; SD = 10.48). Upon restriction of the analysis to these short proteins the *r* for the original formula remained approximately the same (r = 0.63, p = 0.01); however Eq. 7 demonstrated an *r* at 0.17 (p = NS). Upon choosing the remaining proteins (n = 11, mean = 250.18, SD 151.29), the situation was reversed: the original formula dropped the *r* to 0.44 (p = NS); whereas Eq. 7 demonstrated an *r* of 0.65 (p = 0.03). Again, because of the restriction in range, these results should be viewed cautiously, but they do suggest that there is a slightly different effect for charge of very short proteins. Indeed, it may be that net charge is attenuated at very short scales by the stronger effect of local charge.

To get a better sense of the performance of Eq. 7, it was applied to a data set from the SWISS-PROT repository (mean length = 347.61, SD = 303.04; none < 50) (see above) in order to check its ability to single out peculiar functional classes allowing us to obtain better insight into the mathematical modelling of aggregation process. Functionally, the proteins were classified as reported in Table 2 (Menne *et al*. database) (11).

Table 2. Functional classification of proteins used to test Eq. 7

Protein class (subclass)	Number in class	Number in subclass
Nuclear proteins (N)	184	
Histones (h)		55
Regulative (r)		114
Other nuclear proteins (a)		15
Enzymes (E)	296	
Monomeric (m)		144
Oligomeric (o) (<4 subunits)		105
Polymeric (p) (		46
Other enzymes (a)		1
Ca++/metal – binding (C)	57	
RNA binding (RNA)	68	
Cell-Cycle proteins (CC)	42	
Membrane proteins (M)	153	
Structural proteins (S)	74	
Neurotransmitters/Transport (NT)	5	
Cornifins (K)	5	
Other proteins (A)	257	
Total	1141	

The analysis of the 1141 proteins shows that most values of Eq. 7 are near or at zero; however, a considerable number also appear to be widely dispersed. It is difficult to evaluate the cases since the taxonomy is based on varying, and/or very general criteria. Thus, many proteins could putatively be assigned to several categories (see Table 2). As a consequence, the strategy was to single out proteins and classifications which appeared to be unambiguous, ignoring details which might be considered unfairly biasing in a post-hoc analysis.

An immediate result of the computation was the finding that 54 cases exhibited values of exactly zero: a highly unlikely result for globular proteins given the nature of the model. Careful examination of these cases indicated that all of them were membrane related peptides which interact to generate complex structures (transient or stable), many of whom are immobilized in membranes (Table 3). It can be argued that having a value of zero is totally consistent (and beneficial) given their functions, and their need to have large, multi-domain structures not repelling each other.

Table 3. Proteins exhibiting formula values of zero (abbreviations from Table 2)

Code	Length	Class	Subclass	Description
P52915	406	A		Proteasome subunit
Q92524	389	A		"
P54815	357	M		Integral membrane (mitochondrial)
P46467	444	A		Intracellular protein transport
Q09143	622	M		Integral membrane (cationic aminoacid transport)
P45594	148	S		Actin-binding
O88813	683	E	m	Lipid Biosynthesis
P10107	345	C		Annexin (exocytosis)
P07150	345	C		"
P04272	338	C		"
P17785	338	C		"
P16587	180	M		ADP-ribosylation factor (subunit)
P18085	179	M		"
P36403	179	M		"
Q94231	178	M		"
Q19705	200	A		"
P91924	182	N		Transcriptional repressor
P36405	182	A		ADP-ribosylation factor
P37996	182	A		"
P32121	409	C		Beta-adrenergic receptor-binding
P51164	291	M		Potassium-transport ATP-ase
Q29473	499	E	m	Cytochrome P450
P27003	96	A		Annexin-binding (tetramer)
P08206	96	A		"
P31949	105	C		S-100 protein (dimer)
P40124	474	M		CAP protein
Q03503	176	E	m	Acetyltrasferase
P32320	146	E	o	Deaminase
P41089	223	E	m	Chalcone isomerase
O45405	273	M		Hypothetical protein (membrane channel ?)
Q64448	416	M		Gap-junction protein
O35089	160	M		Embryo development, membrane (potential)
Q63532	152	K		Cornifin
Q14061	62	A		Copper chaperone
P24878	365	M		Cytochrome b (subunit)
P22781	480	E		Decarboxylase
P38866	373	A		Hypothetical protein
P14942	222	E		Dimer
P24472	222	E		"
P46433	210	E		"
P53795	130	A		Hypothetical protein
Q00288	457	N	r	Cellular differentiation regulation
P46871	742	S		Hypothetical protein
Q05315	141	E	m	Carbohydrate-binding
P25791	158	N	a	Basic protein-binding
P80367	65	M		Metallothionein
P04734	64	C		"
Q05935	728	N	r	Transcriptional activator
Q07016	163	N	r	Transcription regulation (dimer)
P08235	984	M		Ribosomal protein
P11658	292	E	p	Subunit
P30044	161	A		Peroxisomal antioxidant enzyme
P49197	88	R		Ribosomal protein
P26490	475	E	p	Subunit
P51668	147	A		Ubiquitin-conjugating enzyme
P29595	81	A		Ubiquitin-like (subunit)

In order to check the consistency of our definition of the equation as "aggregation propensity" quantitation, we selected the 22 proteins reported in Table 4 (11), constituting the highest 2% of values for Eq. 7, and hence the least "aggregating prone." Surprisingly, they were all made of histones and histone-like proteins, such as RNA-binding proteins. It is worth noting that at the extreme of the ranking, namely P42129 and P42132 are two sperm protamins whose role is to pack chromatin, i.e., forming particularly dense aggregates.

Table 4. Proteins exhibiting the highest (2%) values for Eq. 7 (abbreviations from Table 2)

Code	Class	Subclass
P42132	N	h
P42129	N	h
P19757	N	h
P13275	N	h
P40631	N	h
P17502	N	h
Q05831	N	h
P07978	N	h
P06144	N	h
P10922	N	h
P02254	N	h
P02259	N	h
P07305	N	h
P17268	N	h
P40262	N	h
P43278	N	h
Q09821	N	H
P15870	N	H
P14798	R	
P06894	N	H
P15796	N	H
P11020	N	H

Histones and RNA-packing proteins are typically involved in the construction of highly specific DNA/RNA protein aggregates. Such supramolecular structures must respond to finely tuned signals (e.g. acetylation) inducing a reversible aggregation/disaggregation of DNA essential for gene expression regulation. Moreover, histones are probably one of the most conserved protein families: there are only very small differences between the same histone proteins across different species. This implies these are "almost deterministic" supramolecular machines exhibiting different states. Given their important work, protection from unwanted aggregation may be crucial. The fact that they are identified as a "minimum" of aggregation propensity suggests they are shielded from the possibility of aggregation, and is thus a strong proof of the biological plausibility of Eq. 7.

As a final check to evaluate the significance of Eq. 7 relative to covariation with length, charge, TREND, LAM, and TT, an analysis of variance was performed for the identified groups. The equation was in all cases significant, as were the covariates (p<.001), except for TT (p = NS).

Discussion and conclusions

These results support our previous finding that TREND and LAM are important determinants of aggregation in conjunction with net molecular charge. What is more surprising is that these variables are solely based on the hydrophobicity patterns of protein sequences. Notwithstanding this, for some time hydrophobicity has been identified as a major determinant of protein dynamics (e.g. 25, 26), it has been difficult, however, to quantitatively describe hydrophobicity patterns able to evoke basic principles. The present findings demonstrate the utility of RQA in this effort, as well as the importance of a correct formulation of TREND, LAM and charge interplay.

In the above perspective, Eq. 3 (the basic functional) is unique in that it shows a singularity at its zero point (Figure 4). At $Q = 0$ the derivatives are not continuous for T. In practice, this means that zero charge is disallowed, and supports the conjecture of Chiti *et al*. (9) that charge is an important factor to maintain intramolecular repulsive forces, thus avoiding aggregation. In the long run, whether a given protein will go to its native fold or an aggregation, may depend upon its characterization by TREND and/or LAM. The probabilities themselves are governed by the boundary conditions (pH, temperature, etc.). This view is in line with the one adopted by Dobson (4) pointing to the stochastic character of aggregation process. Indeed, this is the implication of phase diagrams exploring protein aggregation (27).

We have previously suggested that hydrophobicity segments broken by laminar patches may tend to be disordered, and exhibit more conformational variability (flexibility), thus tending to avoid aggregation. An explanation for this increased flexibility relates to the fact that the *|T|^(L^TT)* quantifies the differential density of patches. This hypothesis is further supported by our earlier work in the analysis of rubredoxins (28). In this study we used RQA to determine features differentiating the function of thermophilic vs mesophilic forms. An important finding was that in the Rubr Clopa (mesophilic) case, the concentration of deterministic patches occurred in unequally distributed areas; whereas in the Rubr Pyrfu case (thermophilic), there is no preferentially populated area and is distributed over the whole backbone. A graph of this finding using a windowed version of RQA demonstrates this more strikingly (Figure 5). Presumably, this is at least one cause for the increased flexibility of the thermophilic rubredoxin over the mesophilic (29).

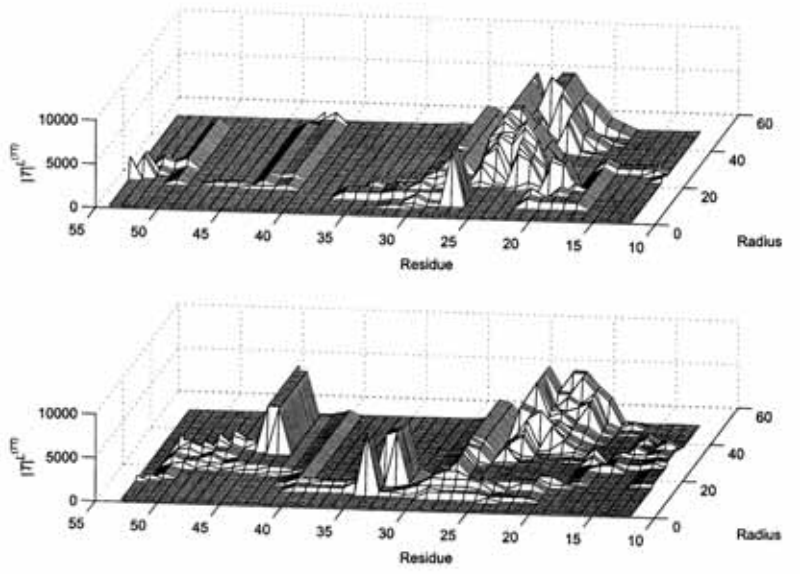

Figure 5. Comparison of Rubr Clopa (top) with Rubr Pyrfu (bottom)

Other putative causes involve the observation that amyloidogenic propensity is associated with a defect in hydrogen bonding exposed to water, making them "sticky" (30-32). Thus it may be that the singular functions address the amount of molecular "patchiness" which may be an inverse indicator of hydrophobic cores. Another view suggests that biopolymers may develop instability and collapse due to soliton-like nonlinear excitations at bends, or patches (33). Previously (34), we have suggested that such instabilities may occur in the form of molecular motions not associated with traditional modes analysis.

Finally, we note the obvious difference between the C3 formulation with ours is their inclusion of the free energy changes based on beta sheet and coil propensities. It may be that our quantification of patches of laminarity may be characterizing a similar phenomenon. Beta sheets and coils in some sense typify types of "patch." In our studies, we have noted a correlation; however, this is not a perfect one. We are currently pursuing additional investigation into this area.

The charge effect in such an explanation takes on a more complex role than that of an indicator of general repulsion between molecules. This is to say that if the patches are sequestered unequally along the series, the inequality may set up a "screening" effect for net charge: the non patchy areas may be related to "blocks" with contrasting solubilities which can, depending upon their size, modify the net charge effect. Given a change in pH which alters a charge, a protein's probability to aggregate may become enhanced. This is in line with recent results obtained by Burke *et al*. (35) with huntingtin-exon 1. The final observation is that the deterministic patches constitute a static factor involved in folding; whereas the net charge effect is a "dynamic" component often modulated by circumstantial factors (boundary conditions) such as pH. Thus, clearly, hydrophobic patterning is a necessary condition for understanding aggregation propensity, but it is insufficient without consideration of charge. It might be of significance to understand the customary milieus of proteins: environments which expose proteins to different pHs may carry a greater likelihood of aggregation as opposed to those which perform their work in relatively circumscribed settings.

Irrespective of the cause, the present results suggest that to understand the aggregation probability for a given protein sequence, unique hydrophobicity patterns need to be considered. This probability may be linked to fixed discrete patches in conjunction with net dynamic electrostatic effects.

Acknowledgements

This work was supported by a joint DMS/NIGMS initiative to support mathematical biology, from the National Science Foundation and National Institutes of Health, (NSF DMS #0240230); J. P. Zbilut, Principal Investigator. JPZ thanks Prof. F. Chiti for kindly providing details of experiments and calculations.

References

1. Kyte J, Doolitle RF. A simple method for displaying the hydropathic character of a protein. J Mol Biol 1982; 157:105-32.
2. Mandell AJ, Selz KA, Shlesinger MF. Protein binding predictions from amino acid primary sequence hydrophobicity. J Mol Liquids 2000;86:163-71.
3. Zimmerman JM, Eliezer N, Simha R. The characterization of amino acid sequences in proteins by statistical methods. J Theor Biol 1968;21:170-201.

4. Dobson CM. Protein folding and disease: a view from the first Horizon Symposium. Nat Rev Drug Discov 2003;2:154-60.
5. Dunker K, Brown CJ, Lawson D, Iakoucheva LM, Obradovic Z. Intrinsic disorder and protein function. Biochemistry 2002;41:6573-82.
6. Chiti F, Taddei N, Baroni F, Capanni C, Stefani M, Ramponi G, Dobson CM. Kinetic partitioning of protein folding and aggregation. Nat Struc Biol 2002;9:137-43.
7. Zbilut JP, Colosimo A, Conti F, Colafranceschi M, Manetti C, Valerio MC, Webber CL Jr., Giuliani A. Protein aggregation/folding: the role of deterministic singularities of sequence hydrophobicity as determined by nonlinear signal analysis of acylphosphatase and Aβ(1-40). Biophys J 2003;85:3544-57.
8. Ortiz AR, Skolnick J. Sequence evolution and the mechanism of protein folding. Biophys. J 2000;79:1787-99.
9. Chiti F, Calamai M, Taddei N, Stefani M, Ramponi G, Dobson CM. Studies of the aggregation of mutant proteins *in vitro* provide insights into the genetics of amyloid diseases. Proc Natl Acad Sci USA 2002;99:16419-26.
10. Chiti F, Stefani M, Taddei N, Ramponi FG, Dobson CM. Rationalization of the effects of mutations on peptide and protein aggregation rates. Nature 2003;424:805-8.
11. Menne KML, Hermjakob H, Apweiler R. A comparison of signal sequence prediction methods using a test set of signal peptides. Bioinformatics 2000;16:741-2.
12. Eckmann JP, Kamporst SO, Ruelle D. Recurrence plots of dynamical systems. Europhys Letts 1987;4:973-7.
13. Webber CL Jr., Zbilut JP. Dynamical assessment of physiological systems and states using recurrence plot strategies. J Appl Physiol 1994;76:965-73.
14. Zbilut JP, Webber CL Jr. Embeddings and delays as derived from quantification of recurrence plots. Phys Lett A 1992;171:199-203.
15. Marwan N, Wessel N, Meyerfeldt U, Schirdewan A, Kurths J. Recurrence plot based measures of complexity and its application to heart rate variability data. Phys Rev E 2002;66:026702-1-026702-7.
16. Trulla LL, Giuliani A, Zbilut JP, Webber CL Jr. Recurrence quantification analysis of the logistic equation with transients. Phys Lett A 1996;223:225-60.
17. Miyazawa S, Jernigan RL. Estimation of effective interresidue contact energies from protein crystal structure: quasi-chemical approximation. Macromolecules 1985;18:534-52.
18. Giuliani A, Benigni R, Zbilut JP, Webber CL Jr, Sirabella P, Colosimo A. Nonlinear signal analysis methods in the elucidation of protein sequence structure relationships. Chem Rev 2002;102:1471-91.
19. Strait BJ, Dewey TG. The Shannon information entropy of protein sequences. Biophys J 1996;71:148-55.
20. Weiss O, Jimenez-Montano MA, Herzel H. Information content of protein sequences. J Theor Biol 2000;206:379-86.
21. Zbilut JP, Sirabella P, Giuliani A, Manetti C, Colosimo A, Webber CL Jr. Review of nonlinear analysis of proteins through recurrence quantification. Cell Biochemistry and Biophysics 2002;36:67-87.
22. Vickers J, Altman DG. Analyzing controlled trials with baseline and follow up measurements. BMJ 2001;323:1123-4.
23. Plaxco KW, Simons KT, Baker D. Contact order, transition state placement and the refolding rates of single domain proteins. J Mol Biol 1998;277:985-94.
24. Ivankov DN, Garbuzynskiy SO, Alm E, Plaxco KW, Baker D, Finkelstein AV. Contact order revisited: influence of protein size on the folding rate. Protein Sci 2003;12:2057-62.

25. Lesk AM, Chothia C. How different amino acid sequences determine similar protein structures: the structure and evolutionary dynamics of the globins. J Mol Biol 1980;136:225-70.
26. Rose GD. Prediction of chain turns in globular proteins on a hydrophobic basis. Nature 1978;272;586-90.
27. Dima RI, Thirumalai D. Exploring protein aggregation and self-propagation using lattice models: Phase diagram and kinetics. Protein Science 2002;11:1036-49.
28. Giuliani A, Benigni R, Sirabella P, Zbilut JP, Colosimo A. Nonlinear methods in the analysis of protein sequences: A case study in rubredoxins. Biophys J 2000;78:136-49.
29. Grottesi A, Ceruso M-A, Colosimo A, Di Nola A. Molecular dynamics study of a hyperthermophilic and a mesophilic rubredoxin. Proteins: Structure, Function and Genetics 2002;486:287-94.
30. Fernández A, Berry RS. Proteins with H-bond packing defects are highly interactive with lipid bilayers: implications for amyloidogenesis. Proc Natl Acad Sci USA 2003;100:2391-6.
31. Fernández A, Scheraga HA. Insufficiently dehydrated hydrogen bonds as determinants of protein interactions. Proc Natl Acad Sci USA 2003;100:113-8.
32. Fernández A, Scott R. Dehydron: a structurally encoded signal for protein interaction. Biophys J 2003;85:1914-28.
33. Mingaleev SF, Gaididei YB, Christiansen PL, Kivshar YS. Nonlinearity-induced conformational instability and dynamics of biopolymers. Europhys. Lett 2002;59:403-9.
34. Manetti C, Giuliani A, Ceruso MA, Webber CL Jr., Zbilut JP. Recurrence analysis of hydration effects on nonlinear protein dynamics: multiplicative scaling and additive processes. Phys Lett A 2001;281:317-23.
35. Burke MG, Woscholski R, Yaliraki SN. Differential hydrophobicity drives self-assembly in Huntington's disease. Proc Natl Acad Sci USA 2003;100:13928-33.

Short communication

METABONOMIC STUDY OF TRANSGENIC MAIZE

Cesare Manetti (a), Cristiano Bianchetti (a), Lorena Casciani (a), Cecilia Castro (a), Maurizio Delfini (a), Maria Enrica Di Cocco (a), Alfredo Miccheli (a), Mario Motto (b), Filippo Conti (a)
(a) Dipartimento di Chimica, University of Rome "La Sapienza", Rome, Italy
(b) Istituto Sperimentale per la cerealicoltura, Sez. Bergamo, Bergamo, Italy

Introduction

Maize (*Zea Mays*) is one of the most important plant crops, used to produce a great number of products, as food, feed, pharmaceutical and industrial manufacture. Unfortunately, insects, pathogens and droughts can be serious threats to maize production, so in these last years scientists have made great efforts to develop a range of improved transgenic varieties that are disease resistant, stress tolerant and high yielding.

Among all the exsisting transgenic species, one of the most studied is the one containing in its genes *Bacillus thurigiensis* (Bt), whose aim is to increase the plant resistence to European Corn Borer, an insect of Lepidoptera.

This work has two aims:

- the comparison of a transgenic maize species with its unmodified control;
- the possibility of recognising and classifying unknown maize seeds samples in classes according to their genetic modification.

In this respect, *metabonomics* is a powerful tool. It is defined as "the quantitative measure of time-related multiparametric metabolic responses of living systems to pathophysiological stimuli or genetic modification" (1).

Metabonomics allows us to define the metabolome of a cell, and in this way to identify and dinamically follow its response to genetic modifications.

Backgrounds

Nuclear Magnetic Resonance (NMR)-based metabonomics combines high-field NMR spectroscopy with chemometric methods and has proved to be a valuable technique in characterizing the changes in metabolome of genetically modified organism.

Among all the chemometric techniques, ^{1}H NMR spectra of cell extracts have been analysed by Partial Least Square-Discriminant Analysis (PLS-DA).

PLS (2) is a supervised regression method, used to construct an empirical model relating y-type variables (e.g., substances concentrations) with x-type variables (e.g., sample absorbance), when the variables are many and highly correlated.

Roughly speaking, PLS can be thought of as doing a PCA on the X block, a PCA on the Y block, and then doing a linear regression to relate the X block principal components to the Y block principal components.

In the particular version of the method PLS-DA, the Y block is a dummy matrix, containing information on the classes to which the different samples belong.

By applying PLS-DA, a model describing maximum separation among pre-defined classes, rather than maximum variation in the data, is obtained.

Separiation is interpreted in terms of X- and Y-scores (T and U), X-Loadings (P), X- and Y-Weights (W, C) and PLS regression coefficients.

In particular, X-scores plots facilitate visualisation of the study-specific clustering/partitioning of samples, while X-Loadings and X-weights plots revealed the characteristic underlying metabolic changes by showing the influence of the different spectral bucket on the latent variables.

Classification of unknown transgenic samples can be performed by projecting their ^{1}H-NMR spectra onto a model obtained by known transgenic classes. The prediction results will give the unknown samples an identity based on the pre-defined classes or provide the equally useful information that the sample does not belong to any of them.

Experimental

Plant material

The seed samples used in this study are shown in Table 1. They were derived from the maize inbred lines La73 (maize3) and La17 (maize5) and their transgenic versions (respectively, maize4 and maize6) containing the *cry1Ab* gene (MON 810) from *Bacillus thuringensis,* conferring resistance to the European corn borer. MON810 was developed and kindly provided by Monsanto Co. (St. Louis, Mo). In addition, a seed sample of the B73 inbred lines (maize1) and its trangenic version (maize2) containing a modified *ZmRpd3-101* maize gene, was included.

Table 1. List of the seed samples used in this study

Sample	Name	Type of sample
Maize1	**C4**	control
Maize2	33 Omozigote AS ZmRpd3/101	transgenic
Maize3	G03-1220 B73+	control
Maize4	03-1216 B73 Bt	transgenic
Maize5	G03-1220 Mo17	control
Maize6	03-1218 Mo17 Bt	transgenic

Plants of inbred lines La73, La17, and B73 and their transgenic versions were grown under greenhouse conditions at 25:18 °C (day:night) with a 16:8 (light:dark) hour cycle. At flowering, plants were self-pollinated; the ears were harvested after physiological maturity, dried at 30 °C and stored in sealed plastic bags at 4 °C. For each genotype, a seed sample derived from the central portion of a single ear was used for chemical analyses.

NMR sample preparation

A Bligh-Dyer modified (4) extractive procedure was used, obtaining an hydro-alcoholic and a chloroformic phases were separated.

NMR data collection

For the NMR spectra, the dried sample was dissolved in 1 ml of 0.5 mM TSP solution in D_2O PBS buffer (pH = 7.4) to avoid chemical-shift changes due to pH variation. The dissolved extracts were transferred to a 5 mm NMR tube.

NMR spectra were recorded on a Bruker (Bruker GmbH, Rheinstetten, Germany) DRX 500 Spectrometer, operating at ^{1}H frequency of 500.13 MHz. ^{1}H NMR spectra were obtained at T=300 K, 256 scans were acquired, with data collected into 64k datapoints, and a spectral width of 12 ppm, using a 20 s delay for a full relaxation condition. A standard 1D presaturation pulse sequence was performed in order to suppress the water signal. Prior to Fourier transformation, an exponential multiplication was performed, using a line broadening equal to 0.09 Hz. Spectra were referenced to TSP (sodium salt of 3-(trimethylsilyl)propionic-2,2,3,3-d_4 acid) at a concentration of 0.5 mM. TSP was used as a reference both for chemical shift and quantitation of the signals.

NMR data pre-processing treatment

One dimensional 500 MHz ^{1}H spectra were reduced to 499 discrete chemical shift regions by digitization to produce a matrix of sequentially integrated regions of 0.02 ppm in width between –0.5 ppm and 9.5 ppm, using ACD/SpecManager 7.00 software (Advanced Chemistry Development Inc., 90 Adelaide Street West, Toronto, Ontario, M5H 3V9, Canada): column 1 corresponds to the bucket –0.5 ppm / –0.48 ppm.

Application of metabonomic analysis to a transgenic-control couple

We applied PLS to a matrix containing pre-processed data relative to samples belonging to the groups maize3 and maize4 (each composed of 8 samples). In the PLS procedure the Y matrix corresponds to a column containing an entry equal to zero or one, according to the seed line - 3 and 4, respectively. The SAS software (Statistical Advanced Software) v.8 (SAS Institute Inc, www.sas.com) was used for all the statistical analysis.

The number of latent variables was chosen in accordance with the percent of explained variability, and was equal to 3. The model was checked by randomly removing some samples from the data set and using them as a test set.

Application of metabonomic analysis to classify unknown samples of maize

We constructed the PLS model with a X matrix containing pre-processed data relative to samples belonging to all the available groups (each composed by 8 samples).

The correct number of latent variables utilised to construct the model was chosen by cross validation.

The constructed model was tested on a set, containing twelve new samples belonging to different groups. The new observation are not used in calculating the PLS-DA model, since they have no assigned values in Y matrix.

Results and discussion

Application of metabonomic analysis to a transgenic-control couple

Transgenic seeds (belonging to the group maize4) and their non modified controls (belonging to the group maize3) have been analysed.

In order to obtain a predictive model that allows us to classify different groups of seeds belonging to the different groups, we took spectral variable correlations into consideration (in this specific case the bucketed spectra regions integrals of the transgenic and control seeds) and applied the supervised PLS-DA analysis technique (as described in the experimental section).

The first factor manages effectively to discriminate between transgenic and their unmodified control seeds.We therefore took the correlation structure into consideration. By analysing the weighting given to each of the original variables, i.e. the degree of correlation between the variables and the direction of the new model, it is possible to determine the hierarchic importance of the variables for the discrimination between the two groups (transgenic and control) of samples. A positive value in the loadings plot implies a positive correlation with the scores in latent variable 1. Thus, all variables with positive values are positively correlated with the samples with positive scores, whilst the variables with negative values are correlated with the samples with negative scores, making it possible to identify the metabolite that discriminates between the two groups (3). In this respect, it is useful to consider the third quadrant.The variables with a greater influence on the discrimination between control and transgenic samples correspond to bucketed spectra regions where there are the signals of choline (*singlet* 3.21 ppm), asparagine (*double doublet* 2.86 ppm; *double doublet* 2.96 ppm), histidine (*multiplet* 7.07 ppm) and trigonelline (*singlet* 9.13 ppm; *multiplet* 8.84 ppm), which were lower in transgenic samples than in controls. The assignment of each substance was based on comparison with the chemical shift values reported in literature.

A large negative value of loading relative to those metabolites indicates higher levels in the control samples (the ones that had negative scores), and lower levels in the transgenic samples (the ones that had positive scores).

By way of example, in Figure 1 the choline regions in maize3, maize4 spectra and in the 1st factor X-weight indicating the signal that contribute to discrimination are shown.

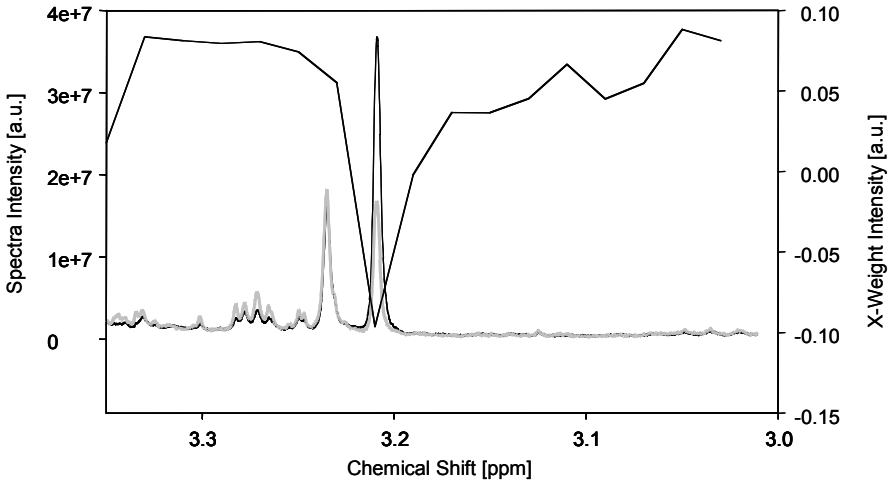

Figure 1. The choline region in maize3 (gray) and maize4 (black) spectra and in the X-Weight of the first latent variable

In this way, elucidate the signals that are key in the separation between the two samples groups has been directly obtained, without pre-analysis derivatization and thus pre-selection of the expected metabolites.

Application of PLS to classify unknown samples of maize

We subsequently considered the possibility of classifying maize seeds, whose genetic modification is not defined *a priori* in the method. This allows us to construct an NMR spectra data-base in order to define maize metabolome, as Nicholson has made for the plasma.

On the basis of the NMR spectra, it was possible to build up a PLS-DA model. In Figure 2, hydro-alcoholic extract spectra are shown, one for each maize group.

We thus took six maize groups into consideration (three different genetic modifications and their own controls), each formed by eight samples. In this case, the input Y "dummy" matrix has a row, for each sample, containing 1 for the y variable corresponding to the right group and 0 for all the others. To choose the latent variable number, a cross validation technique was used.

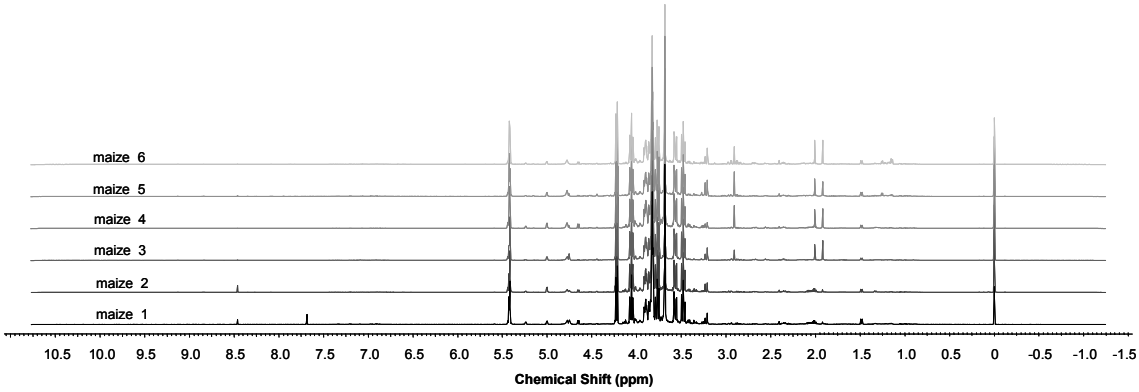

Figure 2. Spectra of the hydro-alcoholic extracts of seeds, one for each maize groups

This model was used to evaluate the predictive capabilities for twelve other seed samples. The output of PLS procedure gives a Y matrix that can be used to classify unknown samples. Indeed, looking at this matrix the sample is assigned to the group that shows the maximum y value. In Table 2 y values for the twelve samples are displayed.

Table 2. Y matrix obtained for the second set of twelve seeds samples

Sample	Group 1	Group 2	Group 3	Group 4	Group 5	Group 6
Maize1I	**0.777006**	0.105033	0.238784	-0.3067	-0.01416	0.200038
Maize1L	**0.822596**	0.364114	-0.00673	-0.05281	-0.43344	0.306276
Maize1M	**0.605178**	-0.14805	0.209341	0.198064	-0.10013	0.2356
Maize1N	**0.407808**	-0.0317	0.225597	0.133936	0.177597	0.086761
Maize3I	0.011782	0.036883	**0.897644**	-0.00734	-0.01609	0.077114
Maize3L	-0.01163	-0.19545	**0.883801**	0.118117	-0.08281	0.287965
Maize3M	-0.08118	-0.06844	**0.923928**	0.123475	0.072519	0.029693
Maize3N	-0.11705	0.117507	**0.859392**	0.156886	0.120912	-0.13765
Maize5I	-0.18455	0.253777	0.259816	0.279073	**0.555209**	-0.16332
Maize5L	-0.14411	0.227277	0.264199	0.161204	**0.58734**	-0.09591
Maize5M	-0.12811	0.222366	0.321713	0.141874	**0.611829**	-0.16967
Maize5N	-0.1625	0.228232	0.287785	0.15676	**0.59786**	-0.10813

Applying PLS it was possible to obtain the correct classification of the twelve samples in three different groups, each composed of four seeds, corresponding to maize1, maize3, maize5.

Conclusions

Metabonomics represents an emerging holistic approach complementary to genomics and proteomics for studying complex biological system behaviour.

In a biological system, the metabolites can be considered the actual phenotypic expression, as the genic function can be viewed as the result of interconnected, non hierarchical, regulatory processes in a gene-transcript-protein-metabolite-metabolic network. The metabolites concentrations in a cell system can be considered as the last response to the chemical, physical environmental as well as genetic changes.

The aim underlying this research was twofold: to evalulate the possible determination of the genetic modification in terms of comparison of the present metabolites with non modified specimens of the same species (equivalence); to identify and classify maize seeds originating from transgenic plants on the basis of analysis using multivariate techniques of the ^{1}H NMR spectra (global system descriptors), which reveals correlations among the different metabolites, without using a targeted analysis of the different metabolites. From these results, it appears useful to construct a NMR spectra data base to evaluate the influence of environmental, chemical, physical and genetic input on the system.

References

1. Lindon JC, Holmes E, Nicholson JK. Pattern recognition methods and application in biomedical magnetic resonance. Prog Nucl Magn Reson Spectrosc 2001;39:1-40.
2. Wold H. Estimation of principal components and related models by iterative least squares. In: Krishnaiah PR (Ed.). Multivariate Analysis. New York: Academic Press; 1966. p. 391-420.
3. Bailey NJC, Oven M, Holmes E, Nicholson JK, Zearl MN. Metabolomic analysis of the consequences of cadmium exposure in *Silene cucubalus* cell cultures via ^{1}H NMR spectroscopy and chemometrics. Phytochemistry 2003;62:851-8.
4. Miccheli A, Aureli T, Delfini M, Di Cocco ME, Viola P, Gobetto R, Conti F. Study on influence of inactivation enzyme techniques and extraction procedures on cerebral phosphorylated metabolite levels by P-31 NMR spectroscopy. Cell Mol Biol 1988;34:591-603.

Short communication

PREDICTION OF HERG AFFINITY VALUES USING INDEPENDENT APPROACHES

Elena Fioravanzo (a), Nicola Cazzolla (b), Lucia Durando (b), Cristina Ferrari (a), Massimo Mabilia (a), Rosella Ombrato (b).
(a) S-IN Soluzioni Informatiche Vicenza, Italy
(b) ACRAF SpA, S. Palomba, Rome, Italy

Introduction

Drug-induced QT interval prolongation, as measured on the human electrocardiogram, was once considered a trivial physiological finding. Now it is believed that drug-induced QT interval prolongation, that has been identified as a critical side effect for numerous drugs, might result in sudden cardiac death. As a consequence, a number of prescription medications associated with QT prolongation have been removed from the market by the European pharmaceutical regulatory authority. The focus of many *in vitro* studies to date is the membrane-bound inward (rapid activating delayed) rectifier potassium channel (I_{Kr}) also known as the product of the human ether-a-go-go gene (hERG). Drugs or their metabolites may block this channel, thereby prolonging the QT interval and in same cases leading to the potentially life-threatening ventricular arrhythmia that may degenerate into ventricular fibrillation and sudden death. Notably, blockade of hERG K^+ channel forms the basis of the therapeutic effect of class III antiarrhythmic drugs, but for all other drugs, it is an unwanted side effect that must be detected as early as possible during drug development (1).

Since at present various *in vivo* and *in vitro* models for QT prolongation and subsequent arrhythmia exist but they may not be entirely predictive for humans, the availability of in silico methods in the early phase of drug development would dramatically increase the screening rate and would also lower the costs compared to experimental assay methods. The possibility of a computational hERG model to be used as a filter in the discovery process would add an extra dimension to lead optimization. Both a quantitative and a qualitative model would theoretically enable virtual selection of candidates with the lowest potential to cause hERG inhibition.

Recent studies on hERG K+ channels involve pharmacophore mapping and CoMFA study. Both approaches, however, are based on the assumption that different compounds bind to the same binding site of the channel using similar binding modes. On the contrary, it is reasonable to assume that the binding affinity of a given compound may vary as a function of the channel states (activated/inactivated), and that structurally diverse molecules may adopt different binding modes. Such considerations are not compatible with a single pharmacophore model nor with a common alignment criterion.

In this study different computational approaches are used to predict hERG K^+ channel affinities.

Methods

Data set. 70 compounds with experimental hERG IC_{50} values were retrieved from the literature (2) (Table 1).

EVA descriptor. The derivation of the EVA descriptor has previously been described elsewhere (3) and only a brief description of the technique will be given here. The descriptor is derived from IR- and Raman-range molecular vibrational frequencies usually calculated through the application of a normal coordinate analysis (NCA) to an energy minimized structure. For a compound with N atoms there are 3N – 6 (or 3N – 5 for a linear structure such as acetylene) normal modes of vibration. Thus, except in the special case where each structure has the same number of atoms, the number of frequencies will be different for each structure; that is, the property is in non-standard form. A technique has thus been developed in order to standardize the property such that each compound is characterized by an equivalent-length descriptor. The frequency set for a given structure is projected onto a linear bounded frequency scale (BFS) covering a range from 1 to 4000 cm^{-1}. A Gaussian kernel of fixed standard deviation (s) is then placed over each and every eigenvalue. The BFS is then sampled at fixed increments of L cm^{-1} and the value of the resulting EVA descriptor at each sample point is the sum of the amplitudes of the overlaid kernels at that point. This procedure is repeated for each dataset compound and then combined to provide a matrix with M rows (compounds) and 4,000/L columns (descriptor variables). Typically, a descriptor set has been derived using a s of 10 cm^{-1} and an L of 5 cm^{-1} giving 800 descriptor variables. For a standard QSAR dataset the number of variables is thus much larger than M and Partial least square to Latent Structure (PLS) is hence used to provide a robust regression analysis. Energy minimization and normal coordinate analysis were carried out by means of Spartan'02 (4) employing Merck Force Field. Calculation of EVA descriptor from vibrational frequencies was carried out using the proprietary program EVA-02 (S-IN).

DRAGON is a software package for the calculation of molecular descriptors developed by Milano Chemometrics and QSAR Research Group. It allows calculation of more than 1600 molecular descriptors for thousands of molecules (5).

PASS (*Prediction of Activity Spectra for Substances*) (6,7) predicts the probability for any given compound to be active (P_a) or inactive (P_i) for each one of over 1000 biological activities, including pharmacological effects, mechanisms of action, mutagenicity, carcinogenicity, teratogenicity, and embryotoxicity. P_a and P_i values vary from 0 to 1, and their sum may be different than 1. PASS predictions are based on the analysis of structure-activity relationships for a training set including a great number of non-congeneric compounds with different biological activities, using the descriptor Multilevel Neighborhoods of Atoms (MNA). PASS training set consists of over 46,000 biologically active compounds: 16,000 are already launched drugs and 30,000 drug-candidates under clinical or advanced preclinical testing.

QikProp (8,9) has been developed by Prof. Bill Jorgensen at Yale University to rapidly predict ADMET properties of drug candidates. QikProp results have been fitted to datasets of drug-like molecules, based on 2-D and 3-D descriptors reflecting Monte Carlo simulation studies as well as experiment. QikProp predictions are calculation-based, as opposed to fragment based. Fragment-based methods can be problematic when they do not recognize parts of a structure or encounter unfamiliar fragment interactions, whereas QikProp will calculate properties based on the whole molecule. The advantage of this approach is that QikProp can be applied to new and unknown scaffolds.

SIMCA-P+ (10) Projections to Latent Structures (PLS) modeling has been used to investigate likely correlations between EVA and experimental pIC_{50} values and, respectively, descriptors generated by DRAGON and experimental pIC_{50} values. The optimal number of components in each PLS model was determined by SIMCA-P+ default cross-validation

procedure. Variables selection was carried out on the basis of VIP parameter and coefficient values. All PLS models here reported were generated considering just the experimental values found in ref. 2(b). Initial models were generated using all 62 compounds - strong outliers were detected and then excluded employing PCA on each X data matrix. The best models were further validated considering half of the compounds as training set and the rest as external test set. Training and test sets were generated by means of Onion/D-Optimal Design with the software MODDE (10).

Table 1. Molecules included in the data set

Primary ID	No.	pIC_{50}			Primary ID	No.	pIC_{50}		
		A	B	C			A	B	C
2-Hydroxymethyl olanzapine	48	-	4.9	-	grepafloxacin	61	4.1	-	4.3
9-OH risperidone	29	-	5.9	-	halofantrine	19	6.7	6.7	6.7
A 56268	58	-	-	4.5	haloperidol	8	7.6	7.6	7.5
Alosetron	35	-	5.5	5.5	ibutilide	4	-	-	8.0
Amiodarone	47	-	-	5.0	imipramine	36	5.5	5.5	5.5
Amitriptyline	45	-	-	5.0	ketoconazole	34	-	-	5.7
Astemizole	1	9.0	-	8.0	levofloxacin	69	-	-	3.0
Azimilide	26	6.3	-	5.9	loratadine	17	6.8	-	6.8
Bepridil	25	6.3	-	6.3	mefloquine	41	-	-	5.3
Carvediol	49	-	-	4.9	mesoridazine	22	-	6.5	6.5
Cetirizine	56	-	-	4.5	mibefradil	31	5.8	-	5.8
Chlorpheniramine	52	-	-	4.7	mizolastine	24	6.5	-	6.4
Chlorpromazine	32	5.8	5.8	5.8	moxifloxacin	65	3.9	-	3.9
ciprofloxacin	70	-	-	3.0	N-desmethylclozapine	57	-	4.5	-
Cisapride	2	8.2	8.2	7.4	nicotine	68	-	3.6	3.6
Citalopram	39	-	-	5.4	nifedipine	59	-	-	4.3
Clozapine	18	6.7	6.5	6.5	nitrendipine	46	-	-	5.0
Cocaina	42	5.2	-	5.1	norastemizole	9	7.6	-	7.6
desipramine	30	-	5.9	5.9	norclozapine	40	-	-	5.4
Desmethyl olanzepine	50	-	4.9		olanzapine	20	-	6.6	6.7
Diltiazem	51	4.8	4.8	4.8	ondansetron	27	-	6.1	6.1
diphenhydramine	55	-	-	4.6	perhexiline	44	5.1	5.1	5.1
disopyramide	62	-	-	4.0	pimozide	7	7.7	7.3	7.3
Dofetilide	5	7.9	-	8.0	quinidine	23	-	-	6.5
Dolasetron	43	5.2	4.9	4.9	risperidone	16	6.8	6.8	6.8
domperidone	15	6.8	-	-	sertindole	6	7.9	7.8	8.0
Droperidol	10	7.5	-	7.5	sildenafil	63	4.0	5.5	5.5
E-4031	3	8.1	7.7	7.7	sparfloxacin	54	4.6	-	4.7
Epinastine	64	-	-	4.0	terfenadine	12	6.9	6.7	6.7
fexofenadine	53	4.7	-	-	terikalant	21	-	-	6.6
Flecainide	38	-	-	5.4	thioridazine	11	7.5	-	6.4
Fluoxetine	33	-	-	5.8	trimethoprin	67	-	-	3.6
gatifloxacin	66	3.9	-	3.9	verapamil	13	6.8	6.8	6.9
glibenclamide	60	4.1	-	-	vesnarinone	28	-	6.0	6.0
granisetron	37	5.4	5.4	-	ziprasidone	14	6.8	6.9	6.9

A: Experimental data from (2a); B: Experimental data from (2c); C: Experimental data from [2b]

Results and discussion

EVA. Molecules A-56268 and perhexiline were detected as outliers by an initial PCA on the whole X matrix and were excluded from the data set. Results are reported in Table 2 and Figure 1..

DRAGON descriptors. Molecules A-56268 and nicotine were detected as outliers by an initial PCA on the whole X matrix and were excluded from the data set.

Different combinations of DRAGON descriptors were tested: the entire matrix, 1399 descriptors, and, alternatively, every single block of descriptors. Best results in terms of predictivity of models were obtained with 2D Autocorrelation (11).

More recently, SIMCA-P+ Orthogonal Signal Correction (OSC) algorithm was used to remove from X data matrices (e.g. EVA, RDF) information that is orthogonal to Y: better models, both in terms of Q^2 and predictive power towards test sets, were thus obtained that will be reported elsewhere.

Table 2. Results of PLS models

Descriptors	X	PCs	Obj.	R2	Q2	SDEC	SDEP
Initial models							
DRAGON ALL	418	3	60	0.817	0.678		
DRAGON 2Dautocorr.	48	2	60	0.657	0.527		
EVA	182	2	60	0.665	0.533		
Final models (R2 Q2 SDEC for training and SDEP for test set)							
DRAGON ALL	329	3	30	0.831	0.703	0.523	0.939
DRAGON 2Dautocorr.	34	2	30	0.727	0.572	0.663	0.827
EVA	86	2	30	0.745	0.615	0.669	0.985

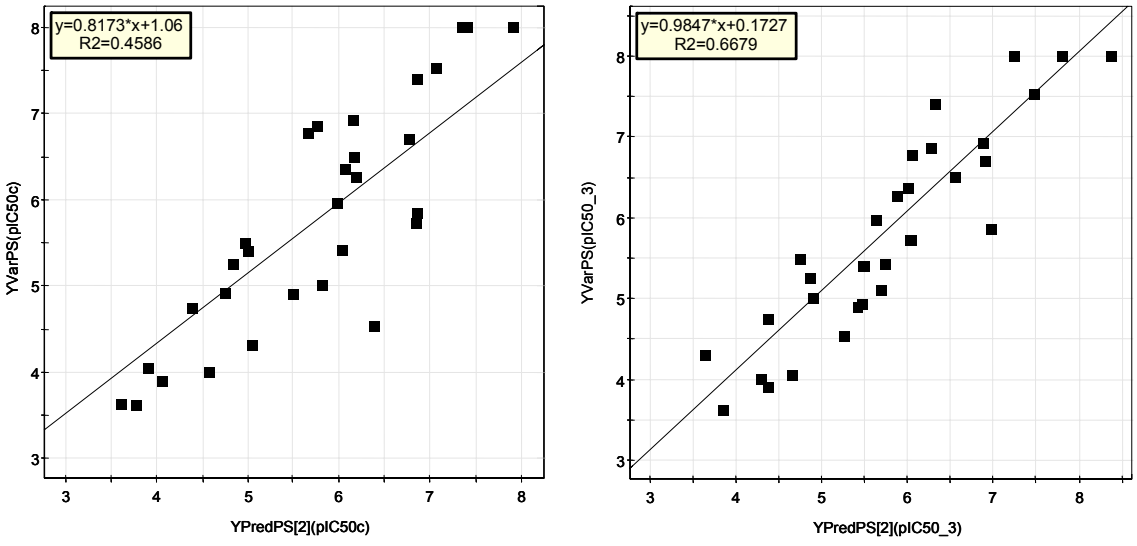

Figure 1. Scatter plot Yexp-Ypred. of final models, EVA on the left and DRAGON all on the right. Training set (box), test set (circle)

The program **PASS** was trained to predict the probability of hERG activity, using a set of molecules with pIC_{50} values grater than or equal to 5.0. Preliminary studies choosing a PASS probability value (p_a) of 0.3 show that 75% of active molecules and, respectively, 73% of "inactive" molecules are predicted correctly, leading to 12 false negative and 6 false positive.

Results of **QikProp** predictions are reported in Figure 2. Considering 5 as the pIC_{50} threshold value between active and inactive compounds, 2 molecules are predicted as false negatives and 12 as false positives.

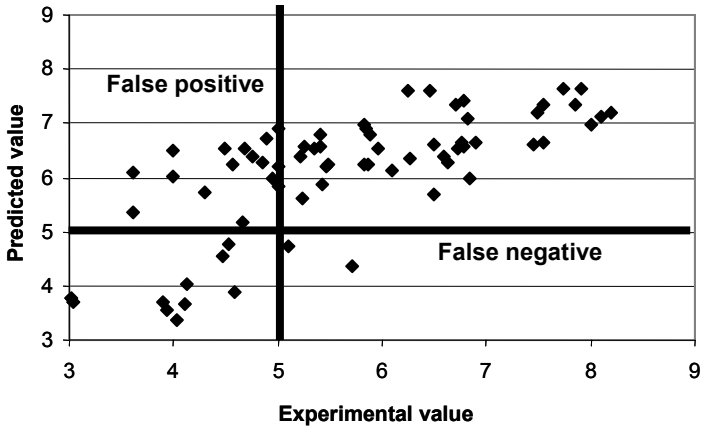

Figure 2. QikProp results

References

1. Mitcheson JS, Chen J, Lin M, Culberson C, Sanguinetti MC. A structural basis for drug-induced long QT syndrome. Proc Natl Acad Scie USA 2000;97:12329-33.
2. Cavalli A, Poluzzi E, De Ponti F, Recanatini M. Toward a pharmacophore for drugs inducing the long QT syndrome: insights froma CoMFA study of HERG K (+) channel blockers. J Med Chem 2002;45:3844-53.
3. Jonathan P, McCarthy WV, Roberts AMI, Discriminant analysis with singular covariance matrices. J Chemometrics 1996;10:189-93.
4. Spartan. [computer software]. Version 2.2. Irvine, CA: Wavefunction, Inc.; 2002.
5. DRAGON. [computer software]. Version 5.1. Milano: Talete srl; 2004.
6. PASS. [computer software]. Version 3.1. Minsk: Institute of Biomedical Chemistry; 2003.
7. Poroikov V, Filimonov D. Computerized prediction of biological activity spectra of chemical substance – New approach to effective drug design. In: Sanz F, Giraldo J, Manaut F (Ed.). QSAR and molecular modeling: concepts, computational tools and biological applications, Proceedings of the 10th European Symposium on Structure-Activity Relationships: QSAR and molecular modelling, Barcelona, Spain. Barcelona: Prous Science; 1995, p. 49-50.
8. QIKPROP [computer software]. Version 1.0. Cambridge, MA: Schrödinger LLC; 2003.
9. Duffy EM, Jorgensen WL. Prediction of properties from simulation: free energies of solvation in hexadecane, octanol and water. J Am Chem Soc 2000:122;2878-88.
10. SIMCA P+. [computer software]. Version 5.4. Umea: Umetrics AB; 2004.
11. Broto P, Moreau G, Vandicke C. Molecular structures: perception, autocorrelation descriptor and SAR studies. Eur. J Med Chem 1984:19;66-84.

Short communication

INFERRING THE ESSENTIALITY OF DIFFERENT MUTATIONS OF SACCHAROMYCES CEREVISIAE FROM THE POSITIONS OF THE CORRESPONDING ENZYMES IN THE METABOLIC NETWORK

Maria Concetta Palombo (a), Alfredo Colosimo (b), Alessandro Giuliani (a), Lorenzo Farina (c)
(a) Dipartimento Ambiente e Connessa Prevenzione Primaria, Istituto Superiore di Sanità, Rome, Italy
(b) Dipartimento di Fisiologia e Farmacologia, University of Rome 'La Sapienza' Rome, Italy
(c) Dipartimento di Informatica e Sistemistica, University of Rome, 'La Sapienza' Rome, Italy

Introduction

Information regarding genomes and metabolic interactions are stored in many databases and scientists have the urgent need for new tools in order to find effective representations and models for such interaction networks.

Only a multidisciplinary approach may lead to significant results, which implies the merging of biological knowledge and methodologies coming from many and diverse fields such as mathematics, statistics, control theory, computer science, etc.

In the present work, following the approach presented in reference (1), the dynamic of fault propagation in metabolic networks is modeled using a Markov chain: to each node (metabolite) is assigned a failure probability varying with time and to each reaction (arc), corresponds a value representing the transition probability. We study two indices potentially useful to describe different aspects of the robustness of the network: the input degree of the nodes (number of incoming arcs) (2) and the failure distribution at steady-state following a transient failure in the network (1). This stems from the need to balance the two competing consequences of the connectivity on robustness:

a) a high number of connections allows the system to react to a damage using different paths;
b) the nodes having many incoming arcs tend to "drain" the damage spreading through the network.

In reference (3) the authors studied the surviving ability of yeast after different gene deletions: they define "essentiality" as the relative lethality coming from the deletion (100% essential = all the mutant colonies die) of the corresponding enzyme. This study provides a large database of experimental data to test our model.

Metabolic networks (Figure 1, left) can be represented as direct graphs (Figure 1, right) in which the nodes are metabolites and the oriented arcs are reactions between them. The orientation of the connections is useful to show the reversibility or irreversibility of the reactions.

A few nodes, called *hubs*, have a high connection degree, while most of the nodes have a low connection degree.

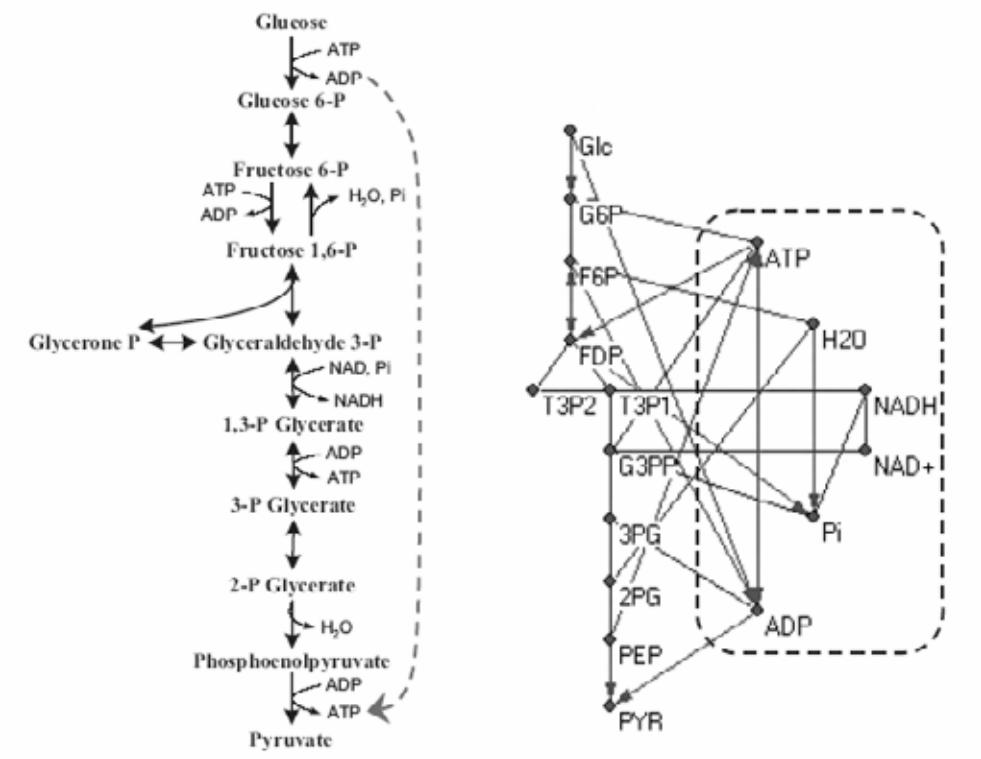

Figure 1. Metabolic networks as direct graph

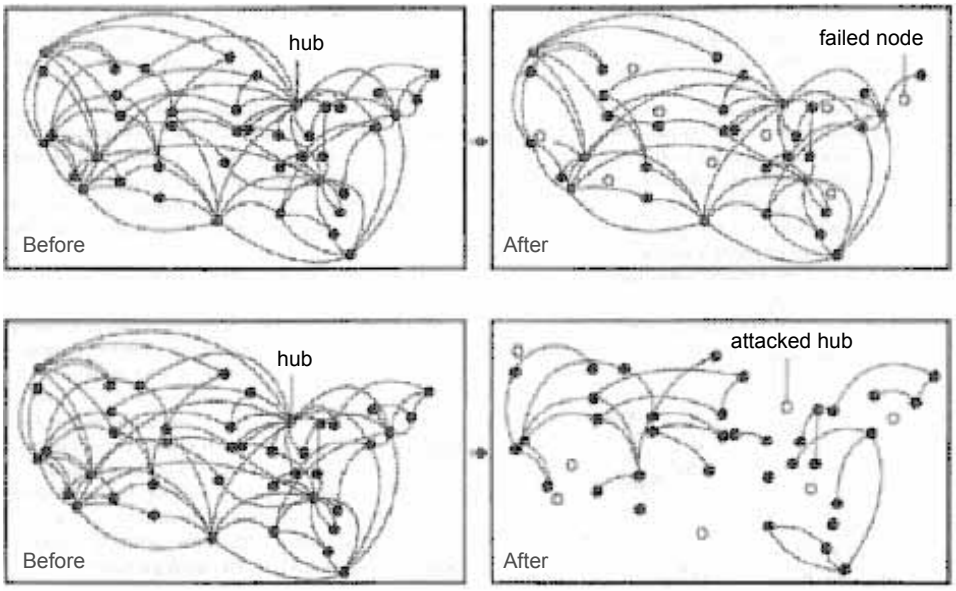

Figure 2. Effects in the network connectivity of the failure in a slightly (upper panels) and a highly (bottom panels) connected node (hub)

In reference (4) Ma and Zeng found that in a metabolic network about half of the metabolites can be only converted in a limited number of metabolites.

At the same time, there exist several fully connected sub-networks in which the metabolite can be converted to each other.

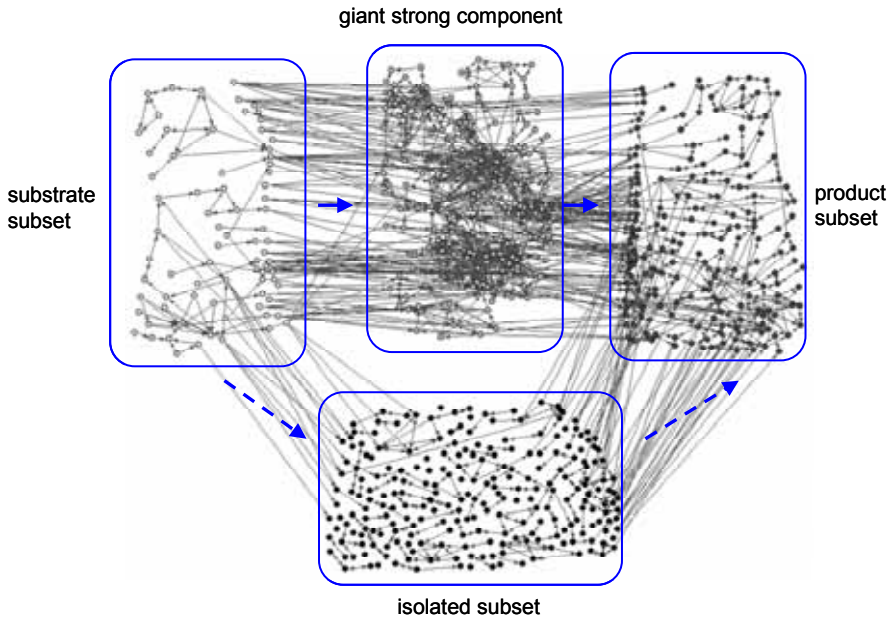

Figure 3. Strong component in metabolic networks

The **strong component** (Figure 3) is defined as a subset of nodes such that for any pair of nodes *i* and *j* in the subset, there is at least one path from *i* to *j*. Consequently, this redundancy makes the network very robust to failure or removal of reactions by gene knock-out or mutations. In a metabolic network several strong components may exist. This peculiar connectivity structure can be found even in the architecture of scale-free network such as Word Wide Web, the electric power transmission grid or airport connections. In this study we analysed the strong components of *Saccharomyces cerevisiae* metabolic network obtained from the KEGG database (5).

Methods

A graph can be represented using an adiacency matrix A, whose values $a_{i,j}$ are associated to the arc connecting node i to node j

$$A = \begin{bmatrix} a_{11} & \dots & a_{1n} \\ \dots & \dots & \dots \\ a_{n1} & \dots & a_{nn} \end{bmatrix} \quad a_{i,j} = \begin{cases} 1 & \text{if exist an arc connecting } i \text{ to } j \\ 0 & \text{otherwise} \end{cases} . \qquad [1]$$

A fault propagation in a network can be modeled using a Markov chain (1). To every node i is associated a state value $x_i(k)$, representing the failure probability of node i at time k. The state

value of *i* can vary at every time instants, depending on the neighbouring nodes, including *i*. As a consequence, self-loops are considered and the new adjacency matrix is

$$\overline{A} = A + I$$

in which the identity matrix *I* takes into account the self-loops. The out-degree of the *i*-th node is defined as $R_i = \sum_{j=1}^{n} \overline{a}_{ij}$ and by dividing every element of $\overline{A}$ by R_i (R_i >0 holds, since we consider the strong component of the network) we obtain the matrix

$$P = \begin{bmatrix} \frac{\overline{a}_{11}}{R_1} & \cdots & \frac{\overline{a}_{1n}}{R_1} \\ \cdots & \cdots & \cdots \\ \frac{\overline{a}_{n1}}{R_n} & \cdots & \frac{\overline{a}_{nn}}{R_n} \end{bmatrix} \qquad [2]$$

in which every element $p_{i,j}$ is such that $0 \le p_{i,j} \le 1$ and *P* is said to be a nonnegative (stochastic) matrix. The evolution of failure with time is defined as the solution of the Markov chain

$$x(k+1) = P^T x(k) \qquad k > 0 . \qquad [3]$$

In [2] we decided to divide by the out-degree because the damage provoked by a failure reactant is assumed to be inversely proportional to the number of reaction the reactant is involved.

Results and discussion

The real eigenvalue of *P* (and of P^T), called Frobenius eigenvalue, is equal to unity and the associated Frobenius eigenvector $x_F = \overline{x}$ with $P^T \overline{x} = \overline{x}$. Since only the strong component of the graph is considered and given the existence of at least one self loop, one can show that the solution $\overline{x}$ is unique, nonnegative and, consequently, the steady-state failure distribution can be obtained from the following equation

$$(P^T - I)\overline{x} = 0 . \qquad [4]$$

The solution is independent of the initial failure in the network and is related only to the connectivity structure of the graph. In order to study the robustness of a metabolic network, in reference (1), we propose to adopt a *tolerance index* T_i given by $T_i = \frac{c_i}{\overline{x}_i}$ in which $c_i = \sum_{j=1}^{n} \overline{a}_{ji}$ is the in-degree (number of incoming arcs) of *i*-th node, and $\overline{x}_i$ is the *i*-th component of the Markov chain solution in [3].

This stems from the need to balance the two competing consequences of the connectivity on robustness. On the one hand a high number of connections allows the system to react to a damage using different paths in order to synthesize the required metabolites; on the other hand the nodes having many incoming arcs tend to "drain" the damage spreading in the network. This balance is evident for *Micoplasma genitalium* (Figure 4).On the left panel we can see the mean

failure distribution $\overline{x}_i$ and the number of metabolites having an in degree between 1 and 6; on the right panel is clear that the mean tolerance has almost the same value for the metabolites having a number of incoming arcs between 1 and 6.

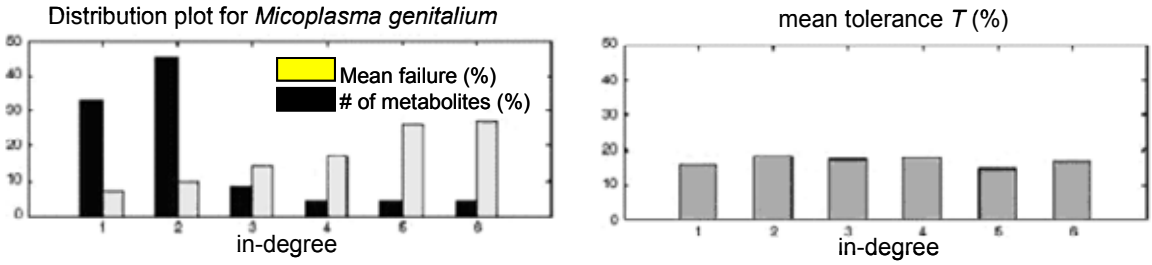

Figure 4. Distribution plot for *Micoplasma genitalium*

The goal of our study is to develop a "tolerance-to-failure" index able to discriminate "essential" and "non-essential" nodes in the network. To this end, we consider a new tolerance index given by a linear equation as follows

$$\overline{T}_i = ac_i + b\overline{x}_i \qquad [5]$$

in which c_i and $\overline{x}_i$ are the same as in reference (1), a and b are estimated using the data provided in reference (2) regarding the surviving ability, called "essentiality", of yeast when gene deletions occur. The consequence of such deletion is the lack of the corresponding enzyme and, as a consequence, a failure in the network. Reference (2) gives us a large database of experimental data on which test our assumptions.

The first step of our analysis is to estimate a and b. Then, as c_i and $\overline{x}_i$ are easy to compute for all the nodes in a network, we can find the 'weak' nodes. The deletion of a high-connected node (a hub) provides a high degree of lethality.

Another direction of this research will include the analysis of the tolerance to damage in metabolic paths. We will also try to extend our work to a number of organisms in order to find the "most important" nodes. Our tolerance index may be a useful tool to develop new drugs, i.e. enzymatic inhibitors, against pathogenic organisms being able to recover the damaged part of the network and whose effect on the network could be easily predicted.

References

1. De Persis C, Farina L. *In silico* analysis of long-run tolerance of metabolic network to transient random faults. In: Doyle G, Dean T (Ed.). Proceedings of the Sixteenth International Symposium on Mathematical Theory of Networks and Systems; 2004 4-6 June; Paris, France. Paris: Masson; 2004. p. 12-9.
2. Albert R, Jeong H, Barabási A-L. Error and attack tolerance in complex networks. Nature 2000;406:378-82.
3. Dezso Z, Oltvai ZN, Barabasi AL. Bioinformatics analysis of experimentally determined protein complexes in the yeast *Saccharomyces cerevisiae*. Genome research 2003; 13:2450-4.

4. Ma HW, Zeng AP. Reconstruction of metabolic networks from genome data and analysis of their global structure for various organisms. Bioinformatics 2003;19:270-277.
5. Ma HW, Zeng AP. The connectivity structure, giant strong component and centrality of metabolic networks. Bioinformatics 2003;19:1423-30.

Molecular modelling

Lecture

CHANGING PARADIGMS IN DRUG DISCOVERY

Hugo Kubinyi
Ruprecht-Karls University Heidelberg, Weisenheim am Sand, Germany; E-mail kubinyi@t-online.de

Introduction

The strategies of drug research did not change too much from the late 19th century till the seventies of the 20th century. New compounds were synthesized and tested in animals or organ preparations, following some chemical or biological hypotheses. Although synthetic output was relatively low, the real bottleneck was constituted by the biological test models. Pharmacological experiments, using dozens of animals for every new compound, most often needed more time for biological characterization than for chemical synthesis.

This situation started to change about thirty years ago. Slowly rational approaches developed, like QSAR and molecular modeling. The consequence was a lower output in such projects, when certain chemical structures had to be synthesized that were proposed by these methods. On the other hand, *in vitro* test systems like enzyme inhibition or the displacement of radio-labeled ligands in membrane preparations enabled a much faster investigation of new analogs. Now chemistry was the bottleneck. About ten to fifteen years ago, another significant shift in drug discovery paradigms happened: combinatorial chemistry suddenly flooded the biology laboratories with an overwhelming number of new compounds. It has been commented that combinatorial chemistry was the "revenge of the chemists" to the development of fast *in vitro* test models, with their large output of data within relatively short time. However, biologists were able to compete: ten thousands of compounds, later even more, could be investigated in just one week by automated High-Throughput Screening (HTS) systems.

In the past, wrong or misleading results were obtained too often just because of the use of animal models. Gene technology made an important contribution to drug discovery: the possibility to produce almost any protein in sufficient quantities enabled biologists to test new compounds at human targets. Genetically modified animals indicate whether a certain principle could work in therapy. The action of an enzyme inhibitor can be simulated before any compounds are synthesized and tested, by a knock-out of the corresponding enzyme; the action of drugs can be investigated in animals bearing a human protein. In addition, the production of larger quantities of a protein of therapeutic relevance allows the determination of its three-dimensional (3D) structure at atomic resolution by protein crystallography, alternatively by multidimensional NMR methods. As a consequence, methods developed for the structure-based design of ligands, by modeling or experimental determination of the 3D structures of protein-ligand complexes. Unfortunately, a new bottleneck resulted! Early combinatorial chemistry was guided by synthetic accessibility and the hype for large numbers. Due to this wrong focus, a huge amount of greasy, high-molecular weight compounds resulted, with all their problems in bioavailability and pharmacokinetics. Biological testing did not produce any valuable hits or supposed hits later failed in preclinical or clinical development. Whereas this situation fortunately changed in the last years, due to the maturation of combinatorial chemistry to an automated parallel synthesis of designed libraries, there was still a need for the fast

measurement or prediction of ADME (Absorption, Distribution, Metabolism, Excretion) properties. Indeed, ADME became the new bottleneck.

Nowadays, we have the information on the sequence of the human genome; our combinatorial chemistry approaches are under control by medicinal chemists and biologists; in addition to structure-based design we apply computer-aided methods for data mining, virtual screening, docking and scoring, to predict valuable leads and optimized candidates; HTS models have developed to ultra-HTS models, with up to a million test points per 24 hours; we even have fast experimental models and prediction tools for some ADME parameters. Is there a new bottleneck? Yes, unfortunately, or better saying: yes, of course. Target validation, the proof that the modulation of a certain target by a small molecule will indeed work in therapy, is one of the new bottlenecks. The other one, even more problematic, is the fact that only for some targets small molecules can be discovered which modulate the protein or a certain protein-protein interaction in the desired manner; "druggable" defines the property of a certain target to be accessible by small molecule intervention.

In the past, serendipity played a big role in the discovery of new drugs (1-3). Some other projects confirmed that the search for new drugs may be more efficient by establishing biological or structure-activity hypotheses and/or selecting certain scaffolds and substituents in the design of new drug candidates. The ratio of 10,000 compounds to produce one new drug is still very often cited. This applies to the situation where research starts from an endogenous ligand or any other lead structure. The "irrational approach", to test huge numbers of in-house compounds, commercially available compounds or chemistry-driven combinatorial libraries in HTS, did not deliver to the expected amount (4). Hundred thousands to millions of compounds have to be investigated if such a search starts from scratch, without any knowledge of an active lead, and even then there is no guarantee for success.

The "druggable genome"

The human genome project has provided the information on all our genes. However, the situation is the same as the one with Egyptian hieroglyphs before the discovery of the Rosetta Stone. We read the text but we understand only a minor part. There are about 30,000 genes in the human genome but we do not know how many of them are disease-related and how many of the gene products will be druggable. It has been estimated that about 600 to 1,500 druggable, disease-related targets exist, if one assumes about 10% disease-related genes on the one hand and about 10% druggable gene products on the other hand (5). However, this number has to be questioned because only the number of genes was considered (6). First of all, much more proteins or protein variants (estimated to be in the range of some 100,000s) are produced by alternative splicing and/or posttranslational modification than there are genes in the genome. Second, proteins can form a multitude of heteromeric complexes that are made up from only a small number of different proteins, e.g. GABA and nicotinic acetylcholine (nACh) receptors, integrins, and heterodimeric G protein-coupled receptors (GPCR). Third, some proteins are involved in more than one signaling chain, interacting with different proteins to modulate certain effects. And, last but not least, many therapeutically used drugs do not interact with just one target but have a balanced effect on several different targets. A striking example for such a promiscuous drug is the atypical neuroleptic olanzapine, which interacts as a nanomolar ligand with many different GPCRs (7-9).

Thus, we should neither discuss a druggable genome, nor a druggable proteome, nor a "druggable targetome", but a "druggable physiome" (6). Our problem is that we do not yet

know how to define and design a drug with the right balance of different target affinities, e.g. for depression, schizophrenia and other CNS diseases.

Virtual screening

Several new strategies have been developed for the structure-based and computer-aided design of active compounds. Drug research has often been compared with the search for a needle in a haystack. If neither active leads are known nor the 3D structure of the biological target, HTS seems to be the only reasonable approach. But much useful information can be derived from virtual screening (10), which reduces the size of the haystack. First of all, reactive compounds and other compounds with undesirable groups can be eliminated by so-called "garbage filters" (11). In a next step, the Lipinski (Pfizer) rule of five may be applied to estimate the potential for oral bioavailability; this set of four rules demands that the molecular weight of a molecule should be lower than 500; the lipophilicity, expressed by log P (P = calculated octanol/water partition coefficient), should be smaller than 5; the number of hydrogen bond donors should not be larger than 5; the sum of oxygen and nitrogen atoms in the molecule (as a rough approximation of the number of hydrogen bond acceptors) should not exceed 10 (12). A high risk of insufficient oral bioavailability is assumed if more than one of these conditions is violated. Often rule of five-compatible molecules are erroneously called "drug-like" (6). However, most of the compounds of the ACD (Available Compounds Directory) (13) would get this label if only the Lipinski rules are applied. "Druglike" or "non-druglike" character can only be attributed by neural nets that have been trained with drugs and chemicals (14-16). In this context it is important to notice that filters are valuable and efficient in the enrichment of interesting candidates out of large libraries. Single compounds should not be evaluated by such filters because the relatively large error rate of about 20% false positives and 20% false negatives would too often provide misleading results.

The situation in drug discovery is much better if already a certain number of active and inactive ligands of a target is known. If a chemical series belongs to a common scaffold or to some related scaffolds, 2D or 3D similarity methods, QSAR and 3D QSAR approaches, and pharmacophore approaches can be applied to derive structure-activity hypotheses (some problems of pharmacophore generation will be discussed in the next section). The results of such analyses are proposals for new syntheses or selections of compounds from a library. A highly valuable tool in this respect are feature tree similarity comparisons (17, 18), where the molecules are coded as strings with nodes, to which the pharmacophoric properties of the corresponding functional group, ring or linker are attributed. Due to this simple representation of the molecules, similarity searches can be performed extremely fast. In this manner, screening hits can be compared in their similarity to a whole in-house compound library, to libraries of commercially available compounds, e.g. the MDL Screening Compounds Directory (19), and to even larger virtual libraries.

If the 3D structure of a new target is known from experimental determination or from reliable homology modeling, the situation seems to be better but in reality it isn't. There remains a high degree of uncertainty about the 3D structure of the protein in the bound state if no information on protein-ligand complex 3D structures is available. Relatively often the protein itself and its ligand complexes have significantly different 3D structures, the most prominent example being HIV protease. In addition, the relatively low resolution of most protein 3D structures does not allow to differentiate between the side chain rotamers of asparagine, glutamine, threonine and histidine; the protonation state of histidine remains unclear; water

molecules being important for the binding of a ligand are sometimes neglected in protein 3D structures.

All these problems exist only to a minor extent if several protein-ligand complexes can be inspected, which leads to the fourth and best situation in ligand design: not only the protein but also some protein-ligand complexes are known. Molecular modeling and docking aids in the design of new ligands with hopefully improved binding affinity and/or selectivity with respect to other targets. It should be emphasized that structure-based design can result in a high-affinity ligand but affinity is only a necessary property of a drug, not a sufficient one. In addition, a drug has to be bioavailable, it must have a proper biological half-life time and is must not be toxic, among some other important properties.

Pharmacophores

The definition of a pharmacophore is simple (20). A 3D pharmacophore corresponds to an arrangement of hydrogen bond donor and acceptor, lipophilic and aromatic groups in space, in such a manner that these moieties can interact with a binding site at the target protein; in addition, steric exclusion volumes can be defined. However, the identification of a pharmacophore within a congeneric group of compounds is far from being trivial. Although there are computer programs for the automated derivation of pharmacophores from series of active and less active analogs (21), a better and more reliable method seems to be a "construction by hand" (22). Four independent problems have to be considered:

- the different pharmacophoric properties of oxygen atoms,
- the protonation and deprotonation of ionizable groups,
- the consideration of tautomeric forms, and
- the superposition of flexible molecules.

Oxygen atoms are strong hydrogen bond acceptors, as long as they are connected to a carbon atom by a double bond (e.g. in aldehydes, ketones, carboxylic acids, carbonyl group of esters) or if they are substituted by hydrogen and/or aliphatic residues (water, aliphatic alcohols and aliphatic ethers). They are weak or even no acceptors at all (e.g. the sp_3 oxygen atom of an ester group) if the direct neighbor atoms are connected to another atom by a double bond or if they are part of an aromatic system, as in oxazoles and isoxazoles (Figure 1) (23,24).

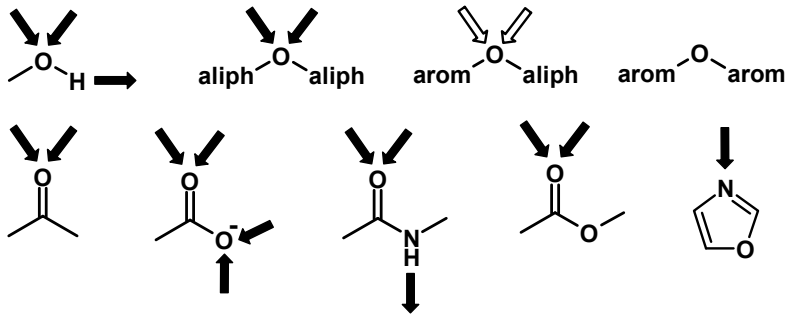

Figure 1. Hydrogen bond acceptors

Ionizable groups must be recognized and defined in the right manner to end up with correct pharmacophores. As this is still a mainly unsolved problem for many compounds that are not simple acids, phenols or anilines (at least considering the speed that is needed in the virtual screening of large libraries), a rule-based system has recently been proposed (25). In this set of rules, all carboxylic acids, the strongly basic amidines and guanidines, and quaternary ammonium compounds are permanently charged. Neutral and protonated forms are generated and investigated in parallel for amines, imidazoles, pyridines and other nitrogen-containing heterocycles. For tetrazoles, thiols, hydroxamic acids, and activated sulfonamides, neutral and deprotonated forms should be investigated in parallel. Certain rules restrict the number of generated species, to avoid combinatorial explosions: there are definitions of the maximum number of charges in a molecule and no identical charges are allowed in adjacent positions of the molecule. Although this approach is definitely better than using all molecules in their neutral form, refined prediction models are urgently needed. An even more difficult problem arises from the fact that ionizable amino acid side chains in proteins may significantly change their pK_a value in dependence of their environment (26, 27).

Protomers and tautomers constitute another serious problem in virtual screening and docking (28, 29). In Figure 2, the two different protomers of imidazole (upper left) present their donor and acceptor moieties in different positions; as imidazole has a pK_a value around 7, also the charged form with two donor functions has to be considered (upper right). The other compounds are typical examples of tautomeric forms of molecules, where donor and acceptor functions change their position. 1,3-Diketones, acetoacetic esters, hydroxypyridines, oxygen-substituted pyrimidines and purines, and many other compounds may exist in several tautomeric forms that have to be recognized and considered.

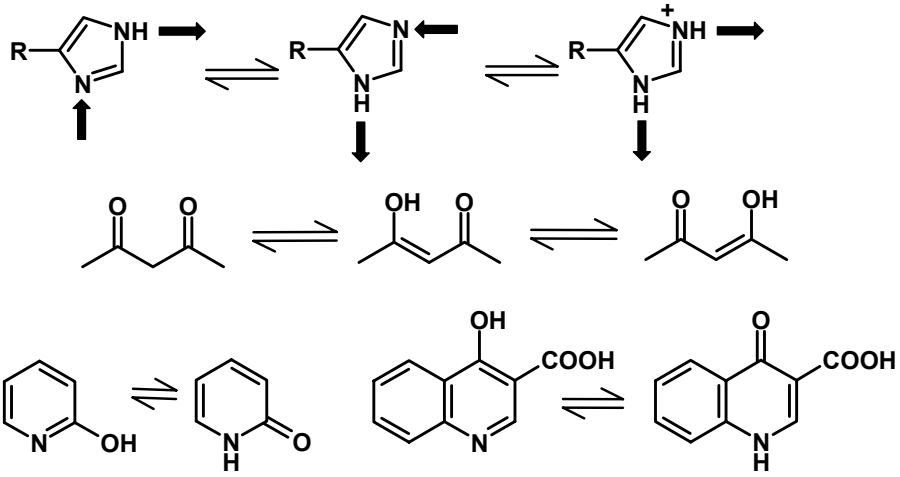

Figure 2. Tautomeric forms of molecules

For the purine base guanine, 15 different tautomers can be formulated (29). In this context it is interesting to note that for long time Watson and Crick had problems to derive the correct 3D structure of DNA because they only considered the enol tautomers of guanine and thymine, instead of the keto forms. As shown in Figure 3, the guanine tautomer in the upper left is the predominant one of 15 possible tautomers, whereas Watson and Crick, for long time, worked with the tautomer shown in the lower left. Ro 200-1770 is a matrix metalloprotease inhibitor.

Only one tautomer can bind with high affinity; the carbonyl form or the other enol form will not form favorable hydrogen bond networks.When their colleague Donohue corrected this error, they immediately arrived at the correct base pairing (30). Sometimes enol forms of a ligand are induced by the binding site, as is the case for the binding of the barbiturate Ro 200-1770 to a matrix metalloprotease (Figure 3) (31). Computer programs for the generation of all possible tautomers have been described (29, 32).

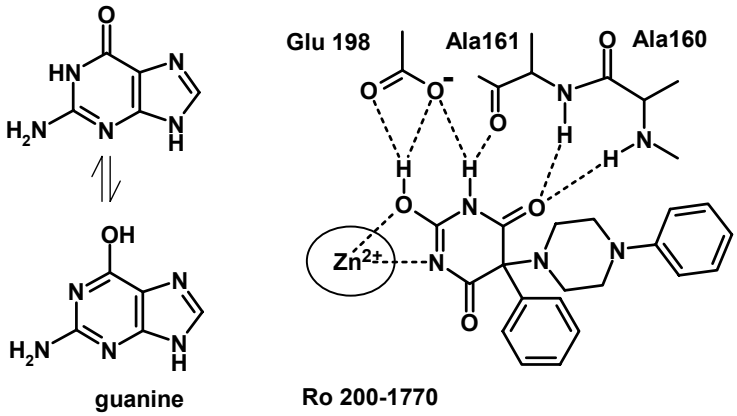

Figure 3. Guanine tautomers

If all these topics are considered in an appropriate manner, the next step is an alignment of the molecules. With rigid molecules, this is most often no problem. But even with steroids the question arises, whether a 3-keto,17-hydroxy-steroid and a 3-hydroxy-17-keto-steroid should be aligned according to their molecular skeleton (which puts the hydrogen bond donor groups of both molecules far apart) or whether a head-to-tail superposition is more favorable; the steric superposition is about as good in this latter case as in the conventional superposition (33). For flexible molecules, the most rigid, active species should be used as template onto which, step by step, the other molecules are superimposed. This can be done by visual inspection or by field fit methods, like SEAL (34, 35); most often several different conformations have to be considered. FlexS is a computer program for flexible superposition; one molecule is used as a rigid template and all other molecules are superimposed in a flexible manner onto this template (36, 37). 3D QSAR methods, like CoMFA (comparative molecular field analysis) (38, 39) or CoMSIA (comparative molecular similarity index analysis) (40), surprisingly do not depend on a knowledge of the bioactive conformation. If all conformations are "wrong" to the same extent, the result of an analysis may nevertheless be useful. Another difficulty in the alignment of molecules arises from different binding modes of seemingly similar molecules; there are no general rules how to recognize such situations.

Once a pharmacophore hypothesis has been derived, 3D searches can be performed, using commercial software (21, 41). However, it must be emphasized that 3D searches are only meaningful if all structures of a database were defined according to their correct pharmacophoric properties; otherwise such searches are just useless.

Structure-based ligand design

In the seventies of the last century, the first structure-based design of ligands was performed. The 3D structure of the 2,3-diphosphoglycerate (2,3-DPG) hemoglobin complex was used to derive simple aromatic dialdehydes which mimicked the function of 2,3-DPG as an allosteric effector molecule. Another early example was the structure-based design of trimethoprim analogs with significantly improved affinities to dihydrofolate reductase. However, neither the hemoglobin ligands nor the trimethoprim analogs could be optimized to become drugs for human therapy (42, 43). The first real success story was the structure-based design of the antihypertensive drug captopril, an angiotensin-converting enzyme (ACE) inhibitor. Its structure was derived in a rational manner from a binding site model, using the 3D information of an inhibitor complex of the closely related zinc protease carboxypeptidase A (44).

With the ongoing progress in protein crystallography and multidimensional NMR techniques, the 3D structures of many important proteins, especially enzymes, have been determined. This information led to the structure-based design of several therapeutically useful enzyme inhibitors, most of them still being in preclinical or clinical development. Marketed drugs that resulted from structure-based design are e.g. the antiglaucoma drug dorzolamide (Merck) and the newer HIV protease inhibitors nelfinavir (Agouron Pharmaceuticals, now Pfizer) and amprenavir (Vertex Pharmaceuticals; developed and marketed by GSK).

Neuraminidase is an interesting target for the structure-based design of anti-influenza drugs. In a very elegant study, Mark von Itzstein used the computer program GRID to estimate interaction energies of the neuraminic acid binding site of this enzyme with different probe atoms or small groups (45). He realized that the introduction of basic groups, like -NH_2, -$C(=NH)NH_2$ or -NH-$C(=NH)NH_2$, into the relatively weak inhibitor neu5ac2en should significantly improve inhibitory activities. This is indeed the case: the neuraminidase inhibitor zanamivir is about 4 orders of magnitude more active than its 4-hydroxy-analog neu5ac2en. Due to its polar character, zanamivir (Relenza®, GSK) is orally inactive; it must be applied by inhalation (46).

Scientists at Gilead Sciences started from the observation that the glycerol side chain of certain zanamivir analogs does not contribute to affinity. In a series of carbocyclic analogs, strongest inhibitor activity was observed for a pent-3-yl ether. Its ethyl ester prodrug oseltamivir (GS 4104, Tamiflu®, Hoffmann-La Roche; Figure 4) shows good oral bioavailability (46, 47). Several other success stories of structure-based design have been published (43, 48-51).

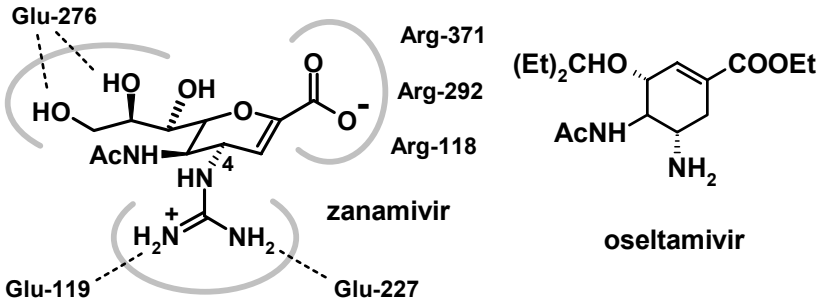

Figure 4. Binding mode of the 4-desoxy-4-guanidino-analog of neu5ac2en, zanamivir, to neuraminidase (left); chemical structure of the orally available prodrug oseltamivir (right)

Computer-aided ligand design

Whereas structure-based design can be regarded as the predominant strategy of the last two decades, several computer-assisted methods were developed more recently. If thousands of candidates and even larger structural databases shall be tested whether they are suited to be ligands of a certain binding site, this cannot any longer be performed by visual inspection. The design process has to be automated with the help of the computer.

The very first computer-based approaches, to search for ligands of a certain binding site, were the programs DOCK (52) and GROW. The *de novo* design program LUDI, developed by Hans-Joachim Böhm at BASF in the early 1990's, was a significant improvement over these early prototypes (53,54). After the definition of a binding site region by the user, the program automatically identifies all hydrogen bond donor and acceptor sites, as well as aliphatic and aromatic hydrophobic areas of this part of the protein surface. From the program-implemented information on the geometry of interaction of such groups with a ligand, the program creates vectors and regions in space, where complementary groups of a ligand should be located. In the next step, LUDI searches any database of 3D structures of small and medium-sized molecules for potential ligands. Every candidate is tested in a multitude of different orientations and interaction modes, optionally also in different conformations. After a rough evaluation, by counting the number of favorable interactions and by checking for unfavorable van der Waals overlap between the ligand and the protein, the remaining candidates are prioritized by a simple but efficient scoring function (55). This scoring function estimates interaction energies on the basis of charged and neutral hydrogen bonding energies, hydrophobic contact areas, and the number of rotatable bonds of the ligand. In a last step, the program is capable to attach groups, fragments and/or rings to a hit or to an already existing lead structure. A flexible docking of ligands onto a rigid binding site can be achieved by the programs DOCK 4.0 (56), GOLD (57), FlexX (58,59), and the public domain program AutoDock (60,61), to mention just the most prominent ones; more docking programs and several success stories of computer-assisted drug design have been reviewed by Schneider and Böhm (62). The FlexX modifications FlexE (63) and Flex-Pharm (64) allow a flexible ligand docking into an ensemble of different binding site conformations and the definition of pharmacophore constraints, respectively. Of course, the pharmacophoric properties of all molecules must be defined in a correct manner also in structure-based and computer-aided design.

Fragment-based and combinatorial ligand design

Several other methods for the design of new ligands have been described in the past, e.g. needle screening (65, 66), which starts from a collection of small drug-like ligands and attempts to extend the best ones to larger ligands. In the binding of biotin to avidin, some molecular fragments have only micromolar affinities, whereas biotin itself binds with femtomolar affinity (67). This principle has recently been used in the rational design of a nanomolar enzyme inhibitor from two low-affinity natural products which bind to different sites of the protein (68). The SAR by NMR method (69-71) searches for small, low-affinity ligands of proteins which bind to adjacent areas of the binding site. A linker combines both molecules to a nanomolar ligand. Some other NMR-based techniques for ligand discovery have been developed (72-78).

Fragment-based ligand design has been applied for combinatorial techniques (79). Up to 10,000 low-molecular weight ligands can be tagged to a gold-coated glass surface (80); binding of any protein to these microarrays of immobilized ligands is detected by surface plasmon

resonance, in this manner avoiding the development of a specific screening method for a new protein. The dynamic assembly of ligands (81-84) generates new molecules from fragments which reversibly react with each other in the presence of a protein. Molecules that fit the binding site are preferentially formed and afterwards trapped by a reaction which freezes the equilibrium. Some other approaches for the combinatorial design of new leads have been described (85-89).

There are also several computer-assisted techniques for the combinatorial combination of fragments to new leads. The program CombiGen (90) designs libraries with a high percentage of drug-like compounds by assembling privileged and/or user-defined fragments and optionally modifying the resulting structures; virtual screening procedures eliminate molecules with undesired properties. TOPAS (91,92) dissects lead structures into fragments and assembles new molecules by re-combining a chemically similar scaffold with fragments that are similar to the original ones; cleavage and assembly of the molecules follow chemical reactions that are defined by a RECAP-like procedure (93). In this manner, new chemistry is generated by "scaffold hopping" (94). In principle, the docking program FlexX (58,59), which performs an incremental construction of a ligand within the binding site, could also arrive at new analogs, if many different building blocks are used instead of the original building blocks; no virtual library of millions of potential candidates needs to be constructed, only favorable intermediate solutions and final candidates are generated. The only unsolved problem in this respect is the lack of reliability of the scoring functions (95).

Conclusions

Virtual screening and fragment-based approaches are powerful techniques in the search for new ligands (10,62,96); promising candidates can be enriched in compound collections and virtual libraries. The integration of protein crystallography, NMR techniques, and virtual screening will "significantly enhance the pace of the discovery process and the quality of compounds selected for further development" (97).

The similarity principle, that similar compounds should exert similar biological activities, has always been a most successful approach in drug research, despite many exceptions to this general concept (98, 99). Chemogenomics is a new term for the dedicated investigation of certain compound classes in target families, like the G Protein-Coupled Receptors (GPCR), kinases, phosphodiesterases, serine proteases, ion channels, etc. (100-104). An analogous concept, the "selective optimization of side activities" (SOSA approach), attempts to develop new drugs in the direction of a side effect of a certain drug (105, 106). Historical examples for the validity of this approach are e.g. antitussive and constipating morphine analogs, diuretic and antidiabetic sulfonamides, and many others (107); some very recent examples have been reviewed (106, 107).

As already mentioned, good ligands are not necessarily good drugs. High-throughput screening of in-house libraries, which originally contained large numbers of reactive, degraded, colored, fluorescent, and highly lipophilic molecules, and screening of combinatorial libraries of large, lipophilic molecules produced hits that could not be optimized to drug candidates. The awareness for the real problems came only after Lipinski had defined his set of rules (12). On the other hand, the massive increase of screening failures due to such inappropriate compound collections or libraries turned this awareness of ADME problems into a hype. Prior statistics of 40% failure in clinical investigation (the most expensive phase of drug development), due to ADME problems (108, 109) are cited in literature, again and again; a closer inspection of the data shows that the ADME-related failure can be neglected if antiinfectives are removed from

the original sample (6,109). This is an indication that medicinal chemists considered, all the time, the importance of ADME properties. Only HTS and early combinatorial chemistry generated so many problems in this direction. In addition to the Lipinski rules, several *in vitro* and *in silico* techniques are now available for the estimation of ADME properties (110).

With respect to biological testing, Horrobin has raised the question whether we are already living in Castalia, the famous virtual land of Hermann Hesse's novel "The Glass Bead Game", where the masters organize and play the most sophisticated, complex and brilliant games - without any context to reality (111). Sometimes, this is also the case in modeling and drug design (6). The new tools of drug research are extremely powerful but they will be successful only if the most important factors, some of them reviewed here, are considered in the right manner. In the fascinating search for better and safer drugs, the new paradigms of drug discovery have to merge with traditional medicinal chemistry experience (2, 112, 113).

Note
This chapter was first published in: Hicks M, *et al*. (Ed.) *Proceedings of the International Beilstein Workshop "The Chemical Theatre of Biological Systems", Bozen, May 24-28, 2004* (with permission from the Editors).

References

1. Roberts R M. Serendipity. Accidental discoveries in science. New York: John Wiley & Sons; 1989.
2. Sneader W. Drug prototypes and their exploitation. Chichester: John Wiley & Sons; 1996.
3. Kubinyi H. Chance favors the prepared mind. From serendipity to rational drug design. J Receptor Signal Transduct Res 1999;19:15-39.
4. Lahana R. How many leads from HTS? Drug Discovery Today 1999;4:447-8.
5. Hopkins AL, Groom CR. The druggable genome. Nature Rev Drug Discov 2002;1:727-30.
6. Kubinyi H. Drug research: myths, hype and reality. Nature Rev Drug Discov 2003;2:665-8.
7. Schaus JM, Bymaster FP. Dopanminergic approaches to antipsychotic agents. Ann Rep Med Chem 1998;33:1-10.
8. Bymaster FP, Calligaro DO, Falcone JF, Marsh RD, Moore NA, Tye NC, Seeman P, Wong DT. Radioreceptor binding profile of the atypical antipsychotic olanzapine. Neuropsychopharmacology 1996;14:87-96.
9. Bymaster FP, Nelson DL, DeLapp NW, Falcone JF, Eckols K, Truex LL, Foreman MM, Lucaites VL, Calligaro DO. Antagonism by olanzapine of dopamine D1, serotonin2, muscarinic, histamine H1 and alpha 1-adrenergic receptors *in vitro*. Schizophr Res 1999;37:107-22.
10. Böhm H-J, Schneider G. Virtual screening for bioactive molecules. In: Mannhold R, Kubinyi H, Timmerman H (Ed.). Methods and principles in medicinal chemistry. vol. 10. Weinheim: Wiley-VCH; 2000. p. 25-31.
11. Rishton GM. Reactive compounds and *in vitro* false positives in HTS. Drug Discov Today 1997;2:9382-4.
12. Lipinski CA, Lombardo F, Dominy BW, Feeney PJ. Experimental and computational approaches to estimate solubility and permeability in drug discovery and development settings. Adv Drug Del Revs 1997;23:3-26.
13. MDL Available compounds directory. San Leandro, CA: MDL Information Systems Inc. Last visited September 13, 2004; available from: www.mdl.com.

14. Ajay, Walters WP, Murcko MA. Can we learn to distinguish between “drug-like” and “nondrug-like” molecules? J Med Chem 1998;41:3314-24.
15. Sadowski J, Kubinyi H. A scoring scheme for discriminating between drugs and nondrugs. J Med Chem 1998;41:3325-9.
16. Walters WP, Murcko MA. Prediction of ‘drug-likeness’. Adv Drug Deliv Rev 2002;54:255-71.
17. Rarey M, Dixon JS. Feature trees: a new molecular similarity measure based on tree matching. J Comput-Aided Mol Design 1998;12: 471-90.
18. Rarey M, Stahl M. Similarity searching in large combinatorial chemistry spaces. J Comput-Aided Mol Design 2001;15:497-520.
19. MDL Screening compounds directory. San Leandro, CA: MDL Information Systems Inc. Last visited September 13, 2004; available from: www.mdl.com.
20. Güner OF (Ed.). Pharmacophore perception, development and use in drug design. La Jolla, CA: International University Line; 2000.
21. Catalyst. San Diego, CA: Accelrys Inc. (cited 2004 September 13). Last visited September 13, 2004; available from: www.accelrys.com.
22. Höltje HD, Sippl W, Rognan D, Folkers G. Molecular modelling. basic principles and applications. 2nd ed. Weinheim: Wiley-VCH; 2003.
23. Lommerse JPM, Price SL, Taylor R. Hydrogen bonding of carbonyl, ether, and ester oxygen atoms with alkanol hydroxyl groups. Comput Chem 1997;18:757-74.
24. Böhm H-J, Brode S, Hesse U, Klebe G. Oxygen and nitrogen in competitive situations: which is the hydrogen-bond acceptor? Chem Eur J 1996;2:1509-13.
25. Sadowski J. A tautomer and protonation pre-processor for virtual screening. In: Totten GE (Ed.). Proceedings of the 224th ACS National Meeting; 2002 August 18-22; Boston, USA. Boston: ACS; 2002. p. 511-20.
26. Nielsen JE, Vriend G. Optimizing the hydrogen-bond network in Poisson-Boltzmann equation-based pKa calculations. Proteins 2001;43:403-12.
27. Nielsen JE, McCammon JA. Calculating pKa values in enzyme active sites. Protein Sci 2003;12:1894-901.
28. Pospisil P, Ballmer P, Scapozza L, Folkers G. Tautomerism in computer-aided drug design. J Recept Signal Transduct Res 2003;23:361-71.
29. Trepalin SV, Skorenko AV, Balakin KV, Nasonov AF, Lang SA, Ivashchenko AA, Savchuk NP. Advanced exact structure searching in large databases of chemical compounds. J Chem Inf Comput Sci 2003;43:852-60.
30. Watson JD, The Double Helix: A Personal Account of the Discovery of the Structure of DNA. New York: Atheneum Press; 1968.
31. Brandstetter H, Grams F, Glitz D, Lang A, Huber R, Bode W, Krell HW, Engh RA. The 1.8-A crystal structure of a matrix metalloproteinase 8-barbiturate inhibitor complex reveals a previously unobserved mechanism for collagenase substrate recognition. J Biol Chem 2001;276:17405-12.
32. Pospisil P, Ballmer P, Scapozza L, Folkers G. Tautomerism in computer-aided drug design. J Recept Signal Transduct 2003;23(4):361-71.
33. Kubinyi H, Hamprecht FA, Mietzner T. Three-dimensional quantitative similarity-activity relationships (3D QSiAR) from SEAL similarity matrices. J Med Chem 1998;41:2553-64.
34. Kearsley SK, Smith GM. An alternative method for the alignment of molecular structures: maximizing electrostatic and steric overlap. Tetrahedron Comp Methodol 1990;3:615-33.

35. Klebe G, Mietzner T, Weber F. Different approaches toward an automatic structural alignment of drug molecules: applications to sterol mimics, thrombin and thermolysin inhibitors. J Comput-Aided Mol Design 1994;8:751-78.

36. Lemmen C, Lengauer T. Time-efficient flexible superposition of medium-sized molecules. J Comput-Aided Mol Design 1997;11:357-68.

37. Lemmen C, Lengauer T. Computational methods for the structural alignment of molecules. J Comput-Aided Mol Design 2000;14:215-32.

38. Cramer III RD, Patterson DE, Bunce JD. Comparative molecular field analysis (CoMFA). 1. Effect of shape on binding of steroids to carrier proteins. J Am Chem Soc 1988;110:5959-67.

39. a) Kubinyi H (Ed.). 3D QSAR in drug design. Theory, methods and applications. Leiden: ESCOM Science Publishers B.V; 1993. b) Kubinyi H, Folkers G, Martin YC (Ed.). 3D QSAR in drug design. Ligand-protein komplexes and molecular similarity. Volume 2. Dordrecht: Kluwer/ESCOM; 1998; also published as Persp Drug Discov Design. 1998;9-11:1-416. c) Kubinyi H, Folkers G, Martin YC (Ed.). 3D QSAR in drug design. Recent advances. Volume 3. Dordrecht: Kluwer/ESCOM; 1998; also published as Persp Drug Discov Design. 1998;12-14:1-352.

40. Klebe G, Abraham U, Mietzner T. Molecular similarity indices in a comparative analysis (CoMSIA) of drug molecules to correlate and predict their biological activity. J Med Chem 1994;37:4130-46.

41. Sybyl [computer software]. Version 3.5. St. Louis, MO: Tripos Inc.; 2004

42. Goodford PJ. Drug design by the method of receptor fit. J Med Chem 1984;27:558-64.

43. Kubinyi H. Structure-based design of enzyme inhibitors and receptor ligands. Curr Opin Drug Discov Dev 1998;1:4-15.

44. Redshaw S. Angiotensin-converting enzyme (ACE) inhibitors and the design of Cilazapril, in: medicinal chemistry. In: Ganellin CR, Roberts SM (Ed.). The Role of organic chemistry in drug research. 2nd edition. London: Academic Press; 1993. p. 163-185.

45. von Itzstein M, Wu WY, Kok GB, Pegg MS, Dyason JC, Jin B, Phan TV, Smythe ML, White HF, Oliver SW, Colman PM, Varghese JN, Ryan DM, Woods JM, Bethell RC, Hotham VJ, Cameron JM, Penn CR. Rational design of potent sialidase-based inhibitors of influenza virus replication. Nature 1993;363:418-23.

46. Abdel-Magid AF, Maryanoff CA, Mehrman SJ. Synthesis of influenza neuraminidase inhibitors. Curr Opin Drug Discov Devel 2001;4:776-91.

47. Kim CU, Lew W, Williams MA, Liu H, Zhang L, Swaminathan S, Bischofberger N, Chen MS, Mendel DB, Tai CY, Laver WG, Stevens RC. Influenza neuraminidase inhibitors possessing a novel hydrophobic interaction in the enzyme active site: design, synthesis and structural analysis of carbocyclic sialic acid analogues with potent anti-influenza activity. J Am Chem Soc 1997;119:681-90.

48. Veerapandian P (Ed.). Structure-based drug design. New York: Marcel Dekker; 1997.

49. Babine RE, Bender SL. Molecular recognition of protein ligand complexes: applications to drug design. Chem Rev 1997;97:1359-472.

50. Gubernator K, Böhm HJ (Ed.). Structure-based ligand design. Weinheim: Wiley-VCH; 1998.

51. Babine RE, Abdel-Meguid SS. Protein Crystallography. Weinheim: Wiley-VCH; 2004.

52. DesJarlais RL, Sheridan RP, Seibel GL, Dixon JS, Kuntz ID, Venkataraghavan R. Using shape complementarity as an initial screen in designing ligands for a receptor binding site of known three-dimensional structure. J Med Chem 1988;31:722-9.

53. Böhm H-J. The computer program LUDI: a new method for the de novo design of enzyme inhibitors. J Comput-Aided Mol Design 1992;6;61-78.

54. Böhm H-J. LUDI: rule-based automatic design of new substituents for enzyme inhibitor leads. J Comput-Aided Mol Design 1992;6:593-606.

55. Böhm H-J. The development of a simple empirical scoring function to estimate the binding constant for a protein-ligand complex of known three-dimensional structure. J Comput-Aided Mol Design 1994;8:243-56.

56. Ewing TJ, Makino S, Skillman AG, Kuntz ID. DOCK 4.0: search strategies for automated molecular docking of flexible molecule databases. J Comput-Aided Mol Design 2001;15:411-28.

57. Jones G, Willett P, Glen RC, Leach AR, Taylor R. Development and validation of a genetic algorithm for flexible docking. J Mol Biol 1997;267:727-48.

58. Rarey M, Kramer B, Lengauer T, Klebe G. A fast flexible docking method using an incremental construction algorithm. J Mol Biol 1996;261:470-89.

59. Lengauer T, Rarey M. Computational methods for biomolecular docking. Curr Opin Struct Biol 1996; 6:402-6.

60. Goodsell DS, Olson AJ. Automated docking of substrates to proteins by simulated annealing. Proteins 1990; 8:195-202.

61. Morris GM, Goodsell DS, Halliday RS, Huey R, Hart WE, Belew RK, Olson AJ. Automated Docking Using a Lamarckian Genetic Algorithm and and Empirical Binding Free Energy Function. J Comput Chem 1998;19:1639-62.

62. Schneider G, Böhm H-J. Virtual screening and fast automated docking methods. Drug Discov Today 2002;7:64-70.

63. Claussen H, Buning C, Rarey M, Lengauer T. FlexE: efficient molecular docking considering protein structure variations. J Mol Biol 2001; 308:377-95.

64. Hindle SA, Rarey M, Buning C, Lengauer T. Flexible docking under pharmacophore type constraints. J Comput-Aided Mol Design 2002; 16:129-49.

65. Hilpert K, Ackermann J, Banner DW, Gast A, Gubernator K, Hadvary P, Labler L, Müller K, Schmid G, Tschopp TB, van de Waterbeemd H. Design and synthesis of potent and highly selective thrombin inhibitors. J Med Chem 1994;37:3889-901.

66. Boehm H-J, Boehringer M, Bur D, Gmuender H, Huber W, Klaus W, Kostrewa D, Kuehne H, Luebbers T, Meunier-Keller N, Mueller F. Novel inhibitors of DNA gyrase: 3D structure based biased needle screening, hit validation by biophysical methods, and 3D guided optimization. A promising alternative to random screening. J Med Chem 2000;43:2664-74.

67. Green NM. Avidin. Adv Protein Chem 1975;29:85-133.

68. Hanessian S, Lu P-P, Sanceau J-Y, Chemla P, Gohda K, Fonne-Pfister R, Prade L, Cowan-Jacob SW. An Enzyme-Bound Bisubstrate Hybrid Inhibitor of Adenylosuccinate Synthetase. Angew Chem Int Ed Engl 1999;38:3159-62.

69. Shuker SB, Hajduk PJ, Meadows RP, Fesik SW. Discovering high-affinity ligands for proteins: SAR by NMR. Science 1996;274:1531-4.

70. Hajduk PJ, Meadows RP, Fesik SW. Discovering high-affinity ligands for proteins. Science. 1997; 278:497-499.

71. Hajduk PJ, Sheppard G, Nettesheim DG, Olejniczak ET, Shuker SB, Meadows RP, Steinman DH, Carrera Jr. GM, Marcotte PA, Severin J, Walter K, Smith H, Gubbins E, Simmer R, Holzman TF, Morgan DW, Davidsen SK, Summers JB, Fesik SW. Discovery of potent nonpeptide inhibitors of stromelysin using SAR by NMR. J Am Chem Soc. 1997; 119:5818-5827.

72. Zerbe O (Ed.). BioNMR in drug research. Weinheim: Wiley-VCH; 2003.

73. Fejzo J, Lepre CA, Peng JW, Bemis GW, Ajay, Murcko MA, Moore JM. The SHAPES strategy: an NMR-based approach for lead generation in drug discovery. Chem Biol 1999;6:755-69.

74. Lepre CA, Peng J, Fejzo J, Abdul-Manan N, Pocas J, Jacobs M, Xie X, Moore JM. Applications of SHAPES screening in drug discovery. Comb Chem High Throughput Screen 2002;5:583-90.

75. Diercks T, Coles M, Kessler H. Applications of NMR in drug discovery. Curr Opin Chem Biol 2001;5:285-91.

76. Pellecchia M, Sem DS, Wüthrich K. NMR in drug discovery. Nature Rev Drug Discov 2002;1:211-9.

77. Jahnke W, Floersheim P, Ostermeier C, Zhang X, Hemmig R, Hurth K, Uzunov DP. NMR reporter screening for the detection of high-affinity ligands. Angew Chem Int Ed Engl 2002;41:3420-3.

78. Meyer B, Peters T. NMR spectroscopy techniques for screening and identifying ligand binding to protein receptors. Angew Chem Int Ed Engl 2003;42:842-90.

79. Kubinyi H. Combinatorial and Computational Approaches in Structure-based Drug Design. Curr Opin Drug Discovery Dev 1998;1:16-27.

80. Metz G, Ottleben H, Vetter D. Small molecule screening on chemical microarrays. In: Böhm, H-J, Schneider G (Ed.). Protein-ligand interactions. From molecular recognition to drug design. Weinheim: Wiley-VCH; 2003. p. 213-36.

81. Huc I, Lehn J-M. Virtual combinatorial libraries: dynamic generation of molecular and supramolecular diversity by self-assembly. Proc Natl Acad Sci USA 1997;94:2106-10; erratum in Proc Natl Acad Sci USA 1997;94:8272.

82. Lehn J-M, Eliseev AV. Dynamic combinatorial chemistry. Science 2001;291:2331-2.

83. Ramström O, Lehn J-M. Drug discovery by dynamic combinatorial libraries. Nature Rev Drug Discov 2002;1:26-36.

84. Hochgürtel M, Kroth H, Piecha D, Hofmann MW, Nicolau C, Krause S, Schaaf O, Sonnenmoser G, Eliseev AV. Target-induced formation of neuraminidase inhibitors from *in vitro* virtual combinatorial libraries. Proc Natl Acad Sci USA 2002;99:3382-7.

85. Erlanson DA, Braisted AC, Raphael DR, Randal M, Stroud RM, Gordon EM, Wells JA. Site-directed ligand discovery. Proc Natl Acad Sci USA 2000;97:9367-72.

86. Erlanson DA, Lam JW, Wiesmann C, Luong TN, Simmons RL, DeLano WL, Choong IC, Burdett MT, Flanagan WM, Lee D, Gordon EM, O'Brien T. In situ assembly of enzyme inhibitors using extended tethering. Nature Biotechnol 2003;21:308-14.

87. Maly DJ, Choong IC, Ellman JA. Combinatorial target-guided ligand assembly: identification of potent subtype-selective c-Src inhibitors. Proc Natl Acad Sci USA 2000;97:2419-24.

88. Swayze EE, Jefferson EA, Sannes-Lowery KA, Blyn LB, Risen LM, Arakawa S, Osgood SA, Hofstadler SA, Griffey RH. SAR by MS: a ligand based technique for drug lead discovery against structured RNA targets. J Med Chem 2002;45:3816-9.

89. Lewis WG, Green LG, Grynszpan F, Radic Z, Carlier PR, Taylor P, Finn MG, Sharpless KB. Click chemistry in situ: acetylcholinesterase as a reaction vessel for the selective assembly of a femtomolar inhibitor from an array of building blocks. Angew Chem Int Ed Engl 2002;41:1053-7.

90. Wolber G, Langer T. Combigen: a novel software package for the rapid generation of virtual combinatorial libraries. In: Höltje H- D, Sippl W (Ed.). Rational approaches to drug design; Proceedings of the 13th European Symposium on Quantitative Structure-Activity Relationships; 2000 August 27 - September 1; Düsseldorf, Germany. Barcelona: Prous Science; 2001. p. 390-9.

91. Schneider G, Clement-Chomienne O, Hilfiger L, Schneider P, Kirsch S, Boehm H-J, Neidhart W. Virtual screening for bioactive molecules by evolutionary de novo design. Angew Chem Int Ed Engl 2000;39:4130-3.

92. Schneider G, Lee ML, Stahl M, Schneider P. De novo design of molecular architectures by evolutionary assembly of drug-derived building blocks. J Comput-Aided Mol Design 2000;14:487-94.

93. Lewell XQ, Judd DB, Watson SP, Hann MM. RECAP -retrosynthetic combinatorial analysis procedure: a powerful new technique for identifying privileged molecular fragments with useful applications in combinatorial chemistry. J Chem Inf Comput Sci 1998; 38:511-22.
94. Schneider G, Neidhart W, Giller T, Schmid G. "Scaffold-hopping" by topological pharmacophore search: a contribution to virtual screening. Angew Chem Int Ed Engl 1999;38:2894-6.
95. Wang R, Lu Y, Wang S. Comparative evaluation of 11 scoring functions for molecular docking. J Med Chem 2003;46:2287-303.
96. Bleicher KH, Böhm H-J, Müller K, Alanine AI. Hit and lead generation: beyond high-throughput screening. Nature Rev Drug Discov 2003;2:369-78.
97. Muchmore SW, Hajduk PJ. Crystallography, NMR and virtual screening: integrated tools for drug discovery. Curr Opin Drug Discovery Dev. 2003; 6:544-549.
98. Kubinyi H. Similarity and dissimilarity: a medicinal chemist's view. Persp Drug Design Discov 1998; 9-11:225-52.
99. Martin YC, Kofron JL, Traphagen LM. Do structurally similar molecules have similar biological activity? J Med Chem 2002;45:4350-8.
100. Caron PR, Mullican MD, Mashal RD, Wilson KP, Su MS, Murcko MA. Chemogenomic approaches to drug discovery. Curr Opin Chem Biol. 2001; 5:464-470.
101. Bleicher KH. Chemogenomics: bridging a drug discovery gap. Curr Med Chem 2002;9:2077-84.
102. Jacoby E, Schuffenhauer A, Floersheim P. Chemogenomics knowledge-based strategies in drug discovery. Drug News Perspect 2003;16:93-102.
103. Müller G. Medicinal chemistry of target family-directed masterkeys. Drug Discov Today 2003;8:681-91.
104. Kubinyi H, Müller G (Ed.). Chemogenomics in drug discovery - A medicinal chemistry perspective. Weinheim: Wiley-VCH; 2004.
105. Wermuth CG. The "SOSA" aproach: an alternative to high-throughput screening. Med Chem Res. 2001; 10:431-439.
106. Wermuth CG. Selective optimization of side activities: another way for drug discovery. J Med Chem 2004;47:1303-14.
107. Kubinyi H. Drug discovery from side effects. In: Kubinyi H, Müller G (Ed.). Chemogenomics in drug discovery - A medicinal chemistry perspective. Weinheim: Wiley-VCH; 2004; p. 43-67.
108. Prentis RA, Lis Y, Walker SR. Pharmaceutical innovation by the seven UK-owned pharmaceutical companies (1964-1985). Br J Clin Pharmac 1988;25:387-96.
109. Kennedy T. Managing the drug discovery/development interface. Drug Discov Today 1997;2:436-44.
110. van de Waterbeemd H, Gifford E. ADMET in silico modelling: towards prediction paradise? Nature Rev Drug Discov 2003;2:192-204.
111. Horrobin DF. Modern biomedical research: an internally self-consistent universe with little contact with medical reality? Nature Rev Drug Discov 2003;2:151-4.
112. Ryan JF (Ed.). The pharmaceutical century. Ten decades of drug discovery. Washington, DC: American Chemical Society; 2000.
113. Wermuth CG (Ed.). The practice of medicinal chemistry. 2nd ed. London: Academic Press; 2003.

Lecture

COMPUTATIONAL EXPLORATIONS OF THE PROPERTY SPACE OF BIOMOLECULES

Bernard Testa (a), Giulio Vistoli (b), Alessandro Pedretti (b), Andrzej J. Bojarski (c), Mateusz Nowak (c)
(a) Pharmacy Dept, University Medical Centre, Lausanne-CHUV, Switzerland
(b) Institute of Pharmaceutical Chemistry, University of Milan, Milan, Italy
(c) Institute of Pharmacology, Polish Academy of Sciences, Krakow, Poland

Introduction

The objective of this paper is to take a global view on molecular structure and to examine how it relates to the biological activity of drugs and other bioactive compounds. The central concept in approaching molecular structure is that of *property space*, namely the ensemble of all distinct states a molecule can exist in. While the concept of conformational space is a well-known one, little has been done to date to explore molecular properties encoding recognition forces (e.g., lipophilicity) and their dependence on conformation. The molecule of the neurotransmitter *acetylcholine* will be used as an example to explore its property space, namely the range of values taken by conformation-dependent properties such as dipole moment and lipophilicity. Furthermore, the conformational space of molecules is well known to be strongly influenced by their molecular environment, as are the dynamics of intramolecular motions. What we have begun to investigate is how constraints on property space mirror constraints on conformational space, as illustrated here.

Other, more drastic constraints are seen when comparing the behaviour of side-chains in amino acids and protein residues. Work in progress with the protein *profilin Ib* will be presented, showing that such constraints generate information as quantified by a decrease in Shannon entropy. It is hypothesized that both backbone and side-chains, by virtue of being conformationally constrained, contribute to the protein's recognition specificity toward other macromolecules and ligands.

The concept of molecular structure

The description of molecules may be approached by considering form, function and fluctuation (1, 2). Molecular *form* ("what a molecule is") can be equated with molecular geometry, namely atom connectivity (2D-structure) and more realistically the 3D-structure. Components of molecular form are called structural attributes. Molecular *function* ("what a molecule does") is interpretable from experimental observations and is expressed as measurable or computable properties. Structure and properties (i.e. form and function) influence each other and are undissociably intertwined. The third component in this approach is molecular dynamics, namely the *fluctuation* in form and function (3).

Form, function and fluctuation cannot be ordered causally or hierarchically. Rather, they are viewed as being of equal importance and feeding on each other, as schematized in Figure 1: a

chemical compound can exist in a number of molecular states differing in conformation, surface area and volume, H-bonding capacity, polarity, lipophilicity, etc. Fluctuation influences form. To give an example, consider how in some compounds a labile hydrogen can jump from one position to another. This changes the atom connectivity (2D-geometry) of the molecule, which experiences a prototropic equilibrium and thus fluctuates between two or more states known as tautomers. Similarly, the 3D-geometry of a molecule can vary markedly depending on its flexibility, resulting in stereoisomers separated by low-energy barriers and well-known to chemists as conformers (conformational isomers). While tautomerism is restricted to a relatively limited number of compounds and involves two (seldom three) tautomeric states, conformational isomerism is a phenomenon of very frequent occurrence that produces a great many (an infinity depending on definition) conformational states. The ensemble of these states defines the conformational space, also known as the conformational hypersurface of a compound.

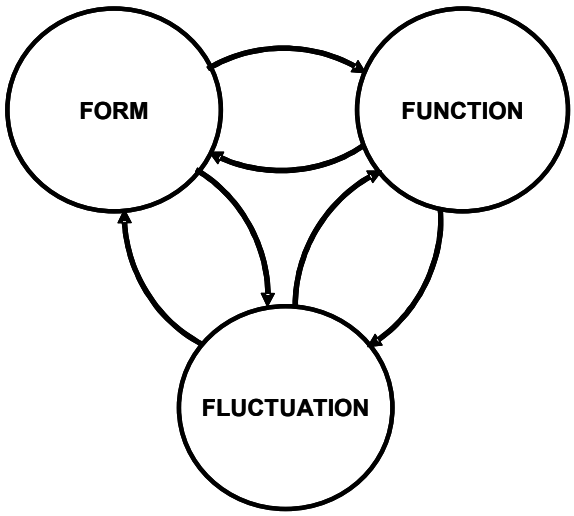

Figure 1. A comprehensive representation of molecular structure in the broadest sense, viewing form, function and fluctuation as its three essential components

Form influences fluctuation. This is a rather trivial statement considering that the capacity of a molecule to oscillate between, e.g., tautomeric or conformational states is entirely pre-determined by its chemical constitution. This makes it clear that form and fluctuation are interdependent and influence each other, in complete similarity with the interdependence between form and function.

Function and fluctuation also influence each other. This is a conclusion that derives logically from the above statements, and which can easily be seen in chemical examples. That tautomers display different chemical properties is again well know to chemists. Similarly, it is common chemical knowledge that electronic properties (e.g. ionization state) will influence conformational behavior.

Molecular states and property space

Molecular fluctuation delineates the ensemble of all probabilistic changes a molecule can undergo in form and function. This generates a very large number of *molecular states*, which are snapshots of the molecule at a given moment in time. Each state is characterized by a unique combination of geometry (form) and associated properties (function). Reciprocally, any property exhibited by a compound will thus have a distinct value for each molecular state occupied by that compound.

The ensemble of all possible states will span a range of values for all properties, thus delineating a *property space*. The latter can also be conceived as the basin of attraction of the property states of a compound. The concept of a basin of attraction can be schematized in pictorial language as shown in Figure 2. A physically more realistic representation of a basin of attraction of all molecular states is afforded by an *energy landscape*, namely a hypersurface whose dimensions are the energy of the system, plus all its other variables (2). Usually, and this is the convention also adopted here, the more probable states of a molecule (i.e., its states of lowest energy) are represented as valleys in the energy landscape, whereas the states of highest energy are represented by peaks and the transition states as mountain passes. There is an energy maximum beyond which the molecule breaks down and ceases to exist, explaining why an energy landscape is finite. A schematic representation of an energy landscape will be shown later (see Figure 4 below). Note that any complex system could *a priori* be represented by an energy landscape, but the hyperdimensionality increases incommensurably for systems of higher complexity.

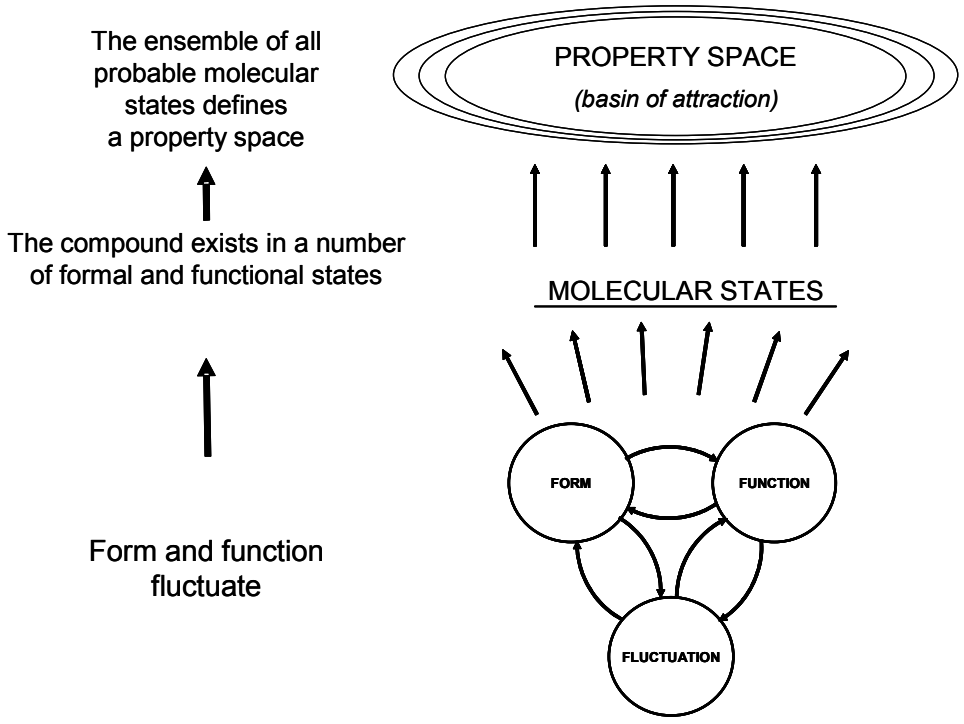

Figure 2. Molecular states are the expression of the mutual interdependence of form, function and fluctuation. The ensemble of all molecular states of a compound defines its property space, namely the range of values each property can span

A molecular property of great biological relevance is *lipophilicity*, namely the preferential affinity of a solute for lipid-like over water-like solvents. This property is commonly measured, but it can also be reliably computed from 2D- and 3D-structures (4). In particular, an algorithm known as the Molecular Lipophilicity Potential (MLP) calculates a virtual lipophilicity for each conformer. The results have revealed large differences between the various conformational states of a compound, up to one order of magnitude or even more (5). This phenomenon, which is particularly marked for large molecules such as various drugs and biomolecules containing both hydrophilic and hydrophobic groups (6), has been termed the chameleonic effect (7). It follows from the above that one way to rank all molecular states of a compound is along an axis of polarity, as will be done below in Figure 4.

Solvent constraints on the property space of solutes

As schematized in Figure 3, the molecule and its environment influence each other. At the macroscopic level, it can be stated that a compound modifies the medium with which it is in contact, as seen for example with changes in physical properties of a solution relative to the pure solvent, a modified fluidity in a membrane, or an allosteric effect in a protein.

But the medium also influences the compound. For example, a solvent will influence the electronic properties of the solute, which may exhibit changes in its color and UV spectrum. Similarly, the conformational behavior of the solute is markedly affected by the medium.

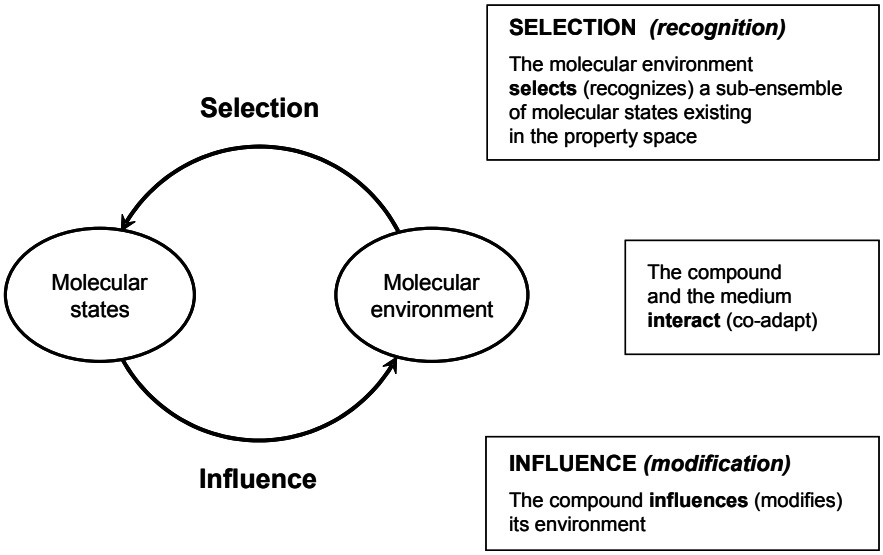

Figure 3. The complex system formed by a chemical compound and its environment results from two types of interactions between its components. The molecular environment selects a sub-ensemble of molecular states in the compound, whereas the latter modifies its environment

In the perspective of Figure 3, the molecule and its environment *co-adapt* to each other within their property space, a phenomenon that can also be viewed as a reversible co-evolution. In this writing, we focus essentially on the influence of the medium on the compound it engulfes. As shown below, this influence involves selection by the environment of a fraction of

the property space accessible to the molecule. Such restrictions in property space have been termed *dissolvence*, being considered as the counterpart of emergence (8).

Figure 3 not only schematizes the transactions between a molecule and its environment, it also raises the question of the intensity of their mutual adaptation. A precise answer appears impossible, but the wealth of available experimental evidence ascertains a qualitative trend. Indeed, the degree of mutual adaptation between a compound and its environment depends mostly on the degree of organization of the latter. Here, we examine the case of a solvent, i.e. a medium with a low degree of organization. Biological media, which are characterized by a relatively high (membranes) or even an extremely highly (functional proteins) degree of organization will be discussed below.

Solvents have a rather high degree of macroscopic (apparent) order, but at the molecular level large random movements and fluctuations take place. The degree of mutual adaptation between solute and solvent will be comparatively low. The solute will have some influence on the solvent, e.g. by local alterations of its structure (e.g. the hydrophobic effect), and by altering slightly some colligative properties such as its freezing point, boiling point, vapor pressure and viscosity. As for the solvent, it usually has a marked influence on the properties of the solute. What is clearly revealed by experimental and computational investigations, for example, is the effect of the solvent on the conformational behavior of the solute, resulting in the selection of some among all the possible molecular states (9, 10).

The hypothesis we wish to explore here is whether polar (hydrophilic) solvents tend to favor the more polar conformations and states, whereas the less polar (lipophilic) solvent will favor less polar conformations and states. In short, can one of the most basic rules in chemistry, *similia similibus solvuntur* (like dissolves like) be expanded to become "like selects like"?

The experimental rule "like selects like" can be depicted by Figure 4, which shows the property space of a hypothetical compound.

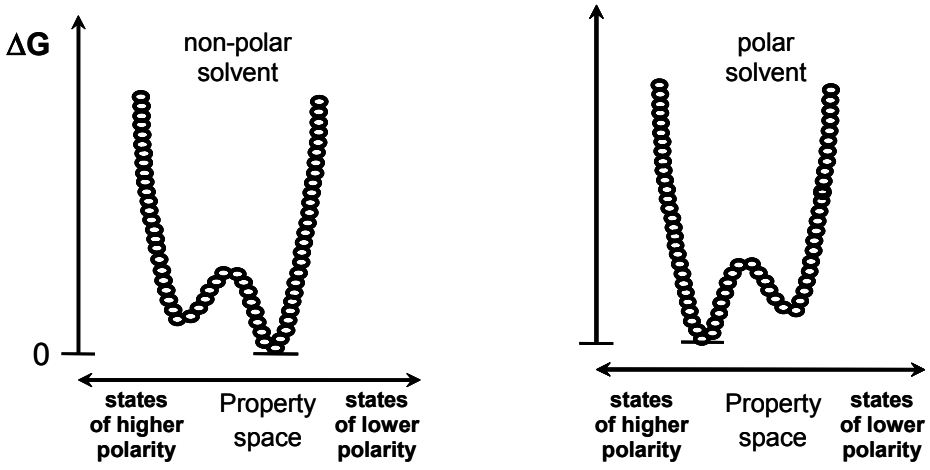

Figure 4. This figure shows the property space of a hypothetical compound as influenced by the molecular environment

Each recognizable state of the molecule is represented by a small circle whose position is defined by its relative energy (ordinate axis) and its relative polarity. In this representation, the property space is condensed to an axis of polarity. The compound is taken to have two low-energy states, with the lest polar being favored in an on-polar solvent. In a polar solvent,

however, "like selects like" and the more polar conformer is preferred. In other words, the property space is reduced to and represented by an axis of polarity. The compound is postulated to have two low-energy states, with the less polar being favored in a non-polar solvent. In a polar solvent, however, "like selects like" and the more polar conformer is preferred.

The property space of acetylcholine

While solvent-dependent conformational equilibria have been extensively investigated, medium-dependent constraints on the hypothetical lipophilicity space remain unexplored. Yet such constraints should not be without influence on the behavior of compounds in biological systems, e.g. when they permeate membranes or bind to biological targets such as enzymes and receptors.

Acetylcholine (Figure 5) was chosen as the object of study given its major biological significance, and the many data (experimental and computational) accumulated on its conformational behavior. Acetylcholine, despite its small MW, has also an interesting molecular structure characterized by a great flexibility and the presence of polar and non-polar groups. In our study, the small size of acetylcholine was both an advantage (since molecular dynamics simulations were very time-effective) and a limitation (since it was obvious at study design that the property space of such a small molecule must be quite limited).

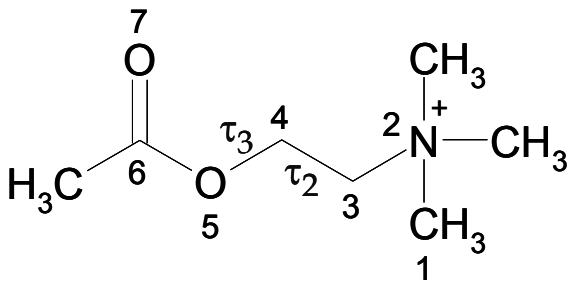

Figure 5. The structure of acetylcholine, with the dihedral angles
τ_1 = C1-N2-C3-C4, τ_2 = N2-C3-C4-O5, τ_3 = C3-C4-O5-C6, τ_4 = C4-O5-C6-O7

Molecular Dynamics (MD) simulations were used to explore the conformational space of acetylcholine in the vacuum, in chloroform and water (11, 12), in water-saturated 1-octanol and in a membrane model (13). A number of geometric and physicochemical properties were calculated for each conformer. The geometric properties were the dihedral angles τ_2 and τ_3 and the distance between $\underline{N}^+$ and (O)$\underline{C}H_3$. The physicochemical properties included lipophilicity (log P), dipole moment, Polar Surface Area (PSA) and Solvent Accessible Surface (SAS), that is a mixed structural and physicochemical property.

In agreement with literature data, it was found that $\tau 1$ and $\tau 4$ vary in a narrow range and independently of the conditions ($\tau_1 = 60° \pm 20°$; and $\tau_4 = 0° \pm 20°$), due to the symmetry of the triple rotor $\tau 1$ and to the rigidity of the ester group (τ_4). Our studies revealed seven low-energy conformational clusters labeled as **+gt**, **+g+g**, **t–g**, **t+g**, **tt**, **–g–g**, and **–gt** (**+g** = 30° to 90°, **t** = 150° to 210°, **–g** = 270° to 330°). The conformational distribution proved that $\tau 2$ was markedly dependent on the medium, whereas τ_3 was not. This is documented in Table 1, which reports the relative populations of the three main groups of conformational clusters. Clearly, the

conformers with τ_2 = trans are poorly populated in the vacuum presumably due to intramolecular attraction between the cationic head and the electron-rich oxygen. The proportion of conformers with τ_2 = trans is markedly increased in the solvents chloroform, water and octanol, with a corresponding increase in the conformers with τ_2 = gauche. In other words, solvent polarity does not appear to significantly affect the conformational preferences of acetylcholine.

Table 1. Populations in the 3 main groups of conformational clusters of acetylcholine

Medium	τ_2 = +g clusters (+gt and +g+g)	τ_2 = t clusters (t+g, t–g and tt)	τ_2 = –g clusters (–g–g and –gt)	Unclustered confor-mers (transition forms)
Vacuum	41%	6%	39%	14%
Chloroform	24%	20%	31%	25%
Water	28%	17%	29%	26%
1-Octanol	19%	23%	20%	38%
Membrane	66%	0.3%	31%	3%

In particular, the comparable increase of extended conformers in both water and chloroform seems just due to the physical presence of the solvent (namely friction and shielding effect) rather than to its specific physicochemical properties (i.e. polarity, H-bonding). This physical incidence also slows down all molecular movements as seen in the significant increase of transitional forms in water and chloroform, whose percentage appears proportional to the molecular weight of the solvent.

A different explanation could be considered when examining the noteworthy abundance of extended geometry in 1-octanol. Indeed when the size of solvent and solute become comparable (as for acetylcholine and 1-octanol) the solute tries to minimize the steric hindrance by mimicking the shape of solvent. On this ground the extended geometries are better able to mimic the classical zig-zag conformation of 1-octanol. Moreover, it must be remembered that the solvent used in the simulations was hydrated octanol rather than the pure solvent, i.e. a solvent formed from H-bonded aggregates of 4 molecules of octanol and one of water. In other words, acetylcholine can receive H-bonds only by competing with solvent molecules.

This modest conformational influence is to be contrasted with the behavior of acetylcholine in a membrane model, where strong constraints are seen (Table 1). Indeed, there are practically no conformers with τ_2 = trans, and the τ_2 = **+g** clusters are more populated than the τ_2 = **–g** clusters. In other words, some specific interactions occur between acetylcholine and phosphatidylcholine (the molecules of which the membrane is made of). Phosphatidylcholine being chiral, it is seen to be able to induce conformational enantiomerism in acetylcholine.

A second objective of our ongoing work is to investigate the influence of solvent on the property space of acetylcholine. Particular attention is being paid to dipole moment and lipophilicity as calculated by the MLP (Molecular Lipophilicity Potential) (4). These two properties vary over a broad range within the conformational space of acetylcholine, and they were highly intercorrelated in each MD simulation.

Figure 6 show histograms of the log P distribution the many acetylcholine conformers obtained in the simulations. Interestingly solvent influences can be seen. Thus, there is a clear shift toward more hydrophilic conformers when going from the vacuum to chloroform to water. The cases of octanol and the membrane deserve separate discussions. Indeed, the lipophilicity space of acetylcholine in octanol resembles that in water more than in chloroform despite octanol and chloroform being of comparatively low polarity.

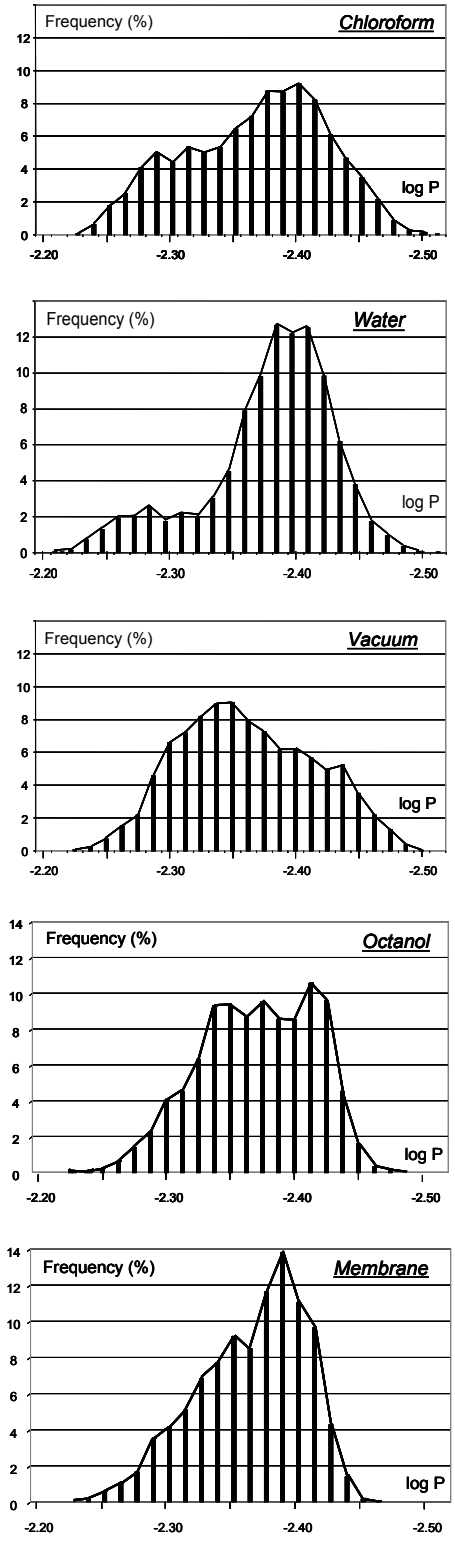

Figure 6. Histograms of the log P values of acetylcholine in a vacuum, in chloroform, in water (30 ns, 6000 conformers), as well as in octanol and in a membrane model (15 ns, 3000 conformers)

When analyzing the log P averages per conformational clusters – namely folded (**gg** and **gt**) and extended (**tg** and **tt**) geometries – one can note that the two averages in water are slightly more hydrophilic than in vacuo and that chloroform yields intermediate averages (Table 2).

Table 2. Property space parameters for virtual log P

Medium	log P average	log P range	log P average (folded forms)	log P average (extended forms)
Vacuum	–2.34	0.37	–2.34	–2.39
Chloroform	–2.36	0.34	–2.36	–2.40
Water	–2.41	0.33	–2.39	–2.42
1-Octanol	–2.39	0.30	–2.37	–2.38
Membrane	–2.38	0.29	–2.38	----

This means that the solvent is able to select the most suitable geometries for each conformational cluster. Considering the similar conformational profile obtained from MD simulations in the two isotropic solvents, we can conclude that the effects on property space predomine over effects on conformational space in order to obtimize the polarity of solute. This suggests that property space and conformational space are not fully correlated and that modifications in the two spaces can occur to different extents. This can happen because each conformational cluster can access a large portion of the property space. This hypothesis finds a convincing proof in the MD simulations in octanol. In this medium, acetylcholine shows the highest percentage of extended conformers in order to gain the abovementioned shape mimicry, but the extended geometries possess in octanol the highest log P average (compared to other solvents and also to the vacuum) in order to preserve an intermediate polarity of solute. This confirms that conformational space and property spaces are only partly interdependent and that a solute can adapt them in opposite ways.

An unexpected finding is that the lipophilicity space of acetylcholine in a membrane strongly resembles that in water despite major conformational differences in the two media (Table 1). In addition Table 2 reports that the folded geometries of acetylcholine in the membrane have an average log P quite identical to the corresponding average in water; this can be explained considering that the solute remains near the phospholipid heads during the simulation. It also suggests that the intermediate polarity of acetylcholine in membrane is totally due to the disappearance of extended conformers. Nevertheless Table 2 shows that the reduction of conformational space doesn't involve a significant decrease in log P range. Our preliminary conclusion is that a medium-dependent reduction in conformational space may not be paralleled by a comparable reduction in property space. The mechanism and significance of this behavior are being investigated.

Conformational constraints on the side-chain of protein residues, and the resulting increase in information content

Constraints imply decreased disorder and hence decreased entropy. And since information is a measure of order (14, 15), constraints imply an increase in information content, in other words an increase in the capacity to select from alternatives (16). We reasoned that good models to

approach this problem would be a comparison of the behavior of side-chains of amino acids in the free state and as residues in proteins. Indeed, the conformational behavior of side-chains (the so-called "Chi space", "χ space") is an important determinant of the surface and recognition properties of proteins (17). Preliminary studies using molecular dynamics simulations and analysis of 3D-molecular fields had shown that the property space of the central residue in tripeptides is indeed constrained compared to the free amino acid (9, 10).

In continuation of previous work (18), we present here new molecular dynamics simulations of profilin Ib, a contractile protein of *Acanthamoeba Castellanii* (Figure 7). This protein contains 125 residues (reference PDB-1ACF in the Protein Data Bank). A comparison of the conformational behavior of the side-chains in the residues and in the corresponding free amino acids revealed strong contraints. These constraints on conformational space were analyzed for their Shannon entropy content (19), which for most residues showed an intriguing reduction relative to the free amino acids.

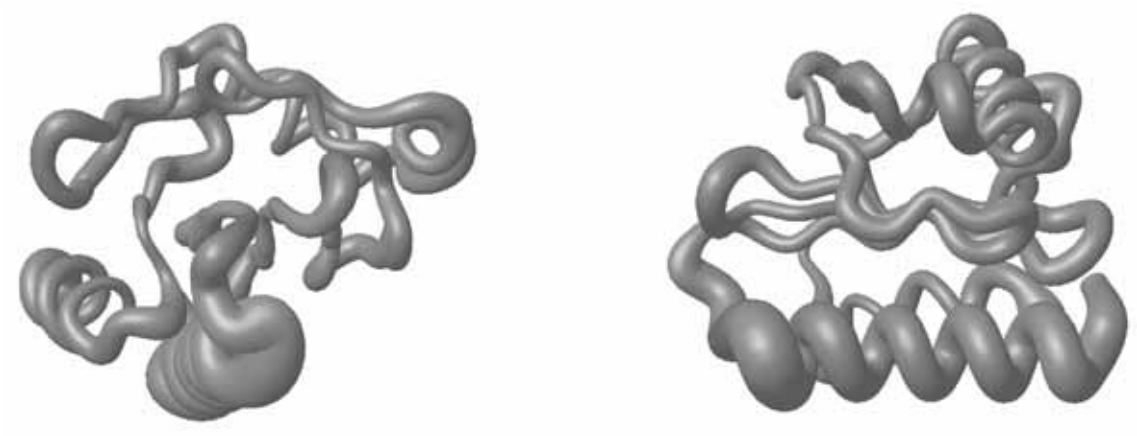

Figure 7. MOLMOL orthogonal views of the 3D-structure of the backbone of profilin Ib, with the backbone thickness being proportional to the amplitude of its movements during the simulation

The dihedral angles of all residue side-chains in profilin Ib were recorded each 5 picoseconds, yielding a 10 ns trajectory for each dihedral angle χ of each residue side-chain. The same was done for the side-chain of the corresponding free amino acids in zwitterionic form. A representative example is shown in Figure 8, where the trajectories of χ_1, χ_2 and χ_3 of the four glutamine residues in profilin Ib (Gln3, Gln18, Gln41 and Gln105) are compared to those of free glutamine. The differences are most impressive and quite revealing. Thus, the $\chi 1$ values of free Gln are clustered in the regions –60° to –90° and –150° to –180°. The same is true for Gln3, whereas the range is mainly –30° to –90° for Gln18 and Gln41, and –150° to –180° for Gln105. The differences are even more marked when comparing χ_2 values.

The occurrence of strong conformational constraints in the side-chains of profilin Ib having been shown, the next step was to quantify and interpret them. This was achieved by a Shannon entropy analysis of the conformational behavior of the side-chains. Shannon entropy is a measure of the relative information content of a dataset (Figure 9), and it allows the information content of two datasets to be compared (19). Thus, SE(2) < SE(1) means that dataset 2 contains more information than dataset 1.

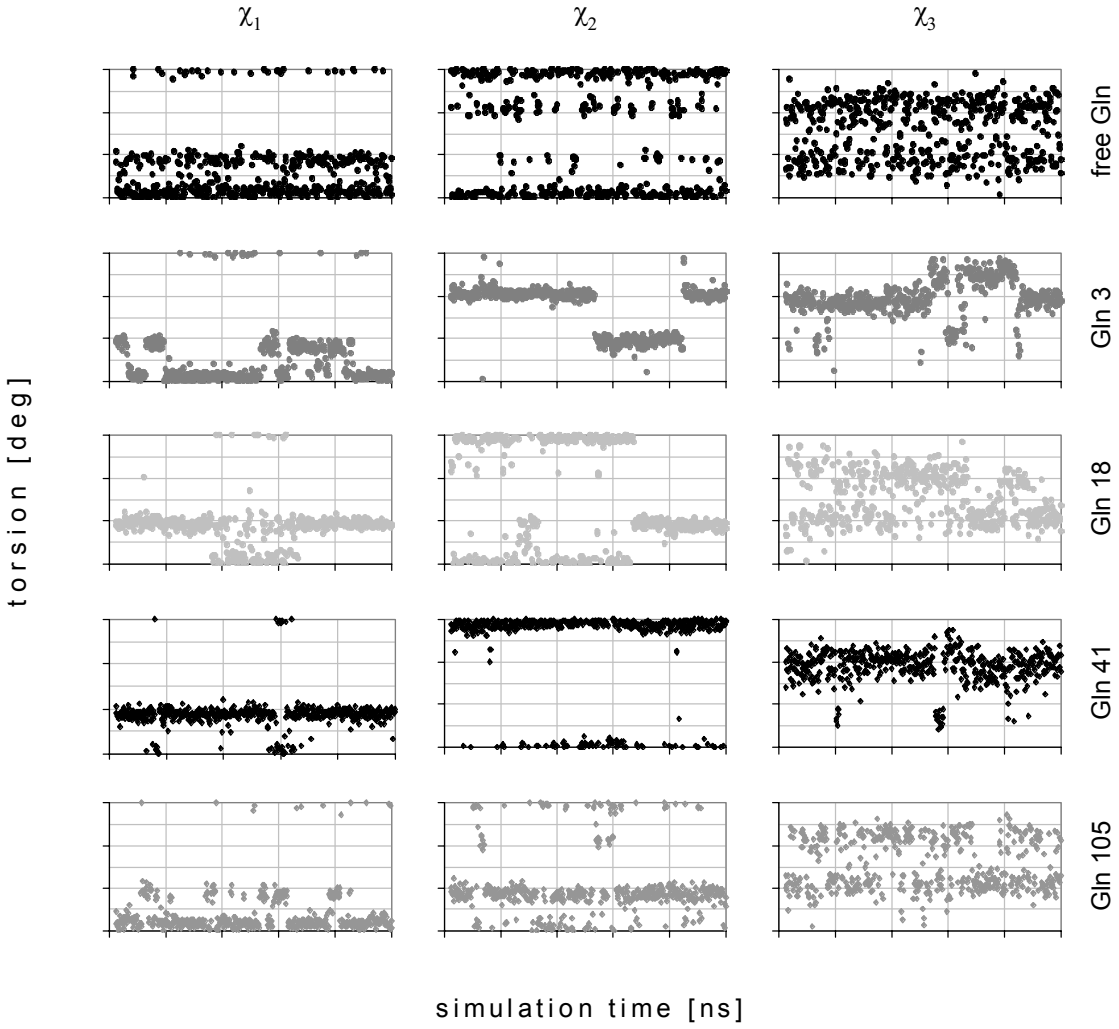

Figure 8. Trajectories of χ_1, χ_2 and χ_3 in the side-chain of free glutamine, Gln3, Gln18, Gln41 and Gln105

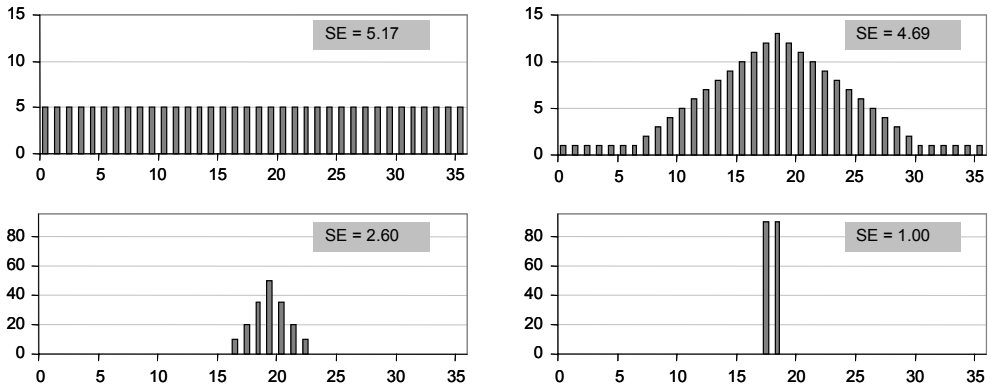

Figure 9. Calculation of Shannon entropy (SE) values, as illustrated here for a hypothetical example with 36 bins

The values of χ_1, χ_2, χ_i of side-chains (except methyl rotors) were distributed in bins of 10°. This allowed the Shannon entropy (SE[χ_i]) to be calculated for each dihedral angle in the free amino acids and in the residues of profilin Ib. A higher conformational constraint on a residue compared to the free amino acid results in a lower SE, and thus a negative ΔSE[χ_i] (defined as SE[χ_i] in residue minus SE[χ_i]), itself synonymous with a greater information content. The results for all side-chains are presented in Figure 10 as a ΔSE[χ_1] versus ΔSE[χ_2] plot. Of the 88 χ_1 and 76 χ_2 (valines excluded) dihedral angles, the majority are located in the lower left (negative-negative) quadrant, with ΔSE[χ_1] and ΔSE[χ_2] values ranging from 0 to –2.3.

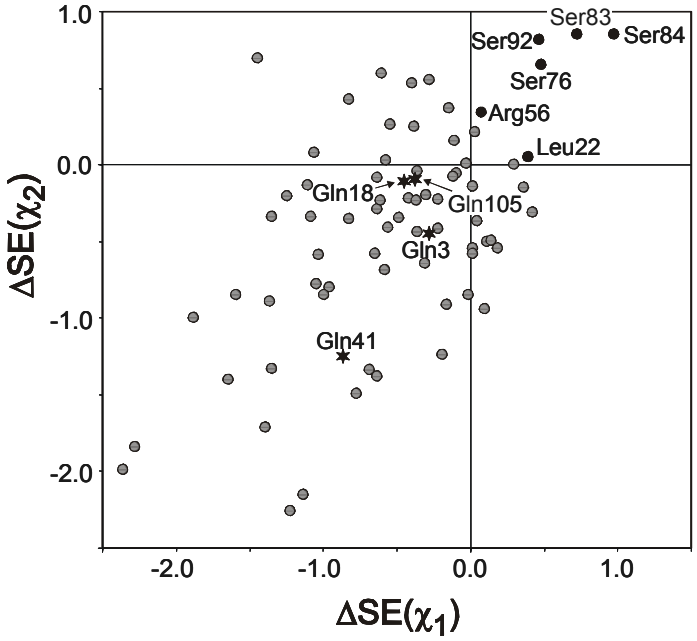

Figure 10. Plot of ΔSE[χ_1] versus ΔSE[χ_2], where ΔSE[χ_i] = SE[χ_i] in residue minus SE[χ_i] in free amino acid

Only nine residues had clearly positive ΔSE[χ_1] values (i.e., ΔSE[χ_1] > 0.2), and only fifteen had clearly positive ΔSE[χ_2] values. Only six residues occupy the upper right quadrant, namely Leu22, Arg56, Ser76, Ser83, Ser84 and Ser92, having ΔSE[χ_i] values between 0 and +1.0. In a free serine, the hydroxy group is H-bonded to the protonated amino group (results not shown), a conformational constraint that is partly removed in serine residues.

The four Gln residues whose behavior has been shown in Figure 8 are highlighted in Figure 10, revealing Gln41 to be the most constrained among the glutamine residues. A majority of residues are located in the lower left quadrant, with ΔSE[χ_1] and ΔSE[χ_2] values ranging from 0 to –2.3. Hence residues in profilin Ib have generally a markedly lower Shannon entropy content in their side-chain than the corresponding amino acids in the free state.

In contrast to χ_1 and χ_2, the results for the few residues having χ_3 and χ_4 dihedral angles were unremarkable, the ΔSE[χ_i] values being modest and without pattern (results not shown). These molecular dynamics simulations demonstrate and quantify the strong conformational constraints felt by residue side-chains in a protein, when compared to the corresponding amino acids in the free state. In profilin Ib, these constraints involve mainly the first two dihedral

angles (χ_1 and χ_2) of the side-chains, with the unpredictable and remarkable consequence that the information content of these side-chains as assessed by Shannon's entropy is markedly affected when comparing residues and free amino acids. In most cases, an important decrease in Shannon's entropy was seen. Given the inverse proportionality between Shannon entropy and information, this is equivalent to stating that most side-chains in residues showed an increase in information content compared to the free amino acids.

But what are the practical implications of the interrelated conformational constraints and information content? We postulate that the increased information content of the side-chain of residues compared to free amino acids contributes to the protein's recognition specificity. In other words, the vastly increased information content of a protein relative to its free monomers is embedded not only in the tertiary structure of its backbone, but also in its side-chains. The implication is that both backbone and side-chains, by virtue of being conformationally constrained, contribute to the protein's recognition specificity toward other macromolecules and ligands, as cogently advocated by Loewenstein (14).

References

1. Testa B, Kier LB. The concept of molecular structure in structure-activity relationship studies and drug design. Med Res Rev 1991;11:35-48.
2. Testa B, Kier LB, Carrupt PA. A systems approach to molecular structure, intermolecular recognition, and emergence-dissolvence in medicinal research. Med Res Rev 1997;17:303-26.
3. Prigogine I, Zeit. Struktur und Fluktuationen (Nobel Lecture). Angew Chem 1978;90:704-15.
4. Carrupt PA, Testa B., Gaillard P. Computational approaches to lipophilicity: methods and applications. In: Lipkowitz KB, Boyd DB (Ed.). Reviews in computational chemistry. Vol. 11. New York: Wiley-VCH; 1997. p. 241-315.
5. Testa B, Carrupt PA, Gaillard P, Billois F, Weber P. Lipophilicity in molecular modeling. Pharm Res 1996;13:335-43.
6. Jiang, XK. Hydrophobic-lipophilic interactions. Aggregation and self-coiling of organic molecules. Acc Chem Res 1988;21:362-7.
7. Carrupt PA, Testa B, Bechalany A, Tayar NE, Descas P. Perrissoud D. Morphine-6-glucuronide and morphine-3-glucuronide as molecular chameleons with unexpected lipophilicity. J Med Chem 1991;34:1272-5.
8. Testa B, Kier LB. Emergence and dissolvence in the self-organization of complex systems. Entropy 2000;2:1-25.
9. Testa B, Bojarski A. Molecules as complex adaptative systems. Constrained molecular properties and their biochemical significance. Eur J Pharm. Sci 2000;11:S3-S14.
10. Testa B, Raynaud I, Kier LB. What differenciates free amino acids and amino acyl residues ? An exploration of conformational and lipophilicity spaces. Helv Chim Acta 1999;82:657-65.
11. Vistoli G, Pedretti A, Villa L. Testa B. The solute-solvent system: Solvent constraints on the conformational dynamics of acetylcholine. J Am Chem Soc 2002;124:7472-80.
12. Vistoli G, Pedretti A, Villa L, Testa B. Solvent constraints on the property space of acetylcholine. I. Isotropic solvents. J Med Chem 2005; in press.
13. Vistoli G, Pedretti A, Villa L, Testa B, Solvent constraints on the property space of acetylcholine. II. Octanol and a membrane model 2005; Submitted.
14. Loewenstein WR. The touchstone of life. Molecular information, cell communication and the foundation of life. London: Penguin; 2000.

15. Fleissner P, Hofkirchner W. Emergent information - Towards a unified information theory. Biosystems 1996;38:243-8.
16. Gell-Mann M. The quark and the jaguar. London: Abacus; 1995.
17. Hruby VJ, Li G, Haskell-Luevano C, Shenderovich M. Design of peptides, proteins and peptidomimetics in Chi space. Biopolymers 1997;43:219-66.
18. Bojarski AJ, Nowak M, Testa B. Conformational constraints on side chains in protein residues increase their information content. Cell Mol Life Sci 2003;60:2526-31.
19. Shannon C. A Mathematical theory of communication. The Bell System Technical Journal 1948;27:379-423 + 623-56.

Short communication

A STOCHASTIC AND COMPUTATIONAL METHOD FOR ESTIMATING THE FOLDING RATES OF WILD TYPE AND MUTANT PROTEINS

Mario Compiani (a,c), Emidio Capriotti (c), Rita Casadio (b,c)
(a) Dept. Chemical Sciences, University of Camerino, Camerino, Italy
(b) Dept. Biology, University of Bologna, Bologna, Italy
(c) CIRB, Centro Interdipartimentale di Ricerche Biotecnologiche, University of Bologna, Bologna, Italy

Introduction

Finding simplified but informative models of protein folding is a major challenge facing theoreticians that are trying to manage the complexity of biomolecules.

Such models are expected to possess the following major requisites: (a) sufficient specificity for sequence details without using representations at atomic level which are too demanding even for computer assisted investigations; (b) capability to describe dynamical events on time scales comparable with the folding time of the protein.

The Foldon Diffusion Collision model (FDC model) (1, 2) meets these requisites since it focuses on the minimal determinants of folding (foldons) and is an effective tool for calculating the kinetics of folding of helical proteins. This paper aims at summarizing the notable properties of the FDC model. We start by outlining the FDC model and the common properties of proteins that provide the physical underpinning for it. We then summarize the main results obtained applying the FDC model to helical proteins and finally comment on its meaning for the general theory of protein folding.

Epitome of the FDC model and its applications

Much of the inherent complexity of the folding process comes from the frustrated character of proteins (3) and the large number of their degrees of freedom. Frustration is the impossibility of optimizing simultaneously the numerous interactions that are dictated on each residue by the native structure of the protein. Trying to remedy this difficulty a stream of research has focused on minimalist descriptions that draw on simplified models of proteins (4-6). Alternatively, one makes use of reductionistic strategies that provide hierarchical pictures of protein folding (7-11).

A key development in the study of the dynamics of protein folding has been marked by the transition from the "pathway perspective'' to the "landscape perspective'' (3, 11). The very essence of the new view is that the process of folding is characterized by multiple and widely different paths running on a funnel-shaped landscape whose basic characteristics are summarized in the minimal frustration requirement (3). This has two basic implications. First, it ensures the existence of a unique and globally stable native state that corresponds to the dominant attractor of the protein viewed as a dynamical system. Secondly, it explains the presence of an energetic bias of the free energy surface that lets different trajectories converge

in a finite time onto the native state. The interpretation of the minimal frustration requirement given in (1) leads to hypothesize the existence of regions of the chain where the constraints imposed by global and local interactions are not in conflict.

The link between minimally frustrated segments and the kinetics of folding has come out of the area of protein structure prediction with neural networks (1). The fundamental finding is that in all-alpha proteins some pieces of information as to the early stages of folding can be extracted from the native structure of the protein under study. In particular, we have illustrated (1) a method to detect minimally frustrated segments with helical structure and have shown that they correspond to the Initiation Sites (IS) of folding.

Here we refer to these segments (or alternatively to their helical structure, depending on the context) as the foldons. Antecedents in the literature for this terminology are found in Refs. (12, 13).

We have argued (1) that foldons comprising contiguous stretches of the sequence with helical structure are stabilized predominantly by local (or short-range) interactions, i.e. interactions that occur between residues that occupy close positions in sequence. Consequently, they are likely to be the precursors of the foldon-containing alpha-helices (IS helices, for brevity) and can be therefore assumed to coincide with the nucleation sites of the IS helices (14).

In (2) we have shown that the coil-to-helix transitions taking place in the IS helices share the same thermodynamic properties of the analogous transitions that occur in the same peptides, as they are isolated from the protein. This implies that the local properties of the IS helices rule the early stages of folding. In (2) we argued that the foldons dictate also the kinetics of the whole folding process. The physical basis for this statement is the general fact that proteins, like all complex systems (15), are characterized by multiscale dynamics. Thus we take advantage of the separation of time scales to simplify the overall picture of the system in that we adopt a more aggregate (usually equilibrium) description of the fast processes and a more detailed (stochastic) treatment of the slow variables (15).

Consistent with the multiscale hypothesis, we exploit the notions of hierarchical dynamics and minimal frustration to reconstruct the salient steps of the folding process by using the minimum possible information from few selected regions of the sequence. We implement the hierarchical organization of folding by splitting the overall dynamics in local fast dynamics and global slow dynamics that are governed, respectively, by short-range (intra-helical) interactions and long-range (inter-helical) interactions. The fast dynamics pertain to the nucleation and elongation of the IS helices. The slow dynamics describe the formation of the tertiary structure via progressive aggregation of the IS helices, as it occurs in the later stages of folding. To integrate the simultaneous fast and slow dynamics in a unified model, we adopt a hybrid strategy. The ensuing model involves the innovative use of neural networks, to locate the foldons and depict the fast dynamics of the fluctuating IS helices, and a stochastic description to account for their slow diffusional motions (15, 16).

The FDC model is inspired by a modular view of folding which envisages that the process is initiated by the fast formation of foldons in the IS helices of the chain (1, 2). Accordingly, the first task to be achieved is the location of the foldons within the protein under study. Following the procedure illustrated in (1) we use a standard feed-forward artificial neural network that is trained to predict alpha-helices of proteins starting from the bare sequence. Thus we adopt the simplest partition of the space of structural classes in alpha and non-alpha structures (or coil for brevity). For any residue being classified the output of the network can be viewed as a discrete probability function defined in the space of structures. Consequently, we can associate the Shannon information entropy with any of such probability distributions. The set of the entropy values along the protein sequence is used to draw an information entropy profile that has been

shown to be equivalent to a measure of frustration (17). The entropy plot is useful to localize the foldons of the protein in correspondence of the minima of the entropy profile.

To account for the average features of the fast dynamics we choose a thermodynamic approach which is applied to the formation of the IS helices. This involves again the entropy plot that is used to extract the pieces of information contained in the native structure to characterize thermodynamically the fast formation of the IS helices. Specifically, the depth and the slope of the entropy minimum allow us to estimate the average stability for an IS helix that fluctuates in length around its average size (2).

The subsequent slow stage of folding comprises the diffusional process that mimics the formation of the tertiary structure. A suitable framework for describing this step is provided by the diffusion-collision model of protein folding (18, 19, 20) (henceforth referred to as the DC model). Following the DC model, we depict the folding process as a sequel of stochastic events where preformed building blocks (microdomains) undergoing Brownian dynamics collide and coalesce. This results in the formation of aggregates of increasing complexity and, eventually, in the stabilization of the native structure. Inherent in this model is a rigid hierarchical view of folding (20). Unlike the original version of the DC model (in which microdomains are identified with the native alpha-helices) we posit that the IS helices with average length are eligible for the role of microdomains.

According to the stochastic treatment the folding time is estimated by the mean first passage time for the formation of the aggregate of highest order, which gathers all the available microdomains. The FDC model has been successfully applied to two-state proteins and we refer the reader to (2) for the detailed presentation of the results.

Rather we turn to the application of the FDC model to the mutants of an intensively studied proteins, the lambda-repressor (1LMB4). The principal goal is to assess the sensitivity of the FDC model to the smallest possible variations in the sequence of the protein (point mutations).

The folding processes of the eight mutants of the lambda-repressor examined in (21) have been modelled with the FDC model. The basic mutant (G46A/G48A) has two point mutations (glycine to alanine) in position 46 and 48. The other seven mutants have undergone a further change (alanine to glycine) in position 15, 20, 37, 49, 63, 66 and 81 respectively. The wild type protein has five helices which, with the exception of helices 2 and 3, do contain a foldon each. The most meaningful results concern the basic mutant and M81. The entropy plot of the basic mutant reveals that helix 3 becomes an IS helix since, as a result of the mutation, the local entropy minimum around residue 48 within helix 3 is thermodynamically stabilized. This signals the birth of a new microdomain which participates in the folding dynamics. The point mutation in the M81 variant has a specular effect since it leads to the deletion of the foldon of helix 5 by destabilizing the helical region around residue 81. The folding rates of the wild type and all the mutants (apart from M66) are predicted with remarkable accuracy by the FDC model (forthcoming paper). The failure to reproduce the rate of M66 stresses the inherent limitations of the present version of the FDC model which underestimates the long range interactions linking the coalesced microdomains. M66 is a typical case where such an approximation is not acceptable since residue 66 affected by the mutation results to be subject to a very strong intramolecular interaction with residue 15 (22).

Discussion

The notable effectivity of the FDC model means that the present approach permits to deduce the kinetic features of helical proteins by relying almost exclusively on sequence information. In this respect it amounts to take a further step toward extending the scope of Anfinsen's

thermodynamic hypothesis (23) (the determinants of the native structure are comprised in the protein sequence) to the province of kinetics (sequence determines the kinetics of folding altogether).

The accurate estimates of the folding rates provided by the FDC model suggest also some notable implications for the general theory of protein folding. In general it has been recognised that the delicate balance of local and non local interactions is crucial in fixing the actual course of folding (24). A recent discussion (25) has made the point that such a balance determines which alternative picture, the DC model or the nucleation-condensation mechanism (NC, for brevity), might be the most appropriate to capture the essence of folding. Let us remind that differently from the DC model (elements of secondary structure precede the collapse), the NC scheme assumes that a collapsed compact conformation and secondary structure elements are formed simultaneously. The two mechanisms are revisited in the general context of the extended nucleus theory (EN theory) (25). In this framework they are considered as the extreme cases of a whole range of possible models, differing for the amount of secondary structure formed in the pre-collapse stages, with secondary structures inherently more stable in the DC model.

The FDC model conforms to the EN theory in that it individuates the mixture of specific secondary and tertiary interactions (25) that are essential for the formation of the rate limiting structure (extended nucleus) in the transition state of the process. The said interactions are those being stabilized within the IS helices and among the IS helices during the fast and the slow stages of the folding process.

The emphasis on the foldons as the essential determinants of the FDC mechanism is a major advancement with respect to previous implementations of the DC model in which all of the helices were included in the computational scheme (18-21). In contrast, our criterion for the identification of foldons is more selective and focuses on a subset of the helical regions of the protein. Therefore, the FDC scenario represents a significant progress toward the definition of the minimal set of the determinants of the folding process. The case of cytochrome c (1HRC) is quite illuminating as to how far such a reduction of the relevant variables can be pushed. As a matter of fact 1HRC has five native helices and only two foldons (2).

The remarkable sensitivity of our model to sequence-specific features can be appreciated if we compare our results with the calculations carried out in (21) on the same set of proteins (1LMB4 and its mutants). The method proposed in (21) is less sensitive than the FDC model to the modulation of the folding times induced by the point mutations. The results obtained in (21) have correlation 0.56 with the experimental values, whereas our results have correlation 0.67. Notably, both the method of (21) and ours fail to reproduce the sensible change of the folding rate exhibited by the M66 mutant. In the case we exclude this unfavorable result, the efficiency gap between our model (correlation 0.98) and (21) (correlation 0.82) further increases.

The FDC model is also useful to provide us with a mechanistic explanation for the noteworthy reduction in the folding time on passing from the wild type to the basic mutant of 1LMB4. The physical ground for this effect hinges on the substantial change in the foldon topology due to the appearance of a new foldon in the region that is affected by the mutation (helix 3 of the basic mutant). The primary importance of topology was pointed out in (26, 27). In full agreement with the FDC model, the detailed analysis of the kinetics of the basic mutant (28) suggested that the early formation and the increased stability of helix 3 is likely to speed up the folding process. This effect is consistent with the general notion that enhanced propensities for local structures may increase the folding rate (29, 30). The opposite effect is expected in the case of M81. This is actually the result predicted by the FDC model although, in agreement with experiments, the decrease in the folding rate is more modest. The reason for this is that a second factor (stability) comes into play in determining the folding rate of proteins (26, 27). In keeping with this finding the deleted foldon in the M81 mutant causes a smaller change in stability than

the newly formed foldon in the basic mutant. In any case the FDC model follows effectively the changes in the folding rate (be they small or large) of the above mentioned mutants of 1LMB4. Quite interestingly, mutations affecting non foldon regions are usually conducive to moderate kinetic effects (our forthcoming paper). The general conclusion is that foldons are the critical targets for mutations that are intended to affect the kinetics of the folding process. Foldons can be likened to the accelerator pedals of the protein in that mutation in these regions are likely to elicit the maximal effect. The 1LMB4 case study shows that the most remarkable effects are due to the death or the birth of foldons.

A further essential feature of the FDC model is its versatility which is well illustrated by the successful description of different folding mechanisms (two-state and three-state mechanisms) (A. Stizza, E. Capriotti and M. Compiani, submitted). This is a hint that the FDC model is a good candidate for the role of unifying picture of the folding of helical proteins, whose main properties were discussed in the recent literature (25, 31, 32). Also, the physical insight afforded by the FDC model turns out to be useful in arguing that the model is capable of describing cooperative as well as hierarchical folding mechanisms. Finally, the FDC model suggests a straightforward way of quantifying the cooperativity (or modularity) of the folding process of helical proteins (M. Compiani, in preparation). This may be a non trivial supplement to the informational content of protein interaction maps. As a matter of fact, modularity or cooperativity features of the folding process may be crucial in determining the number and properties of the interactions of individual proteins with the cellular machinery.

References

1. Compiani M, Fariselli P, Martelli P-L. Casadio R. An entropy criterion to detect minimally frustrated intermediates in native proteins. Proc Natl Acad Sci USA 1998;95:9290-4.
2. Compiani M, Capriotti E, Casadio R. Dynamics of the minimally frustrated helices determine the hierarchical folding of small helical proteins. Phys Rev E 2004;69:051905(1-8).
3. Bryngelson JD, Onuchic JN, Socci ND, Wolynes PG. Funnels, pathways and the energy landscape of protein folding: a synthesis. Proteins: Struct Funct Genet 1995;21:167-95.
4. Alm E, Baker D. Prediction of protein folding mechanisms from free-energies derived from native structures. Proc Natl Acad Sci USA 1999;96:11305-10.
5. Muñoz V, Eaton WA. A simple model for calculating the kinetics of protein folding from three-dimensional structures. Proc Natl Acad Sci USA 1999;96:11311-6.
6. Plaxco KW, Riddle DS, Grantcharova V, Baker D. Simplified proteins: minimalist solutions to the protein folding problem. Curr Opin Struct Biol 1998;8:80-5.
7. Lesk AM, Rose GD. Folding units in globular proteins. Proc Natl Acad Sci USA 1981;78:4304-8.
8. Panchenko A, Luthey-Schulten Z, Wolynes PG. Foldons, protein structural modules and exons. Proc Natl Acad Sci USA 1996;93:2008-13.
9. Baldwin RL, Rose GD. Is protein folding hierarchic? I. Local structure and peptide folding. Trends Biochem Sci 1999; 26-33.
10. Baldwin RL, Rose GD. Is protein folding hierarchic? II. Folding intermediates and transition states. Trends Biochem Sci 1999; 77-83.
11. Dill KA, Chan HS. From Levinthal to pathways to funnels. Nature Struct Biol 1999;4:10-19.
12. Yu MH, King J. Single amino acid substitutions influencing the folding pathway of the phage P22 tail spike endorhamnosidase. Proc Natl Acad Sci USA 1984;81:6584-8.

13. Panchenko A, Luthey-Schulten, Z., Cole, R. Wolynes, P.G. The foldons universe: a survey of structural similarity and self-recognition of independently folding units. J Mol Biol 1997;272:95-105.
14. Engel J. Conformational transitions in biopolymers. In: Hoppe W, Lohmann W, Markl H, Ziegler H (Ed.). Biophysics. Berlin: Springer Verlag; 1983. p. 233-43.
15. Serra R, Zanarini G, Andretta M, Compiani M. Introduction to the physics of complex systems. Oxford: Pergamon Books; 1986.
16. Casadio R, Compiani M, Fariselli P, Jacoboni I, Martelli PL. Neural networks predict protein folding and structure: Artificial Intelligence faces biomolecular complexity. SAR QSAR Environm Res 2000;11:149-82.
17. Compiani M, Fariselli P, Casadio R. Noise and randomlike behavior of perceptrons: theory and application to protein structure prediction. Phys Rev E 1997;55:7334-43.
18. Karplus M, Weaver DL. Protein-folding dynamics. Nature 1976;260:404-6.
19. Karplus M, Weaver DL. Diffusion-collision model for protein folding. Biopolymers 1979;18:1421-37.
20. Karplus M, Weaver DL. Protein folding dynamics: the diffusion-collision model and experimental data. Protein Sci 1994;3:650-68.
21. Burton RE, Myers JK, Oas TG. Protein folding dynamics: quantitative comparison between theory and experiment. Biochemistry 1998;37:5337-43.
22. Hilser VJ, Dowdy D Oas, TG, Freire E. The structural distribution of cooperative interactions in proteins: analysis of the native state ensemble. Proc Natl Acad Sci USA 1998;95:9903-8.
23. Anfinsen CB, Principles that govern the folding of protein chains. Science 1973;181:223-30.
24. Abkevich VI, Gutin AM, Shakhnovich EI. Impact of local and non-local interactions on thermodynamics and kinetics of protein folding. J Mol Biol 1995;252:460-71.
25. Fersht AR. Transition-state structure as a unifying basis in protein-folding mechanisms: Contact order, chain topology, stability, and the extended nucleus mechanism. Proc Natl Acad Sci USA 2000;97:1525-9.
26. Dinner A, Karplus M. The roles of stability and contact order in determining protein folding rates. Nature Struct Biol. 2001; 8:21-22.
27. Plaxco KW, Simons KT, Ruczinski I, Baker D. Topology, stability, sequence and length: defining the determinants of two-state protein folding kinetics. Biochemistry 2000; 39: 11177-11183.
28. Burton RE, Guewha SH, Daugherty MA, Oas TG. Microsecond protein folding through a compact transition state. J Mol Biol 1998;263:311-22.
29. Viguera AR and Serrano L, Loop length, intramolecular diffusion and protein folding. Nature Struct Biol 1997;4:939-46.
30. Viguera AR, Villegas V, Aviles FX, Serrano L. Favourable native-like helical local interactions can accelerate protein folding. Fold Des 1996;2:23-33.
31. Daggett V, Fersht AR. Is there a unifying mechanism for protein folding? Trends Biochem Sci 2003;28:18-25
32. Gianni S, Guydosh NR, Khan F, Caldas TD, Mayor U, White GWN, DeMarco ML, Daggett V, Fersht AR. Unifying features in protein-folding mechanisms. Proc Natl Acad Sci USA 2003;100:13286-91.

Short communication

ADAPTIVE PROCESSING OF COMPLEX DATA STRUCTURES IN QSPR/QSAR ANALYSIS

Alessio Micheli, Antonina Starita
Informatics Department, University of Pisa, Pisa, Italy
E-mail: micheli@di.unipi.it

Introduction

A central problem in modeling complex systems is to provide the model with a proper and expressive representation of the real-world data. For instance, biological and chemical problems are characterized by quite complex domains where the managing of relationships and structures is relevant to achieve suitable modeling of the solutions. Among studies of complexity in the living, the Quantitative Structure Property Relationship/Quantitative Structure Activity Relationship (QSPR/QSAR) approach allows an analysis of the interactions between chemicals and biological systems abstracted by a quantitative mathematical model, where the treatment of chemical structures (molecular graphs) plays a major role.

On the side of the mathematical models, the Machine Learning (ML) approach is ideally suited to tackle complex problems where there is a lack of a clear theory explaining the molecular interactions, and the presence of noisy experimental data. Specifically, ML has contributed powerful data modeling tool that are able to approximate complex non-linear input/output dependencies. However, standard ML techniques are often restricted to the treatment of finite dimensional vectors of features.

Traditional QSPR/QSAR approaches inherited the same assumptions that lead to a case-dependent extraction of features, guided by the knowledge of experts, to obtain a finite set of suitable structural descriptors of the molecules, i.e. a flat representation of the problem domain where a complete representation of the molecular structures is difficult.

Since molecules are more naturally described via a varying size structured representation, the study of general approaches to the processing of structured information is needed.

Methodology

With respect to the traditional descriptors-based QSPR/QSAR analysis, we propose a completely different approach to deal directly with a structured representation of molecules. The approach is based on Recursive Neural Network (RNN), a Neural Network model able to handle the complexity of variable-size structured data through a recursive encoding process (see (1) for a unified presentation and recent developments and the references therein for historical background). In particular, RNN works directly with hierarchical structured data that represent molecules. By construction, according to the recursive approach, the encoding process mimics the morphology of each input hierarchical structure. For each vertex of the structure the model computes a numerical code using information both of the vertex label and of the code of the sub-graphs descending from the current vertex. At the end of the process, a code of the whole

molecular structure is computed. Since the model is equipped with tunable free-parameters, the encoding process can be adapted to the prediction task: the learning algorithm fits the parameters values to the given set of input/output training examples.

Globally, the model directly takes as input molecular structured representations and it simultaneously learns both how to numerically represent (encode) and to map chemical structures to their property/activity values. Through this adaptive encoding the model can compute structural descriptors that are specific for the data and computational problem at hand. In other words, the map of (chemical) similarities among molecules is automatically adapted by the model to the task, according to the property/activity target values. Note that the process can consider both the 2D graph topology and the atom types (or the chemical functionalities). Hence, exploiting the richness of a structured molecular representation and avoiding the use of any fixed structure-coding (or similarity) scheme, we offer a new perspective to the QSPR/QSAR studies.

It must be stressed that the proposed methodology, relying on the generality and flexibility of a structured representation, defines a unified approach that can be used to tackle different problems on different kind of molecular data.

Applications overview

The capability of the proposed approach to the adaptive processing of structured domains has been progressively proved by the application of the RNN models to various QSPR/QSAR problems, basically involving either congeneric series or simple organic compounds.

In particular, we considered QSPR problems, such are the prediction of the boiling point for alkanes (2) and the prediction of thermodynamical properties of the solvation process (3), and QSAR problems, such are the prediction of the non-specific activity (affinity) towards the benzodiazepine/GABA receptor (2,4,5), and the prediction of A1 adenosine receptor ligands affinity toward the receptor (6).

As a general result, we found that generality of the RNN approach is not at the expense of predictive accuracy, as our results were competitive with results achieved by traditional QSPR/QSAR treatment. Moreover, studies of the numerical code developed by the RNN shown that the model is able to discover relevant features for the problem at hand just on the basis of the associations between the molecular morphology and the target property (5).

Conclusions

In this work an overview of a Machine Learning approach (based on Recursive Neural Network) to the modeling of complex data in the area of cheminformatics has been presented.

Through the proposed methodology we intended to show that the ML-based modeling of complex systems can be effectively equipped with expressive representation of complex data in the form of structured representation. As a result, concerning biological and chemical problems, we have shown that predictions can be done directly from molecular structures, introducing potential benefits in the current QSPR/QSAR methodology. In particular, since universal approximation capabilities of the RNN have been proved (specifically for tree-structured domains (7)), RNN can be considered a general tool useful especially to deal with new tasks where the relevance of the traditional molecular descriptors is unknown.

More generally, the presented approach can be seen as a paradigmatic example of the studies aiming at extending machine learning techniques (considering either neucomputing, kernel-based, probabilistic or symbolic approaches) to the treatment of various structured classes of data (see (1) and the references therein).

Our aim here is also to propose the new approach as a general methodology to tackle various structured problems in the area of cheminformatics and bioinformatics. Main potentially developments concern hard tasks in toxicology and bioinformatics whenever is natural to find useful structured representation of chemical/biological data.

References

1. Micheli A. Recursive processing of structured domains in machine learning. (PhD thesis TD-13/03) Pisa (Italy): Department of Computer Science, University of Pisa; 2003.
2. Bianucci AM, Micheli A, Sperduti A, Starita A. Application of Cascade Correlation Networks for Structures to Chemistry. Applied Intelligence Journal 2000;12:117-46.
3. Bernazzani L, Duce C, Mollica V, Tinè MR, Micheli A, Sperduti A, Starita A. Predicting thermodynamic properties from molecular structures by recursive neural networks. In: Galli G, Solaro R (Ed.). Proceedings of the International Workshop on "Advanced Frontiers in Polymer Science"; 2002 12-13 September; Pisa, Italy. Pisa: Università di Pisa; 2002. p. 62.
4. Bianucci AM, Micheli A, Sperduti A, Starita. Quantitative structure-activity relationships of benzodiazepines by recursive cascade correlation. In: Sekercioglu YA, Pitsillites A, Vasilakos A (Ed.). IEEE Workshop on application of computational intelligence; Proceedings of the IEEE World Congress on Computational Intelligence; 1998 May 4-9; Anchorage, Alaska. Anchorage: IEEE; 1998. p. 117-122.
5. Micheli A, Sperduti A, Starita A, Bianucci AM. Analysis of the internal representations developed by neural networks for structures applied to quantitative structure-activity relationship studies of benzodiazepines. J Chem Inf Comp Sci 2001;41(1):202-18.
6. Micheli A, Sperduti A, Starita A, Bianucci AM. Design of new biologically active molecules by recursive neural networks. In: Oja M, Kaski S, Kohonen T (Ed.). Proceedings of the IEEE International Joint Conference on Neural Networks. 2001 July 15-19*;* Washington, DC, USA. Washington: IEEE; 2001. 4: 2732-7.
7. Hammer B. Learning with recurrent neural networks. Lecture notes in control and information sciences. Berlin: Springer-Verlag; 2000.

Short communication

LOOKING FOR CONSTITUTIVE GENE REGULATION WEBS BY MICROARRAY STUDIES: A RECURSIVE NEURAL NETWORK APPROACH

Monica Francesca Blasi (a), Ida Casorelli (a), Alfredo Colosimo (b), Francesco Simone Blasi (c), Margherita Bignami (a), Alessandro Giuliani (a)
(a) Dipartimento di Ambiente e Connessa Prevenzione Primaria, Istituto Superiore di Sanità, Rome, Italy
(b) Department of Human Physiology and Pharmacology, University of Rome "La Sapienza", Rome, Italy
(c) Department of Mathematics, Università di Roma "Tor Vergata", Rome, Italy

Introduction

To fully exploit the information present in microarray data, we applied the recursive feature of network architectures to identify possible gene regulation circuits (1-3). The success of the proposed approach is based on the concept of invariance: thus the presence of constitutive co-regulation circuits is proven by the ability to construct networks showing the same asymptotic behaviour starting from gene expression data derived from different biological specimens in independent experiments. Our analysis is based on microarray data made accessible to the public in the web (4-6).

The method was experimentally validated by applying it to two examples of circuits formed by components interacting with their partners in permanent or transient complexes, i.e. 1) ribosomal proteins forming stable multimeric structures, and 2) genes involved in the control of genome stability. We demonstrate that the network algorithm can single out the presence of a regulation circuit which is not apparent when more traditional linear methods are applied (7).

Strategy of analysis

The idea is to generate a network whose nodes and edges corresponded to gene expression values measured in microarray experiments, and to empirical correlation coefficients between genes, respectively. Such a network receives as initial "input" an n-dimensional vector (n being the number of genes) of arbitrary initial expression values, which is transformed by the application of the network according to a recursive algorithm. The transformation rule active in the network, corresponding to the gene expression rate, is the following:

$$dy_i/dt = k_{1i}\, G_{1i} - k_{2i}\, y_i \qquad [1]$$

where k_{1i} and k_{2i} are the accumulation and degradation rate constants of the i-th gene product, respectively; $G_{1i} = \{1+ e^{-(\Sigma_j Wij\ yj + bi)}\}^{-1}$ is the regulatory effect on each gene, defined by a set of weights (w_{ij}) estimating the regulatory influence of gene i on gene j, by an external input (b_i), and by the actual concentrations of gene products (y_i). Vohradsky and his associates (8-10) proposed the above architecture to study regulatory genetic networks such as those involved in the transcriptional and translational control of gene expression. We can choose the parameters of the models to obtain only stable states at the end of the simulation. As a consequence we can

assume the existence of t' such that, for t>t' we can put y(t)=const., and then we can write the Eq. [1] in the form:

$$dy_i/dt = 0 \quad [2]$$

Fixing the parameters of the model as $k_{2i}/k_{1i} = k_2/k_1 = k = \text{const.} > 0$, $b_i = 0$ and $w_{ij} = (w_{ii} = 1, -1 \leq w_{iJ} = w_{ji} \leq 1)$ we obtain:

$$y_i = k/(1+e^{-\Sigma W_{ijyj}}) \quad [3]$$

We selected a subset of genes from a complete set of independent experiments and use their mutual correlations as synaptic weights of the genetic network algorithm. The chosen experiments gave rise to four data sets we named A to D. They are: A) 64 primary adenocarcinoma and 12 metastatic carcinomas; B) 74 leukemias; C) 13 determinations in human synchronized cells in a time course experiment; D) 60 NCI model cell lines.

The value of the correlation depends on both the actual link between the two variables (partial correlation) and the links that two nodes share with all the other elements of the network. The symmetric character of the correlation matrix and the constraints derived from the mutual interference between the nodes forces the network to relax on a bi-stable behaviour. Thus each gene, at equilibrium, can only attain a maximum level corresponding to the k value or a state corresponding to a null activity.

The concordance between different experiments is measured by the percentage of communality correspondent to the number of genes attaining the same stable state in all the experiments.

To verify whether our approach was able to identify a regulation circuit we compared the asymptotic behaviour of networks based on different data sets made of genes known to be involved in co-regulation circuits with networks constituted by "random extractions" of genes. We define the occurrence of a regulation circuit in a set of genes by a) the invariance of their correlation structure; b) the lack of invariance in randomly assorted genes; c) the percentage of genes having the same asymptotic expression values in different data sets (commonality).

Results

To verify whether our approach was able to identify a regulation circuit we analysed the mRNA expression levels of genes that are known to cooperate in the construction of the ribosome machinery. The application of the four recursive neural networks with the correlation coefficients derived from the data sets A-D resulted into a high level of commonality between the ribosomal genes (Figure 1). This high percentage of commonality (85.5%) was further increased to 90.6% by the analysis of a smaller data set (44 genes) from which homolog and isoformic genes as well as mithocondrial and partial cDNAs were eliminated. When this analysis was applied to a random extraction of genes from the same data sets, the percentage of commonality decreased dramatically. The percentage of communality between 58 ribosomal genes as well as in the subset of 44 genes is indicated together with RC for randomly selected genes. The dotted line represents the 50% of communality. On the contrary, only a very weak linear relation was observed between different pairs of correlation matrixes (Figure 2). This lack of concordance between the linear correlation structures of the different data sets was confirmed by the variations in the component loadings of the four data sets (data not shown).

This result clearly indicates the ability of the proposed strategy to identify gene regulation networks from the background of general genetic activities.

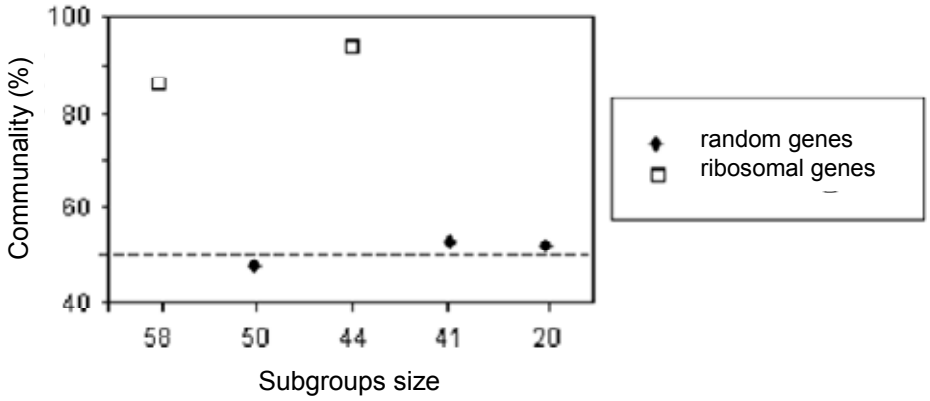

Figure 1. Recursive correlation applied to ribosomal genes in the various data sets

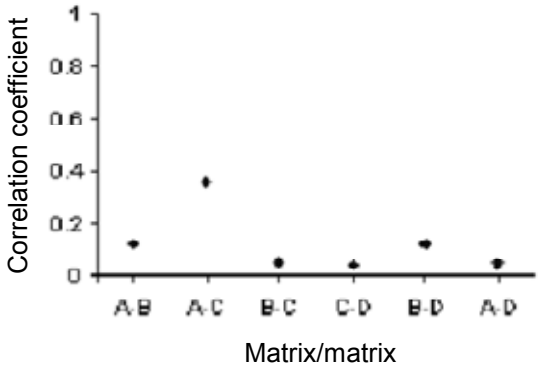

Figure 2. Correlation beetween matrices relative to gene expression data for ribosomal genes

The same strategy was applied to 41 genes involved in DNA repair/DNA damage signalling/cell cycle control which might represent a transient regulation structure. The linear correlation structures were each other independent, failing to highlight any mechanistic relationship linking the 41 genes (Figure 3).

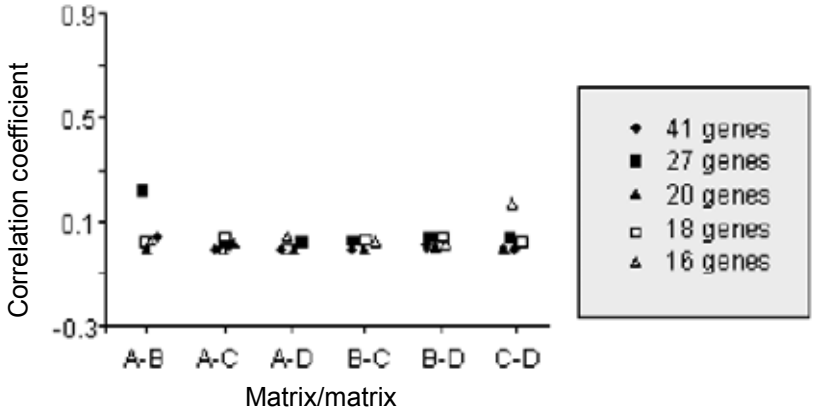

Figure 3. Correlation between matrices relative to gene expression data for genome stability genes

The application of principal component analysis to the four data sets confirmed the lack of any linear superposition between the correlation structures, reaching different eigenvector profiles for the four sets (data not shown) in accordance with other studies.

From the initial group of 41 genes we selected four subgroups of 27, 20, 18, and 16 genes, respectively, which were obtained by a progressive elimination of possible sources of redundancy (repeated genes, partial cDNAs, etc.).

For each of the five selections (41, 27, 20, 18, 16 genes) independent recursive networks were generated, each having a synaptic weight matrix equal to the between-gene correlation matrix. Furthermore, random extractions of 50, 41 and 20 genes were generated from the same data sets, and the relative correlation matrices were used to build the corresponding networks. After the application of the recursive network algorithm, the average percentage of equally expressed genes is marginally increased from 50% in the randomly chosen groups to 62% in the 41 genes group (Figure 4A).

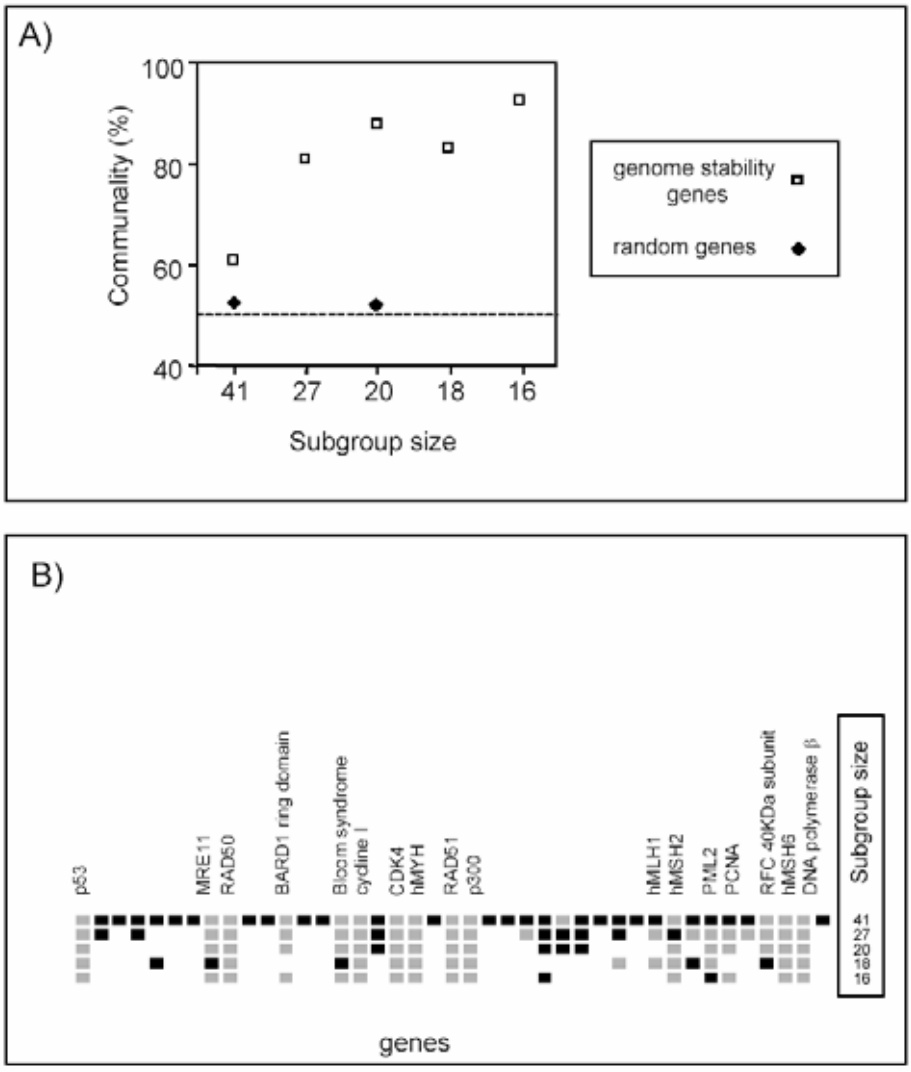

Figure 4. Commonality in the binary classification of genome stability genes in the various data sets

The clearance of the 41 genes from redundancies, produced an increase of this percentage close to 93% in the 16 gene subgroup. In contrast, the average percentage of the "random gene set" (from 41 to 20 genes) did not change at all, remaining very close to the 50% value expected by chance.

This implies that the behaviour of the DNA repair/DNA damage signalling/cell cycle control can be isolated from the background of the general expression activity and is partially independent from the number and kind of the analysed genes (Figure 4B). The percentage of communality relative to genes belonging to the pathway for the control of gene stability is indicated together with RC for randomly selected genes (Panel A). An overview of the asymptotic expression pattern of genes in different contexts is reported in Panel B. The whole name of genes is reported whenever it is asymptotically expressed in at least four of the five examined subgroups. Black symbols refer to genes which are coherently not expressed, grey symbols correspond to genes expressed at level k in all the experiments

Conclusions

The technique of microarrays might provide an opportunity to study the actual functioning of gene regulation networks in approximately natural settings by modifying the classical scheme of perturbation analysis (i.e. switch off of one or more elements followed by analysis of the induced functional modifications) (11). In the reconstruction of regulation networks from microarray derived data, however, some basic problems emerge. A recent finding by Ueda and colleagues (12) demonstrated a power law distribution in the changing of expression levels from bacteria to human. This effect cannot only be considered a purely statistical feature, but might be linked to the coordinated change of the expression of the genes coding for multimeric stable complexes. In addition concentration fluctuations, intrinsic to the nature of the biological system, can affect the regulation of protein synthesis. However the interactions among these molecules occur in a random fashion and there has been a considerable recent interest in studying experimentally the effect of this intrinsic noise (13). Another indication of the general relevance of transcriptional regulation in the general functioning of biological regulation network is of theoretical nature and comes from the model set by Goutsias and Kim (14) where the dynamical link between transcription and translation steps is carefully exploited.

The recurrent neural network approach allows to overcome some of the limitations in the analysis of microarray data and allows to identify biologically-based regulation circuits over random gene assortments. This outcome is reminiscent of a classical result in statistical mechanics, i.e. the dynamics of associative memories (15). In the present study we demonstrate how our approach is able to identify both strong and weak interaction networks as commonality between data sets from different biological conditions. It is worth noting that the "transiently interacting" network (genome stability genes) attained an invariance level not too dissimilar from that reached by the "permanently interacting" network represented by ribosomal proteins when depurated by spurious components. In addition the selection procedure operated on the genome stability genes allowed to attain the maximal convergence and robustness of the data through a fine tuning of the optimal composition of the circuit. The relative robustness of the network to different amounts of noise is another feature that RC model shares with content-addressable memories (not shown).

Our model lays in between the mathematically-intensive methods based on differential equations (16) and statistical mechanics-oriented theoretical models. The first ones, although very accurate, are forcedly limited to small sets of genes while the second ones are difficult to implement with empirical data. We adopted a completely data-driven strategy which a) is easily

applicable starting from actual microarray experiments; b) does not impose any pre-conceived model on studied interactions; c) can be useful for the generation of biologically sound hypotheses on diverse regulation circuits.

References

1. Jansen R, Greenbaum D, Gerstein M. Relating whole-genome expression data with protein-protein interactions. Genome Research 2002;12:37-46.
2. Jansen R, Yu H, Greenbaum D, Kluger Y, Krogan NJ, Chung S, Emili A, Snyder M, Greenblatt JF, Gerstein M. A Bayesian networks approach for predicting protein-protein interactions from genomic data. Science 2003;302:449-53.
3. Barabàsi AL, Ravasz E, Vicsek T. Deterministic scale-free networks. Physica A 2001;299:559-64.
4. Ramaswamy S, Ross KN, Landern ES, Golub TR. A molecular signature of metastasis in primary solid tumors. Nat Genet 2002;33:49-54.
5. Cho RJ, Huang M, Campbell MJ, Dong H, Steinmetz L, Sapinoso L, Hampton G, Elledge SJ, Davis RW, Lockhart DJ. Transcriptional regulation and function during the human cell cycle. Nature Genetics 2001;27:48-54.
6. Ross DT, Scherf U, Eisen MB, Perou CM, Rees C, Spellman P, Iyer V, Jeffrey SS, Van de Rijn M, Waltham M, Pergamenschikov A, Lee JC, Lashkari D, Shalon D, T.G Myers, Weinstein JN, Botstein D, Brown PO. Systematic variation in gene expression patterns in human cancer cell lines. Nat Genet 2000;24:227-35.
7. Farkas I, Derényi I, Jeong H, Néda Z, Oltvai ZN, Ravasz E, Schubert A, Barabàsi AL. Vicsek T. Networks in life: scaling properties and eigenvalue spectra. Physica A 2002;314:25-34.
8. Vu TT, Vohradsky J. Genexp-a genetic network simulation environment. Bioinformatics 2002;18:1400-1.
9. Vohradsky J. Neural network model of gene expression. FASEB J 2001;15:846-54.
10. Vohradsky J. Neural model of the genetic network. J Biol Chem 2001;276:36168 - 73.
11. Chu T, Glymour C, Scheines R, Spirtes PA. Statistical problem for inference to regulatory structure from associations of gene expression measurements with microarrays. Bioinformatics 2003;19:1147-52.
12. Ueda HR, Hayashi S, Matsuyama S, Yomo T, Hashimoto S, Kay SA, Hogenesch JB, Iino M. Universality and flexibility in gene expression from bacteria to human. Proc Natl Acad Sci USA 2004;101:3765-9.
13. Blake WJ, Kaern M, Cantor CR, Collins JJ. Noise in eukaryotic gene expression. Nature 2003;422:633-7.
14. Goutsias J, Kim S. A nonlinear discrete dynamical model for transcriptional regulation: construction and properties. Biophys J 2004;86:1922-45.
15. Farhat NH, Psaltis D, Prata A, Paek E. Optical implementation of the Hopfield model. Applied Optics 1985;24:1469-75.
16. Gardner TS, Di Bernardo D, Lorenz D, Collins JJ. Inferring Genetic networks and identifying compound mode of action via expression profiling. Science 2003;301:102-5.

Integrative neuroscience

Lecture

NON INVASIVE BRAIN COMPUTER INTERFACE FOR COMMUNICATION AND CONTROL

Fabio Babiloni (a,d), Donatella Mattia (a), Marco Mattiocco (a), Alessandro Timperi (a), Serenella Salinari (b), Maria G. Marciani (a,c), Febo Cincotti (a)
(a) Fondazione Santa Lucia IRCCS, Rome, Italy
(b) Dept. of Computer and Systems Science, University of Rome "La Sapienza", Rome, Italy
(c) Dept. of Neuroscience, University of Rome "Tor Vergata", Rome, Italy
(d) Dept. of Human Physiology and Pharmacology, University of Rome "La Sapienza", Rome, Italy

Introduction

Recently, it has been suggested that with the use of the modern high resolution EEG technologies (1) it could be possible to estimate the cortical activity associated to the mental imagery of the upper limbs movements in humans (2). However, a verification of such statement on a group of normal subjects has not been yet performed. The scientific question at the base of the present work is whether the estimated cortical activity related to the mental imagery of the upper limbs returns more useful features with respect to those obtained by using scalp EEG recordings. To address this issue, we performed high resolution EEG recordings during the imagination of upper limb movements in a group of five healthy subjects. Comparisons between the waveforms from scalp electrodes and those from the estimated cortical activity in particular Region of Interest (ROIs) were then performed. These comparisons returned information about the usefulness of the use of cortical activity for the recognition of mental states with respect to the use of the scalp recorded data.

Methods

Five healthy subjects participated voluntarily in experiments, in which they were asked to perform the imagination of right finger movements when they perform the protrusion of their lips. EEG was recorded by using a high resolution EEG cap with 64 electrodes disposed accordingly to an extension of the 10-20 international system. Subjects were asked to imagine the movement of their right middle finger during the simultaneous protrusion of their lips. This provided the necessary EMG trigger to synchronize the average of the recorded movements. Eighty single EEG trials were recorded for each subject. Each single EEG trial was acquired from 2 second before the arrival of the visual trigger to 1 s after. For all subjects analyzed in this study, sequential MR images were acquired and realistic head models were generated. A cortical surface reconstruction was accomplished for each subject's head with a tessellation of about 10,000 triangles on average. The estimation of cortical activity during the mental imagery task was performed in each subject by using the depth-weighted minimum norm algorithm (3). Such estimation returns a current density estimate for each of the five thousand dipoles constituting the modelled cortical source space. Each dipole returns a time-varying amplitude representing the brain activity of a restricted patch of cerebral cortex during the entire task time-

course. This rather large amount of data can be synthesized by computing the ensemble average of all the dipoles magnitudes belonging to the same cortical region of interest (ROI). Each ROI was defined on each subject's cortical model adopted in accordance with its Brodmann areas (BAs). In the present study, the activity in the primary left and right motor area, related to the B.A. 4 for the lips as well as hand regions have been taken into account. Artifacts correction by visual and automatic inspection was performed on each single EEG trial recorded. Threshold criteria were used to discard EEG trials contaminated by electrooculogram (EOG) or EMG activity at the resting arms. Visual inspection has been used to discard trials with unusual sub-threshold artifacts. On average, about the 10% of the acquired EEG trials were discarded in the recorded population. Each artifacts-free single trials was then subjected to the linear inverse procedure, and the time varying cortical distributions associated was estimated. The collapsing procedure explained above was then applied to retrieve the cortical waveforms related to each particular ROI analyzed.

Results

Figure 1 shows the event related potentials gathered from the scalp electrodes C3 and C4 (right bottom) and the event related mean current densities obtained from the bilateral MI-hand and MI-lips (right top and middle, respectively) areas for a representative subject (Subjet 5). In the figure the head model utilized for the solution of linear inverse problem is reported. Cortical RoIs are evidenced in red (MI-hand) and blue (MI-lips). Electrode leads (58) are represented in green; C3 and C4 electrodes are evidenced with a darker color. In the right panel of Figure 1 the *t*op and middle waveforms represent the average current densities estimated on MI-hand and MI-lips RoIs, respectively; bottom waveforms represent the potential measured from C3 and C4 electrodes. Solid and dashed lines are for left and right side, respectively.

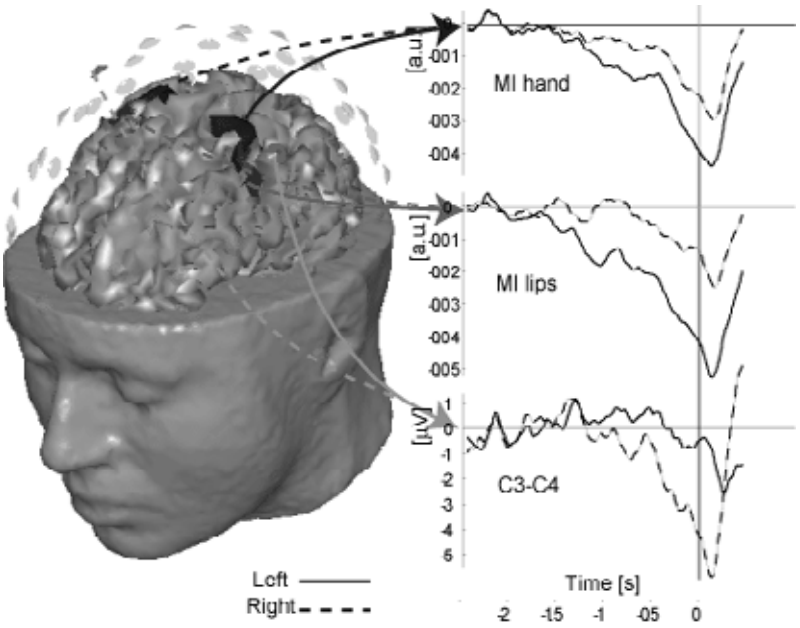

Figure 1. *Left panel*: Realistic head model utilized for the solution of linear inverse problem. *Right panel*: Current densities waveforms

Estimated current density underlying motor imagery is characterized by a negative slope peaking around 100ms before the EMG onset (0 Time) over the left M1 hand-ROI (namely contralateral to the imagined hand movements); no relevant activity was present over the right M1-hand ROI. As for the estimated current density underlying lip pursing, the negative slope involved bilaterally the M1-lips ROI. Scalp potential related to the task displayed a higher peak amplitude over C3 electrode lead with respect to C4. Analysis of the time varying current density distributions over the cortical mantle showed the presence of a bilateral negative (i.e. inward directed) activity on the supplementary motor area.

Table 1 reports the values of the measured current density in the different BAs examined at the peak of the motor potential for all the subjects employed in this study. Table 1 Table shows the amplitude values at the peak of the motor potentials in all the subjects analyzed. BA4finger label stands for Brodmann area 4 (B.A.; primary motor area relative to the fingers area), BA4lips label stands for B.A. area 4 for the lips movements while C3 and C4 labels refer to the values measured at the electrode position of the international 10-20 system. The L and R letters refer to the left and right hemispheres, respectively. Values for the C3 and C4 measurements are in uV, values for the current density measurements are in arbitrary units.

Table 1 Amplitude values at the peak of the motor potentials in all the subjects analyzed

SUBJECT	BA4fingerL	BA4fingerR	BA4lipsL	BA4lipsR	C3	C4
#1	-8.2	-5.4	-0.88	0.01	0.34	0.06
#2	-8.6	-7.2	-0.57	-0.35	-0.48	-0.04
#3	-12.5	-10.2	-1.42	-0.96	-0.81	-0.51
#4	-5.8	-6.9	-0.68	-0.34	-0.37	0.38
#5	-8.3	-5.4	-0.23	-0.02	-0.19	-0.13

It is worth note as the potentials amplitudes at MP peak (gathered from C3 and C4 leads) are less unbalanced between left and right scalp areas when compared to the estimated current density activity in the primary motor areas related to the finger movements (BA4Rfinger, BA4Lfinger). Furthermore, the estimated cortical current density values in the primary motor areas related to the lips movements are rather symmetrical, i.e. the values are similar for the left and right ROI considered (BA4Llips and BA4Rlips, respectively).

A statistical analysis of this unbalancing for the gathered scalp potentials as well as for the estimated cortical activity was then performed by using the t-paired Student test. Results obtained indicating; 1) a greater cortical activity estimated over the left primary motor cortical areas for finger movements (BA4Lfinger) with respect to the right one (BA4Rfinger), with a significance equal to $p < 0.0011$; 2) a statistical similar estimated cortical activity for the left (BA4Llips) and right (BA4Rlips) ROIs for the lips movement ($p < 0.36$); and a statistically significant differences between the MP peak for the scalp potentials gathered from the left scalp areas (C3) with respect to the right (C4) one, with a statistical significance of $p < 0.04$.

Discussion

The data reported here suggest that it is possible to retrieve the cortical activity related to the mental imagery by using sophisticated high resolution EEG techniques, obtained by solving the linear inverse problem with the use of realistic head models. Of course, the analysis of the

distribution of the potential fields associated to the motor imagery in humans have been already described (4).

However, in the context of the Brain Computer Interface, it assumes importance if the activity related to the imagination of arm movement could be unbalanced between the two hemispheres. In fact, the greater this unbalance between the scalp activity gathered in scalp electrodes C3 and C4 the easier is the task of recognizing it by a classifier (5). The relevant finding here is that the group analysis of the cortical waveforms associated to the mental imagery suggested the presence of a more pronounced unbalance between the cortical activity estimated in the primary motor areas of the right and left hemispheres with respect to those gathered from scalp electrodes. It is also worth to note that this unbalancing of the estimated cortical activity between left and right primary motor areas related to the finger movement imagination was not found in the primary motor areas related to the actual performed lips movements. The rather bilateral cortical activity for the lips cortices is consistent with the bilateral activations seen in fMRI activations in a previous study (6). On the other hand, it is worth of note that the cortical estimation methodology illustrated above is suitable for the on-line applications needed for the BCI device. In fact, despite of the use of sophisticated realistic head models for scalp, skull, dura mater and cortical surface, the estimation of the instantaneous cortical distribution from the acquired potential measures required a limited amount of time necessary for a matrix multiplication. Such multiplication occurs between the data vector gathered and the pseudoinverse matrix, that is stored off-line before the start of the EEG acquisition process. In the pseudoinverse matrix is enclosed the complexity of the geometrical head modeling with the Boundary Element or with the Finite Element Modeling techniques, as well as the a priori constraints used for the minimum norm solutions.

There is a large trend in the modern neuroscience field to move toward invasive electrodes implants for the recording of cortical activity in both animals and humans for the realization of an efficient BCI device (7). In this paper we have presented evidences that suggest an alternative methodology for the estimation of such cortical activity in a non invasive way, by using the possibilities offered by an accurate modeling of the principal head structures involved in the transmission of the cortical potential from the brain surface to the scalp electrodes

References

1. Gevins A, Brickett P, Costales B, Le J, Reutter B. Beyond topographic mapping: towards functional-anatomical imaging with 124-channel EEG and 3-D MRIs. Brain Topogr 1990;1:53-64.
2. Cincotti F, Mattia D, Babiloni C, et al. Classification of EEG mental patterns by using two scalp electrodes and Mahalanobis distance-based classifiers. Methods Inf Med 2002;41:337-41.
3. Babiloni F, Babiloni C, Locche L, et al. High resolution EEG: source estimates of Laplacian-transformed somatosensory-evoked potentials using a realistic subject head model constructed from magnetic resonance images. Medical & Biological Engineering & Computing 2000;38:512-9.
4. Pfurtscheller G, Neuper C. Motor imagery activates primary sensorimotor area in man. Neurosci Lett 1997;239:65-8.
5. Neuper C, Schlögl A, Pfurtscheller G. Enhancement of left-right sensorimotor EEG differences during motor imagery. J Clin Neurophysiol 1999;16:373-82.
6. Lotze M, Flor H, Grodd W. Larbig and Birbaumer Phantom movements and pain: an fMRI study in upper limb amputees. Brain 2001;124:2268-72.
7. Donoghue JP. Connecting cortex to machines: recent advances in brain interfaces. Nature Neuroscience 2002;5:1085-8.

Lecture

TIME-DEPENDENT MEASURES OF DYNAMICAL COMPLEXITY

Paul E. Rapp (a), Christopher J. Cellucci (b), Toshio A. A. Watanabe (c), Richard S. Hernandez (d)
(a) Drexel University College of Medicine and The Naval Medical Research Center, Philadelphia
(b) Ursinus College and The Naval Medical Research Center, Philadelphia
(c) Naval Medical Research Cente, Philadelphia
(d) Uniformed Services University of the Health Sciences, Philadelphia

Introduction

The term complexity is losing rather than gaining specificity as it comes to be applied to an ever-expanding collection of measures for characterizing time-dependent dynamical behavior. This being the case, it seems helpful to begin this contribution by defining how the term will be used here. In this paper, the analytic process begins with time series data from a discrete map, for example the Hénon system, or from a discretely sampled continuous system, for example solutions to ordinary differential equations like the Rössler and Lorenz equations or a digitized electroencephalographic signal. These data are then partitioned onto a finite symbol set. This process is best described by considering an example. Suppose a single channel EEG signal is to be examined. The signal's median voltage is determined. Each element of the voltage signal is then mapped to symbol 'a' if it is less than the median value or to symbol 'b' if it is greater than or equal to the median. A two-symbol, that is a binary, symbol sequence results. Alternative procedures for mapping time series data onto a symbol set and different specifications of that set can be considered. This is a nontrivial process. Care must be exercised. Inappropriate symbolic partitioning protocols can produce fallacious results (1).

The rest of the analysis is performed with the symbol sequence. Kolmogorov (2) and Chaitin (3) introduced the concept of complexity, as we use the term here, to characterize quantitatively the degree of disorder in a symbol sequence. Consider, for example, sequences M_1 and M_2:

$$M_1 = a\ a\ a\ a\ a\ a\ a\ a\ b\ b\ b\ b\ b\ b\ b\ b$$
$$M_2 = a\ b\ a\ b\ b\ a\ b\ a\ b\ b\ a\ a\ b\ a\ a\ b$$

These messages have the same distributions, that is the symbol 'a' and 'symbol b' appear the same number of times in each message. Nonetheless, the second message seems more irregular than the first. Measures of symbolic complexity bring a quantitative precision to this intuitive understanding. Several dozen measures of symbolic complexity have been published, and it is now possible to construct a taxonomy of complexity measures based on their defining characteristics (4). In this paper, all complexity calculations are performed with the Lempel-Ziv measure (5). A didactic presentation of the measure with examples and pseudocode for its calculation is given in an appendix of Watanabe *et al*. (6).

In common with most complexity measures, the numerical value of Lempel-Ziv complexity is sensitive to both the dynamics of the process generating the symbol sequence and to the number of symbols in the message (how long the process was observed). It is also sensitive to

the sampling frequency (how often measurements were taken). This is a significant limitation when comparing complexity values from different experiments. These limitations are addressed in the next two sections of this paper. While these normalization procedures are helpful, fundamental limitations of this form of analysis remain and should be recognized. Specifically, an absolute measure of complexity is impossible. Rather, we can only report the complexity observed during an observational period of some specified duration. A numerical demonstration of this limitation is presented below. The paper concludes with a description of how time-dependent measures of instantaneous complexity can be constructed.

Normalization for data set size

The upper half of Figure 1 shows the Lempel-Ziv complexity of five computationally generated signals: uniformly distributed random numbers, the Hénon system, the Lorenz equations, the Rössler equations and a constant signal. With the exception of the constant signal, the complexity is a linearly increasing function of data set size. The lower panel shows the corresponding normalized complexity. Values of Lempel-Ziv complexity were normalized against complexity values obtained from equiprobable, random surrogates.

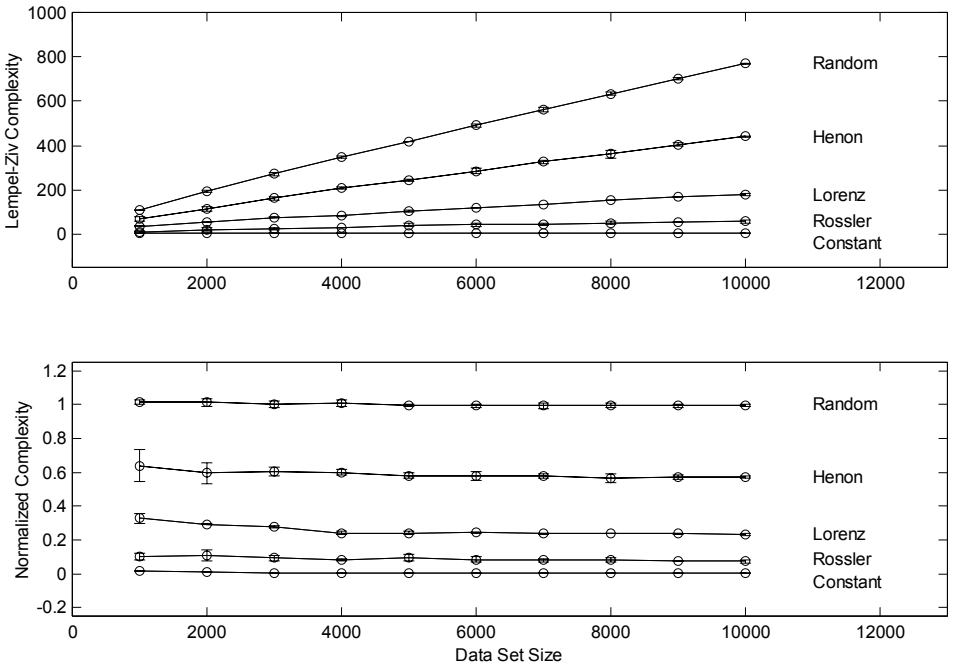

Figure 1. Lempel-Ziv complexity and normalized complexity as a function of data set size

The random numbers are uniformly distributed on [0,1] and were generated with the L'Ecuyer's algorithm incorporating a Bays-Durham shuffle (7). Specifications of the Hénon, Lorenz and Rössler systems are given in the appendix. The constant signal consisted of a single repeated symbol. The uncertainty in the complexity was estimated by comparing the values obtained with the first half and the second half of the symbol sequence. C_{ORIG} is the complexity

of the entire symbol sequence. (The subscript ORIG is used to denote the 'original' and will serve to contrast that value from values obtained with surrogate data sets.) Let C_A denote the value of complexity obtained using the first half of the symbol sequence. Let C_B denote the value computed with the second half. The uncertainty in C_{ORIG} is given by

$$\Delta C_{ORIG} = \frac{|C_A - C_B|}{(|C_A| + |C_B|)/2}$$

With the exception of the constant signal, the Lempel-Ziv complexity increases linearly with data set size. We now define a normalized complexity C_N.

$$C_N = C_{ORIG} / < C_0 >$$

$< C_0 >$ is the average complexity obtained with equiprobable, random symbol sequences formed on the same symbol set used to construct the symbolic partition of the original data and having the same length as the original sequence. These symbol sequences are referred to as surrogate data sets. The normalized complexity defined here is related to a previously introduced definition of algorithmic redundancy (8) which is a sequence sensitive generalization of Shannon's information redundancy. It is possible to estimate the uncertainty in C_N with the following:

$$(\Delta C_N)^2 = \left(\frac{\partial C_N}{\partial C_{ORIG}}\right)^2 \Delta C_{ORIG}^2 + \left(\frac{\partial C_N}{\partial < C_0 >}\right)^2 (\Delta < C_0 >)^2$$

$$(\Delta C_N)^2 = \left(\frac{1}{< C_0 >}\right)^2 \Delta C_{ORIG}^2 + \left(\frac{C_{ORIG}}{< C_0 >^2}\right)^2 (\Delta < C_0 >)^2$$

$\Delta < C_0 >$ is the standard deviation of the mean formed by calculating the complexity of several surrogate symbol sets. In the calculations shown here, ten surrogates were used. ΔC_{ORIG} is estimated by the previously described procedure. This normalization gives values of C_N that range from nearly zero for a constant signal, to the maximum value of one which is obtained when random numbers are partitioned.

A casual reading of this description might suggest that the surrogate symbol sequences were formed by a random shuffle of the original sequence. This is not the case. The surrogates are random, equiprobable symbol sequences. Equiprobable is defined here in the following manner. Let N_α be the number of symbols in the symbol set. This is not the length of the message. In the previous example of a partition onto 'a' and 'b', $N_\alpha = 2$. An equiprobable symbol sequence is one in which the probability of each symbol is $1/N_\alpha$.

The reason for using random, equiprobable surrogates rather than random shuffles of the original symbol sequence is discovered by considering cases where the symbols in the original message are not equally likely. In the limiting case of a constant signal, every symbol is the same. In that case, the complexity does not change in response to a random shuffle; C_{CORIG} /<C_0> would be equal to one, the maximum value of complexity, if surrogates were formed by a random shuffle. The lower half of Figure 1 shows the results obtained with this normalization. It is seen that for these stationary systems (and stationarity is the key to the process), a value of complexity that is insensitive to data set size is obtained provided that a sufficiently large data set is used.

With this normalization it is possible to compare complexity values obtained in different conditions. An example is shown in Figure 2. Signals were acquired in two behavioral

conditions: eyes-closed resting and eyes-closed performing mental arithmetic. The upper panel shows the Lempel-Ziv complexity. The lower panel shows the corresponding normalized complexity computed with equiprobable, random surrogates. The average complexity obtained in the rest condition is .31±.02. The average complexity obtained in the cognitively active condition is .40±.02.

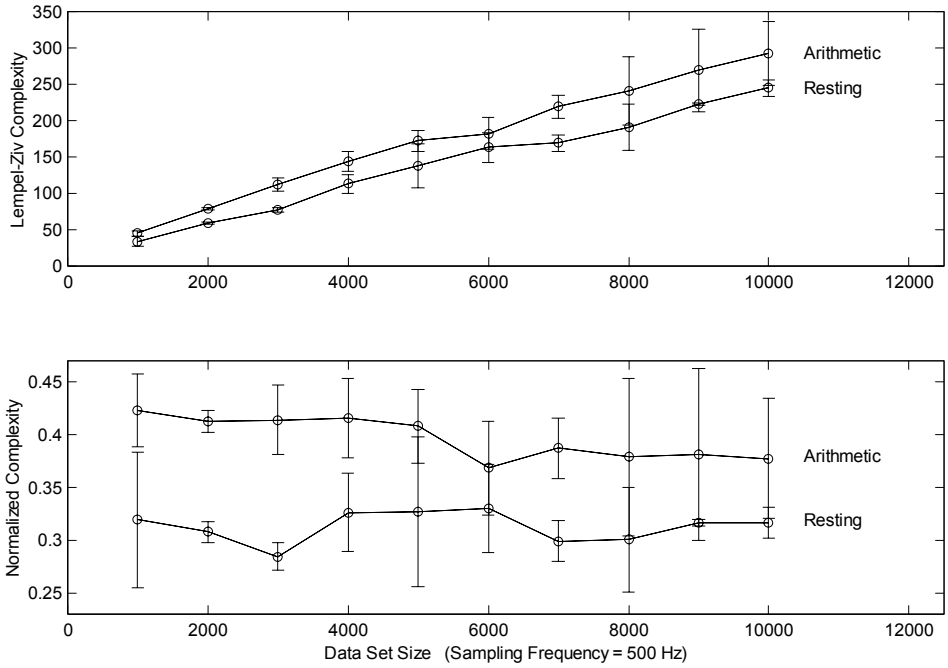

Figure 2. Lempel-Ziv complexity and normalized complexity of EEG signals obtained from a healthy, adult control subject

EEG signals from a healthy control subject were sampled at scalp site Oz at 500 Hz in two behavioral condition, eyes closed resting and eyes closed performing mental arithmetic (a silent backward count in steps of seven). As before, the binary Lempel-Ziv complexity increases with the size of the data set. The normalized complexity, however, does not display a linear sensitivity to data set size. An average value for each behavioral condition can be found by taking the mean of the values obtained with 1000, 2000, …..10,000 element records. In the resting condition $< C_N > = .31 \pm .02$. During mental arithmetic $< C_N > = .40 \pm .02$

Normalization for sampling interval

The normalization introduced in the preceding section can successfully address differences in complexity measures due to the number of elements in the symbol sequence, but it will not normalize for differences in sampling frequency. For example, the results in Figure 2 show that random equiprobable normalization can be used to compare EEG signals recorded for different epoch lengths at the same sampling frequency. If, however, the same normalization were used with a signal digitized at 1000 Hz, a different value of normalized complexity would be

obtained. Specifically, a higher value of complexity would result because a 1000 Hz sampling frequency will reveal fine grained dynamical structure that cannot be observed at 500 Hz. This is shown in Figure 3: the upper panel shows the Lempel-Ziv complexity of data generated by the Lorenz equations over an equal temporal interval when h=.01, .02, .04 and .08. The Lempel-Ziv complexity decreases with the sampling interval. The lower panel shows the corresponding normalized complexity where, in contrast with Figures 1 and 2, the Lempel-Ziv complexity is normalized against random phase surrogates.

Problems introduced by comparing signals obtained at different sampling frequencies can be addressed by normalizing against a different class of surrogates.

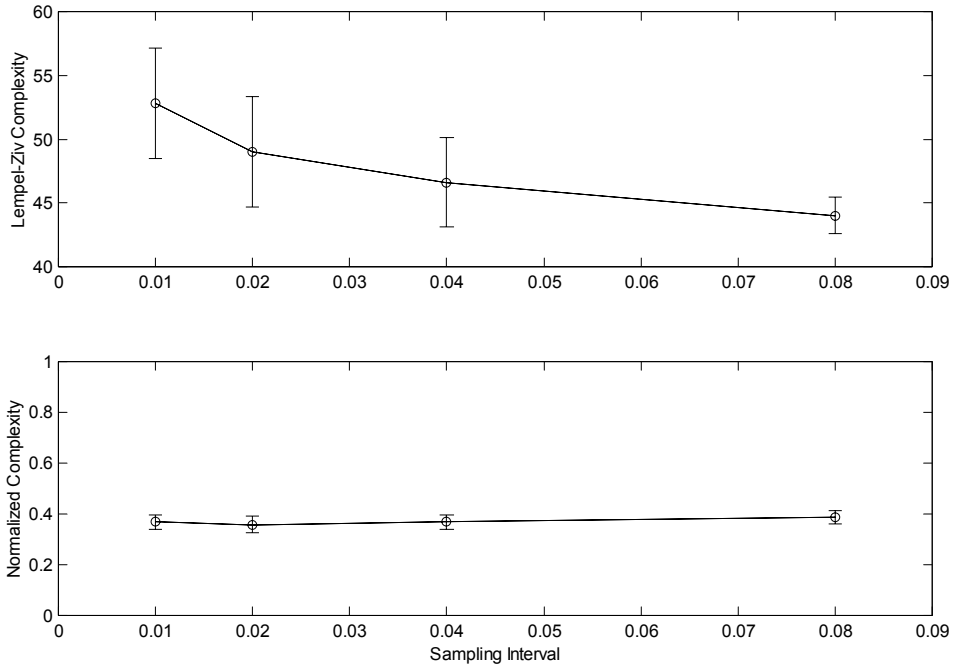

Figure 3. Lempel-Ziv complexity and normalized complexity as a function of sampling interval

Random phase surrogates (9,10) are formed by taking the original time series (this is the original data prior to partitioning onto a symbol set) and calculating its Fourier transform, assigning a random value to the phase at each harmonic and calculating the inverse transform. The time series obtained by calculating the inverse Fourier transform is the random phase surrogate. The same symbolic partitioning and complexity calculation is applied to the original signal and to its random phase surrogates. A new normalized complexity is defined by

$$(C_N)_1 = C_{ORIG} / < C_1 >$$

$< C_1 >$ is the mean value of complexity obtained with the surrogates. The subscript 1 is employed because random phase surrogates are referred to as Algorithm 1 surrogates in the earlier literature (9). By construction, a random phase surrogate is a stochastic signal filtered to have the same power spectrum as the original signal. Because the surrogate and the original signal have the same power spectra, they have the same autocorrelation times. The surrogate therefore changes on the same time scale as the original signal. This class of surrogate can provide a normalization for different sampling frequencies. An example is shown in Figure 3.

The normalized complexity is denoted by $(C_N)_1$. In this example, the Lorenz system was sampled at four different frequencies. While the Lempel-Ziv complexity is different, the normalized complexity is approximately constant.

Three points should be emphasized. First, care must be exercised in the construction of random phase surrogates. Seemingly minor numerical errors in the calculations of the original signal's Fourier transform can result in the false positive rejection of the surrogate null hypothesis (11). Second, when reporting a value of normalized complexity it is essential to identify the type of surrogate used in the normalization. Other classes of surrogate can be considered. They include Algorithm 2, gaussian-scaled surrogates (9) and an iterative surrogate that combines properties of Algorithm 1 and Algorithm 2 surrogates (12). Third, in addition to identifying the type of surrogates used, a report of normalized complexity must also include a specification of the complexity measure used to characterize symbol sequences. In these examples, the Lempel-Ziv complexity measure was used. However, as previously indicated, many alternative complexity algorithms can be considered.

The procedures presented here show that it can be possible to control to some degree for differences in sampling duration and frequency when stationary processes are examined. While this is important in facilitating a comparison of complexity assessments between different conditions, these procedures do not address the fundamental limitation of complexity measures that is addressed in the next section

An absolute measure of complexity is impossible

The near constant values of normalized complexity seen in the two preceding sections are obtained only if the observed dynamical process is stationary. An example of a departure from stationarity based on a Mahler symphony has been presented in a previous contribution (13). On a single listening, a Mahler symphony might well be deemed to be a highly complex signal. Suppose, however, it was played in a tape loop and observed for several years. Under these circumstances, it becomes a periodic signal with, presumably, a low complexity.

Results from a demonstration of this process are shown in Figure 4. The Lempel-Ziv complexity normalized against equiprobable, random surrogates is shown for a signal constructed by repeating the same one hundred element segment of uniformly distributed random numbers. Calculated in isolation, the complexity of this segment has a value expected from random numbers, 1.06±.11. With increasing repetition of the same segment, the complexity of the compound signal has value indicating that the signal is periodic**.**The initial signal is a one hundred-point set of uniformly distributed random numbers. The Lempel-Ziv complexity of this data set normalized against equiprobable random surrogates is $(C_N)_0 = 1.06 \pm .11$. (The complexity is denoted by $(C_N)_0$ to identify the kind of surrogate used in the normalization. Random surrogates are often referred to as Algorithm 0 surrogates.) A value greater than one and the comparatively high value of uncertainty were obtained because only one hundred points are in the data set. A two hundred point data set was formed by repeating the one hundred element component twice. In this case, $(C_N)_0 = 0.68 \pm .02$.

Figure 4 shows the value of $(C_N)_0$ as a function of the number of times that the one hundred element data set is repeated. Even though when examined in isolation the one hundred element segment has the highest possible value of normalized complexity, the value of complexity decreases to a value typically observed with simple periodic signals when the segment is repeated.

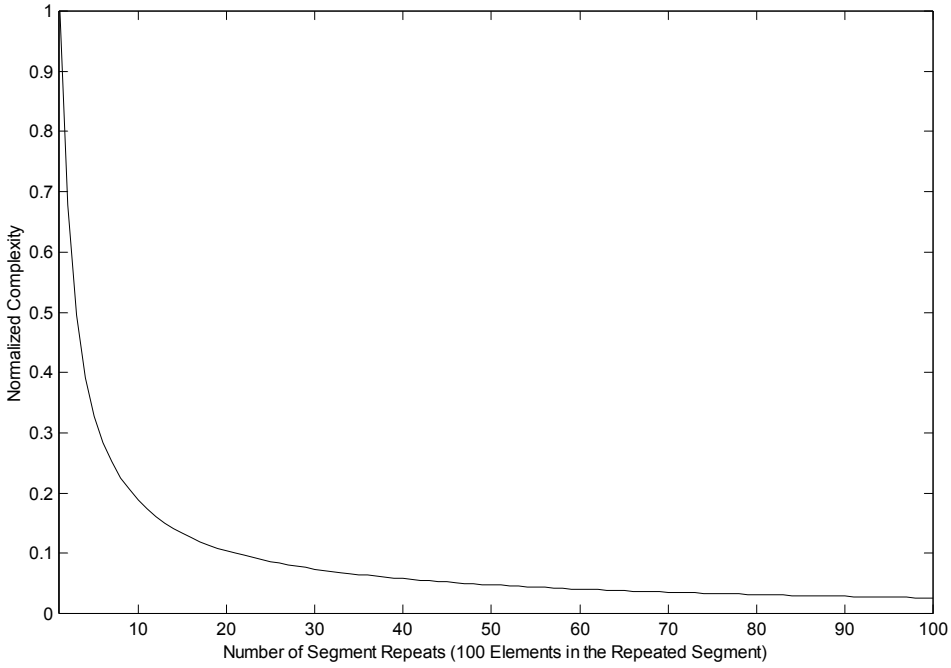

Figure 4. Normalized complexity for repeated segments

We therefore conclude that all complexity measures are time constrained. At best we can only report the value of normalized complexity observed under explicitly specified operational conditions which include a report of the temporal duration of the observation. An absolute value of complexity can never be measured.

There is a further limitation inherent to this class of complexity measure. As stated in the preceding paragraph, these kinds of complexity measurements can only report the complexity observed over a designated period of time. They cannot indicate the complexity of a signal at a specific point in time. A response to this limitation is outlined in the next section.

Instantaneous complexity

To use an analogy from mechanics, a value of complexity determined over a specified period of time is analogous to the mean velocity computed over a journey. The determination of dynamical complexity at a single point in time would be analogous to an instantaneous velocity, and we therefore use the term instantaneous complexity to describe it. If one restricts oneself to complexity measures based on symbolic dynamics, then the best approximation of an instantaneous complexity would be the complexity obtained in a short subepoch of the total signal in a moving window calculation. As with all moving window calculations, there is a trade off between temporal resolution (a short window gives a better temporal resolution) and the accuracy of the complexity estimate (a shorter window gives lower accuracy in the complexity calculation). We wish to outline here an alternative program for constructing an instantaneous measure of dynamical complexity. This requires a transition to a different area of mathematics.

The proposed measure is derived from the theory of continuous dynamical systems rather than from symbolic dynamics.

As before, the process begins with the acquisition of time series data, for example a digitized EEG signal, denoted by (x_1, x_2, ……., x_{NDATA}). We consider here the single channel case. Generalizations to multichannel signals can be constructed. The next step is a mathematical procedure called embedding in which the time series is used to form a trajectory in m-dimensional space. The points in this space are denoted by Z_j,

$$\{Z_j\} \subseteq \Re^m,$$

and are formed by the rule:

$$Z_j = (x_j, x_{j+L}, x_{j+2L}, ..., x_{j+(m-1)L})$$

(Alternative, equally acceptable, embedding protocols are possible.) For each Z_j there is a corresponding time t_j which is the midpoint of the time interval between the observation of x_j and $x_{j+(m-1)L}$. The embedding process requires the specification of appropriate values for m, the embedding dimension, and L, the lag. There is a large literature discussing criteria for choosing m and L. This literature is reviewed and the results of a comparative study of embedding criteria are given in Cellucci *et al*. (14). Based on that study, we set L equal to the first minimum of the time series' mutual information function, and embedding dimension m is determined by a false nearest neighbors argument (15).

Transformation of the time series into an m-dimensional set is motivated by the Takens embedding (16). A didactic statement of the theorem is given in Cellucci *et al*. (14). Stated informally, the theorem shows that if several conditions are met, then there is an intimate relationship, a diffeomorphism, between the dynamical structure of the system that generated the observed signal and the geometry of the embedded set $\{Z_j\}$. In practice these conditions cannot be met with finite data sets. Nonetheless it is sometimes possible to make meaningful inferences about the generating system from an examination of $\{Z_j\}$. The complexity of the signal generator at time t_k will be reflected in the complexity of the set of points in the immediate vicinity of point Z_k. Let $\{N_k\}$ denote the neighbor set of Z_k where we establish the convention that Z_k is an element of $\{N_k\}$. Procedures for identifying $\{N_k\}$ will be considered presently. By the preceding argument, the instantaneous complexity of the observed dynamical system at time t_k can be estimated by constructing a measure of the geometrical complexity of the m-dimensional set of points $\{N_k\}$.

If it were possible to rotate $\{N_k\}$ so that all of its elements lined up on a single axis of m-space, we would conclude that $\{N_k\}$ had a simple geometry. A less simple, but still fairly simple, case would be obtained if it were possible to rotate $\{N_k\}$ so that all of its elements fell on a single plane. Conversely, if points of $\{N_k\}$ were distributed so that no rotation caused a simplification of its geometry, we would conclude that $\{N_k\}$, and hence instantaneous complexity at time t_k, had a high value of complexity. Based on this reasoning, we conclude that a systematic procedure for examining the geometrical complexity of $\{N_k\}$ can be constructed using the singular value decomposition. Let A denote the local embedding matrix of point Z_k. Each point of $\{N_k\}$ becomes a row in matrix A. Therefore, A has m columns. The number of rows is equal to the number of points in $\{N_k\}$ which must be at least equal to m. In practice it will be much larger. The singular value decomposition of matrix A is given by $A = VDU^T$. Matrix U is the orthogonal transformation that rotates matrix A to its principal components; that is, the first column of matrix AU is the first principal component. The second column is the second principal component, and so on. Matrix D is the diagonal matrix of singular values.

$$D = \mathrm{diag}(\lambda_1, \lambda_2, ..., \lambda_m)$$

where we adopt the ordering convention $\lambda_i \geq \lambda_{i+1}$. The fraction of total signal variance in the j-th principal component, Var_j, is given by:

$$\lambda_j^2 \setminus \sum_i^m \lambda_i^2 .$$

If the elements of (x_1, x_2,… x_{NDATA}) are randomly distributed, then the variance is distributed equally across all components and $Var_j = 1/m$, j=1,2,……,m. In the other limiting case of an extremely simple matrix A, all variance would be in the first principal component. In this case, $Var_j = 1$ and the variance of the remaining components would be zero. Thus the complexity of $\{N_k\}$ can be expressed by a measure that gives a low value for $Var_j = 1$, $Var_j = 0$, j=2,….,m and a high value for the case $Var_j = 1/m$, j=1,2,….m. Morgera (17) has pointed out that this can be done with the functional form used to define Shannon entropy. In the present context, this is referred to as the covariance complexity, C_{COV}.

$$C_{COV} = -\sum_{i=1}^{m} Var_i \log Var_i / \log(m)$$

It can be shown that the maximum value of C_{COV} is one and that it is obtained in the case of random x's where $Var_j = 1/m$ for all j. The lowest value of C_{COV} is zero, and it is obtained when $Var_j = 1$, and $Var_j = 0$, j=2,….,m,.

With the exception of a specification of a procedure for constructing $\{N_k\}$, this completes the outline of a program for calculating the instantaneous complexity of a time series based on Takens theorem. This is a six step process:

1. The time series (x_1, x_2,… x_{NDATA}) is acquired.
2. Embedding parameters m and L are determined and the embedding set $\{Z_j\}$ is constructed.
3. For a given time t_k, the set $\{N_k\}$ consisting of Z_k and its neighbors is identified.
4. Local embedding matrix A is constructed from the points of $\{N_k\}$.
5. The singular value decomposition of A is performed to give the singular value spectrum.
6. The covariance complexity corresponding to time t_k, $C_{COV}(k)$ is calculated.

The remaining requirements are criteria for determining the number of elements in $\{N_k\}$ and the procedure for selecting its elements. These are matters of ongoing research. Three approaches are now being investigated: (i.) temporally contiguous neighbor sets, (ii.) geometrically contiguous neighbor sets, and (iii.) selective, geometrically contiguous neighbor sets.

As before let t_k denote the time corresponding to point Z_k. $\{N_k\}$ is its neighbor set, and N_N denotes the number of points in $\{N_k\}$. The easiest procedure for constructing $\{N_k\}$ is to use points temporally contiguous to Z_k. In this case, $\{N_k\}$ consists of the points recorded immediately before and immediately after Z_k.

$$\{N_k\} = \{Z_{k-N_N/2}, \ldots\ldots Z_K, \ldots\ldots, Z_{k+N_N/2}\}$$

This is equivalent to a moving window calculation that proceeds along the trajectory in embedding space. The effect of changing N_N can be investigated empirically.

The second procedure for constructing $\{N_k\}$, geometrically contiguous neighbor sets, uses the N_N points closest to Z_k irrespective of when they were recorded. This is a theoretically attractive option. C_{COV} is determined by the topological properties of the embedding space in the immediate vicinity of Z_k and uses topological information gained throughout the entire time series. This approach has much in common with recurrence diagrams (18-20) which has been shown to be effective in detecting transitions in dynamical systems.

The third procedure, selective, geometrically contiguous neighbor sets, is related to the second in that it finds points close to Z_k in the embedding space without reference to when they were recorded, but it tries to refine this selection criterion beyond a simple "take the N_N closest points" criterion. The practice of using selective nearest neighbor sets has a long history in the development of prediction algorithms based on the properties of embedded data (21, 22). For example, Short (23) constructed a prediction algorithm in which elements of $\{N_k\}$ are selected not only on the basis of their position, but also according to having tangent vectors that are close in Euclidean norm to the tangent vector at point Z_k. This criterion addresses problems caused by the self-intersection of reconstructed attractors.

These procedures can be used to calculate $C_{COV}(k)$ which gives a time-dependent measure of dynamical behavior. In principal, this technology could be used in any investigation that seeks to detect transitions in noisy time series. It is hypothesized that methods for detecting change based on local embedding space geometry can provide a valuable noise-robust complement to other transition detection procedures, for example ARMA modeling. This hypothesis can be confirmed or rejected only with additional research.

Acknowledgements

This research was supported by Grant Number 601135N.4508.518.A0247 from the Office of Naval Research and the Navy Bureau of Medicine to the Naval Medical Research Center. The opinions and assertions contained herein are the private ones of the authors and are not to be constructed as official or reflecting the views of the Navy Department or the naval service at large.

References

1. Rapp PE, Albano AM, Zimmerman ID, Jiménez-Montaño MA. Phase-randomized surrogates can produce spurious identifications of non-random structure. Physics Letters 1994;192A:27-33.
2. Kolmogorov AN. Three approaches to the definition of the concept of quantity of information. Problems of Information Processing 1965;1:3-11. (Translated from the Russian Edition).
3. Chaitin GJ. On the length of programs for computing finite binary sequences. Journal of the Association for Computing Machinery 1966;13:547-69.
4. Rapp PE, Schmah TI. Dynamical analysis in clinical practice. In: Lehnertz K, Arnhold J, Grassberger P, Elger CE (Ed.). Chaos in brain? Singapore: World Scientific; 2000. p. 52-65.
5. Lempel A, Ziv J. On the complexity of finite sequences. IEEE Transactions on Information Theory 1976;IT-22:75-81.
6. Watanabe TAA, Cellucci CJ, Kohegyi E, Bashore TR, Josiassen RC, Greenbaun NN, Rapp PE. The algorithmic complexity of multichannel EEGs is sensitive to changes in behavior. Psychophysiology 2003; 40:77-97.
7. Press WH, Flannery BP, Teukolsky SA, Vetterling WT. Numerical recipes (The art of scientific computing). Cambridge: Cambridge University Press; 1986.
8. Rapp PE, Cellucci CJ, Korslund KE, Watanabe TAA, Jiménez-Montaño MA. An effective normalization of complexity measurements for epoch length and sampling frequency. Physical Review E 2001;64(016209):1-9.
9. Theiler J, Eubank S, Longtin A, Galdrikian B, Farmer JD. Testing for nonlinearity in time series: The method of surrogate data. Physica D 1992;58:77-94.
10. Rapp PE, Albano AM, Schmah TI, Farwell LA. Filtered noise can mimic low dimensional chaotic attractors. Physical Review E 1993;47:2289-97.

11. Rapp PE, Cellucci CJ, Watanabe TAA, Albano AM, Schmah TI. Surrogate data pathologies and the false-positive rejection of the null hypothesis. International Journal of Bifurcation and Chaos 2001;11:983-97.
12. Schreiber T, Schmitz A. Improved surrogate data for nonlinearity tests. Physical Review Letters 1996;77:635-8.
13. Rapp PE, Schmah TI. Complexity measures in molecular psychiatry. Molecular Psychiatry 1996;1:408-16.
14. Cellucci CJ, Albano AM, Rapp PE. Comparative study of embedding methods. Physical Review E 2003; 67(066210):1-13.
15. Abarbanel HDI, Kennel MB. Local false nearest neighbors and dynamical dimensions from observed chaotic data. Physical Review E 1993;47:3057-68.
16. Takens F. Detecting strange attractors in turbulence. In: Rand DA, Young LS (Ed.). Lecture notes in mathematics. Vol. 898. New York: Springer-Verlag; 1980: p. 365-81.
17. Morgera SD. Information theoretic covariance complexity and its relation to pattern recognition. IEEE Transactions on Systems, Man and Cybernetics 1985;15:608-19.
18. Eckmann JP, Kamporst SO, Ruelle D. Recurrence plots of dynamical systems. Europhys Letts 1987; 4:973-7.
19. Webber CL Jr, Zbilut JP. Dynamical assessment of physiological systems and states using recurrence plot strategies. J Appl Physiol 1994; 76:965-73.
20. Zbilut JP, Sirabella P, Giuliani A, Manetti C, Colosimo A, Webber CL Jr. Review of nonlinear analysis of proteins through recurrence quantification. Cell Biochemistry and Biophysics 2002;36:67-87.
21. Judd K, Mees A. On selecting models for nonlinear time series. Physica 1995;82D:426-44.
22. Mees AI. Dynamical systems and tesselations: Detecting determinism in data. Int J Bifurcation Chaos 1991;1:777-94.
23. Short KM. Detection of teleseismic events in seismic sensor data using nonlinear dynamic forecasting. Int J Bifurcation Chaos 1997;8:1833-45.

Appendix: Specification of model systems

Hénon System

$$x_{t+1} = 1 - ax_t^2 + y_t \quad a=1.4$$
$$y_{t+1} = bx_t \quad b=0.3$$

Lorenz Equations:

$$dx/dt = -\sigma(x - y)$$
$$dy/dt = -xz + rx - y$$
$$dz/dt = xy - bz$$

σ=10, b=8/3, r=28, h=.1

Rössler Equations:

$$dx/dt = -y - z$$
$$dy/dt = x + ay$$
$$dz/dt = b + xz - cz$$

a=.2, b=.4, c=5.7, h=.1

Short communication

MODEL, DYNAMICAL BEHAVIOUR AND SYNCHRONIZATION PROPERTIES IN NETWORKS OF FAST-SPIKING INTERNEURONS

Angelo Di Garbo, Alessandro Panarese, Michele Barbi, Santi Chillemi
Istituto di Biofisica, Consiglio Nazionale delle Ricerche – Sezione di Pisa, Pisa, Italy

Introduction

Recently it was found that in the neocortex the Fast Spiking (FS) inhibitory interneurons are interconnected by electrical synapses too (1, 2). At present the specific functional role of the activity patterns of FS interneurons for cortical information processing are not well known. In a recent study it was shown that FS cells are strongly excited by thalamocortical inputs, thus it was suggested that this group of interneurons operates as a local source of neocortical inhibition (3). Moreover, additional experimental findings suggest that FS cells could play a relevant role in the detection of synchronous activity (4).

On the theoretical side, by using computational and analytical tools it was shown that a network of mutually inhibiting interneurons is capable to generate synchronous oscillatory activity provided that specific constraints on the time course of the postsynaptic inhibitory conductance, tonic excitatory drive etc. are satisfied (5-9). In the most recent work concerning this problem (10), the existence and the stability of the phase locking states of a pair of identical Leaky Integrate-and-Fire (LIF) neural models, coupled by electrical and chemical synapses, were investigated. In the present report we perform a study similar to the latter by using a single compartment biophysical model for each FS cell. Our principal aim is to study how electrical and inhibitory synapses affect the synchronization properties of a pair of coupled FS cells and compare our results with those obtained with the LIF model.

Models and methods

The activity of each FS cell is described by a single compartment biophysical model derived from that proposed recently (10), consisting of an isopotential sphere (the soma). To better match the main experimental electrophysiological properties of an FS cell the maximal conductances and the kinetics of the ionic currents were modified, and the new model reads:

$$C dV/dt = I_E - g_{Na} m^3 h (V - V_{Na}) - g_K n^4 (V - V_K) - g_L (V - V_L) \quad [1a]$$

$$dx/dt = (x_\infty - x) / \tau_x,\ x_\infty = \alpha_x / (\alpha_x + \beta_x),\ \tau_x = 1 / (\alpha_x + \beta_x),\ (x = m, h, n) \quad [1b]$$

where $C = 1 \mu F/cm^2$, I_E is the external stimulation current, and $\alpha_m = 4.2\ exp[(V+34.5)/11.57]$, $\beta_m = 4.2\ exp[-(V+34.5)/27]$, $\alpha_h = 0.09\ exp[-(V+45)/33]$, $\beta_h = 0.09\ exp[(V+45)/12.2]$, $\alpha_n = 0.3\ exp[(V+35)/13.83]$, $\beta_n = 0.3\ exp[-(V+35)/14.06]$. The maximal specific conductances and the reversal potentials are, respectively: $g_{Na} = 52\ mS/cm^2$, $g_K = 250\ mS/cm^2$, $g_L = 1.6\ mS/cm^2$ and V_{Na}

= 58 mV, V_K = -90 mV and V_L = - 72 mV. In this model the onset of periodic firing occurs through a Hopf bifurcation for $I_E \cong 28.7\ \mu A/cm^2$ with a well defined frequency (~37 Hz), according to the type II excitability property (11).

The inhibitory synapse is modelled as follows: if a presynaptic neuron generates N spikes at times t_j (j =1, 2,..N) the magnitude of the inhibitory current at time $t > t_N$ in the postsynaptic cell is $I_{Sy} = g_{Sy} \sum_j s(t - t_j)\ (V_{Post}\ (t) - V_{Rev})$, with $s(t) = \{[1 - exp(-t/\tau_{Rise})]\ exp(-t/\tau_{Decay})\}/\max[s(t)]$, V_{Rev} = -80 mV and g_{Sy} is the maximal conductance of the inhibitory synapse (in mS/cm^2 unit). In the following we will keep τ_{Rise} = 0.289 ms and $\tau_{Decay} = <\tau_{Exp}> = 2.6\ ms$; moreover, where stated, the τ_{Decay} value will be varied. The electrical synapse is modelled as $I_{El} = g_{El}\ (V_{Post} - V_{Pre})$ and g_{El} is the maximal conductance of the gap junction (in mS/cm^2).

Let us consider a pair of coupled nonlinear oscillators and assume that in absence of coupling the state of each one is a stable limit cycle. Then, in the weak coupling limit the state of each oscillator can be described by its phase θ_i (i = 1, 2) and the time evolution of $\phi = \theta_1 - \theta_2$ is determined by $d\phi/dt = [H_2(-\phi) - H_1(\phi)] = - D(\phi)$ (for details see (12)). The phase locked states can be found by searching the solutions of the equation $D(\phi^*) = 0$.

In numerical simulations of a pair of FS cells subject to Poissonian synaptic bombardment we used the normalized cross-correlation histogram to quantify their synchronization level: this measure is denoted by $\Gamma(t)$. The adopted time bin is 1 $msec$.

Results

Firstly let us consider a pair of identical FS cells reciprocally coupled by inhibitory synapses alone to investigate the existence and stability of phase locked states as the decay time constant τ_{Decay} of the inhibitory current is varied. The stimulation current I_E is the same for both interneurons and the results are reported in left and middle panels of Figure 1: bifurcation diagrams of the phase difference against τDecay for a pair of FS cells weakly coupled by inhibitory and electrical synapses are reported. For both the left and middle panels it is gE =0, while for the right one it is gEl / gSy =0.3. For both panels νFree is the free firing frequency of each cell for the used IE values. For all panels the black (gray) dots represent stable (unstable) states. It is important to note that there is a critical value τ_C of the decay time constant such that for $\tau_{Decay} < \tau_C$ there is bistability (synchrony and antisynchrony), while for $\tau_{Decay} > \tau_C$ the only stable states are the synchronous ones. As the value of the stimulation current I_E increases synchronization is promoted. As the electrical coupling is set on, the probability to get stable synchronous states increases (right panel of Figure 1). From a dynamical point of view for $\tau_{Decay} = \tau_C$ a subcritical pitchfork bifurcation occurs: the antiphase state loses its stability and two unstable branches, behaving as separatrices between antiphase and inphase states, appear. Thus, for a fixed τ_{Decay}, the quantity $2 - 2\phi(\tau)$ gives a rough estimation of the probability of asymptotically reaching a synchronous regime for random initial conditions ($\phi(\tau)$ being the phase of the corresponding state in the top unstable branch). The existence and stability of phase locked states in a pair of FS cell models were investigated against I_E by keeping $\tau_{Decay} = <\tau_{Exp}> = 2.6\ ms$ and the results were qualitatively similar to those shown in figure 1 (data not shown). The above results are qualitatively the same as those found for a LIF pair.

To quantify the effects of electrical coupling on the synchronization level of a pair of FS cell models we used the following protocol: for any fixed value of the ratio $Q = g_{El} / g_{Sy}$ we evaluated $I_C(Q)$ from the associated bifurcation diagram (for I_E ranging in the interval 29.2 - 30.5 $\mu A/cm^2$); next, we considered the rectangle with unity height and base $I_C(Q) - 29.2$ and

calculated the area A_{UB}, of the region contained within the unstable branches. Then, the probability of synchronous firing was estimated as follows: $P_S = 1 - A_{UB} / A_{Tot}$, being $A_{Tot} = I_C(Q) - 29.2$. By plotting the value of P_S against g_{El} / g_{Sy} for $\tau_{Decay} = 5.2$ *ms* and $\tau_{Decay} = 2.6$ *ms* we found that for both fast and slow synapses the increase of g_{El} promotes synchronization (data not shown). These results are qualitatively in keeping for fast synapses, but at odds for slow ones, with those obtained by Lewis and Rinzel (10).

The above findings were obtained for symmetrical inhibitory coupling. We found that using two different values for the conductances of the inhibitory synapses destroys, as expected, the symmetry of the bifurcation diagrams as shown in Figure 2. However, when the intensity of the electrical coupling is increased, the synchronization is enhanced: i.e. the probability to get synchronous states starting with arbitrary initial conditions increases and the symmetry of the bifurcation diagram is partially recovered.

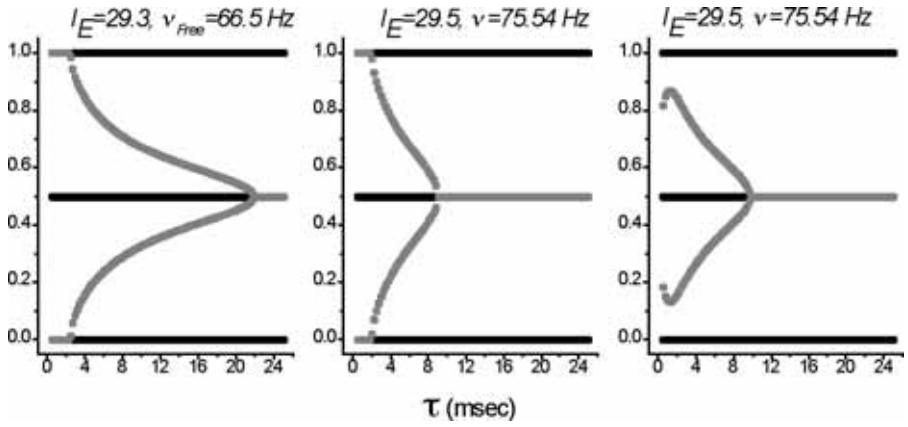

Figure 1. Bifurcation diagrams of the phase difference against τDecay for a pair of FS cells weakly coupled by inhibitory and electrical synapses

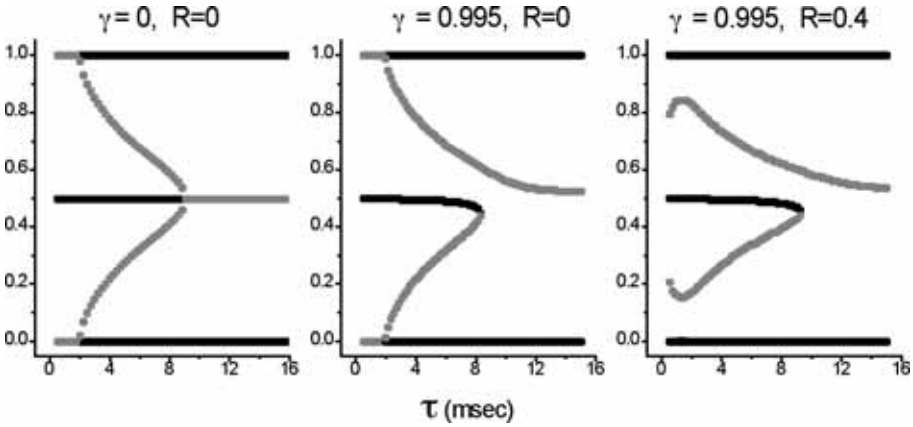

Figure 2. Bifurcation diagrams of the phase difference against τDecay in the presence of heterogeneities

FS interneurons receive excitatory inputs from pyramidal neurons and the properties of these synapses were studied experimentally (4). We used these experimental data to model excitatory postsynaptic currents (EPSC) from pyramidal to FS cells. Poissonian spike trains (of 1000 Hz rate) were generated, convolved with the experimental waveform of EPSC and added to the right hand side of equation (1a). Then the corresponding equations were integrated numerically. For the discharges recorded from neocortical FS cells *in vitro* a very low value of the coefficient of variation (*CV*) of the interspike intervals (*ISIs*) was measured: $CV = 0.086$ (13). Thus, the amplitude of the EPSC for our computer experiments was fixed in order to yield for the uncoupled FS cell a *CV* value of the same magnitude as the experimental one. By adopting $g_{EPSC} = 0.0047\ mS/cm^2$ for the maximal conductance of the excitatory synapses, we got $CV \sim 0.085$. The plots of $\Gamma(t)$ are shown in Figure 3: for $g_{El} = g_{Sy} = 0$ the corresponding Γ curve is flat and the discharges of the two interneurons are uncorrelated as expected. The figure reports the Normalized cross-correlation histograms for a pair of coupled FS cell models when each cell receives uncorrelated Poisson distributed excitatory inputs of 1000 Hz rate and maximal amplitude $g_{EPSC} = 0.0047\ mS/cm^2$. Left panel: $g_{El} = g_{Sy} = 0$, middle: $g_{El} = 0$, $g_{Sy} = 0.11\ mS/cm^2$ and right: $g_{El} = 0.05\ mS/cm^2$, $g_{Sy} = 0.11\ mS/cm^2$. For both cells it is $I_E = 29.4\ \mu A/cm^2$ and $\tau_{Decay} = \langle\tau_{Exp}\rangle = 2.6\ ms$.

The introduction of the inhibitory coupling leads to the emergence of an oscillatory activity. The addition of electrical coupling reinforces the oscillatory activity and promotes the synchronization by increasing the number of events in which action potentials are generated within 1 *ms* time scale.

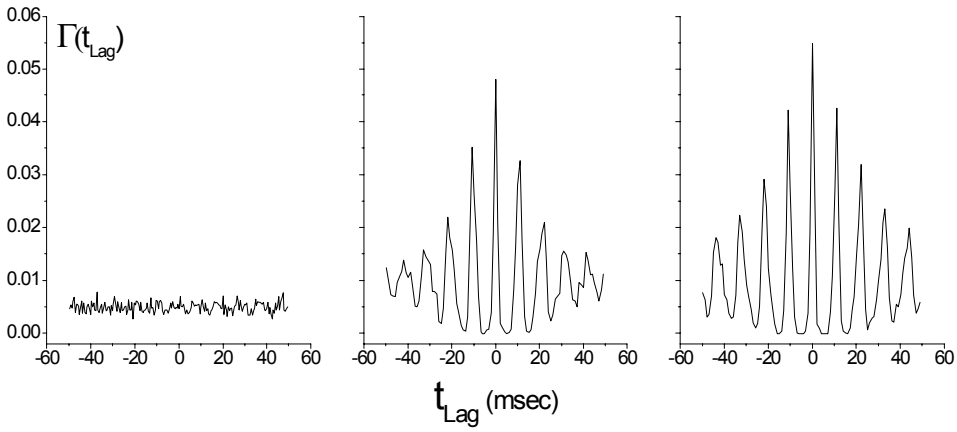

Figure 3. Normalized cross-correlation histograms for a pair of coupled FS cell models

Conclusions

We studied the synchronization phenomena occurring in a pair of FS cell models coupled by electrical and inhibitory synapses. We found that increasing either the stimulation current or the decay time constant of IPCS enhances the probability to get synchronous firing regimes starting with arbitrary random initial conditions. These results are qualitatively in agreement with those obtained for a pair of coupled LIF models (10). By increasing the conductance of the electrical

synapse we found that for fast synapses (τ_{Decay} = 2.6 *ms*) our results agree qualitatively with those obtained for a LIF model pair, while for slow (τ_{Decay} = 5.2 *ms*) synapses they are conflicting.

We showed that the presence of heterogeneities deteriorates the coherence levels of the network. However, the effects of heterogeneities on the synchronization level between cells can be balanced by increasing the g_{El} value.

Lastly, the synchronization phenomena occurring in more realistic conditions were studied too by injecting each cell by uncorrelated Poisson distributed excitatory inputs of 1000Hz rate. The main finding was the enhancement of the synchronization level as the electrical coupling condunctance was set on.

References

1. Galarreta M, Hestrin S. A network of fast-spiking cells in the cortex connected by electrical synapses. Nature 1999;402:72-5.
2. Gibson JR, Beierlein M, Connors BW. Two networks of electrically coupled inhibitory neurons in neocortex. Nature 1999;402:75-9.
3. Beierlein M, Gibson JR, Connors BW. Two dynamically distinct inhibitory networks in layer 4 of the neocortex. J Neurophysiol 2003;90:2987-3000.
4. Galarreta M, Hestrin S. Spike transmission and synchrony detection in networks of GABAergic interneurons. Science 2001;292:2295-9.
5. Wang XJ, Rinzel J. Alternating and synchronous rhythms in reciprocally inhibitory model neurons. Neural Comput 1992;4:84-97.
6. Van Vreeswijk CA, Abbott LF, Ermentrout GB. Inhibition, not excitation, synchronizes coupled neurons. J Comp Neurosci 1995;1:303-13.
7. Whittington MA, Traub RD, Jefferys JGR. Synchronised oscillations in interneuron networks driven by metabotropic glutamate receptor activation. Nature 1995;373:612-5.
8. White JA, Chow CC, Rit J, Soto-Trevino C, Kopell N. Synchronization and oscillatory dynamics in heterogeneous, mutually inhibited neurons. J Comp Neurosci 1998;5:5-16.
9. Di Garbo A, Barbi M, Chillemi S. Synchronization in a network of fast-spiking interneurons. BioSystems. 2005; in press.
10. Lewis T, Rinzel J. Dynamics of spiking neurons connected by both inhibitory and electrical coupling. J Comp Neuroscience 2003;14:283-309.
11. Rinzel J, Ermentrout B. Analysis of neural excitability and oscillations. In: Koch C, Segev I (Ed.). Methods in neuronal modeling. Cambridge: MIT Press; 1989.
12. Ermentrout B. Neural networks as spatio-temporal pattern-forming systems. Rep Prog Phys 1998; 61:353-430.
13. Galarreta M, Hestrin S. Electrical and chemical synapses among parvalbumin fast-spiking GABAergic interneurons in adult mouse neocortex. Proc Natl Acad Sci USA. 2002; 99:12438-12443.

Short communication

ANALYZING SPATIAL DISTRIBUTIONS OF FMRI "BOLD" SIGNALS BY RQA VARIABLES

Marta Bianciardi (a), Paolo Sirabella (b), Gisela E. Hagberg (a), Alessandro Giuliani (c), Joseph P. Zbilut (d), Alfredo Colosimo (b)
(a) Laboratory of Neuroimaging, Foundation Santa Lucia, Rome, Italy
(b) Dept. of Human Physiology and Pharmacology, University of Rome "La Sapienza", Rome, Italy
(c) Dipartimento di Ambiente e Connessa Prevenzione Primaria, Istituto Superiore di Sanità, Rome, Italy
(d) Department of Molecular Biophysics and Physiology, Rush College of Medicine, Chicago, USA

Introduction

Recurrence Quantification Analysis (RQA) is a model-free method sensitive to both linear and non-linear time-dependent processes. The assumption-free RQ estimation of brain activation patterns thus offers an extension and improvement of conventional General Linear Modeling (GLM) approaches. In the present work we check the conjecture that parameters obtained by RQA can be used as indicators of significant MR signal changes during activation in the human brain. We produced recurrence plots of experimental fMRI data acquired on a subject performing a motor task and, by means of RQA variables, we analyzed signals generated from different areas or volume elements of the brain. If brain activity can be reliably identified and imaged by such an approach, a spatial picture of the time dependent changes in the system may be developed and active/non active areas discriminated without too strict a priori assumptions.

BOLD fMRI signals and their analysis

One common form of functional MRI is known as blood oxygen level dependent imaging, or BOLD. The BOLD technique is based on measurements that are sensitive to changes of the effective transverse relaxation time of a magnetic resonance (MR) signal. These changes occur due to varying deoxy-hemoglobin concentrations following locally increased neuronal metabolic rates. To put it in different words, these physiological processes induce activation related signal variations in each volume element of a brain that can be detected with the BOLD technique.

With conventional analysis methods (1), activated brain areas can be revealed by comparing the temporal evolution of the MR signal in each voxel with an external reference model that represents the expected activation time-course. The overall results are transformed into a visual output, where active volume elements are rendered by false colors corresponding to the statistical significance of the difference of the dynamic features of the signal in that volume element, as compared to an external reference model. Unfortunately the choice of such a reference model remains arbitrary and subject to systematic and unforeseeable pitfalls, such as those induced by delays or differences in the shape between the MR signal variation and the adopted reference model. Thus, any conclusion drawn from conventional statistical regression

analysis of BOLD images will depend on the choice of reference model and therefore will be somewhat subjective.

One analytical technique that has proven successful for the quantitative analysis of dynamic systems is Recurrence Quantification Analysis (RQA). This method (2-4) identifies and quantifies recurrent patterns in dynamic systems without relying on assumptions and models. A number of dynamic systems have been studied using RQA techniques. In the present work RQA was applied to analyze the spatial distribution of RQA variables generated from time varying signals that have spatial contiguity, i.e. fMRI signals collected from a plurality of area or volume elements, of the human brain.

Analytical approach

For each collected MR voxel time-series, $\mathbf{y}_{raw}$, (see below) three preprocessing steps are performed previous to statistical analysis. Correction for involuntary motion during MR-scanning; then, in order to increase the MR signal-to-noise-ratio, a spatial smoothing filter is applied for each brain 3D-volume by convolution with an isotropic Gaussian kernel (FWHM = 6 mm for our data); afterwards, removal of low frequency noise (e.g. static magnetic field drift and other aliased effects) is achieved by temporal linear detrending of each time-series.

In conventional analysis, a reference model **H** is fitted to the data **y**, pre-processed in this fashion. **H** is obtained after convolution of a train of stimulus events (delta functions centered on instants when the event occurred, $T_{\delta(t-tE)}$) with an impulse hemodynamic response function (iHRF). The shape of the iHRF can be arbitrary chosen and usually is set as a linear combination of gamma functions, with a positive peak around 5 s, followed by an undershoot, with maximum ca 10 sec after the event. The output of conventional analysis applied on each voxel time-series consists of a β–value, which is proportional to the effect size (activation amplitude), and of a t-value, by which assesses quantitatively the statistical significance of the activation.

In RQ analysis, a recurrence 2D-plot is first worked out. Given the time-series $\mathbf{y}$ = (y(1)… y(i)…y(n)), an embedding procedure will produce a vector $\mathbf{y_i}$ = (y(i) y(i+L)… y(i+(m-1)L)), where m is the embedding dimension and L the lag. Distances between vectors $\mathbf{y_i}$, $\mathbf{y_j}$, if less than an established radius r, will embody the element i,j of the auto-recurrence matrix visualized in the 2D-plot. Dissimilarly, when the two axes of the recurrence plot represent an external reference function (the stimulus train, $T_{\delta(t-tE)}$) and the response signals **y**, respectively, the matrix will be representative of cross-recurrences. In order to quantify important features of the recurrence plot, several strategies are developed, which lead to the generation of ten variables: recurrence, determinism, entropy, max-line, mean-line, laminarity, trap-time, max-vert, recurrence time1, recurrence time2

In Figure 1, conventional (linear regression) and RQA steps described above are shown in synthesis. Recurrence (REC) provides a measure of the percentage of recurrence plots (RPs) filled with recurrent points. Determinism (DET) represents the percentage of recurrent points that form diagonal lines, with a minimum of two adjacent points. This is significant because recurrent points forming a diagonal line segment are considered as deterministic (as opposed to random). Entropy (ENT) is the Shannon information entropy of the line length distribution in a RP. The length of the longest line segment parallel to the diagonal is called max-line (MAXLIN), and, similarly, the mean length of such segments is called mean-line (MEALIN). Laminarity (LAM) represents the fraction of recurrence points forming continuous vertical alignments, and the average length of such vertical alignments is called trapping time (TRAPT).

The maximum number of consecutive recurrence dots arranged in a vertical line is termed max-vert (MAXVERT). The time distance between a state of a system at time *i* and at its recurrence at time *j*"RECUTIME1") may be measured by vertical distances of the line segments in a RP. Discarding the states at time *j-1* (sojourn times) leads to recurrence times of a second type (i.e., "RECUTIME2").

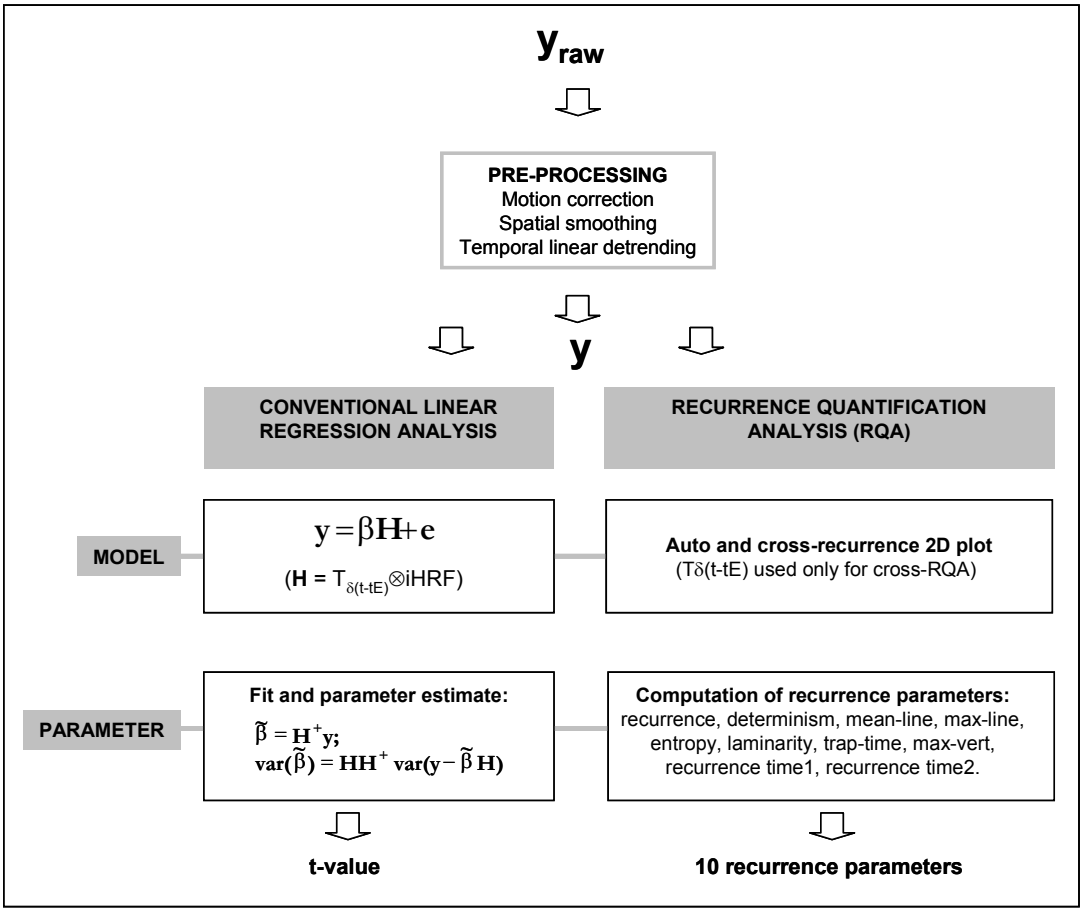

Figure 1. Analysis approaches

Application to fMRI BOLD data

A 24 year-old male volunteered to participate in this study, approved by the local ethics committee. A total of 270 BOLD sensitive image volumes were acquired with a Siemens Vision Magnetom MR system (Siemens Medical Systems, Erlangen, Germany) operating at 1.5 T and equipped for echo-planar imaging. Each volume was subdivided in 11 planes, starting from the vertex and stretching caudally (radio-frequency pulse: 60°; TR: 1000 ms; TE: 60 ms; in-plane resolution: 3x3 mm, slice thickness = 4 mm and gap between slices = 0.4 mm). The 14 initial BOLD images were discarded from further analysis to remove any possible T1 saturation effects. Visual stimuli indicating onset of the events (finger tapping) were projected via

mirroring to a front projection screen using a LCD video projector (Model VPL-351QM, Sony Corp., Tokyo) located inside the MR room and connected to a PC located outside the MR room.

The subject had to fixate the front projection screen on which the visual stimuli were presented. In response to the occurrence of a green dot on the monitor (with a 16 MR scans ON/OFF cycle), the volunteer had to push a button of a response box.

Figure 2 shows the magnetic resonance signals obtained from five contiguous voxels in an active region of the brain (left) and the magnetic resonance signals obtained from five contiguous voxels in a non-active region of the brain (right). Notice that in the present context, activity is determined by means of the conventional approach (statistical threshold $p < 0.001$, uncorrected for multiple comparisons, and $t > 3.01$). Statistical t-values ranged from 7.8 to 10.8 and from –0.4 to –1 for time series "a" and "b", respectively.

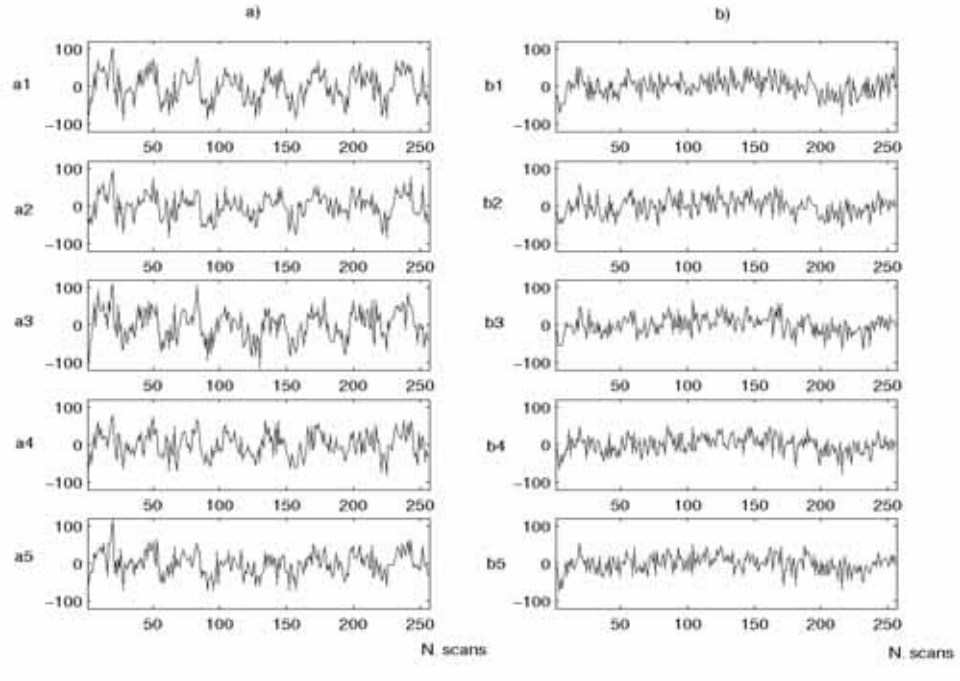

Figure 2. MR signals (Siemens Vision 1.5 Tesla, GE-EPI, 256 scans, TR = 1 s, TE = 60 ms, voxel dim = 3x3x4.8 mm) related to 5 contiguous voxels pertaining to two different brain areas a), b)

The two classes of time-series, "a" and "b", could also be discriminated by RQA variables. Auto- and cross- recurrence plots were generated for each time-series and examples relative to time-series 3a and 3b of Figure 1 are shown in Figure 3. A repetitive pattern is clearly evident in Figure 3a (for example, on the diagonal 8 mini-blocks, about 16 points long, as the design ON periods, can be distinguished); for time-series 3b (Figure 3b) recurrences are less pronounced, although the presence of some structure indicates the somewhat colored feature of the noise. Quantification of recurrences leads to a variable REC that was twice as high for time-series 2a, than for 2b.

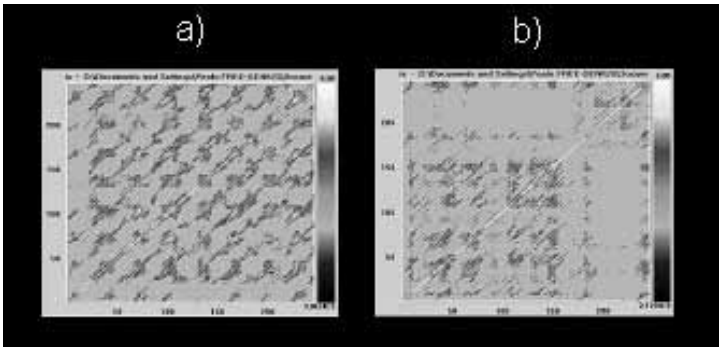

Figure 3. Auto-recurrence plot relative to time-series 3a and 3b of Figure 2, respectively

The same analytical strategies (conventional and RQA) were applied to the entire 3D brain-volume collected by fMRI. Ten RQA variables were calculated for each of the volume elements in the volume element array and an image showing the spatial distribution of the RQA variables of each brain slice was generated for each of the ten variables (calculated both for auto- and cross-recurrence plots, see Table 1, right). Figure 4 (upper panels) shows the resulting images for two of the ten RQA variables relative to one slice, namely cross-REC and cross-MAXLIN.

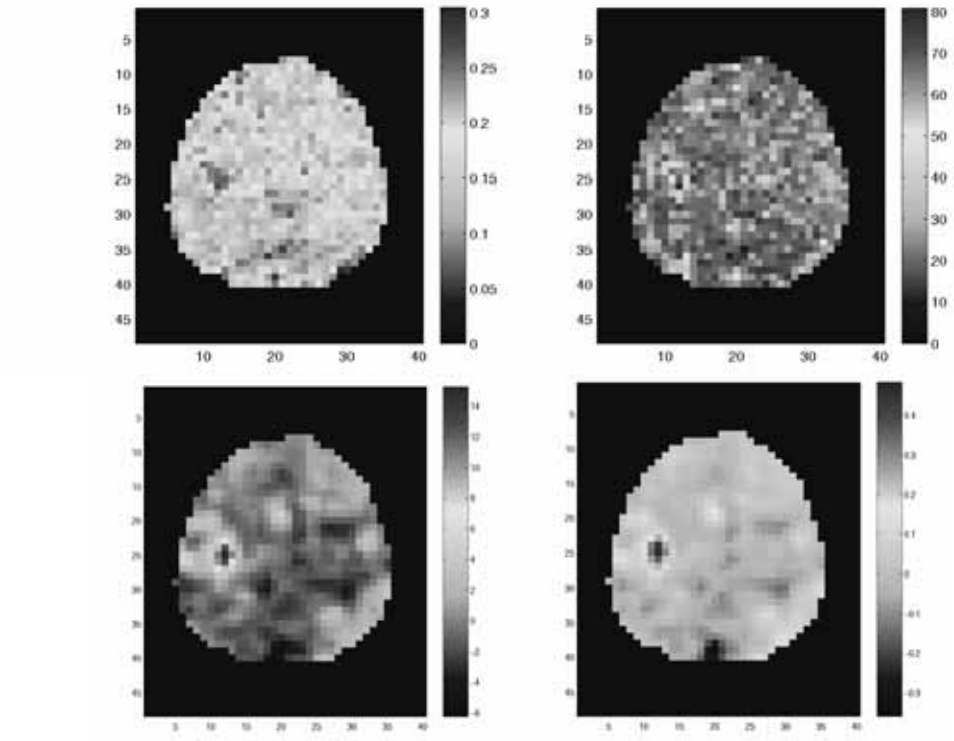

Figure 4. Upper panels: Cross-recurrence (left) and cross-maxline (right) computed on the experimental data-set (The working parameters of RQA were adjusted to the following values and kept the same in all cases: embedding dimension = 8; shift length (lag between subsequent windows) = 1; distance = Euclidean; radius = 1.7 standard deviation (SD) units in the distribution of distances; deterministic line = 2). Bottom panels: Results of conventional analysis: (left) estimated β-values; (right) t-values)

The bottom panels in Figure 4 contain the results (β- and t-values) over the same brain regions obtained by conventional linear regression analysis (see Figure 1, left). Notice that the graphical representation of Figure 3a,b is based on a false color scale.

Four RQA descriptors (auto-recurrence, auto-laminarity, cross-recurrence and cross-max-line) were able to detecte regions common to conventional analysis activation maps. In the former maps the activated regions appear somewhat more blurred; their location, however, could be characterized by a completely iHRF-assumption-free approach.

Conclusions

Preliminary results obtained by RQA on fMRI data of a volunteer performing a motor task showed clear activation clusters corresponding to the outcome of linear analysis. Although the exact relationship and statistical significance of the RQA parameters need to be established, this method seems a promising tool for the analysis of functional MR images of the human brain. With respect to conventional GLM techniques, in fact, RQA has the exclusive feature of being model-free and of detecting potentially both linear and non-linear dynamic processes, without requiring stationarity of the signal under investigation.

References

1. Friston KJ, Holmes AP, Poline JB, Grasby PJ, Williams SCR, Frackowiak RSJ, Turner R. Analysis of fMRI Time-Series Revisited. Neuroimage 1995;2:45-53
2. Eckmann JP, Kamporst SO, Ruelle D. Recurrence plots of dynamical systems. Europhys Letts 1987;4:973-977.
3. Zbilut JP, Sirabella P, Giuliani A, Manetti C, Colosimo A, Webber CL Jr. Review of nonlinear analysis of proteins through recurrence quantification. Cell Bioch Bioph 2002;36:67-87.
4. Webber CL Jr., Zbilut JP. Dynamical assessment of physiological systems and states using recurrence plot strategies. J Appl Physiol 1994;76:965-973.

Short communication

OTOACOUSTIC EMISSIONS AT DIFFERENT MATURATION STAGES: PRE-TERM AND FULL TERM SUBJECTS COMPARISON

Giovanna Zimatore (a), Alessandro Giuliani (b), Stavros Hatzopoulos (c), Alfredo Colosimo (a)
(a) Dept. of Human Physiology and Pharmacology, University of Rome "La Sapienza", Rome, Italy
(b) Dipartimento di Ambiente e Connessa Prevenzione Primaria, Istituto Superiore di Sanità, Rome, Italy
(a) Dept. of Audiology, University of Ferrara, Ferrara, Italy

Introduction

Otoacoustic signals allow a non-invasive inspection of cochlear function, and the information contained in their complex structure reveals the details of many auditory processes concerning not only the auditory periphery but the central nervous system as well (1). The click-evoked otoacoustic emissions (CEOAEs) can be characterized by means of their deterministic structuring and, by appropriate combination of Recurrence Quantification Analysis (RQA) and of Principal Components Analysis (PCA), in these signals we showed the presence of: i) significant individual features in adults and, ii) a large intra-subject variability in newborns (2-4). These observations provide the opportunity to determine whether a given morphoanatomical maturation stage in the ear system corresponds to a well defined functional maturation in newborns (5, 6). In the present study, we extend to newborns the same analytical strategy used in our previous characterization of adult signals (2,3) to get additional insight into the dynamic characteristics of CEOAEs through the systematic comparison of different age classes and of individual-linked features from non-pathological subjects.

Data sets and methods

A total of 124 CEOAE signals were collected in the Audiology Department of the University of Ferrara. In the case of 22 pre-term and 29 full-term subjects, the signals were recorded only once; in the case of 3 pre-term and 4 full-term subjects, the signals were recorded more than once, for a total of 30 and 43 signals, respectively. Pre-term signals are divided into two classes based on gestational age (before and after 33 weeks).

Recurrence variables. %Rec, %Det, Maxline, Ent, Trend, Lam and Trap (for a definition of the whole set of RQA variables see (1) or the J. Zbilut's contribution to this volume) were calculated by means of the software available from http://homepages.luc.edu/~cwebber/ (RQA62.EXE), with the following choice of working parameters: lag (delay in the embedding procedure) = 1; embedding dimension (number of elements in the rows of the embedding matrix) = 10; radius = 15 (expressed as a percentage of the maximum Euclidean distance between rows, to make variance and amplitude independent of the observed dynamic features of the signal); and line (minimum number of consecutive, recurrent points scored as deterministic) = 8. This choice derives from our previous experience in applying RQA to TEOAEs (2, 3), and,

in all cases, the results were checked for robustness against alternative choices. For a complete discussion of the RQA variables and working parameters, see reff. (1, 3).

Principal component analysis (PCA) was used to reduce the redundancy in the original variables (7). Since the principal components are, by construction, orthogonal to each other, a clear-cut separation of the different and independent features characterizing the data set is made possible. We applied PCA on the space spanned by the RQA variables to estimate the subject-dependent features of CEOAEs.

Results

Comparing full-term and pre-term responses

Fifty-one CEOAE responses of 22 pre-term and 29 full-term normoacousic newborns were projected into a principal component plane. Principal components are extracted from the 7 RQA variables listed in the previous paragraph. A two-sample t-test indicates that the dynamical variables %Rec, %Det, Maxline and Ent can significantly separate the two groups (see also Figure 1). Moreover, among pre-term newborns, two further groups (born before and after 33 weeks) are considered and compared by two-sample t-test: in that case all the 7 RQA variables were significantly different among the two groups.

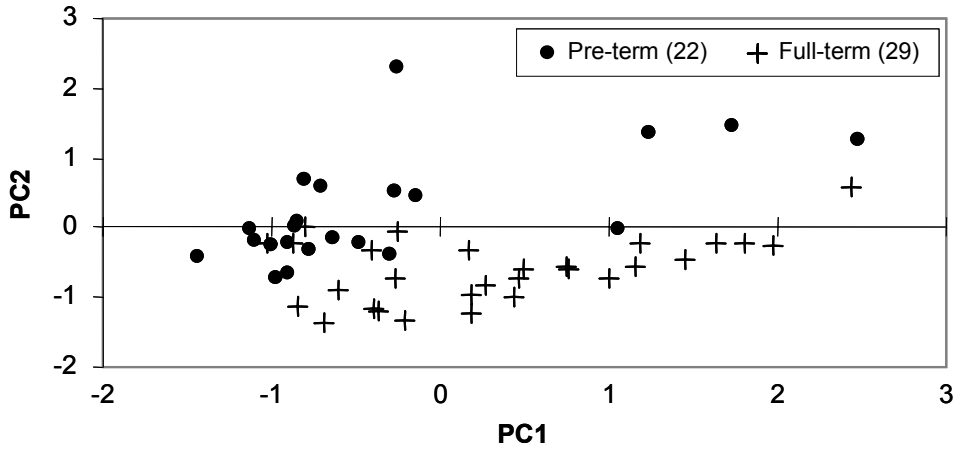

Figure 1. CEOAE responses evoked in full-term and pre-term subjects

Individual features

The average and standard deviation values of %DET were calculated over repeated records from 3 pre-term and 5 full-term newborns. 30 and 43 signals were considered for pre-term and full-term subjects, respectively and the results reported in Table 1.

Table 1. % Det variability in pre-term and full-term subjects

Variability	Inter	Intra	Inter/intra
PRE-TERM	3.72	1.10	3.40
FULL-TERM	2.79	0.73	3.83

Inter-subject variability (inter) is the standard deviation of the averages relative to the different individuals of that group.
Intra-subject variability (intra) is the average of the standard deviations relative to each single individual in that class.

In a previous work (5) we found very similar values for inter/intra ratios estimated from newborns and adults signals (3.70 and 3.79, respectively). In the present case the inter/intra ratio seems also independent from the maturation state of newborns, indicating that genetic factors (influencing the middle ear structure and distribution patterns of outer hair cells) prevail over the functional/physiological ones in accounting for the differences observed between the two gestational groups. This is evident in Figure 2 reporting the clustering in the first two components plane of individual TEOAE responses from newborns. The same symbol is used for responses of the same ear of the same subject in different experimental sessions. Each response was separately analyzed and plotted in the plane of the first two principal components (PC1, PC2) extracted from 9 RQA variables (7 dynamic variables plus the average and the standard deviation) in a previous set of signals (training set) recorded under identical conditions.

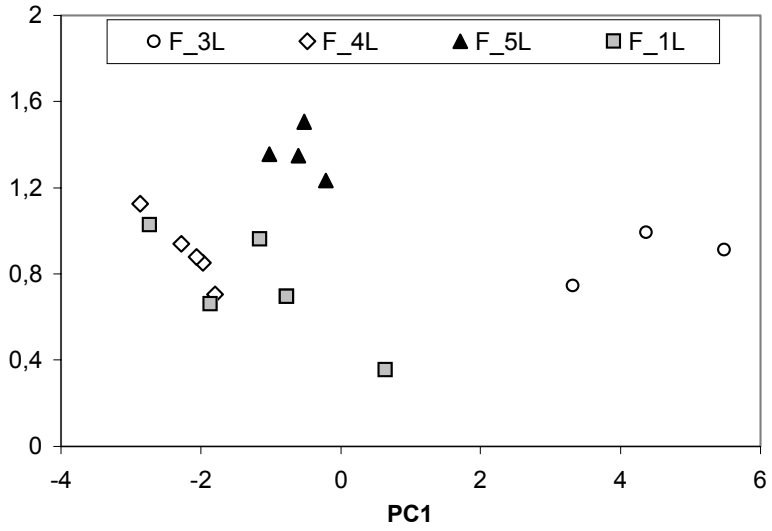

Figure 2. Clustering in a PC1/PC2 plane of individual TEOAE responses from newborns

Lateralization

For a number (20) of full-term subjects signals from both ears were available, which allowed us to compare signals from right and left ears. The paired samples t-test carried out over standard deviations (‘static’ variables) provided a significant difference between the two groups at the 5% significance level.

Conclusions

The main result of this work is the identification of a new estimator of the auditory functions of newborns at different gestational age. In particular, variables from recurrence quantification analysis of CEOAE signals can distinguish between pre-term babies born before and after 33 gestation weeks. A cut-off of %DET can be defined, and signals showing values of %DET lower than the thresholds cut-off may indicate no complete maturation. Moreover, our results indicate that individual features and distinction between Right and Left ear already exist in pre-term babies born before 33 gestation weeks.

This finding looks of peculiar interest in the light of the more general problem of identifying individual-linked features in complex physiological signals by appropriate use of non-linear analytical tools.

References

1. Kemp DT. Stimulated otoacoustic emissions from within the human auditory system. J Acoust Soc Am 1978;64:1386-91.
2. Zimatore G, Giuliani A, Hatzopoulos S, Martini A, Colosimo A. Otoacoustic emissions at different click intensities: invariant and subject dependent features. J Appl Physiol 2003;95:2299-305.
3. Zimatore G, Giuliani A, Parlapiano C, Grisanti G, and Colosimo A. Revealing deterministic structures in click-evoked otoacoustic emissions. J Appl Physiol 2000;88:1431-7.
4. Webber CL and Zbilut JP. Dynamical assessment of physiological systems and states using recurrence plot strategy. J Appl Physiol 1994;76:965-74.
5. Zimatore G, Hatzopoulos S, Giuliani A, Martini A, Colosimo A. Comparison of transient otoacoustic emission (CEOAE) responses from neonatal and adult ear. J Appl Physiol 2002;92:2521-8.
6. Hatzopoulos S, Tsakanikos M, Grzanka A, Ratynska J, and Martini A. A comparison of neonatal CEOAE responses recorded with linear and QuickScreen protocols. Audiology 2000;39:70-9.
7. Bartholomew DJ. The foundation of factor analysis. Biometrika 1984;71:221-32.

Stampato da Tipografia Facciotti srl
Vicolo Pian Due Torri 74, 00146 Roma

Roma, settembre 2005 (n. 3) 8° Suppl.